# Channel Estimation for Gigabit Multi-user MIMO-OFDM Systems

Franklin Mung'au

A Thesis Submitted in Partial Fulfillment
of the Requirements for the Degree of
Doctor of Philosophy
in
Engineering

©The University of Hull
31st March, 2008

The University of Hull holds the copyright of this thesis. Any person(s) intending to use a part or the whole of the materials in this thesis in a proposed publication must seek copyright release from the Dean of the Graduate School.

# Abstract

The fundamental detection problem in fading channels involves the correct estimation of transmitted symbols at the receiver in the presence of Additive White Gaussian Noise (AWGN). Detection can be considered when the receiver is assumed not to know the channel (non-coherent detection), or alternatively, when the random channel is tracked at the receiver (coherent detection). It can be shown that for a given error probability, coherent detection schemes require a Signal to Noise Ratio (SNR) that is 3dB less than the SNR required for non-coherent detection schemes. It is also known that the performance of coherent detection schemes can be further improved using space-frequency diversity techniques, for example, when multiple-input multiple-output (MIMO) antenna technologies are employed in conjunction with Orthogonal Frequency Division Multiplexing (OFDM).

However, the superior performance promised by the MIMO-OFDM technology relies on the availability of accurate Channel State Information (CSI) at the receiver. In the literature, the Mean Square Error (MSE) performance of MIMO-OFDM CSI estimators is known to be limited by the SNR. This thesis adopts a different view to estimator performance, by evaluating the accuracy of CSI estimates as limited by the maximum delay spread of the multipath channel. These considerations are particularly warranted for high data rate multi-user MIMO-OFDM systems which deploy large numbers of transmit antennas at either end of the wireless link. In fact, overloaded multi-user CSI estimation can be effectively studied by considering the grouping together of the user antennas for the uplink while conversely, considering a small number of antennas due to size constraints for the downlink. Therefore, most of the work developed in this thesis is concerned with improving existing single-user MIMO-OFDM CSI estimators but the results can be extended to multi-user system.

# Acknowledgments

This thesis is dedicated to my parents, Jacob Mung'au and Mary Mung'au. My dad, an Engineer and Mathematician, who has inspired me to achieve the best results academically, but more than that, personally. My mom for putting her career on hold to raise me and my sisters, and moulding us into the people we are today. To both parents; I would not have achieved what I have today were it not for your guidance, encouragement and faith in my abilities.

This thesis could also not have been done (on time at least!) were it not for my wife, Becky, who has been very supportive in every way and also made sure that I didn't spend too much time on capoeira! It is also dedicated to my two golden girls, Ayla and Leilani who are very special to me. Thanks to all those York capoeira who would play me in the roda even when the stress was evident and I was playing a bit too hard, axe, meu irmao.

Special thanks to Kai-Kit Wong, who introduced me to MIMO-OFDM and the problem of channel estimation in overloaded systems. Thanks also to K. Paulson, and Nick G. Riley for their contributions.

# Contents

# List of Figures

# List of Tables

# List of symbols

| | |
|---|---|
| $n_t$ | number of transmit antennas for a point to point MIMO system. |
| $n_r$ | number of receive antennas for a point to point MIMO system. |
| $E_s(t)$ | energy per symbol. The term symbol refers to the modulated IQ carriers for a QAM system. |
| $T_s$ | Symbol period. The duration for which information representing a binary sequence is modulated onto the IQ carriers. |
| $f_c$ | Carrier frequency. The carrier frequency is set at 2.4GHz. |
| $s_m(t)$ | A QAM symbol which has one of $m$ possible messages encoded onto the IQ carriers. |
| ${s_m}^{rx}(t)$ | The received QAM symbol. Includes the carrier and base band signals. |
| ${s_m}^{tx}(t)$ | The transmitted QAM symbol. Includes the carrier and base band signals. |
| $W_N^{k,n}$ | Complex exponential elements of the fourier transformation matrix. $W_N^{k,n} = \frac{1}{\sqrt{N}} e^{j2\pi kn/N}$. |

| | |
|---|---|
| $\mathbf{s}_k$ | OFDM subcarrier. OFDM transmits a vector of symbol via $K$ parallel subcarrier channels such that the duration of a symbol is extended from $T_s$ to $KT_s$. |
| $X[k]$ | Complex QAM symbol. The real part and imaginary parts correspond to the amplitude of the I and Q carriers respectively. |
| $x[n]$ | Complex OFDM sample. These samples are formed after the IFFT stage of an OFDM transmitter. |
| $R[k]$ | Received QAM symbol. These are formed when the received QAM symbols $r[n]$ are premultiplied by the FFT matrix. |
| $H_I(t), H_Q(t)$ | Complex gain of the channel. The real part and imaginary parts correspond to the gain experienced by I and Q carriers respectively. |
| $n_L$ | The number of OFDM symbols that are transmitted in the joint optimization scheme. |
| $\lambda$ | Wavelength of the carrier frequency. The wavelength is related to the carrier frequency $f_c$ via $\lambda = c/f_c$. |
| c | speed of an electromagnetic (EM) waves in free space, $c = 3 \times 10^8$ meters per second. |
| $k$ | wave number, the number of radians per wavelength for a given carrier frequency, $k = 2\pi/\lambda$. |

# Chapter 1

# An Introduction to MIMO-OFDM Systems

The multiple Input Multiple Output (MIMO) technology employs multiple transmit and receive antennas at either end of the wireless link to increase data rates or the reliability with which data is received. MIMO systems offer an efficient way of improving the performance of a wireless link through the exploitation of the spatial resource. MIMO equipped systems can also implement the discrete multitone technique Orthogonal Frequency Division Multiplexing (OFDM) which has the advantage of eliminating Inter-Symbol Interference (ISI), an effect prevalent at high data rates due to multipath propagation. The MIMO-OFDM technology is therefore poised to deliver the high data throughput and quality of service projected for future wireless systems.

As a starting point, this chapter introduces the MIMO-OFDM system model and discusses the process of communicating a sequence of bits (binary digits) from an application such as a camera on a mobile device equipped with MIMO-OFDM. The MIMO-OFDM system is described in terms of the air interface (QAM and OFDM), MIMO transmit/receive function (Spatial multiplexing and space-frequency coding) and the MIMO wireless link. The concept of multi-user MIMO-OFDM systems is then introduced after which the objectives of this thesis are formally stated.

## 1.1 Predicting the Emerging and Future Wireless Communications Technologies

In a little over two decades, the mobile phone has gone from being an expensive piece of hardware to a pervasive low cost technology enabling users to communicate regardless of their location. Other technologies such as Wi-Fi, which allow users to deploy network connections without cabling, provide mobile access to services such as internet and gaming applications, and have become ubiquitous in modern personal communications devices. Future wireless systems will aim to deliver high data rates and quality of service (QoS) for both indoor and outdoor environments. In addition to extending the range of applications available on personal communications devices, it is expected that standards such as the fourth generation of mobile systems (4G) will integrate mobile communications specified by International Mobile Telecommunications (IMT) standards and Wireless Local Area Networks (WLAN) [1]. Such projections have motivated extensive studies on the achievable capacity gains associated with multi-user MIMO systems [2].

Each new generation of mobile systems has required a particular technology in order to make the next evolutionary step forward. The step from the first generation (1G - 1982) of mobile systems (e.g., Advanced Mobile Phone System - AMPS) to the second generation (2G - 1992) of mobile systems (e.g., Global System of Mobile Communications - GSM) required the digitization of both speech and signaling [3]. The digitization of speech using full rate coders (such as the GSM 06.10 codec, also called the Regular Pulse Excitation - Long Term Prediction RPE-LTP codec [4]) allowed for high quality, low data rate voice digitization, which helped to establish GSM as a global system used by 82 percent of the global market. Indeed, GSM is used by over 2 billion people in 212 countries and territories.

The data handling capabilities of 2G systems are limited and the third generation (3G - 2004) of mobile phone systems has been deployed to provide the high bit rate services that enable high quality images and video to be transmitted and received. The third generation of mobile systems are based on the Code Division Multiple Access (CDMA) technologies, including CDMA2000 and WCDMA [5], which allow for greater bandwidth allocation per user (and hence higher data rates) when compared to the Frequency and Time Division Multiple Access (FDMA/TDMA) technologies implemented in 2G. Whereas 2G provides mobile data rates of up to 270kbps and 3G delivers rates of 2Mbps, the mobile data rates for the fourth generation (4G - 2014–2018?) of mobile systems are expected to reach 50-100Mbps [1], 10-20 times the rates available currently for broadband!

One technology that is poised to deliver the enhanced capabilities of the future systems is the Multiple Input Multiple Output[1] (MIMO) system technology [7]. Such systems promise to deliver high data throughput, and reliable detection, without additional bandwidth or transmission power. This is achieved through spatial multiplexing (when more data can be transmitted simultaneously from multiple antennas), diversity (sending coded bit sequences that allow for correct detection), as well as beamforming. Alternatively, methods that combine the spatial multiplexing and diversity advantages of MIMO transmission can be implemented, for example, the layered approach [8] and joint optimization schemes [9]. However, in order to realize the MIMO advantage, the elements of the antennas arrays at the transmitter and receiver must be adequately separated [10], where the minimum separation is typically considered to be on the order of a single wavelength. This separation of the antenna elements in the arrays ensures independent fading (Chapter 2) between transmit and receive antenna pairs. In practice, such independence of

[1]the notation $(n_t, n_r)$ will be used to denote a MIMO system with $n_t$ transmit antennas and $n_r$ receive antennas.

the MIMO links is possible because of multipath propagation. The probability of all the links being in deep fade is reduced; hence the spatial diversity gain, or alternatively, the information transmitted via each link can be detected using a well designed receiver in the spatial multiplexing schemes.

Multipath propagation, despite being essential for MIMO transmission, results in Inter-Symbol Interference (ISI). Inter-symbol interference here refers to the phenomena where symbols that have been transmitted previously arrive via a longer, non-direct path at the same time as the symbols arriving currently via the direct path. Orthogonal Frequency Division Multiplexing (OFDM) is a digital modulation technique that solves the ISI problem [6]. The use of multiple antennas with OFDM (MIMO-OFDM) therefore represents a robust technology for high data rate communications systems. However, in order to benefit from the opportunities presented by the new technology, industry will have to accept higher complexity and accuracy in the implementation, otherwise the accumulated implementation losses may significantly degrade the system performance [1].

This thesis is concerned with achieving accurate channel estimates (referred to as Complete Channel State Information C-CSI in the literature) for multi-user MIMO-OFDM system. The following is a description of the main topics and conclusion for each chapter.

## 1.2 Chapter Summary

Chapter 1 provides a background of the MIMO-OFDM technology considered in the thesis by describing the motivation and limitations of this technology. This introductory chapter is written as a starting point to the concepts of MIMO-OFDM and assumes only a fundamental understanding of communications theory. Chapter 2 introduces the mathematical model for the frequency selective channel which is used to develop various channel estimators in the thesis. The Wide-Sense-Stationary Uncorrelated Scattering (WSSUS) channel model is introduced to indicate the limits of the conventional MIMO-OFDM channel estimator.

Chapter 3 derives and evaluates various 1-D and 2-D channel estimators for SISO-OFDM systems based on the convolution channel model. Channel estimation performance is evaluated through extensive simulation for doubly selective (time and frequency varying) channels and it is shown that 2-D estimators outperform 1-D estimators at the cost of increased computational complexity at the receiver. In conclusion, it is noted that the filtering and predictive functions of the 2-D estimators are separable and can be optimized independently for MIMO-OFDM channel estimators. This conclusion provides the motivation for the development of robust 1-D MIMO-OFDM channel estimators, which is the main body of work presented in this thesis.

In Chapter 4, Reduced Parameter Channel State Information estimators (RP-CSI) based on OFDM symbol correlations and OFDM sub-symbol correlations are developed. Novel bases are investigated for the representation of CSI variations using a reduced parameter set. As it is explained, such considerations are warranted for the operations of high data rate MIMO-OFDM systems which deploy large numbers of transmit antennas in multipath channels. A generic estimator is derived which is capable of implementing an arbitrary basis for 1-D CSI parameter estimation exploiting either time or frequency correlations.

Chapter 5 evaluates the Mean Square Error (MSE) performance of MIMO-OFDM channel estimators as a function of the maximum delay spread of the multipath channel. RP-CSI estimators based on OFDM symbol correlations are analyzed and shown to provide a lower bound on the MSE which is comparable to similar results in several literatures on the subject. The implications of the number of channel estimation parameters are then extended to the OFDM sub-symbol based estimators, where it is shown that interpolation plays a crucial role in obtaining accurate CSI. Finally an iterative approach is introduced to reduce the error in CSI estimates which occur due to variations of CSI within a coherence bandwidth for OFDM sub-symbol based estimators.

Chapter 6 is the concluding chapter in which the estimation of channels using the RP-CSI is extended to the time domain. Clarke's model is introduced as a means of predicting the variation of CSI for a receiver traveling at a constant velocity away from the transmitter. The Slepian basis is implemented within the RP-CSI framework. As an alternative, Kalman filters are introduced to track the time variations of the channel with the aim of investigating the effect of RP-CSI estimation error on tracking performance.

In summary, the contributions of the thesis are as follows:

- A generic MIMO-OFDM channel estimator, the Reduced Parameter Channel State Information (RP-CSI) estimator, is developed and the optimal frequency domain basis is determined. In this thesis, an optimal basis is defined as a basis that spans typical channel variation using the least number of coefficients.

- The RP-CSI estimator is adapted for channel estimation in the time domain, by choosing a suitable basis (Slepian Basis) and by developing a suitable filter (the Kalman filter). The RP-CSI estimator developed can also be adapted for time-frequency channel estimation, a particularly useful approach when combined with orthogonal training sequence channel estimation (future work).

- An iterative approach exploiting the CSI correlations between adjacent OFDM sub-carriers is developed and shown to improve the accuracy of channel estimation when orthogonal training sequences are implemented.

## 1.3 The MIMO-OFDM System Model

Figure 1.1 depicts a generic MIMO-OFDM system where a sequence of bits is coded for space-frequency communication, transmitted via the wireless channel, and subsequently decoded at the receiver. It can be noted that the MIMO-OFDM system derives data from a single application (e.g. a video frame) on the mobile device, for which each sample (e.g. a pixel), is encoded as a binary number. The sample is digitally encoded to increase the security of a transmission, minimize errors at the receiver, or maximize the rate at which data is sent [12]. The binary data corresponding to several contiguous samples forms a serial bit stream which constitutes the input bit sequence $\mathbf{b}^{tx}[n]$ in Figure 1.1. The input bit sequence is converted into a sequence of complex symbols (each with real and imaginary components) through the process of In phase and Quadrature (IQ) constellation mapping. IQ constellation mapping is an intermediate step in Quadrature Amplitude Modulation (QAM) which is usually followed by quantization of the complex symbols (QAM symbols), Digital to Analogue Conversion (DAC) and carrier modulation. However, for a system implementing Orthogonal Frequency Division Multiplexing (OFDM) modulation, an IFFT process is implemented after the IQ constellation mapping. In order to implemented the IFFT, $N$ QAM symbols are arranged in a column vector which is then pre-multiplying by the inverse of the Fourier transformation matrix. For the remainder of the thesis, the column vector of $N$ symbols will be referred to as the *OFDM symbol* which is in the frequency domain before the IFFT and in the time domain after the IFFT. In addition, the elements of the OFDM symbol will be referred to as *QAM symbols* before the IFFT, whilst the elements of the OFDM symbol will be referred to as *OFDM samples* after the IFFT. The OFDM modulation process is repeated $n_t$ times resulting in a stack of OFDM symbols as depicted at the transmitter in Figure 1.1.

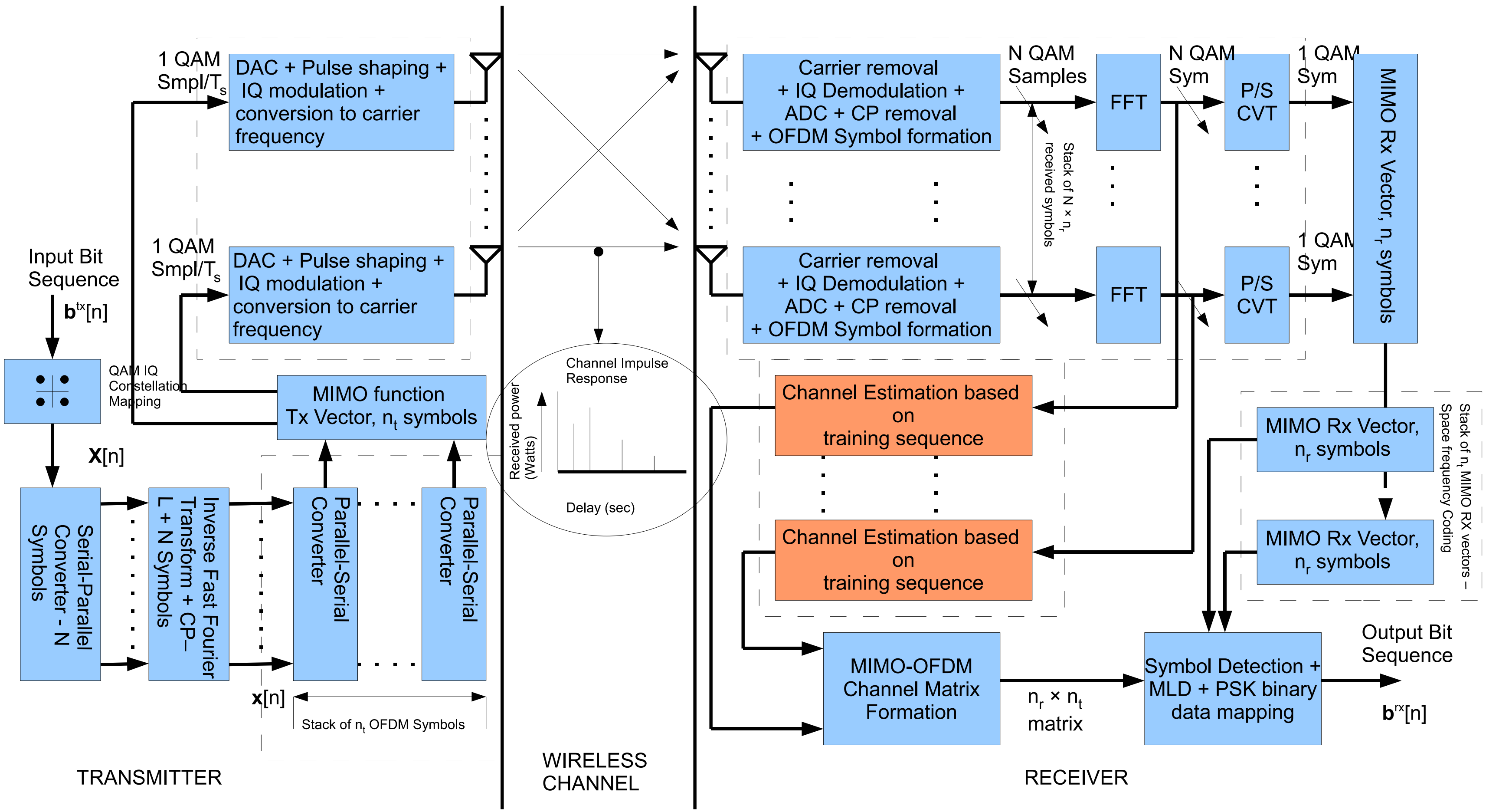


Figure 1.1: A generic MIMO-OFDM communications system. Data flow in the diagram is directed by the arrows, starting with the "Input bit sequence" at the transmitter, and ending at the "Output bit sequence" at the receiver. The wireless channel is the transmission medium.

The stack of OFDM symbols can then be mapped onto the $n_t$ antenna elements at the transmitter array using spatial diversity, spatial multiplexing, layered or joint optimization functions. The OFDM samples then go through the process of quantization, pulse shaping for spectral efficiency, digital to analogue conversion and carrier modulation. At the receiver, various schemes can be implemented to detect the transmitted symbols as is described in the Sections on space-frequency coding (1.5.1), spatial multiplexing (1.5.2) and multi-user MIMO-OFDM (1.6). A full discussion on some of the components of the MIMO-OFDM system such as the cyclic prefix (CP) and Channel estimation are differed for later chapters.

The main functions within the MIMO-OFDM system are the **MIMO-OFDM air interface**, **MIMO-OFDM mapping/de-mapping** and the **MIMO-OFDM channel**. Perhaps the most significant function in the MIMO-OFDM wireless system is the wireless channel/link, a snapshot of which is depicted in Figure 1.1. The Channel Impulse Response (CIR) is a description of the output of a wireless channel when the input is an impulse, or typically, a wideband signal representing the maximum communications system bandwidth. An ideal channel will reproduce the input signal (in this case an impulse) exactly at the output. Such ideal channels are called *flat fading* channels because the frequency response of the channel (the fourier transform of the channel impulse response) is constant/flat across all frequencies [12, 13]. A flat fading channel represents a wireless channel where there is effectively only one propagation path between the transmitter and the receiver. A more realistic channel will however have several paths by which the transmitted impulse signal can propagate to the receiver due to several mechanisms cf. Chapter 2 in the wireless environment. As a result, several impulses will be observed at the receiver, and the paths corresponding to the furthest reflectors will show significant delay and attenuation in the received power profile. The power delay profile (PDP), is a plot of the received power against time when an impulse is transmitted. Channels that are characterized by multipath have a frequency response that varies depending on the frequency and are called *frequency selective* channels [12, 13]. Chapter 2 and 6 will describe the wireless channel in greater detail.

The MIMO-OFDM air interface can be defined as the protocol that allows for the exchange of information between transmitter and receiver stations for the MIMO-OFDM system. Alternatively, the air interface can be defined as the radio-frequency portion of the system. The MIMO-OFDM air interface consists of a combination of Quadrature Amplitude Modulation (QAM) constellation mapping and Orthogonal Frequency Division Multiplexing (OFDM). QAM constellation mapping is used to generate symbols with real and imaginary components for the FFT process used in OFDM modulation. On the one hand, the implementation of M-QAM in MIMO is motivated by the realization of greater spectral efficiency for the overall digital modulation scheme [2, 11]. On the other hand, OFDM modulation effectively divides a wideband frequency selective channel into numerous narrowband channels that are, as a result, flat fading [6]. The combination of the two modulation schemes is used to convey data by changing the phase of a carrier signal that is then transmitted as an electromagnetic wave via an antenna. Both these modulation schemes are discussed in more detail in subsequent sections of this chapter.

The MIMO-OFDM mapping/de-mapping function determines how the transmit vector of $n_t$ symbols is formed and how the receive vector of $n_r$ symbols can be manipulated in order to detect the transmitted vector. Depending on the mapping/de-mapping function specified for the MIMO system, data communications can be improved in terms of increased data throughput or data detection reliability. Link reliability can be improved by sending correlated data streams from the transmitter antenna array and exploiting these correlations at the receiver to improve data detection [17, 18]. Data throughput may be increase by transmitting $n_t$ uncorrelated data streams from the transmitter antenna array [19, 20, 21]. The receiver has then to be specially designed in order to detect the transmitted data as each received symbol at a given antenna is a weighted sum of the $n_t$ transmitted symbols. It can be shown that at a particular Signal to Noise Ratio (SNR), the data detection error rates can be reduced for particular transmission schemes using MIMO antenna [12]. Both the spatial multiplexing and diversity MIMO functions will be discussed in subsequent sections of this chapter.

## 1.4 The MIMO-OFDM Air Interface

This section describes how digital information in the form of binary data is transmitted over an analogue radio channel. As mentioned previously, MIMO-OFDM combines the representation of binary data as Quadrature Amplitude Modulation (QAM) symbols and the multitone modulation to simultaneously transmit data using Inphase and Quadrature sinusoidal carrier waveforms. The implementation of M-QAM allows for high data rate, efficient multiple access strategies and resistance to channel imperfections, amongst other advantages [2, 12]. This section focuses on the improved data rates and Inter-Symbol Interference (ISI) cancelation in frequency selective channels.

### 1.4.1 IQ Constellation Mapping

For QAM digital modulation, the phase of sinusoidal carrier waves is modulated, meaning changed or 'keyed', to represent the binary data signal. 4-QAM is discussed as a suitable example as it is simple yet the formulation can easily be extended when considering the implementation of the general M-QAM. The sinusoidal carrier waveform used to transmit the digital data is given by the equation

$$s_m(t) = \sqrt{\frac{2E_s(t)}{T_s}} \cos\left(2\pi f_c t - (2m-1)\frac{\pi}{4}\right) \tag{1.1}$$

$$= \sqrt{\frac{2E_s(t)}{T_s}} cos\left(2\pi f_c t - \phi_m\right) \tag{1.2}$$

$E_s(t)$ is the energy per symbol which is a function of time $t$, $T_s$ is the symbol period, and $f_c$ is the carrier frequency. Typically, for 4-QAM, the bit sequences $\{00_2, 01_2, 10_2, 11_2\}$ are mapped onto the numbers $\{m = 1, 2, 3, 4\}$ which determine the phase $\phi_m$ of the carrier signal $s_m(t)$ . In fact, to aid with Forward Error Correction (FEC), the bit sequences are assigned a particular phase so that adjacent symbols on the constellation diagram differ by only one bit (cf. Figure 1.2) which is the Gray Coding scheme. It is known that noise and the channel induce arbitrary phase changes in the received signal $s_m^{rx}(t)$ and that maximum likelihood detectors can be used to estimate the transmitted signal phase $s_m^{tx}(t)$ (cf. Section 1.4.3). The idea is that if the received bit sequence is wrongly decoded, the likelihood is that only one bit will be in error. FEC techniques such as convolution coding and Hamming codes can then be used to correct these errors. These techniques leads to improved reliability of the communications link when the QAM modulation scheme is implemented [12].

The expansion of the sinusoidal carrier cf. (1.1) into Inphase and Quadrature components is a result that is used extensively in Chapter 2 and in particular when deriving the convolution model of the channel. This expansion can be achieved using the trigonometric identity $\cos(A-B) = \cos(A)\cos(B) + \sin(A)\sin(B)$ which results in the expression

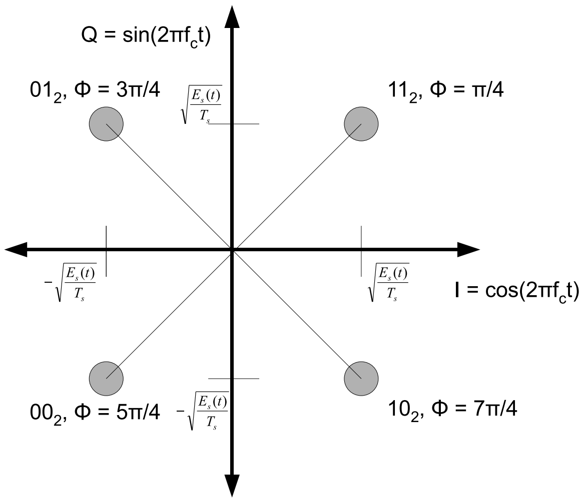


Figure 1.2: Constellation diagram of 4-QAM with Gray Coding

$$\cos(2\pi f_c t - \phi_m) = \cos(2\pi f_c t)\cos(\phi_m) + \sin(2\pi f_c t)\sin(\phi_m) \tag{1.3}$$

$$= \pm\frac{1}{\sqrt{2}}\cos(2\pi f_c t) \pm \frac{1}{\sqrt{2}}\sin(2\pi f_c t) \tag{1.4}$$

$$= \pm\frac{1}{\sqrt{2}}s_I(t) \pm \frac{1}{\sqrt{2}}s_Q(t) \tag{1.5}$$

The QAM symbol $s_m(t)$ is generated from two unit magnitude basis functions, $s_I(t) = \cos(2\pi f_c t)$ and $s_Q(t) = \sin(2\pi f_c t)$, the *inphase* and *quadrature* carriers respectively. The two unit magnitude basis functions are sinusoidal carrier waves that are 90 degrees out of phase and are orthogonal or separable at the receiver, cf. Section 1.4.3. Because the symbol $s_m(t)$ has an amplitude given by $\sqrt{\frac{2E_s(t)}{T_s}}$, and the inphase and quadrature components can be separated at the receiver, each bit sequence can be represented by the complex number with real and imaginary components $\cos(\phi_m)A(t) + j\sin(\phi_m)A(t) = A(t)(I_m + jQ_m)$ where $A(t) = \sqrt{\frac{2E_s(t)}{T_s}}$. The index $m$ indicates that the I and Q factors can take positive or negative signs depending phase generated by the number $m$ (cf. Figure 1.2).

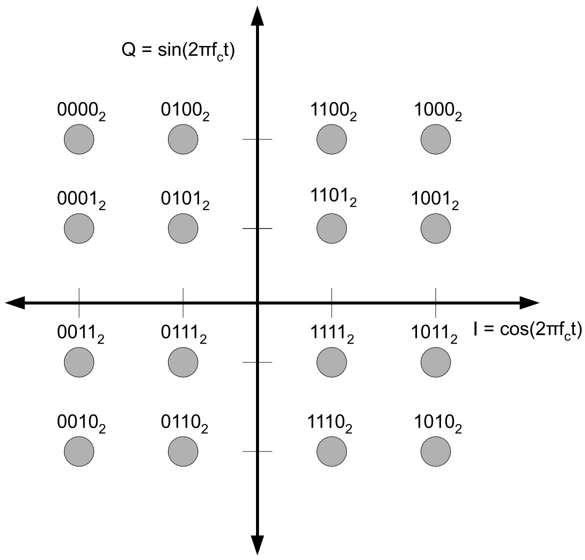


Figure 1.3: Constellation diagram of rectangular 16-QAM with Gray Coding

As was mentioned previously, errors in symbol detection occur due to arbitrary phase changes which are induced by noise as well as channel fading. The problem becomes significant when the keyed phase changes are too closely spaced on the constellation diagram. For Rectangular QAM, the probability of error per carrier [12] is given by

$$P_{sc} = 2\left(1 - \frac{1}{\sqrt{M}}\right) Q\left(\sqrt{\frac{3E_s(t)}{N_0(M-1)}}\right) \tag{1.6}$$

$M$ is the number of symbols used in the modulation constellation, $E_s(t)$ is the energy per symbol, $N_0$ is the noise power spectral density and $Q(x) = \frac{1}{2}erfc\left(\frac{x}{\sqrt{2}}\right)$ is related to the complementary Gaussian error function $erfc = \frac{2}{\sqrt{\pi}}\int_x^{\infty} e^{-t^2}dt$. The literature [2] and [12] have detailed discussion on the performance of Digital Modulation schemes over wireless channels. For IQ constellation mapping using QAM, $M$ bits can be transmitted simultaneously over the $I$ and $Q$ resulting in spectral efficiency but the bit error rate increases proportionally to $M$.

### 1.4.2 Digital multitone/multi-carrier modulation

In addition to sending $M$ bits in parallel using QAM based IQ constellation mapping, the MIMO-OFDM air interface is equipped to transmit $N$ QAM symbols in parallel using $K$ orthogonal carriers where $K = N$ (the indices $K$ and $N$ are used interchangeably to indicate time/frequency domain vectors cf. Figure 1.4). Some of the early work on OFDM modulation can be found in the literature [14] and [15]. Amplitude modulation onto $K$ orthogonal carriers is efficiently implemented using the Fast Fourier Transform (FFT).

The collection of $N$ OFDM samples to be transmitted $\mathbf{x} = [x[0], x[1], \ldots, x[N-1]]^T$, is generated from the QAM symbol source $\tilde{\mathbf{x}} = [X[0], X[1], \ldots, X[K-1]]^T$ through the Inverse FFT (IFFT).

$$\mathbf{x} = \begin{bmatrix} W_N^{0,0} & W_N^{1,0} & \ldots & W_N^{K-1,0} \\ W_N^{0,1} & W_N^{1,1} & \ldots & W_N^{K-1,1} \\ \vdots & \vdots & \ddots & \vdots \\ W_N^{0,N-1} & W_N^{1,N-1} & \ldots & W_N^{K-1,N-1} \end{bmatrix} \begin{bmatrix} X[0] \\ X[1] \\ \vdots \\ X[K-1] \end{bmatrix} \tag{1.7}$$

The vector $\mathbf{x}$ is the IFFT of the vector $\tilde{\mathbf{x}}$. The index $k$ is the frequency index, $n$ is the time index and the FFT complex exponentials are denoted by $W_N^{k,n} = \frac{1}{\sqrt{N}} e^{j2\pi kn/N}$. The Inverse FFT can be viewed as multiplying a QAM symbol $X[k]$ by a length $N$ vector of complex exponential at a fixed frequency index $k$ to obtain a vector $\mathbf{x}_k$. The transmitted vector $\mathbf{x}$ is then obtained by summing the vectors $\mathbf{x}_k$.

$$\mathbf{x}_k = X[k]\mathbf{s}_k \tag{1.8}$$

$$\mathbf{x} = \sum_{k=0}^{K-1} \mathbf{x}_k \tag{1.9}$$

$\mathbf{s}_k = \left[W_N^{k,0}, W_N^{k,1}, \ldots, W_N^{k,N-1}\right]^T$ is an OFDM carrier (these are commonly

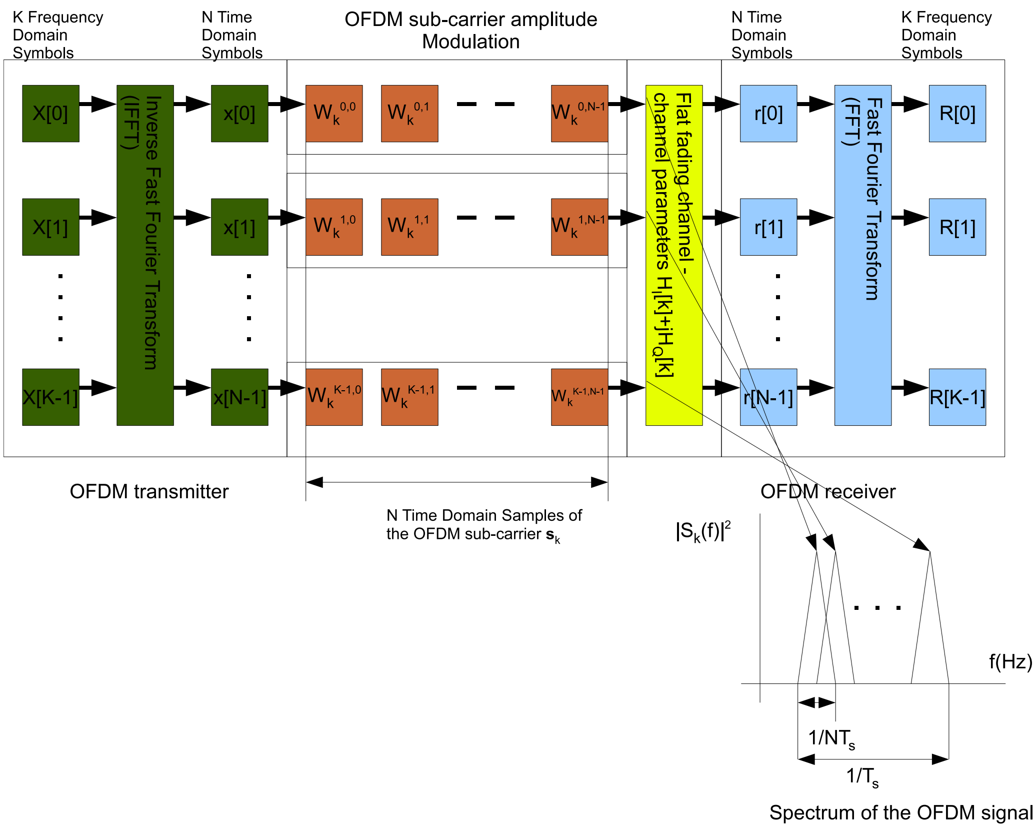


Figure 1.4: Block Diagram representation of OFDM modulation. Because the sub-carrier channels are orthogonal and separable at the receiver, they are depicted as parallel channels. The symbols and channel parameters are complex numbers representing the separable I and Q components. The square blocks represent complex variables.

referred to as orthogonal *OFDM sub-carrier* as they are separable at the receiver cf. Chapter 3). The sub-carriers form the columns of the IFFT matrix cf. equation (1.7).

For OFDM modulation, each QAM symbol $X[k]$ is used to modulate the amplitude of a sub-carrier $\mathbf{s}_k$ for the duration $NT_s$ cf. equation (1.8) and $K$ such symbols are transmitted simultaneously cf. equation (1.9). The symbol period for each of the $N$ QAM symbols ($NT_s/N = T_s$) is equal to the QAM symbol period but the symbol rate over each sub-carrier channel is reduced to

$NT_s$. Multitone modulation is also equivalent to transmitting the QAM symbols $X[k]$ over narrow bandwidth channels ($B_{SC} = 1/NT_s$) that are at precise intervals over the system bandwidth ($B = 1/2T_s$) [16]. Typically the QAM symbol rate ($1/T_s$) is determined by the spectral allocation for the radio frequency channel. In other words, *data can be clocked at rates determined by the hardware within the mobile and receiver hardware devices but on transmission, the rate $T_s$ has to be observed.* For example, GSM has a 200kHz bandwidth assigned to a particular user frequency channel which, based on Gaussian pulse shaping, constrains the data rate to 270kbps. The long OFDM vector period $NT_s$ per sub-carrier $\mathbf{s}_k$ results in narrow band channels which are effectively flat fading. The received OFDM vector can the be written in the form

$$R[k] = H[k]X[k] \tag{1.10}$$

$$\tilde{\mathbf{r}} = \mathsf{diag}\left(H[k]\right)\tilde{\mathbf{x}} \tag{1.11}$$

Note that $\tilde{\mathbf{x}}$ is the OFDM vector *before* the IFFT and $\mathsf{diag}\left(H[k]\right)$ is a diagonal matrix of the gain of the channel $\mathbf{s}_k$. For the remainder of the thesis we shall refer to OFDM vectors as OFDM symbols. The flat fading channel gain $\{H[k]\}$ will be referred to as Channel State Information (CSI). We emphasize here that OFDM amounts to sending $K$ symbols in parallel through a single link between a transmit and receive antenna, which is referred to as frequency diversity in the literature [12]. A mathematically rigorous derivation of the OFDM input-output relationship can be found in chapter 3 of this thesis.

### 1.4.3 Maximum Likelihood Detection

This section describes the Maximum Likelihood Detector (MLD) based on equation (1.10) for the input-output OFDM symbol relationship. These are discussed in order to highlight the importance of CSI estimation in single antenna systems but the results are similarly applicable to multiple antennas.

It will be shown that IQ modulation results in parallel channels and greater spectral efficiency because the symbols in the I and Q channels can be detected separately.

The source OFDM symbol $\tilde{\mathbf{x}} \equiv [X[0], X[1], \ldots, X[K-1]]^T$ consists of a series of the QAM symbols $X[k] = I_m[k] + jQ_m[k]$ with the real and imaginary components that are modulated onto the quadrature carriers cf. Figure 1.4. The index $k$ denotes the frequency of the OFDM sub-carrier and $m$ indicates the phase of the QAM symbol. After Digital to Analogue Conversion (DAC), the base band signal for the OFDM symbol would have the form

$$I_m(t) = \sum_{k=0}^{K-1} I_m[k]p(t - kT_s) \tag{1.12}$$

$$Q_m(t) = \sum_{k=0}^{K-1} Q_m[k]p(t - kT_s) \tag{1.13}$$

$p(t)$ is a pulse which has a width $T_s$, $I_m(t)$ and $Q_m(t)$ are the real and imaginary components of the OFDM symbol $\tilde{\mathbf{x}}$ that form the baseband signals to be modulated onto the quadrature carriers [2] .

$$p(t) = \begin{cases} 1 & \text{if } 0 \le t \le T_s \\ 0 & \text{elsewhere} \end{cases} \tag{1.14}$$

The transmitted OFDM signal is formed by mixing (multiplying) the baseband signals $I_m(t)$ and $Q_m(t)$ with the inphase and quadrature carriers[3] .

$$s_m^{tx}(t) = I_m(t)\cos(2\pi f_c t) + Q_m(t)\sin(2\pi f_c t) \tag{1.15}$$

The QAM symbol amplitude $A(t)$ is suppressed to simplify the notation. At the receiver the two modulated baseband signals can be demodulated using a

[2]the baseband signals $I_m(t)$ and $Q_m(t)$ are processed using a pulse shaping filter to limit their bandwidth at the transmitter

[3]we consider the source OFDM symbol rather than the transmitted OFDM symbol because the received OFDM symbol is a function of the former in equation 1.10

*coherent demodulator*. Coherent demodulators can detect the $I_m(t)$ and $Q_m(t)$ signals separately by multiplying the received signal by cosine and sine signals respectively.

If the received signal has an Inphase gain of $H_I(t)$ and a quadrature gain of $H_Q(t)$, the demodulated Inphase component can be extracted from the received QAM symbol as follows

$$s_m^{rx}(t) = I_m(t)H_I(t)\cos(2\pi f_c t) + Q_m(t)H_Q(t)\sin(2\pi f_c t) \tag{1.16}$$

$$I_m^{rx}(t) = \Gamma\left(s^{\ rx}(t)\cos(2\pi f_c t)\right) \tag{1.17}$$

In equation (1.17) the function $\Gamma(.)$ is a low pass filter. Combining equations (1.16) and (1.17) yields the result

$$I_m^{rx}(t) = \Gamma\left(\hat{I}_m(t)\cos(2\pi f_c t)\cos(2\pi f_c t) + \hat{Q}_m(t)\sin(2\pi f_c t)\cos(2\pi f_c t)\right) \tag{1.18}$$

$\hat{I}_m(t) = I(t)H_I(t)$ and $\hat{Q}_m(t) = Q_m(t)H_Q(t)$. Using trigonometric identities $\cos(A)\cos(B) = [\cos(A+B) + \cos(A-B)]/2$ and $\sin(A)\cos(B) = [\sin(A+B) + \sin(A-B)]/2$, the received symbol for the Inphase component can be written as

$$I_m^{rx}(t) = \Gamma\left(\frac{1}{2}\hat{I}_m(t) + \frac{1}{2}\left[\hat{I}_m(t)\cos(4\pi f_c t) + \hat{Q}_m(t)\sin(4\pi f_c t)\right]\right) \tag{1.19}$$

$$I_m^{rx}(t) = \frac{1}{2}\hat{I}(t) \tag{1.20}$$

Similarly we may multiply $s^{\ rx}(t)$ by a sine wave and then low-pass filter to extract $Q^{\ rx}(t)$.

$$Q_m^{rx}(t) = \Gamma\left(s^{\ rx}(t)\sin(2\pi f_c t)\right) \tag{1.21}$$

$$Q_m^{rx}(t) = \Gamma\left(\frac{1}{2}\hat{Q}_m(t) + \frac{1}{2}\left[\hat{I}_m(t)\sin(4\pi f_c t) - \hat{Q}_m(t)\cos(4\pi f_c t)\right]\right) \tag{1.22}$$

$$Q_m^{rx}(t) = \frac{1}{2}\hat{Q}_m(t) \tag{1.23}$$

After being passed through an Analogue to Digital Converter (ADC), the demodulated baseband inphase ($\hat{I}_m[k] = \hat{I}_m(t)\delta(t - kT_s)$) and quadrature ($\hat{Q}_m[k] = \hat{Q}_m(t)\delta(t - kT_s)$) signals are used to determine the transmitted symbols $I_m[k]$ and $Q_m[k]$ by using Maximum Likelihood Detector (MLD) for a particular sub-carrier $k$.

$$\min_{\{\hat{I}_m[k], \hat{Q}_m[k]\}:\forall m} \varepsilon \triangleq \left|\hat{I}_m[k] - I_m[k]\right|^2 + \left|\hat{Q}_m[k] - Q_m[k]\right|^2 \tag{1.24}$$

The channel parameters (CSI) $H_I(t)$ and $H_Q(t)$ are used to quantify the effects of the channel and will be discussed in Chapter (2). An arbitrary phase change in the received QAM symbol is observed as a result of the gain factors $H_I(t)$ and $H_Q(t)$ .

$$s_m^{rx}(t) = I_m(t)H_I(t)\cos(2\pi f_c t) + Q_m(t)H_Q(t)\sin(2\pi f_c t) \tag{1.25}$$

$$= A_m(t)\cos(2\pi f_c t - \hat{\phi}_m) \tag{1.26}$$

The received carrier signal $s_m^{rx}(t)$ has amplitude and phase terms given by $A_m(t)^2 = (I_m(t)H_I(t))^2 + (Q_m(t)H_Q(t))^2$ and $\hat{\phi}_m = \arctan(\frac{Q_m(t)H_Q(t)}{I_m(t)H_I(t)})$ (this result can be confirmed by using the trigonometric expansion $A_m(t)\cos(2\pi f_c t - \hat{\phi}_m) = A_m(t)\cos(2\pi f_c t)\cos(\hat{\phi}_m) + A_m(t)\sin(2\pi f_c t)\sin(\hat{\phi}_m)$ and comparing like terms in equation 1.25). The channel parameters are random for a particular channel and hence will cause random phase changes and amplitude fluctuations (fading) in the received signal.

Note also that the received QAM symbols $R[k] = I_m[k]H_I[k]+jQ_m[k]H_Q[k]$ form the received OFDM symbol $\tilde{\mathbf{r}}$. In order to reduce the error in data detection using the MLD, estimation of the channel parameters is vital and forms the subject of this thesis (in Figure 1.1 the channel estimation function has been highlighted in the block diagram). For a well designed channel estimator, errors in data detection are mainly due to the noise in the system as discussed in chapter 5 of the thesis.

## 1.5 The MIMO-OFDM Mapping/De-mapping Function

As mentioned previously MIMO-OFDM mapping functions are used to form combinations of $n_t$ QAM symbols that are transmitted on an antenna array. Generally, the transmitted symbols will be correlated or uncorrelated over space and frequency depending on the function of the MIMO-OFDM system. MIMO-OFDM de-mapping functions operate on a vector of $n_r$ received symbols to produce an estimate of the transmitted symbols based on channel parameter estimates (cf. Figure 1.1).

One of the most reliable channel estimation methods uses the received symbols as well as knowledge of some known transmitted symbols (generally known as training symbols) to form estimates of the channel parameters. This process is known as *data based* channel estimation. Once the training symbols have been transmitted and the channel estimated, data can be transmitted and detected based on the channel estimates (cf. Figure 1.1). This scheme assumes that the channel remains unchanged when the data is transmitted and is called *coherent detection*[4] (cf. Chapter 3). Recall that in Section 1.4.3, knowledge of the channel parameters reduced errors in Maximum Likelihood

[4]not to be confused with a *coherent demodulator* used in QAM receivers

Detection and is an important function even within Single Input Single Output (SISO) wireless systems.

The next sections describe space-frequency coding and spatial multiplexing MIMO-OFDM mapping/de-mapping functions which rely on coherent detection. In particular, a description of how spectral efficiency and diversity are achieved depending on the MIMO-OFDM mapping/de-mapping function is given.

### 1.5.1 Space-Frequency Coding

The source QAM symbols to be transmitted can be correlated in space and frequency using MIMO antennas. A space-frequency coding technique for a ($n_t = 2, n_r = 2$) MIMO-OFDM system based on Alamouti codes [17] is depicted in Figure 1.5. The Alamouti scheme is generalized to orthogonal designs in the literature [18].

The stacking of OFDM symbols in figure 1.1 would therefore consist of a single OFDM symbol that has been arranged into two OFDM symbols as depicted in Figure 1.5. The data throughput of a space frequency coding MIMO-OFDM system is therefore the same as a SISO-OFDM system.

At the receiver, the unknown data in the transmit vector can be deduced from two successive received symbols (a stack of $n_t$ MIMO receive vector $\tilde{\mathbf{r}}_{\mathbf{S}}$ is formed for spatial-frequency coding - cf. Figure 1.1).

$$R_1[k] = H_{1,1}[k]X_1[k] + H_{2,1}[k]X_2[k] + N_1[k] \tag{1.27}$$

$$R_2[k] = H_{1,2}[k]X_1[k] + H_{2,2}[k]X_2[k] + N_1[k] \tag{1.28}$$

$$R_1[k+1] = H_{1,1}[k+1]X_1[k+1] + H_{2,1}[k+1]X_2[k+1] + N_1[k+1] \tag{1.29}$$

$$R_2[k+1] = H_{1,2}[k+1]X_1[k+1] + H_{2,2}[k+1]X_2[k+1] + N_1[k+1] \tag{1.30}$$

The Alamouti scheme assumes that the channel parameters in adjacent sub-carriers are highly correlated so that the channel parameters for sub-carrier $k$

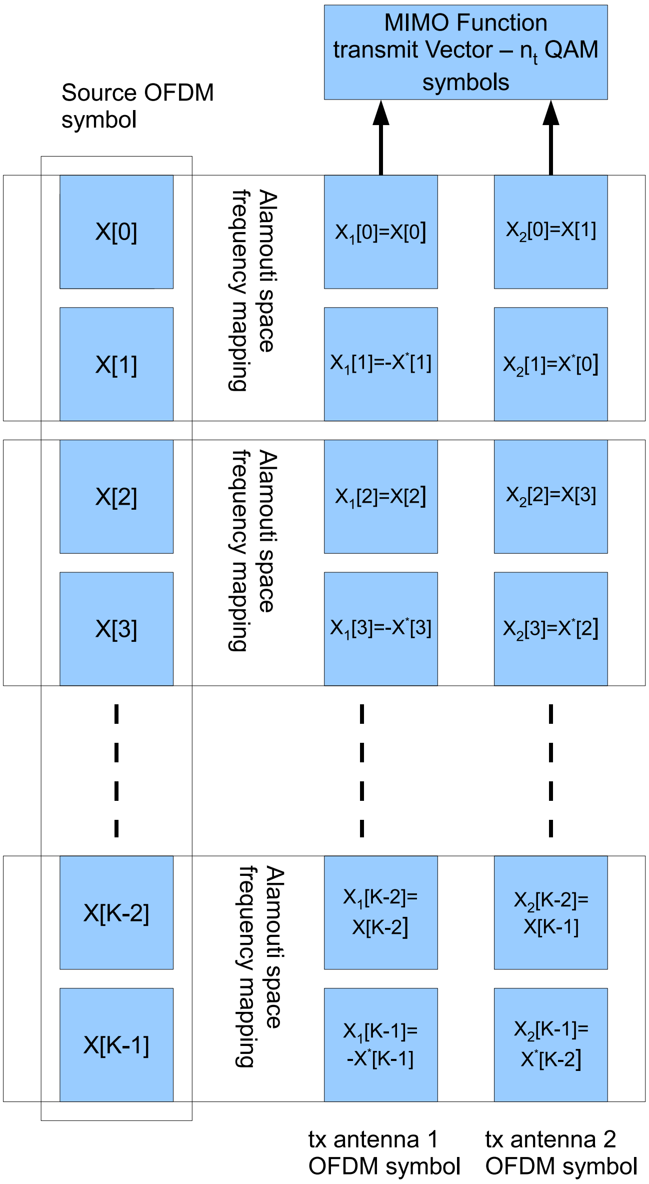


Figure 1.5: Space-Frequency Alamouti Coding for a (2,2) MIMO-OFDM system. The source OFDM symbol is mapped onto two OFDM stacks which have space-frequency correlations.

are equal to the channel parameters of sub-carrier $k+1$ for the MIMO-OFDM system. The combiner at the receiver performs a weighted sum of the four received QAM (1.27–1.30) symbols to form two QAM symbols and that are sent to a maximum likelihood detector.

$$\hat{X}_1[k] = H^*_{1,1}[k]R_1[k] + H_{2,1}[k]R^*_1[k+1] + H^*_{1,2}[k]R_2[k] + H_{2,2}[k]R^*_2[k+1] \tag{1.31}$$

$$\hat{X}_2[k] = H^*_{2,1}[k]R_1[k] - H_{1,1}[k]R^*_1[k+1] + H^*_{2,2}[k]R_2[k] - H_{1,2}[k]R^*_2[k+1] \tag{1.32}$$

$z^*$ is the complex conjugate of a complex number $z$. Substituting the appropriate equations for the received symbols with the correlation assumption $H_{i,j}[k] = H_{i,j}[k+1]$ in place yields

$$\hat{X}_1[k] = \sqrt{\frac{E_s(t)}{2}}\left[|H_{1,1}[k]|^2 + |H_{2,1}[k]|^2 + |H_{1,2}[k]|^2 + |H_{2,2}[k]|^2\right]X_1[k] + \hat{N}_1[k] \tag{1.33}$$

$$\hat{X}_2[k] = \sqrt{\frac{E_s(t)}{2}}\left[|H_{1,1}[k]|^2 + |H_{2,1}[k]|^2 + |H_{1,2}[k]|^2 + |H_{2,2}[k]|^2\right]X_2[k] + \hat{N}_2[k] \tag{1.34}$$

$|z|$ is the magnitude of a complex number $z$. Note that the symbols $\hat{X}_1[k]$ and $\hat{X}_2[k]$ are approximations of $X_1[k]$ and $X_2[k]$. Referring to Figure 1.5, these two QAM symbols represent the two source QAM symbols $X[k]$ and $X[k+1]$. $\hat{N}_1[k]$ and $\hat{N}_2[k]$ are linear combinations of the noise at the receiver

$$\hat{N}_1[k] = H^*_{1,1}[k]N_1[k] + H_{2,1}[k]N^*_1[k+1] + H^*_{1,2}[k]N_2[k] + H_{2,2}[k]N^*_2[k+1] \tag{1.35}$$

$$\hat{N}_2[k] = H^*_{2,1}[k]N_1[k] - H_{1,1}[k]N^*_1[k+1] + H^*_{2,2}[k]N_2[k] - H_{1,2}[k]N^*_2[k+1] \tag{1.36}$$

For the $(2, 2)$ diversity scheme, the SNR is proportional to the sum of the squared magnitude of all four channels which is found to be better by about 20dB when compared to a single transmitter, single receiver SISO system. The impact of antenna diversity on the capacity of wireless communication systems is studied in the literature [21]. When compared to spatial multiplexing cf. Section 1.5.2, however, the data rate is less by a factor of $1/n_t$. Importantly, channel state information is required at the receiver for the Alamouti scheme cf. (1.31) hence Space-Frequency Coding is a MIMO-OFDM coherent detection scheme.

### 1.5.2 Spatial Multiplexing

In section 1.4.2 an input-output relationship was given for the QAM symbols for an OFDM system cf. (1.10). This relationship applies to a SISO system which has a single transmit and receive antenna. Here, we shall consider a MIMO system with $n_t$ transmit antennas and $n_r$ receive antenna employing spatial multiplexing [20].

If we denote the antenna in the transmitter array using an index $i$ and the antennas in the receiver array using the index $j$, then the input-output equation for QAM symbols for a MIMO-OFDM system becomes

$$R_j[k] = \sum_{i=1}^{n_t} H_{i,j}[k] X_i[k] \tag{1.37}$$

Therefore, each received QAM symbol at antenna $j$ ($R_j[k]$) is a weighted sum of the QAM symbols $\{X_i[k]\}$ transmitted from the antenna array for the index $\{i = 1, 2, ..n_t\}$. Recall that there are $K$ QAM symbols that are transmitted through a channel (at frequency $f_c$) in equation (1.16) but there are $n_t \times n_r$ such channels (at the *same* frequency $f_c$[5] ) in a MIMO-OFDM system. Each channel has the parameters $H_{i,j}[k] = H_I^{i,j}[k] + jH_Q^{i,j}[k]$ that

[5] hence the increase in data transmission for a MIMO-OFDM systems does not require an increase in bandwidth!

affect the QAM symbols that are transmitted between the transmit antenna $i$ and receive antenna $j$ - the MIMO-OFDM channel.

If the received QAM symbols across the antenna array $\{j = 1, 2, ..n_r\}$ are stacked into a vector $\tilde{\mathbf{r}}_{\mathsf{S}} = [R_1[k], R_2[k], \ldots, R_{n_r}[k]]^T$ (the subscript $\mathsf{S}$ is used to denote a collection of QAM symbols at the same sub-carrier index for all the receive antennas), then we can write the matrix equation

$$\tilde{\mathbf{r}}_{\mathsf{S}} = \begin{bmatrix} H_{1,1}[k] & H_{2,1}[k] & \ldots & H_{n_t,1}[k] \\ H_{1,2}[k] & H_{2,2}[k] & \ldots & H_{n_t,2}[k] \\ \vdots & \vdots & \ddots & \vdots \\ H_{1,n_r}[k] & H_{2,n_r}[k] & \ldots & H_{n_t,n_r}[k] \end{bmatrix} \begin{bmatrix} X_1[k] \\ X_2[k] \\ \vdots \\ X_{n_t}[k] \end{bmatrix} \tag{1.38}$$

$$\tilde{\mathbf{r}}_{\mathsf{S}} = \mathbf{H}_{\mathsf{S}}\tilde{\mathbf{x}}_{\mathsf{S}} \tag{1.39}$$

$\tilde{\mathbf{x}}_{\mathsf{S}} = [R_1[k], R_2[k], \ldots, R_{n_r}[k]]^T$ is the transmit MIMO-OFDM vector (cf. Figure 1.1). If the number of receive antennas is greater than or equal to the number of transmit vectors ($n_r \geq n_t$), and the channel matrix $\mathbf{H}_{\mathsf{S}} \in \mathbb{C}^{n_r \times n_t}$ has been estimated, then the unknown data in the transmitted vector can be determined using the equation

$$\tilde{\mathbf{x}}_{\mathsf{S}} = \mathbf{H}_{\mathsf{S}}^{\dagger}\tilde{\mathbf{r}}_{\mathsf{S}} \tag{1.40}$$

$\mathbf{H}_{\mathsf{S}}^{\dagger} = (\mathbf{H}_{\mathsf{S}}^{H}\mathbf{H}_{\mathsf{S}})^{-1}\mathbf{H}_{\mathsf{S}}^{H}$ is the pseudo inverse of the channel matrix cf. Section 3.3.1. $\mathbf{A}^H$ is the complex conjugate (Hermitian) of the matrix $\mathbf{A}$. A receiver implementing equation 1.40 is called a *Zero-Forcing* MIMO-OFDM receiver.

The spatial-multiplexing MIMO-OFDM system increases the data throughput of a MIMO-OFDM by a factor of $n_t$ over a SISO-OFDM system. A performance analysis for spatial multiplexing MIMO systems is provided in the literature [20]. Figure 1.1 depicts how $n_t$ OFDM symbols are stacked prior to transmission. Note that the MIMO receive vector $\tilde{\mathbf{r}}_{\mathsf{S}}$ is NOT stacked for spatial multiplexing as only one QAM symbol is required per receiver antenna.

## 1.6 Multi-user MIMO-OFDM

This section describes how MIMO-OFDM systems can be extended from the single user or point-to-point applications that have been described previously, to multi-user systems capable of communicating messages to $P$ decentralized users. The scheme presented here is the joint optimization scheme described in the literature [22, 23]. The joint optimization scheme combines the spatial multiplexing and diversity schemes discussed previously. All the sub-carriers in the OFDM scheme are used by all the users.

Let us assume that the number of transmit antennas at the base station is $n_t$ and the mobile device for user $p$ is equipped with $n_r^p$ antennas. The OFDM source symbols[6] are stacked as $n_L$ parallel OFDM symbols (in contrast, the single user MIMO-OFDM system stacks $n_t$ OFDM symbols at the transmitter in Figure 1.1). A MIMO-OFDM transmit vector $\tilde{\mathbf{x}}_{n_L,\mathsf{S}} \in \mathbb{C}^{n_L \times 1}$ can then be formed at the base station by selecting the QAM symbols $\tilde{\mathbf{x}}_{n_L,\mathsf{S}} \equiv \{X_l[k] : l = 1, 2, \ldots, n_L\}$ for a particular sub-carrier $k$. The first step in transmission is to place a power constraint on the vector $\tilde{\mathbf{x}}_{n_L,\mathsf{S}}$ through multiplication by a matrix $\mathbf{E}_{n_L,\mathsf{S}} = \{\mathsf{diag}(E_l[k]) : l = 1, 2, \ldots, n_L\}$. The next step is to process the resulting length $n_L$ vector so that it can be transmitted on $n_t$ antennas. The vector transmitted from the multi-user MIMO-OFDM system antennas array $\tilde{\mathbf{x}}_{\mathsf{S}} \in \mathbb{C}^{n_t \times 1}$ for downlink communications can be written as follows.

$$\tilde{\mathbf{x}}_{\mathsf{S}} = \mathbf{U}\mathbf{E}_{n_L,\mathsf{S}}\tilde{\mathbf{x}}_{n_L,\mathsf{S}} \tag{1.41}$$

The linear precoder $\mathbf{U} \in \mathbb{C}^{n_t \times L}$ transforms a length $L$ vector into a length $n_t$ vector that can be transmitted using the MIMO antennas. The received MIMO-OFDM vector can be determined using equation (1.39). Substituting the equation for the transmitted MIMO-OFDM vector (1.41), the received vector $\tilde{\mathbf{r}}_{p,\mathsf{S}} \in \mathbb{C}^{n_r^p \times 1}$ for user $p$ can be written as

[6] OFDM source symbols are the Fourier transform of OFDM symbols in section 1.4.2

$$\tilde{\mathbf{r}}_{p,\mathsf{S}} = \mathbf{H}_{p,\mathsf{S}}\tilde{\mathbf{x}}_{\mathsf{S}} = \mathbf{H}_{p,\mathsf{S}}\mathbf{U}\mathbf{E}_{n_L,\mathsf{S}}\tilde{\mathbf{x}}_{n_L,\mathsf{S}} \tag{1.42}$$

The MIMO-OFDM channel $\mathbf{H}_{p,\mathsf{S}} \in \mathbb{C}^{n_r^p \times n_t}$ matrix is different for each user $p$ due to their physical location in the space-frequency system. The multi-user MIMO-OFDM system has $n_L$ symbols in total to communicate to $P$ number of users. Each user $p$ has a unique linear decoder that allows them to decode a message of $n_{L,p}$ symbols, where $\sum_{p=1}^{P} n_{L,p} = n_L$. At the receiver, user $p$'s message $\tilde{\mathbf{x}}_{p,\mathsf{S}} \in \mathbb{C}^{n_{L,p}\times 1}$ can be decoded as follows.

$$\tilde{\mathbf{x}}_{p,\mathsf{S}} = \mathbf{V}_p^H \tilde{\mathbf{r}}_{p,\mathsf{S}} = \mathbf{V}_p^H \mathbf{H}_{p,\mathsf{S}}\mathbf{U}\mathbf{E}_{n_L,\mathsf{S}}\tilde{\mathbf{x}}_{n_L,\mathsf{S}} \tag{1.43}$$

The linear decoder $\mathbf{V}_p^H \in \mathbb{C}^{n_{L,p}\times n_r^p}$ is designed to extract the message symbols ($\tilde{\mathbf{x}}_{p,\mathsf{S}}$) from the vector received at the antennas array ($\tilde{\mathbf{r}}_{p,\mathsf{S}}$). By implication, the linear precoder is also designed as an encoder for user $p$ message and we can write $\mathbf{U} = [\mathbf{U}_1, \mathbf{U}_2, \ldots, \mathbf{U}_P]$ with $\mathbf{U}_p \in \mathbb{C}^{n_t \times n_{L,p}}$. Note that each users message cf. (1.43) forms part of the vector transmitted at the base station prior to linear precoding so that $\tilde{\mathbf{x}}_{n_L,\mathsf{S}} = \left[\tilde{\mathbf{x}}_{1,\mathsf{S}}^T, \tilde{\mathbf{x}}_{2,\mathsf{S}}^T, \ldots, \tilde{\mathbf{x}}_{P,\mathsf{S}}^T\right]^T$. The power constraint vector is designed to minimize the bit error rate.

The linear precoders and decoders described above can also be used for uplink communications where the users communicate with the base station. The equation for the vector received at the base station and the message extracted from user $p$ are given by

$$\tilde{\mathbf{r}}_{\mathsf{S}} = \sum_{p=1}^{P} \mathbf{H}_{p,\mathsf{S}}^H \mathbf{V}_p \mathbf{D}_{n_L,\mathsf{S}} \tilde{\mathbf{x}}_{p,\mathsf{S}} \tag{1.44}$$

$$\tilde{\mathbf{x}}_{p,\mathsf{S}} = \mathbf{U}_{p,\mathsf{S}}^H \tilde{\mathbf{r}}_{\mathsf{S}} \tag{1.45}$$

$\mathbf{D}_{n_L,\mathsf{S}} = \{\mathsf{diag}(D_l[k]) : l = 1, 2 : \ldots, n_L\}$ is the power constraint vector for user $p$. In both the uplink and downlink equation, we assume that there is no noise at the receiver.

## 1.7 Research Objectives of the Thesis

The MIMO-OFDM system technology that will be considered in this thesis has been introduced in this chapter. In addition, a multi-user MIMO-OFDM system capable of downlink and uplink communications was described and contrasted to a single user MIMO-OFDM system. In Section 1.4.2, it was shown that a SISO-OFDM channel is described by $K$ channel parameters. Because OFDM transmission converts the link between a transmitter and receiver into $K$ low symbol rate sub-carrier channels and the MIMO system employs $n_t \times n_r$ such links, the total number of channel parameters to be estimated in the MIMO-OFDM system is $n_t \times n_r \times K$.

For downlink communications in multi-user systems, the number of transmit base station antennas $n_t$ may be large when compared to the number receiving antennas for a particular user $n_r^p$ (cf. section 1.6) due to size constraints on the mobile device. For uplink communications, the transmitting antennas from the $P$ users may be very large $\sum_{p=1}^{P} n_r^p = n_r$ when compared to the receiving antennas at the base station $n_t$. Both these scenarios can be investigated by considering a single user $(n_t, n_r)$ MIMO-OFDM system where $(n_t, n_r)$ represents base station and user $p$'s antenna respectively for the downlink or the grouping of the user antennas and the base station antennas respectively for the uplink. The objective of the thesis is to investigate the performance of MIMO-OFDM channel estimators when the number of transmitting antennas is disproportionately large. It can be shown that in such cases, the MSE performance of the MIMO-OFDM channel estimator is limited by the maximum delay spread of the wireless channel.

Whereas several well established estimators have been developed with optimal SNR performance, the optimal performance of MIMO-OFDM estimators as limited by the maximum delay spread of the wireless channel is a question that remains largely unanswered. The research objective as presented in this thesis is to; *extend current MIMO-OFDM channel estimators with the aim of improving their MSE performance as limited by the maximum delay spread of the wireless channel*. For GSM900, the total available bandwidth of 25MHz is divided into 125 channels with a bandwidth of 200kHz. Assuming that a frequency reuse factor of 7 is implemented to reduce co-channel interference, approximately 18 channels are available in each cell. However, these channels may be divided between 5 mobile phone operators, for example, so that approximately 4 channels are available in each cell, based purely on frequency Division Multiple Access (FDMA). Due to the digitization of speech and signaling, Time Division Multiple Access (TDMA) time slots can be implemented, increasing the number of users to 29, for 8 TDMA time slots per frequency channel. This example sets the precedent for multi-user MIMO-OFDM systems, which have to be able to support the user capacity described in this example in order to be competitive with the current technology.

# Chapter 2

# The Wireless Channel

The effect of transmitting Quadrature Amplitude Modulation (QAM) symbols through a wireless channel may be an arbitrary phase change, which corrupts the information carried by the signal, as well as fluctuations in the received symbol level (fast fading). Another effect of wireless transmission is the addition of white noise which is typically wideband, so that the wider the bandwidth of the system, the greater the effect of the noise. A mobile receiver will experience decreasing signal power with increasing separation from the transmitter (slow fading) and hence a degradation in the Signal to Noise Ratio (SNR). Indeed, the two ray ground reflection model that is widely used in cellular system design calculations, predicts that the received power falls off with distance raised to the fourth power, or at a rate of 40 dB/decade [24].

This section describes the mathematical modeling of the wireless channel for which there is effectively a single propagation path for the wireless link. This channel model is derived from a multipath propagation model, where the output QAM symbol vector is given by the convolution of the input QAM symbol vector and the Channel Impulse Response (CIR) vector. For both the single path and multipath propagation models, Non-Line of Sight (NLOS) communications between the transmitter and receiver is assumed. Finally, the Saleh-Valenzuela model is used to determine the multipath component amplitude, phase and delay for a frequency selective channel.

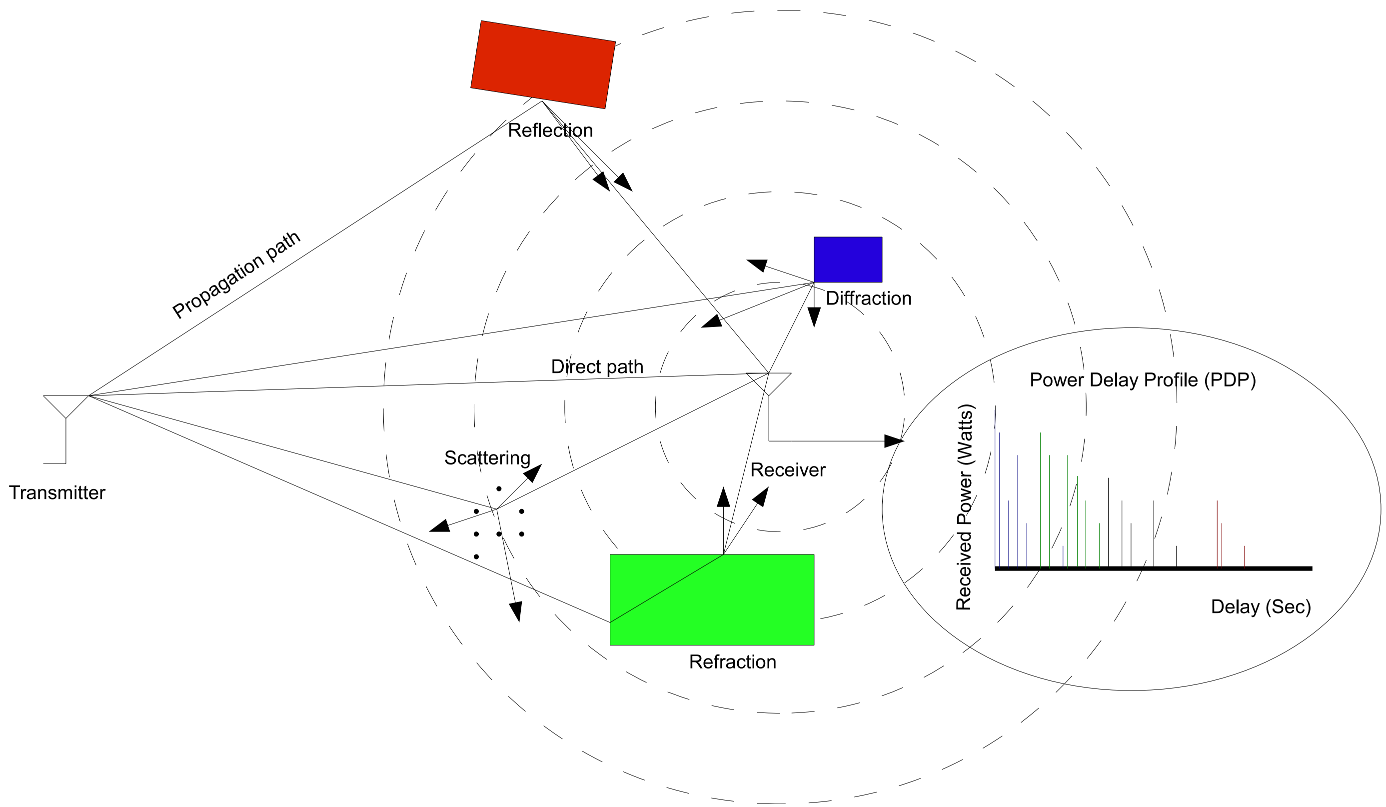


Figure 2.1: Different mechanisms for creating multipath propagation distributed in rings around the receiver. Note that generally speaking, the mechanisms that are close to the receiver result in high received power and the mechanisms that are further away result in low received power. The proximity of the multipath mechanism to the receiver is indicated by the concentric circle. The color coding in the Power Delay Profile relates the received power to a particular multipath mechanism. Each propagation path results in numerous received rays which arrive in clusters.

## 2.1 Multipath Propagation

The transmitted OFDM symbol for a MIMO-OFDM system consists of a vector of QAM symbols that are transmitted for a duration of $KT_s$ seconds, where $K$ is the number of QAM symbols in the OFDM symbol and $T_s$ is the QAM symbol period which is determined by the bandwidth of the radio frequency channel. The effects of the channel on the transmitted OFDM symbol can be divided into QAM symbol effects (fading and random phase changes), and the OFDM symbol effects (Inter-Symbol Interference - ISI, which is the interference of the transmitted QAM symbols at the receiver). The channel model that is derived in this section is based on the response of the channel to a transmitted impulse, or more precisely, a wideband signal representing the bandwidth under consideration, and as such, the model encompasses all the effects mentioned above. In this section, an intuitive discussion on the Channel Impulse Response (CIR) is presented which will be followed by the detailed mathematical modeling of the wireless channel in subsequent sections.

Iospan Wireless Inc., a leader in fixed wireless broadband multiple antenna technology, is widely credited for combining the MIMO and OFDM technologies to transmit radio signals particularly for Non-Line-of-Sight (NLOS) functionality. According to Iospan, speaking of outdoor propagation,

"In this environment, radio signals bounce off buildings, trees and other objects as they travel between the two antennas. This bouncing effect produces multiple "echoes" or "images" of the signal. As a result, the original signal and the individual echoes each arrive at the receiver antenna at slightly different times causing the echoes to interfere with one another thus degrading signal quality."

Figure 2.1 depicts a range of mechanisms leading to multipath propagation. Note that any one, a few, or all of these mechanisms may be present in the wireless environment in different physical locations. Rings of mechanisms around the receive antenna can be consider and it can be noted that broadly speaking, the mechanisms that are furthest from the receiver result in longest delays and lowest received signal strength when an impulse is transmitted. The direct path (Line-of-Sight) may or may not be available due to obstructions, but the straight line between the transmitter and receiver, represents the path of the shortest length which is associated with the shortest achievable propagation delay, and highest achievable signal strength. The description given here is the basis of the one ring model [25]. The mechanisms for Non-Line-of-Sight communications can be defined as follows.

- *Scattering.* Scattering occurs when an electromagnetic wave strikes objects that are small compared to the wavelength of the carrier frequency. Scattering can occur when radio waves impinge on rain drops in the outdoors, or ornamental beads in an indoor environment.

- *Refraction.* Refraction occurs when an electromagnetic wave traveling though one medium experiences a diversion in its path as it enters another medium due to a difference in refractive index of the separate mediums. An example of refraction is when radio waves traveling through the air penetrate walls and emerge at an angle in the direction of the receiver (Snell's law).

- *Reflection.* Reflection occurs when an electromagnetic wave traveling through one medium changes direction at the interface formed between the propagation medium and a second medium. An example of reflection is when signals are reflect off walls towards the receiver.

- *Diffraction.* Diffraction occurs when the electromagnetic wave impinges on an edge or corner of a structure that is large compared to a wavelength. The incident rays in diffraction follow Keller's law of diffraction [13] for example when radio waves impinge on a wall corner or furniture edges.

For free space propagation, the received signal is exclusively a result of direct path propagation and the signal strength calculations are deterministic (Friis transmission equation). The two ray ground reflection model (also called the flat earth model) is another example of a deterministic model that can be used to predict the total received field in some outdoor wireless environments based on the wireless systems physical characteristics such as antenna heights and the ground reflection coefficient ([13] in Chapter 6). However, deterministic models cannot be used to predict the received signal characteristics in a wireless channel in which there are multiple propagation paths. Such channels are described using statistical models which are necessary because of the large number of propagation paths that can be attributed to the different mechanisms through which multipath propagation may occur (Figure 2.1).

Each of the numerous propagation paths constitutes a multipath "channel" through which the transmitted signal arrives at the receiver. Each channel is characterized by the amplitude gain, phase change and propagation delay affecting the transmitted signal. The number of paths, the propagation delays and complex gain (amplitude and phase) attributed to each path can be regarded as random variables across a range of wireless environments and system geometries. In the following sections, the mathematical model of a wireless environment used to develop various channel estimators in the thesis is developed. The channel model encapsulates the effects of fading, random phase change and ISI affecting the sequence of QAM symbol transmitted in the MIMO-OFDM system.

## 2.2 Tapped-Delay-Line System Model

In this section a model for the input/output relationship for QAM symbol transmission through a frequency selective channel is developed. This is achieved by modeling the received QAM symbol as a finite sum of QAM symbols arriving at the receiver as a result of the multipath propagation of the transmitted QAM symbol. This mathematical model leads to a tapped-delay-line (TDL) model of a frequency selective channel where the output QAM symbols have independent Inphase and Quadrature gain.

Recall that the transmitted QAM symbol can be written as a product of the base band (information carrying) and carrier frequency signals for IQ QAM modulation (see Section 1.4.1[1] ).

$$s_m^{tx}(t) = I_m(t)\cos(2\pi f_c t) + Q_m(t)\sin(2\pi f_c t) \tag{2.1}$$

$$= A_m(t)\cos(2\pi f_c t - \phi_m(t)) = \Re\Big(\bar{s}_m^{tx}(t)e^{j2\pi f_c t}\Big) \tag{2.2}$$

$\Re(\bar{z})$ denotes the real part of a complex number $\bar{z}$. The phasor $\bar{s}_m^{tx}(t) = A_m(t)e^{-j\phi_m(t)}$ is the *complex envelope* at the input of the frequency selective channel. The amplitude and phase terms of the phasor $\bar{s}_m^{tx}(t)$ are given by $A_m(t)^2 = I_m(t)^2 + Q_m(t)^2$ and $\phi_m(t) = \arctan(\frac{Q_m(t)}{I_m(t)})$ (because $A_m(t)\cos(2\pi f_c t - \phi_m(t)) = A_m(t)\cos(2\pi f_c t)\cos(\phi_m(t)) + A_m(t)\sin(2\pi f_c t)\sin(\phi_m(t))$ and comparing like terms in (2.2)). For $N$ discrete propagation paths, the received QAM symbol (the baseband signal mixed with the IQ carriers) can be modeled as the sum of the QAM symbols arising from the multipath propagation of the transmitted QAM symbol [26].

$$s_m^{rx}(t) = \sum_{n=0}^{N-1} \gamma_n(t) s_m^{tx}(t - \tau_n(t)) \tag{2.3}$$

In this formulation, a QAM symbol is the time domain waveform which carries the digital data as successive pulse waveforms or more suitable pulse shapes cf. Section 2.2.2. Note that the $n$th path contributes a delayed and attenuated replica of the transmitted QAM symbol to the received symbol.

[1]The QAM symbol amplitude $A(t)$ is suppressed to simplify the notation.

$\gamma_n(t)$ is the amplitude attenuation when the symbol $s_m^{tx}(t)$ propagates via the $n$th path. The time delay $\tau_n(t)$ is the difference in the time of arrival for the QAM symbol propagating via the $n$th path and the time of arrival of the first perceptible QAM symbol at the receiver. Substituting the complex representation of the transmitted QAM symbol $s_m^{tx}(t)$ in (2.2) into the equation for the received QAM symbol $s_m^{rx}(t)$ in (2.3),

$$s_m^{rx}(t) = \Re\Bigg(\Bigg[\sum_{n=0}^{N-1} \gamma_n(t) e^{-j2\pi f_c \tau_n(t)} \bar{s}_m^{tx}(t - \tau_n(t))\Bigg] e^{j2\pi f_c t}\Bigg) \tag{2.4}$$

$$= \Re\Big(\bar{s}_m^{rx}(t) e^{j2\pi f_c t}\Big) \tag{2.5}$$

The phasor $\bar{s}_m^{rx}(t)$ in (2.5) is the complex envelope at the output of the frequency selective channel. Typically the carrier signal can be removed through coherent demodulation cf. Section 1.4.3 and is not of interest when modeling the frequency selective channel. Referring to equation (2.4–2.5)

$$\bar{s}_m^{rx}(t) = \sum_{n=0}^{N-1} \gamma_n(t) e^{-j2\pi f_c \tau_n(t)} \bar{s}_m^{tx}(t - \tau_n(t)) \tag{2.6}$$

$$= \sum_{n=0}^{N-1} \bar{\gamma}_n(\tau_n(t), t) \bar{s}_m^{tx}(t - \tau_n(t)) \tag{2.7}$$

$\bar{\gamma}_n(\tau_n(t), t) = \gamma_n(t) e^{-j2\pi f_c \tau_n(t)}$ in (2.7) is the time varying channel gain of the $n$th path (the multipath gain). Note that equation (2.7) is a convolution sum[2] of two complex variables in the form $\bar{y}[m] = \sum_{n=0}^{N-1} \bar{h}[n]\bar{x}[m-n]$ where the vectors $\{\bar{x}[n]\}$ and $\{\bar{y}[n]\}$ are the input and output variables respectively and $\{\bar{h}[m]\}$ is the impulse response. The convolution model gives rise to ISI which is overcome using OFDM modulation cf. Section 3.1.

The multipath component gain for each propagation path can be evaluated further by noting that each term in the summation (2.4) can be interpreted as a delayed received symbol $s_m^{rx}(t - \tau_n(t))$ which is given by

[2] the input-output relationship for a multipath channel is given by convolution as opposed to multiplication for LOS channels as discussed in 1.4.3

$$s_m^{rx}(t - \tau_n(t)) = \Re\Big(\gamma_n(t)e^{-j2\pi f_c \tau_n(t)}\bar{s}_m^{tx}(t - \tau_n(t))e^{j2\pi f_c t}\Big) \tag{2.8}$$

Recall that the transmitted QAM symbol phasor can be written as $\bar{s}_m^{tx}(t) = A_m(t)e^{-j\phi_m(t)}$ so that the received QAM symbol is given by

$$s_m^{rx}(t - \tau_n(t)) = \Re\left(\Big[\gamma_n(t)e^{-j2\pi f_c \tau_n(t)}A_m(t - \tau_n(t))e^{-j\phi_m(t-\tau_n(t))}\Big]e^{j2\pi f_c t}\right) \tag{2.9}$$

$$= \bar{\gamma}_n(\tau_n(t), t)\Big[I_m(t - \tau_n(t))\cos\left(2\pi f_c(t - \tau_n(t))\right) + \ldots$$
$$Q_m(t - \tau_n(t))\sin\left(2\pi f_c(t - \tau_n(t))\right)\Big] \tag{2.10}$$

$$= I_m(t)H_I(t)\cos(2\pi f_c t) + Q_m(t)H_Q(t)\sin(2\pi f_c t) \tag{2.11}$$

The QAM symbol arriving via the $n$th path will therefore experience an arbitrary phase change, depending on the Inphase and quadrature gain

$$H_I(t) = \frac{\bar{\gamma}_n(\tau_n(t), t)I_m(t - \tau_n(t))\cos(2\pi f_c\,(t - \tau_n(t))}{I_m(t)\cos(2\pi f_c t)} \tag{2.12}$$

$$H_Q(t) = \frac{\bar{\gamma}_n(\tau_n(t), t)Q_m(t - \tau_n(t))\sin(2\pi f_c\,(t - \tau_n(t))}{Q_m(t)\sin(2\pi f_c t)} \tag{2.13}$$

From the analysis in 2.9–2.13, the Inphase and Quadrature multipath component gain $H_I(t)$ and $H_Q(t)$ are independent as they depend on the independent baseband signals $I_m(t)$ and $Q_m(t)$.

The evolution in time of the multipath component gain $\bar{\gamma}_n(\tau(t), t)$ in (2.8) can be modeled by considering $M$ distinct multipath components arriving at a delay $\tau_n(t)$ (Clarke's Model cf. [13]). The $M$ multipath components can be thought of as propagation paths with the same path length, but different angle of arrival at the receiver. The QAM symbol and complex envelope received via path $n$ are then

$$s_m^{rx}(t-\tau_n(t)) = \Re\Big(\sum_{n=0}^{M-1}\gamma_n(t)e^{-j2\pi f_c\tau_n(t)}\bar{s}_m^{tx}(t-\tau_n(t))e^{j2\pi f_c t}\Big) \tag{2.14}$$

$$\bar{s}_m^{rx}(t-\tau_n(t)) = \Big[\sum_{n=0}^{M-1}\gamma_n(t)e^{-j2\pi f_c\tau_n(t)}\Big]\bar{s}_m^{tx}(t-\tau_n(t)) \tag{2.15}$$

The $M$ multipath components in the summation (2.15) arrive with the same delay independent of the measurement time so that $\tau_n(t) = \tau_n$, and the multipath component gain in (2.15)is given by the model

$$\bar{\gamma}(t) = \sum_{n=0}^{M-1}\gamma_n(t)e^{-j2\pi f_c\tau_n} \tag{2.16}$$

$\tau_n$ can be assumed to be some time invariant constant. The multipath component gain model in (2.16) can be extended to include the effects of Doppler frequency shifts, cf. - Chapter 6 and it can be shown that the multipath component gain has a rapidly changing envelope (fast fading). In the next section, the multipath channel gain $\{\bar{\gamma}_n(\tau_n(t), t)\}$ is modeled.

### 2.2.1 Statistical Model of a Multipath Channel

Having described the input/output relationship for frequency selective channels as a convolution, this section describes the statistical characteristics of a wireless channel. These statistical descriptions are used later to generate random realizations of the channel impulse response for simulation purposes. Having shown that the channel gain is a function of both delay and time, we now discuss how the variation of the channel gain as a function of the delay and time variables can be modeled mathematically. Recall that because there are a large number of irresolvable multipath components, a statistical rather than a deterministic approach is expedient.

From the description of the multipath channel given, it is expected that a discrete number of multipath components will be observed at delays $\tau_n(t)$,

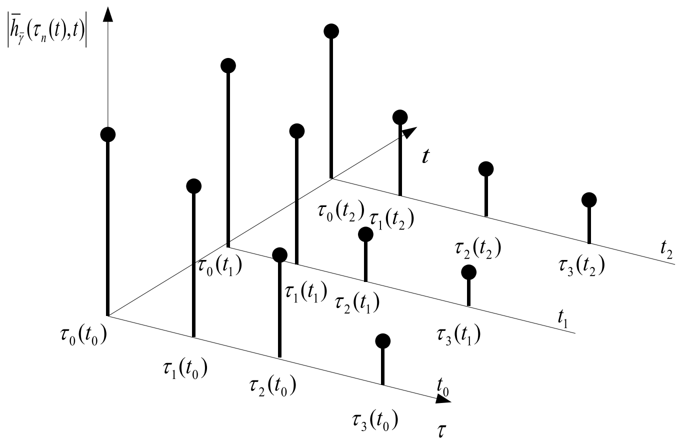


Figure 2.2: Channel Impulse Response (CIR) at three measurement time instances. The first ray to arrive at measurement time $t_n$ corresponds to the shortest path or the direct/LOS path.

depending upon the measurement time $t$. Also, these multipath components will have amplitudes that generally diminish with increasing delay (see Figure 2.2). *This time-delay model of the multipath component gain is used to develop 1-D and 2-D channel estimators in Chapter 3.* The variation of channel gain $\bar{\gamma}_n(\tau_n(t), t)$ with delay $\tau_n(t)$ (the *channel impulse response* (CIR)) can be written as

$$\bar{h}_{\bar{\gamma}}(t, \tau) = \sum_{n=0}^{N-1} \bar{\gamma}_n(\tau_n(t), t)\delta(t - \tau_n(t)) \tag{2.17}$$

The Channel Impulse Response in (2.17) can be modeled as a *wide sense stationary* (WSS) random process in $t$. This means that the expectation of the multipath gain $\bar{\gamma}_n(\tau_n(t), t)$ is constant in time and the correlation function depends only on the separation in time (delay) between two channel gain samples and not on the measurement time $t$ [27]. The correlation function of the WSS channel gain process is written as

$$R_{\bar{\gamma}}(\tau_n, \tau_{n+k}) = E\left[\bar{\gamma}^*(\tau_n, t)\bar{\gamma}(\tau_{n+k}, t)\right] \tag{2.18}$$

$$= R_{\bar{\gamma}}(\tau_n, \tau_{n+k}, \Delta t) = E\left[\bar{\gamma}^*(\tau_n, t)\bar{\gamma}(\tau_{n+k}, t + \Delta t)\right] \tag{2.19}$$

$\Delta t$ is a small time step, $E[.]$ is the expectation operator and the notation $\tau_n(t)$ shortened to $\tau_n$ to ease the notation. In most multipath channels, the channel gain associated with different paths can be assumed to be uncorrelated [26]; this is the uncorrelated scattering (US) assumption, which leads to

$$R_{\bar{\gamma}}(\tau_n, \tau_{n+k}, \Delta t) = R_{\bar{\gamma}}(\tau_n, \Delta t)\delta(\tau_n - \tau_{n+k}) \tag{2.20}$$

Equation 2.20 embodies the WSS and US assumptions and is called the WSSUS model for fading. A discussion similar to the one presented here can be found in the literature [13] and [26],. Because the WSSUS mathematical model of the frequency selective channel assumes that the multipath gain is uncorrelated, *knowledge of the multi-path gain at a particular delay $\tau_n$ cannot be used to predict the multipath gain at another delay $\tau_{n+k}$*, and from this model it appears that a compact representation of the CIR in (2.17) is not possible. However, because the frequency selective channels linking MIMO-OFDM antennas are the Fourier transform of the CIR in (2.17), a compact representation of MIMO-OFDM CSI (Section 1.4.2) is possible. Also Clarke's Model (Section 6) of the multipath channel has a finite spectrum (Jakes' Spectrum) and the Discrete Prolate Spheroidal Sequences provide a compact representation of the CIR in (2.17). For the notional continuous random variable $\tau$, the autocorrelation function is denoted as $R_{\bar{\gamma}}(\tau, \Delta t)$,

$$R_{\bar{\gamma}}(\tau, \Delta t) = E\left[\bar{\gamma}^*(\tau, t)\bar{\gamma}(\tau, t + \Delta t)\right] \tag{2.21}$$

The *scattering function*, $S(\tau, \nu)$ is obtained by performing the Fourier transform on the variable $t$ of the autocorrelation function cf. Appendix B.

$$S(\tau,\nu) = F_{\Delta t}\left[R_{\bar{\gamma}}(\tau,\Delta t)\right] = \int_{-\infty}^{\infty} R_{\hat{\gamma}}(\tau,\Delta t)e^{j2\pi\nu\Delta t}d\Delta t \tag{2.22}$$

Note that we can perform the Fourier transform on either $\tau$ or $t$ or both, but from the engineer's point of view, it is more useful to have a model that simultaneously provides a description of the channel properties with respect to the delay variable $\tau$ and a frequency domain variable $\nu$ called the *Doppler frequency*. The scattering function provides a single measure of the average power output of the channel as a function of the delay $\tau$ and Doppler frequency $\nu$. More commonly, the Power Delay Profile (PDP) [33] which represents the average received power as a function of delay $\tau$ *for a zero Doppler frequency*, is provided for the channel.

$$p(\tau) = R_{\bar{\gamma}}(\tau,0) = E\left[|\bar{\gamma}(\tau,t)|^2\right] \tag{2.23}$$

$$= \sum_{n=0}^{N-1} P_n\delta(t-\tau_n) \tag{2.24}$$

$P_n = E\left[|\bar{\gamma}(\tau,t)|^2\right]$ is the power of the $n$th multipath component. The scatter function (2.22) and power delay profile (also called the multipath intensity profile- 2.23) are related via

$$p(\tau) = \int_{-\infty}^{\infty} S(\tau,\nu)d\nu \tag{2.25}$$

Another function that is useful in characterizing fading is the Doppler power spectrum, which is derived from the scattering function through

$$S(\nu) = \int_{-\infty}^{\infty} S(\tau,\nu)d\tau \tag{2.26}$$

When developing the MU-MIMO-OFDM Channel Estimation Algorithm, we shall assume that the mobile user is stationary and therefore describe the channel in terms of the PDP. The Doppler Spectrum will be considered in Chapter 6.

### 2.2.2 Bandlimited transmission

Bandlimiting the transmitted QAM symbols is necessary to reduce the interference of communication devices in Frequency Division Multiple Access (FDMA) multi-user systems and more generally for communications devices operating in different bands of the Electromagnetic spectrum. In FDMA multi-user systems, the QAM symbols are transmitted and received at a symbol rate which is determined by the channel bandwidth $B = 1/2T_s$, where $T_s$ is the QAM symbol period [16]. It can be shown that when the transmitted QAM symbols are bandlimited, the received QAM symbols are filtered by two successive filters namely, the bandlimiting filter and the channel. Both of these filters can be cascaded when simulating the effects of the channel on the transmitted QAM symbol. In addition due to the process of bandlimiting, the total power received from multipath components within the delay $nT_s \leq \tau \leq (n+1)T_s$ where $n$ is an integer, can be used to model the channel gain affecting a QAM symbol. In this section, the simulation of the CIR for a bandlimited system is described.

A simple example of the impulse response of a bandlimiting filter is the sinc function which yields sinc shaped pulses corresponding to the QAM symbol [16]. The sinc function is extremely spectrally efficient[3] but results in the interference of adjacent symbols at the source. The solution to this problem is to use the damped sinc waveform (raised cosine) pulse shape which has a narrower main lobe and finite duration [28]–[30]. This discussion will consider sinc pulses as an example of pulse shaping. For a bandlimited system, the transmit symbol $s_m^{tx}$ in equation (2.2) becomes

$$\bar{s}_m^{tx,BL}(t) = \sum_{n=-\infty}^{\infty} \bar{s}_m^{tx}(t - nT_s)\,\mathsf{sinc}\left(\pi B(nT_s)\right) \tag{2.27}$$

For the multipath channel, the bandlimited QAM symbol propagating via

[3] The Fourier transform of a time domain sinc function is a rectangular pulse.

the $n$th path has a delay $\tau_n(t)$ and is given by

$$\bar{s}_m^{tx,BL}(t - \tau_n(t)) = \sum_{n=-\infty}^{\infty} \bar{s}_m^{tx}(t - \tau_n(t) - nT_s)\,\mathsf{sinc}\,(\pi B(nT_s)) \quad (2.28)$$

$$= \sum_{n=-\infty}^{\infty} \bar{s}_m^{tx}(t - nT_s)\,\delta\,(nT_s - \tau_n(t))\,\mathsf{sinc}\,(\pi B(nT_s)) \quad (2.29)$$

$$= \sum_{n=-\infty}^{\infty} \bar{s}_m^{tx}(t - nT_s)\,\mathsf{sinc}\,(\pi B(nT_s - \tau_n(t))) \quad (2.30)$$

Substituting the equation for the delayed QAM symbol (2.30) into the convolution sum model of the received symbol (2.7)

$$\bar{s}_m^{rx}(t) = \sum_{n=0}^{N-1} \bar{\gamma}_n(\tau_n(t), t)\left[\sum_{n=-\infty}^{\infty} \bar{s}_m^{tx}(t - nT_s)\,\mathsf{sinc}\,(\pi B(nT_s - \tau_n(t)))\right] \quad (2.31)$$

By rearranging the terms in (2.31) and defining the CIR $\bar{g}_{\bar{\gamma}}(t, \tau_n(t)) = \sum_{n=-\infty}^{\infty} \bar{\gamma}_n(\tau_n(t), t)\mathsf{sinc}\,(\pi B(nT_s - \tau_n(t)))$, the LHS of (2.31) simplifies to the convolution

$$\bar{s}_m^{rx}(t) = \sum_{n=0}^{N-1} \bar{s}_m^{tx}(t - nT_s)\,\bar{g}_{\bar{\gamma}}(t, \tau_n(t)) \quad (2.32)$$

We can conclude from this analysis that the CIR $\bar{g}_{\bar{\gamma}}(t, \tau_n(t))$ for a bandlimited communications system is the convolution of the CIR $\bar{h}_{\bar{\gamma}}(t, \tau_n(t)$ cf. equation (2.17) with the pulse shaping filter[4] . The received QAM symbol can be simulated using the tapped-delay-line model (Figure 2.3). However, in order to simulate the frequency selective channel, random realizations of the CIR have to be generated.

Assuming that mobile user is stationary at the measurement time, it is expected that the complex channel gain $\bar{\gamma}_n(\tau_n(t), t)$ will vary rapidly whilst the relative delays $\tau_n(t)$ vary slowly [87] at different user locations. However,

[4] when the system is not bandlimited, the pulse shaping function is a delta function (equation 2.17). The delta function has infinite bandwidth.

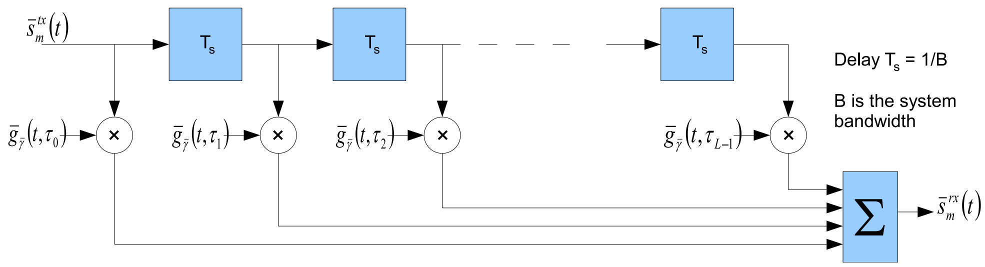


Figure 2.3: Tapped-delay-line model for the input/output relationship of a frequency selective wireless system. The channel taps $\bar{g}_\gamma(t, \tau_n)$ are assumed to be uncorrelated when there are a large number of multipath components. The multipath components within a symbol period are summed up when modeling the received symbol because the transmit symbol remains unchanged for this duration.

because the channel is a WSSUS process, the PDP is expected to be constant at different measurement locations. In the Section 2.2.3, it is shown that a Gaussian complex channel gain process can be derived from the PDP of the channel. The PDP can also be used to classify the channel by defining the maximum delay $\tau_{max}$ which is the delay beyond which the received power falls below a predefined threshold (e.g 20dB) [13] and [26]. The maximum delay $\tau_{max}$ can be used to classify the wireless channel as follows.

- Channels are said to exhibit frequency selective fading if the maximum delay is greater than the symbol period $\tau_{max} > T_s$.
- A channel is said to exhibit flat fading if the maximum delay is much smaller than the symbol period $\tau_{max} \ll T_s$.

The wireless channel can be classified further by specifying the root mean square (rms) delay spread $\tau_{rms}$ of the PDP.

$$\tau_{rms} = \left[ \frac{\sum_{n=0}^{N-1} (\tau_n^2 - \tau_n) p(\tau_n)}{\sum_{n=0}^{N-1} p(\tau_n)} \right]^{\frac{1}{2}} \tag{2.33}$$

The rms delay spread $\tau_{rms}$ is the square root of the difference between the second and the first moment of the power delay profile. The first moment of the power delay profile is called the mean excess delay and is defined as

$$E[\tau_n] = \frac{\sum_{n=0}^{N-1} \tau_n p(\tau_n)}{\sum_{n=0}^{N-1} p(\tau_n)} \tag{2.34}$$

$p(\tau_n)$ is the received power at the delay $\tau_n$ (2.23). In the calculation of the mean delay $E[\tau_n]$ and the rms delay spread $\tau_{rms}$, the power for the path delay $\tau_n$ is divided by the sum of the received power $\sum_{n=0}^{N-1} p(\tau_n)$ so that weak multipath components contribute less to the statistical distributions of the channel than strong multipath components. In many applications the requirement for a channel to be frequency-nonselective is $\tau_{rms} \leq 0.1T_s$.

### 2.2.3 Rayleigh Fading Channels

In this section, the multipath component gain $\bar{\gamma}(t)$ in equation (2.16) is shown to be a Gaussian random variable with Rayleigh distributed amplitude and uniformly distributed phase. Furthermore, because the relationship between the mean square value (expected power of the Gaussian process) and the standard deviation (statistics of the Gaussian process) of the multipath component gain is well known, a random realization of the multipath component gain can be generated from the PDP.

Recall that the multipath component gain can be modeled as the total gain of $M$ separate paths which have the same path length (2.16). Since the number of multipath components due to various mechanisms is considered to be large, then by virtue of the central limit theorem[5] the channel gain $\bar{\gamma}(t)$ can be modeled as a complex Gaussian process (see Chapter 6 and [26]).

The complex Gaussian process $\bar{\gamma}(t)$ can be written in polar and Cartesian form as follows

[5]the central limit theorem states that if the sum of independent identically distributed random variables has a finite variance, then it will be approximately normally distributed (i.e., following a Gaussian distribution, or bell-shaped curve)

$$\bar{\gamma}(t) = \gamma(t)e^{j\psi(t)} \tag{2.35}$$
$$= \gamma(t)\cos(\psi(t)) + j\gamma(t)\sin(\psi(t)) \tag{2.36}$$

The Cartesian form of the complex process can be written as $\bar{\gamma}(t) = x(t) + jy(t)$, where $\gamma(t) = \sqrt{x(t)^2 + y(t)^2}$, $\tan(\psi(t)) = \frac{y(t)}{x(t)}$ and the coordinates $(x(t), y(t))$ are Gaussian distributed random variables with zero mean and variance $\sigma$. The probability density functions $p(x)$ and $p(y)$ can be written as

$$p(x) = \sqrt{\frac{1}{2\pi\sigma^2}}\exp\left(\frac{-x^2}{2\sigma^2}\right) \tag{2.37}$$
$$p(y) = \sqrt{\frac{1}{2\pi\sigma^2}}\exp\left(\frac{-y^2}{2\sigma^2}\right) \tag{2.38}$$

Assuming that $x(t)$ and $y(t)$ are independently random processes, the joint probability density function $p(x, y)$ is given by the multiplicative rule,

$$p(x, y) = p(x)p(y) = \frac{1}{2\pi\sigma^2}\left(\exp\frac{-(x^2 + y^2)}{2\sigma^2}\right) \tag{2.39}$$

The joint probability density function of the amplitude $\gamma(t)$ and phase $\psi(t)$ of the multipath component gain (2.35) is calculated from $p(x, y)$ by transforming an area element[6] in rectangular coordinates $(x, y)$ to polar coordinates $(\gamma, \psi)$ using $dxdy = \gamma d\gamma d\psi$.

$$p(\gamma, \psi) = \frac{\gamma}{2\pi\sigma^2}\left(\exp\frac{-(x^2 + y^2)}{2\sigma^2}\right) \tag{2.40}$$

Since $p(\gamma, \psi)$ is independent of the phase $\psi(t)$, then the variables $\gamma(t)$ and $\psi(t)$ are independent.

[6]given the probability density function f(x), the probability of the interval [a,b] is given by the area under a curve $\int_a^b f(x)dx$.

$$p(\gamma, \psi) = p(\gamma)p(\psi) \tag{2.41}$$

$$p(\psi) = \int_0^\infty p(\gamma, \psi) d\gamma = \frac{1}{2\pi} \quad for \quad 0 \leq \psi \leq 2\pi \tag{2.42}$$

$$p(\gamma) = \int_0^{2\pi} p(\gamma, \psi) d\psi = \frac{\gamma}{2\pi\sigma^2} \left( \exp \frac{-\gamma^2}{2\sigma^2} \right) \quad for \quad \gamma(t) \geq 0 \tag{2.43}$$

This shows that the random variable $\gamma(t)$ is *Rayleigh distributed* whilst the random variable $\psi(t)$ is uniform distributed. The mean square value of the Rayleigh distributed variable $\gamma(t)$ is related to the standard deviation of the Gaussian distribution as follows [24]

$$E\left[|\gamma(t)|^2\right] = 2\sigma^2 \tag{2.44}$$

In Section (2.3), the PDP is modeled using the well known Saleh-Valenzuela model. The PDP provides the expected power of each multipath component ($E\left[|\gamma(t)|^2\right]$) which is then used to generate a complex gain process $\bar{\gamma}(t)$ with variance $\sigma$. Note that because of the WSSUS assumption, it is reasonable to expect that the mean square value for a multipath component is not dependant on measurement time, or for stationary users, the measurement location. For this reason, the Saleh-Valenzuela model appears extendable (by changing some basic parameters) to represent the channel within any building.

## 2.3 Saleh-Valenzuela channel Model

The Saleh-Valenzuela (SV) model [32] can be used to generate the PDP of an indoor environment which is then used to simulate the CIR with Rayleigh distributed amplitudes and uniform distributed phase. It is assumed that the transmitter and receiver links in the MIMO-OFDM systems are uncorrelated and the condition under which this assumption can be made are stated in the discussion in section 2.4. The SV model is used to generate that uncorrelated channel taps for wireless channels in an indoor environment by generating independent power delay profiles. In this section, the SV model is described in detail and some simplifying assumptions used in the computer simulations for this thesis are stated. In the following discussion, $K$ is the source OFDM symbol length as described in section 1.4.2.

The Channel Impulse Response of a wireless channel can be described by a simplification of the model described in section 2.2.1

$$h(t, \tau_n) = \sum_{n=0}^{N-1} \bar{\gamma}(t)\delta(t - \tau_n) \tag{2.45}$$

Note that the multipath component gain model in (2.16) is used in (2.45) which implies multipath channel gain measurements at the time $t$ or random location. Each term in the summation corresponds to a particular reflected path (the so-called multipath component) which we will refer to as a *ray*. Observations of measured channel impulse responses indicate that the rays generally arrive in clusters and that the cluster arrival times, defined as the cluster arrival time of the first ray in the cluster, are a Poisson process with some fixed rate $\Lambda(s^{-1})$. Typically each cluster consists of many rays which also arrive according to a Poisson process with another fixed rate $\lambda(s^{-1})$, so that $1/\lambda \ll 1/\Lambda$ ($1/\lambda \approx 5ns$ and $1/\Lambda \approx 200ns$ from room measurements [32]). The cluster and ray inter-arrival times are exponentially distributed. The Saleh-Valenzuela model assumes that the complex gain $\bar{\gamma}_n$ is independent of the associated delay and is a zero-mean, complex Gaussian random variable, i.e., the real and imaginary components are independent samples from the same Gaussian distribution cf. Section 2.2.3. The power of the multipath component gain $\bar{\gamma}_n$ decays exponentially with delay $\tau_n$ to reflect the decreasing power in multi-path components that have traveled further. The magnitude and phase of $\bar{\gamma}_n$ will follow Rayleigh and Uniform distributions respectively.

The first step in simulating the wireless channel between a transmitting and receiving antenna pair is to generate the expected number of clusters within the OFDM symbol duration $KT_s$. The probability of $N$ arrivals in the OFDM block period is given by the Poisson distribution with mean $\Lambda T_s$

$$P_N(KT_s) = \frac{(\Lambda KT_s)^N}{N!} e^{-\Lambda KT_s}; \quad N = 0, 1, 2, \ldots \tag{2.46}$$

The times between consecutive arrivals of clusters $T_\ell - T_{\ell-1}$ are Negative-Exponentially distributed with mean $1/\Lambda$ and by definition $T_0 = 0$ and $T_N < KT_s$. A random number of $N+1$ inter-arrival times are generated such that the probability density of the arrival time $T_\ell$ is given by the exponential distribution

$$P_{T_\ell}(KT_s) = \Lambda e^{-\Lambda KT_s}. \tag{2.47}$$

For a random channel realization, clusters for which the arrival time exceeded the OFDM block period are ignored because rays within such clusters far exceed the maximum delay of $200ns$ for indoor channels. At this point the number of rays and the inter-arrival times between the rays within each cluster can be generated from the distributions (2.46) and (2.47) using the ray arrival rate $1/\lambda$ within the cluster inter-arrival times $T_\ell - T_{\ell-1}$. If the arrival time of the $k$th ray measured from the beginning of the $\ell$th cluster is denoted by $\tau_{k\ell}$, the arrival time of the $k$th ray in the $\ell$th cluster is such that $\tau_{0\ell} = T_\ell$ and $\tau_{k\ell} = T_\ell + \tau_k$. Ray arrival times $\tau_{k\ell}$ that exceed the OFDM block period are ignored.

The next step is to determine the average power gain of the $k$th ray in the $\ell$th cluster $\overline{\beta^2_{k\ell}}$. The average multipath gain $\overline{G}$ is related to the average power gain of the first ray of the first cluster $\overline{\beta^2_{00}}$ by the equation

$$\overline{\beta^2_{00}} = (\gamma\lambda)^{-1}\overline{G} = (\gamma\lambda)^{-1} G_t G_r \frac{\lambda_0^2}{16\pi^2} \tag{2.48}$$

where $G_t$ and $G_r$ are the gains of the transmitting and receiving antennas

(3dB - International Telecommunications Union ITU1238 statistical description of a typical homes operating conditions), $\lambda_0$ is the RF wavelength (0.125m at 2.4GHz) and $\gamma$ is the power-delay time constant for the rays (20ns - from room measurements [32]). Using (2.48), the average power gain $\overline{\beta_{00}^2}$ is determined and then used to calculate the monotonically decreasing mean square values $\overline{\beta_{k\ell}^2}$ according to the relationship

$$\overline{\beta_{k\ell}^2} = \overline{\beta_{00}^2} e^{-T_\ell/\Gamma} e^{-\tau_{k\ell}/\gamma}. \tag{2.49}$$

$\Gamma$ is the power-delay time constant for the clusters (60ns - from room measurements [32]). The multi-path component gain amplitudes $\{\gamma_{k\ell}\}$ are generated from a Rayleigh distribution with the Rayleigh distribution parameter $2\sigma^2 = \overline{\beta_{k\ell}^2}$. $\sigma$ is therefore the standard deviation associated with the Gaussian distribution of the real and imaginary part of the complex gain $\bar{\gamma}_n = \gamma_{k\ell} e^{j\theta_{k\ell}}$ of the path. The phase of the ray channel gain $0 \leq \theta_{k\ell} \leq 2\pi$ is uniformly distributed.

Note that the arrival time of the $k$th ray in the $\ell$th cluster $\tau_{k\ell}$ is simply $\tau_n$ and that the $(k, \ell)$ notation makes it easier to index the rays associated with particular clusters. Also $E[|\bar{\gamma}_{k\ell}|^2]$ is equivalent to $\overline{\beta_{k\ell}^2}$, but the later notation as used in this section has been adopted from the literature [32]. Generally the clusters will overlap but typically the expected power of the rays in the cluster decays faster than the expected power of the first ray of the next cluster.

From room measurements in [32] and [33], rays and clusters outside a $200ns$ window, although they existed, were generally too small to be detected. The simulation results with the parameters specified in this section exhibit the same characteristics with $\tau_{max} \ll KT_s$. We will assume that the delays in the impulse response model (2.45) are multiples of the symbol period $T_s$. This approach assumes that the amplitude and phase terms of the transmitted symbol $\bar{s}_m^{tx}(t)$ remain constant over the symbol period $T_s$, and the summation in equation 2.7 can be simplified by factoring out the transmitted symbol and

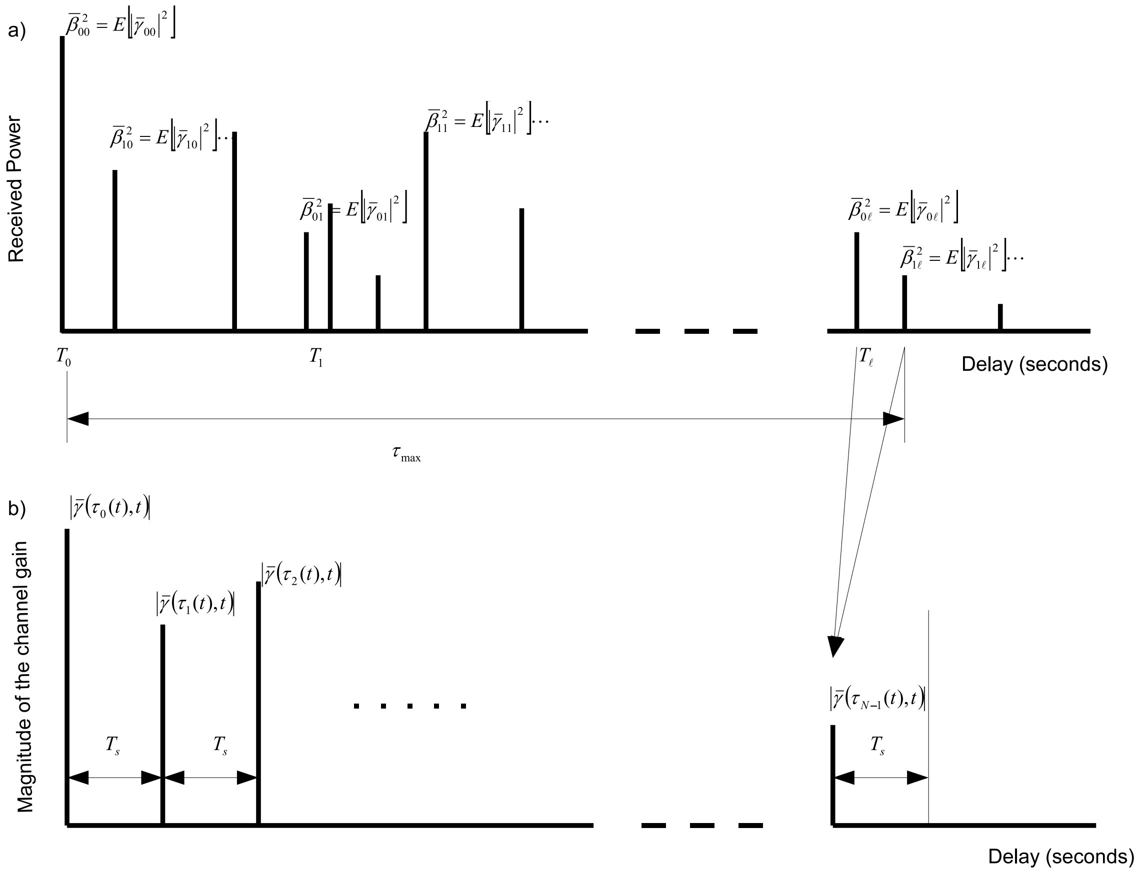


Figure 2.4: a) The power delay profile and b) channel impulse response of a wireless channel. Note that the rays in the PDP arrive in clusters as described by the Saleh-Valenzuela model. The CIR is realized by summing the average received multipath power ($\overline{\beta_{k\ell}^2}$) within the period $T_s$ and generating a complex Gaussian random variable with $\sigma = \sqrt{\overline{\beta_{k\ell}^2}/2}$

adding the multipath component gain. The power gain of multiple paths with delays that vary by less than $T_s$ superimpose to yield a single ray gain, $\overline{\beta_{k\ell}^2}$ (Figure 2.4). Having discretised in time, the impulse response $\mathbf{h} \in \mathbb{C}^{K\times 1}$ may be written as a sparse vector having non-zero elements $\bar{\gamma}_n$ at indices $\eta(n) : \eta(n)T_s = \tau_n$, e.g.,

$$\mathbf{h} = [\bar{\gamma}_1, 0, \cdots, \bar{\gamma}_2, 0, \cdots, \bar{\gamma}_n, 0, \cdots, 0]^T. \tag{2.50}$$

A single PDP generated by the Saleh-Valenzuela model can be used to simulate numerous random realizations of a CIR. However, because we wish to evaluate the performance of the channel estimation algorithm for varying maximum delay spread $\tau_{max}$, we generate random PDPs using the Saleh-Valenzuela model for *each* CIR realization. Because the user is stationary, we can assume that the CIR in our simulation corresponds to channel measurements that are performed in different locations within the indoor environment.

## 2.4 Correlation of the channel gain parameters of MIMO antennas

This section describes the correlation of the channel gain parameters (gain and phase) for the separate antenna elements in an array at the receiver of a MIMO system. The path analysis presented in this section can also be extended to the transmit antenna array. Uncorrelated channel gain parameters at each antenna element are desirable for MIMO functionality, that is, the so-called spatial multiplexing, diversity, beamforming and joint optimization schemes.

Figure 2.5 shows a far field wavefront impinging on two antennas at the receiver of a MIMO system. The two antenna elements in the array are separated by a distance $L$ which is typically of the order of a wavelength $\lambda$. The wavefront arriving at an azimuth angle of $\phi_n$ at transmit antenna 1, has to travel a

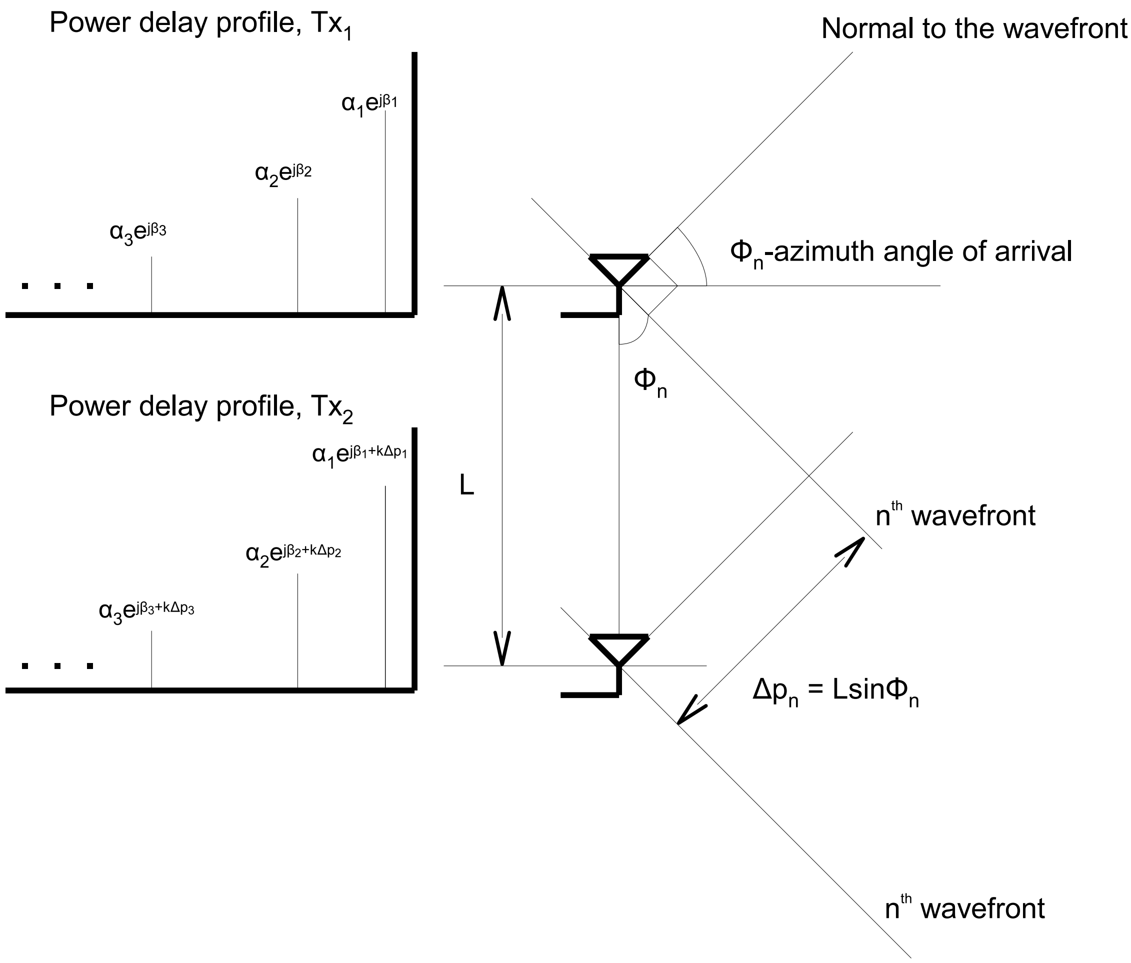


Figure 2.5: A far field wavefront impinging on two antenna elements at the receiver of a MIMO system. The path difference $\Delta p_n$ causes an additional phase change and delay for the multipath components at the second antenna elements, ultimately leading to uncorrelated channel gain parameters at either antenna. Each multipath component will have a unique path difference depending on its azimuth angle of arrival.

distance $\Delta p_n = L\sin(\phi_n)$ before reaching the second antenna in the antenna array. This path difference results in an additional phase change of $k\Delta p_n$ radians and delay $\delta\tau_n = \Delta p_n/c$ seconds for each received multipath component, where $k$ is the wave number, $\lambda$ is the carrier wavelength and $c = 3 \times 10^8$ is the speed of an electromagnetic (EM) waves in free space . Note that the delay $\delta\tau_n$ is typically very small and its effects can be considered negligible, particularly when compared to the effects of path differences.

If the antennas are adequately spaced (the separation is in the order of a wavelength), and there is a large number of multipath components, then the channel for each receiver antenna can be considered to be independent. Typically, when the symbol period is much longer than the maximum delay (flat fading), then the summation of a large number of multipath components result in uncorrelated channel gain parameters at the different antenna elements in the array. Similarly, when the symbol period is a fraction of the maximum delay, the multipath component gain can be summed up over the symbol period, again resulting in uncorrelated channel gain parameters for each antenna element. An analysis of the correlation of MIMO channels is presented in the literature [34].

In this thesis, it is assumed that the MIMO channels are uncorrelated for each transmit receive antenna pair.

## 2.5 Chapter Summary

This chapter is concerned with the effects of the wireless channel on the transmitted QAM symbol vectors used in MIMO-OFDM systems. Mathematical models are used to predict the effects of Inter-symbol interference (ISI), arbitrary phase change and fading that are typically experienced in Non-Line-of-Sight (NLOS) multi-path channels. The convolution model of the channel is later used in the thesis to develop the theoretical framework for data aided channel estimators based on the time and frequency correlations of the MIMO-OFDM channel.

The convolution model (which leads to ISI) is derived by formulating the received QAM symbol as the sum of the delayed and attenuated transmitted QAM symbol propagating via a finite number of paths (the so called multi-path components). In this formulation, a QAM symbol is the time domain waveform which carries the digital data as successive pulse waveforms, or alternatively, more suitable pulse shapes. Different models of the channel can be formulated depending on the pulse shaping function and the sampled, discrete, Channel Impulse Response (CIR) can be used in the tapped-delay-line (TDL) model to simulate the received symbol. Bandlimited transmission therefore has two implications for communications systems modeling:

- The Channel Impulse Response is a convolution of the multi-path CIR and the pulse shaping filter impulse response. This extended CIR model predicts that the multi-path component gain at a particular delay may be 'blurred' due to pulse shaping.

- Simulation of the tapped-delay-line (TDL) model can be simplified by using impulses at the symbol period $T_s$ to represent multi-path component gain. This channel model assumes a maximum likelihood based timing recovery scheme is implemented at the receiver.

The symbol period $T_s$ together with the maximum delay of the channel $\tau_{max}$ determine whether the channel can be classified as a frequency selective channel or a flat fading channel. This thesis is concerned with high data rate systems operating in sever multipath conditions, and hence a frequency selective channel model is adopted.

From the QAM symbol formulation of the received signal, it can be noted that each multipath component has a complex gain (representing the IQ components gain) whose real and imaginary components are independent random variables. This observation is made by considering the signal received from each multi-path component and comparing the form of this received symbol to the transmitted symbol. If each multi-path component is itself a sum of finite components arriving at the same time from different directions, the central limit theorem can be used to model the IQ components of the gain as independent Gaussian random variables. The resulting complex process has Rayleigh distributed amplitude and uniformly distributed phase.

In order to simulate the multipath component gain, the relationship between the Power Delay Profile (PDP) and the variance of the Rayleigh distributed channel amplitude is exploited. Because the multipath component gain is assumed to be a wide sense stationary (WSS) process, average power measurements are sufficient for describing the channel in any location with a room when the user is stationary. The Saleh-Valenzuela model is used to simulate the PDP using the exponential decay of the multi-path component power with increasing delay, and the Poisson process to predict the number of multipath components and their inter-arrival times.

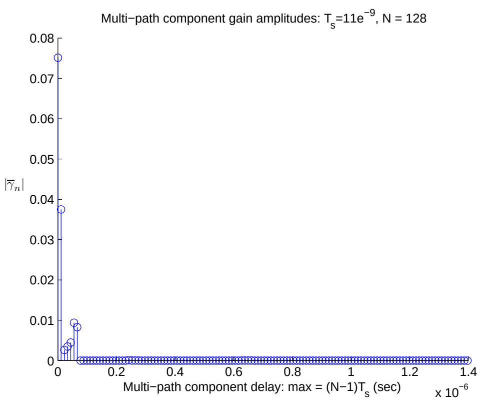


Figure 2.7: Simulation results for random channel gain amplitudes generated using the Saleh-Valenzuela PDP and i.i.d Gaussian IQ processes.

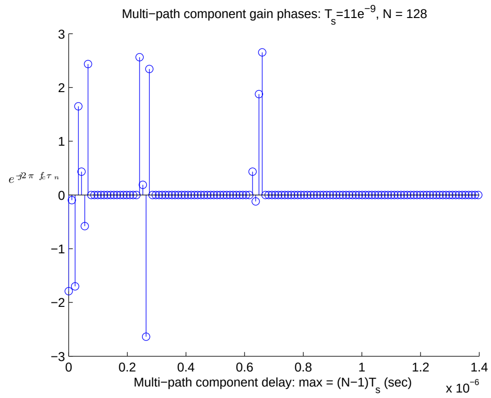


Figure 2.8: Simulation results for random channel gain phases generated using the Saleh-Valenzuela PDP and i.i.d Gaussian IQ processes.

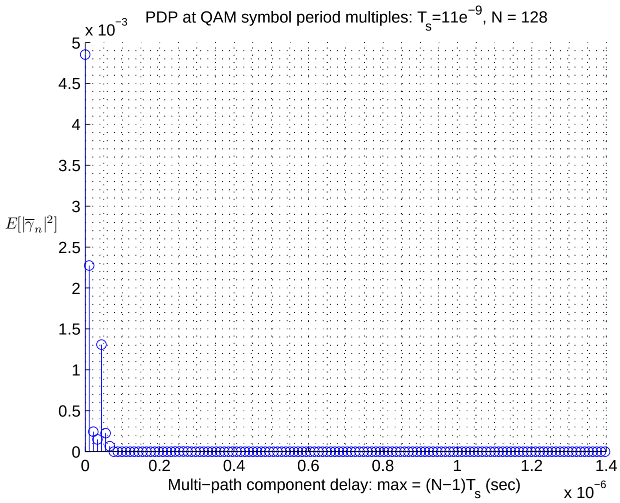


Figure 2.6: Simulation results for a random channel Power Delay Profile (PDP) (c.f. 2.24) generated using the Saleh-Valenzuela model. The value $E[|\bar{\gamma}_n|^2]$ is calculated at multiples of the QAM symbol period $T_s$.

# Chapter 3

# Coherent Detection for MIMO-OFDM Systems

A simple and accurate method of estimating the channel gain parameters (amplitude and phase) of a wireless system is to send a sequence of QAM symbols known to the receiver and use the received QAM symbols as well as the underlying convolution model of the frequency selective channel to form channel estimates. For MIMO-OFDM systems, channel gain estimation can be performed in the time domain followed by a transformation into the frequency domain using a Fourier transform. This approach has the advantage of reducing the number of channel gain parameters to be estimated for the MIMO-OFDM system.

In this chapter, a data aided channel estimation algorithm for the MIMO-OFDM systems is described. As a starting point, the mathematical description of the equalization of frequency selective channels using OFDM is given. OFDM equalization results in flat fading channel gain parameters for each sub-carrier in the MIMO-OFDM system. In order to develop a MIMO-OFDM estimator, SISO-OFDM channel estimators are considered after which a MISO-OFDM channel estimator that calculates the channel at a single receive antenna is developed. The MISO-OFDM channel estimator can then be generalized to a MIMO-OFDM system.

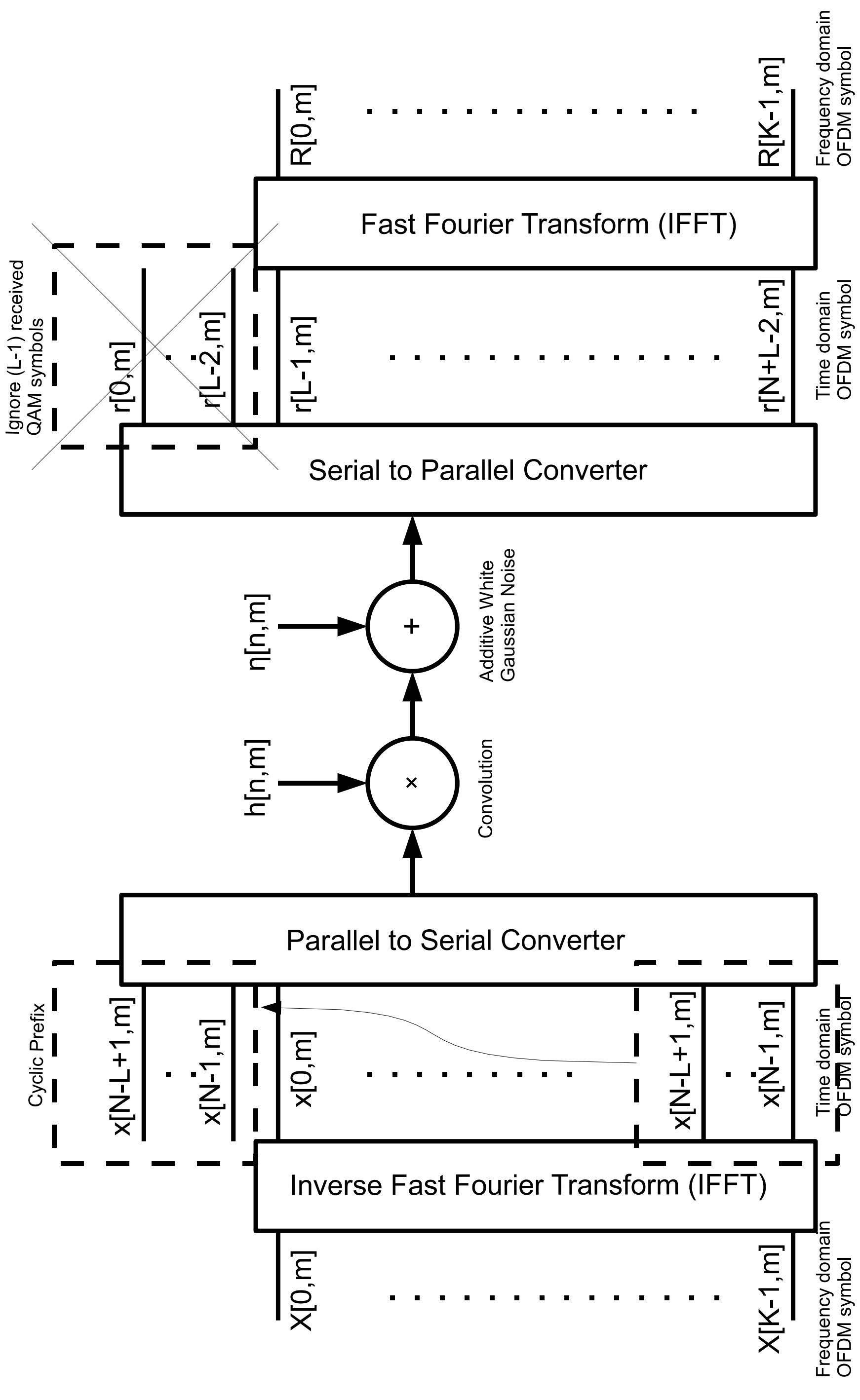


Figure 3.1: The SISO-OFDM System Model. The index $n$ denotes multiples of the QAM symbol period $T_s$ whilst the index $m$ is used to denote multiples of the OFDM symbol period $NT_s$.

## 3.1 OFDM Equalization

In Section 2.2, the QAM symbols at the output of a frequency selective channel are shown to be a convolution of the QAM symbols at the channel input and the Channel Impulse Response vector (the CIR vector is derived in Section 2.3). One undesirable effect of the convolution is Inter-Symbol Interference (ISI) by which it is meant that the current output QAM symbol is a weighted sum of the current and past input QAM symbols. Frequency selective channels are said to exhibit a memory of previously transmitted symbols. The single multipath component or a single sub-carrier in OFDM will be referred to as a *channel* depending on the context, and the amplitude and phase of the channel as the channel parameters or Channel State Information (CSI).

Recall that for OFDM transmission, a length $K$ source OFDM symbol $\{X[k]\}$ is processed using the FFT at the transmitter resulting in a length $N$ transmit OFDM symbol $\{x[n]\}$ (Figure 3.1). $K$ is the number of OFDM sub-carriers $\mathbf{s}_k$ cf. (1.8) which are amplitude modulated by the QAM symbols $\{X[k]\}$ for the duration $NT_s$. For the transmission of OFDM symbol in multipath channels, redundancy must be added to the vector $\{x[n]\}$ in order to maintain orthogonality of the sub-carriers [35]. This is done by adding a repetition of the some of the transmit QAM samples to the beginning of each burst resulting in a length $(N+L-1)$ OFDM symbol $\{x^{CP}[n]\}$ (Figure 3.1). $L$ is the maximum number of non-zero elements in the CIR vector which is found by dividing the maximum delay spread $\tau_{max}$ by the symbol period $T_s$. The convolution model is then used to determine the received OFDM symbol $\{r^{CP}[n]\}$.

$$r^{CP}[m] = \sum_{n=0}^{L-1} h[m-n]x^{CP}[n] \tag{3.1}$$

The convolution sum in equation (3.1) is derived from (2.7). For a length $(N+L-1)$ OFDM symbol $\{x^{CP}[n]\}$ and length $L$ Channel Impulse Response vector $\{h[n]\}$, the channel output $\{r^{CP}[n]\}$ has a length $N + 2(L-1)$[1] . The output QAM symbol vector can be written as a product of a channel gain matrix and the input QAM symbol vector.

$$\begin{bmatrix} r[0] \\ r[1] \\ r[2] \\ \vdots \\ r[L-1] \\ \vdots \\ r[N+2(L-1)-2 \\ r[N+2(L-1)-1] \end{bmatrix} = \begin{bmatrix} h[0] & 0 & 0 & \dots & 0 & 0 \\ h[1] & h[0] & 0 & \dots & 0 & 0 \\ h[2] & h[1] & h[0] & \dots & 0 & 0 \\ \vdots & \vdots & \vdots & \ddots & \vdots & \vdots \\ h[L-1] & h[L-2] & h[L-3] & \dots & 0 & 0 \\ \vdots & \vdots & \vdots & \ddots & \vdots & \vdots \\ 0 & 0 & 0 & \dots & h[L-1] & h[L-2] \\ 0 & 0 & 0 & \dots & 0 & h[L-1] \end{bmatrix} \begin{bmatrix} x[N-L+1] \\ x[N-L+2] \\ x[N-L+3] \\ \vdots \\ x[0] \\ \vdots \\ x[N-2] \\ x[N-1] \end{bmatrix} \tag{3.2}$$

At the receiver, the first and last $L-1$ symbols of the vector $\{r^{CP}[n]\}$ in equation (3.2) are removed leaving a length $N$ vector $\{r[n]\}$. Note that the added redundancy due to a cyclic prefix can be 5% to 20% of the transmitted data vector [3]. After removal of the cyclic prefix, the output QAM symbol vector $\mathbf{r} \equiv \{r[n]\}$ equation (3.2) can be written as the product of a circulant matrix $\mathbf{H}_{\mathsf{C}}$ and the input QAM symbol vector $\mathbf{x} \equiv \{x[n]\}$.

$$\mathbf{r} = \mathbf{H}_{\mathsf{C}}\mathbf{x} \tag{3.3}$$

The circulant matrix $\mathbf{H}_{\mathsf{C}}$ is an special kind of Toeplitz matrix where each column is obtained by doing a wrap-around downshift of the column vector $\mathbf{h} \equiv [h[0], h[1], \dots, h[N-1]]^T$ cf. Section 2.3.

$$\mathbf{H}_{\mathsf{C}} = \begin{bmatrix} h[0] & h[N-1] & h[N-2] & \dots & h[1] \\ h[1] & h[0] & h[N-1] & \dots & h[2] \\ h[2] & h[1] & h[0] & \dots & h[3] \\ \vdots & \vdots & \vdots & \ddots & \vdots \\ h[N-1] & h[N-2] & h[N-3] & \dots & h[0] \end{bmatrix} \in \mathbb{C}^{N \times N} \tag{3.4}$$

[1]this result is a well known result for the convolution sum

The downshift operator can be written as a matrix $\mathbf{R} = [\mathbf{e}_2, \mathbf{e}_3, \ldots, \mathbf{e}_N, \mathbf{e}_1]$, where $\mathbf{e}_k$ is the $k$th column of the identity matrix from which it can be noted that $\mathbf{H}_\mathsf{C} = \left[ \begin{array}{cccc} \mathbf{h} & \mathbf{Rh} & \ldots & \mathbf{R}^{N-1}\mathbf{h} \end{array} \right]$. The special property of the circulant matrix[2] is that it is diagonalized by the Fourier transformation matrix. Denoting the FFT complex exponentials by $W_N^{k,n} = \frac{1}{\sqrt{N}} e^{j2\pi kn/N}$, Fourier transformation matrix can be written as

$$\mathbf{F} = \begin{bmatrix} W_N^{0,0} & W_N^{0,1} & \ldots & W_N^{0,N-1} \\ W_N^{1,0} & W_N^{1,1} & \ldots & W_N^{1,N-1} \\ \vdots & \vdots & \ddots & \vdots \\ W_N^{K-1,0} & W_N^{K-1,1} & \ldots & W_N^{K-1,N-1} \end{bmatrix} \tag{3.5}$$

In the next section, the proof [36] of the diagonalization of the circulant channel matrix using the FFT is provided. This result implies that OFDM transmission with a redundant cyclic prefix leads to channel equalization. Another important result arising from OFDM modulation is that the flat fading channel gain for each sub-carrier and the CIR vector are related via $\tilde{\mathbf{h}} = \mathbf{Fh}$. Because the vector $\mathbf{h}$ is sparse, this result is used to reduce the number of channel estimation parameters $\tilde{\mathbf{h}}$. The following theorem and related proofs are used extensively throughout the thesis. The presentation of the formal proof also highlights some of the simulation assumptions stated later.

**Theorem 3.1** If $\mathbf{H}_\mathsf{C}$ is a circulant matrix, then it is diagonalized by $\mathbf{F}$. More precisely

$$\mathbf{H}_\mathsf{C} = \mathbf{F}^H \mathsf{diag}\left(\{H[k]\}\right)\mathbf{F} \tag{3.6}$$

where $\mathsf{diag}\left(\{H[k]\}\right) = \mathsf{diag}\left(\mathbf{Fh}\right)$ is a diagonal matrix.

When a vector $\mathbf{x}$ is multiplied by $\mathbf{F}$ the result is the discrete Fourier transform of $\mathbf{x}$. Thus, the theorem claims that the eigenvalues of $\mathbf{H}_\mathsf{C}$ are the discrete

[2]this property motivates the addition of the redundant cyclic prefix

Fourier transform of the first column in $\mathbf{H}_{\mathsf{C}}$. To prove this theorem we need two lemmas. First we verify that a circulant matrix is a polynomial in the downshift operator $\mathbf{R}$.

**Lemma 3.2** The circulant channel matrix is a polynomial in the downshift operator.

$$\mathbf{H}_{\mathsf{C}} = h[0]\mathbf{I} + h[1]\mathbf{R} + \cdots + h[N-1]\mathbf{R}^{N-1} \tag{3.7}$$

Recall that $\{h[n]\}$ are the elements of the Channel Impulse Response column vector $\mathbf{h}$. The vector $\mathbf{h} \equiv \{h[n]\}$ is also the first column of the matrix $\mathbf{H}_{\mathsf{C}}$.

**Proof**: Expanding the $j$th columns of equation (3.7) and using the result $\mathbf{R}^k\mathbf{e}_j = \mathbf{e}_{(j+k) \mod (N+1)}$ yields

$$\begin{aligned}
\left(h[0]\mathbf{I} + h[1]\mathbf{R} + \cdots + h[N-1]\mathbf{R}^{N-1}\right)\mathbf{e}_j &= h[0]\mathbf{e}_j + h[1]\mathbf{e}_{j+1} + \dots \\
&\quad + h[N-j]\mathbf{e}_N + h[N-j+1]\mathbf{e}_1 + \dots \\
&\quad + h[N-1]\mathbf{e}_{j-1} && (3.8)\\
&= \mathbf{R}^{j-1}\mathbf{h} && (3.9)\\
&= \mathbf{H}_{\mathsf{C}}\mathbf{e}_j && (3.10)
\end{aligned}$$

Hence, the $j$th column in the matrix polynomial equals the $j$th column in $\mathbf{H}_{\mathsf{C}}$. Since this holds for all $j$ the lemma is established.

Note that $\mathbf{R}$ is also a circulant matrix, so Theorem (3.1) should hold for this special matrix. We first show that the Fourier matrix diagonalizes $\mathbf{R}$ and, using Lemma (3.2) we can then show that $\mathbf{F}$ diagonalizes more general circulant matrices.

**Lemma 3.3**

$$\mathbf{FR} = \mathbf{DF} \tag{3.11}$$

where $\mathbf{D} = \mathsf{diag}\left(W_N^{0,1}, W_N^{1,1}, W_N^{2,1}, \ldots, W_K^{K-1,1}\right)$

**Proof**: We prove this lemma by comparing the $(k, j)$th element of $\mathbf{FR}$ with the $(kj, )$th element of $\mathbf{DF}$.

$$[\mathbf{FR}]_{k,j} = \left[W_N^{(k-1),1}, W_N^{(k-1),2}, W_N^{(k-1),3}, \ldots, W_N^{(k-1),N}\right] \mathbf{e}_j = W_N^{(k-1),j} \tag{3.12}$$

$$[\mathbf{DF}]_{k,j} = W_N^{(k-1),1}\mathbf{e}_k^T \begin{bmatrix} W_N^{0,(j-1)} \\ W_N^{1,(j-1)} \\ W_N^{2,(j-1)} \\ \vdots \\ W_N^{N-1,(j-1))} \end{bmatrix} = W_N^{(k-1),1} W_N^{(k-1),(j-1)} \tag{3.13}$$

$$= W_N^{(k-1),j} \tag{3.14}$$

Since $k$ and $j$ are arbitrary the statement $\mathbf{FR} = \mathbf{DF}$ holds. We now have the results needed to prove Theorem (3.1) above.

**Proof** [Theorem (3.1) ]: We start by showing that $\mathbf{F}\mathbf{H}_{\mathsf{C}}\mathbf{F}^H$ is diagonal. Replacing $\mathbf{H}_{\mathsf{C}}$ with the matrix polynomial (3.7) and using $\mathbf{FRF}^H = \mathbf{D}$ from Lemma (3.3) gives

$$\mathbf{F}\mathbf{H}_{\mathsf{C}}\mathbf{F}^H = \mathbf{F}\left(\sum_{k=0}^{N-1} h[k]\mathbf{R}^k\right)\mathbf{F}^H = \sum_{k=0}^{N-1} h[k]\mathbf{F}\mathbf{R}^k\mathbf{F}^H \tag{3.15}$$

$$= \sum_{k=0}^{N-1} h[k]\left(\mathbf{FRF}^H\right)^k = \sum_{k=0}^{N-1} h[k]\mathbf{D}^k = P(\mathbf{D}) \tag{3.16}$$

where $P(z) = h[0] + h[1]z + \cdots + h[N-1]z^{N-1}$. Since $\mathbf{D}$ is diagonal $\mathbf{D}^k$ is also diagonal,

$$\mathbf{D}^k = \mathsf{diag}\left(W_N^{0,k}, W_N^{1,k}, W_N^{2,k}, \ldots, W_N^{N-1,k}\right) \tag{3.17}$$

Thus $P(\mathbf{D})$ is a diagonal matrix. It remains to show that $P(\mathbf{D}) = \mathsf{diag}\left(\mathbf{Fh}\right)$. Using 3.17 the $(k, k)$th element in $P(\mathbf{D})$ can be found,

$$[P(\mathbf{D})]_{k,k} = \left[h[0]\mathbf{I} + h[1]\mathbf{D} + \cdots + h[N-1]\mathbf{D}^{N-1}\right]_{k,k} \tag{3.18}$$

$$= h[0]W_N^{k-1,0} + h[1]W_N^{k-1,1} + \cdots + h[N-1]W_N^{k-1,N-1} = \mathbf{Fh}[k] \tag{3.19}$$

This proves the theorem.

## 3.2 SISO-OFDM Channel Estimation

In order to achieve low error rates for data detection, OFDM systems employ coherent detection which relies on the knowledge of the amplitude and phase variations that are present on each flat fading sub-carrier channel. The most common channel parameter estimation technique involves the use of a training sequence, where the transmitter sends a known sequence of QAM symbols which are used to derive knowledge of the channel parameters at the receiver. The correlation of the channel parameters for successive sub-carrier channels, the so called frequency correlations, can be exploited to reduce the number of channel estimation parameters. Alternatively, correlations of the channel parameters for successive OFDM symbols, time correlations, can be exploited for the same purpose. The time-frequency model cf. (2.17) of a SISO-OFDM system is introduced, which makes it possible to estimate the channel along one or both of these dimensions.

For a single user, Single Input Single Output OFDM (SU-SISO-MIMO) communications system, the system model is expressed as a Hadamard (i.e element wise) product of the columns of the data matrix $\tilde{\mathbf{X}}$ and the channel matrix $\tilde{\mathbf{H}}$.

$$\tilde{\mathbf{R}} = \tilde{\mathbf{X}} \bullet \tilde{\mathbf{H}} + \tilde{\mathbf{N}} \tag{3.20}$$

Each column of the the matrix $\tilde{\mathbf{X}} \equiv [\tilde{\mathbf{x}}_1, \tilde{\mathbf{x}}_2, \ldots, \tilde{\mathbf{x}}_M]$ represents an OFDM symbol whilst each column of $\tilde{\mathbf{H}} \equiv \left[\tilde{\mathbf{h}}_1, \tilde{\mathbf{h}}_2, \ldots, \tilde{\mathbf{h}}_M\right]$ is the FFT of the CIR cf. Section 3.1. $\tilde{\mathbf{N}} \equiv [\tilde{\mathbf{n}}_1, \tilde{\mathbf{n}}_2, \ldots, \tilde{\mathbf{n}}_M]$ is an Additive White Gaussian Noise (AWGN) matrix with columns $\tilde{\mathbf{n}}_m$ corresponding to the AWGN affecting the $m$th OFDM symbol. $\tilde{\mathbf{x}}_m \equiv [X[0,m], X[1,m], \ldots, X[K-1,m]]^T$ is the OFDM symbol where $\{k : k = 0, 1, \ldots, K-1\}$ is the sub-carrier/frequency index cf. Section 1.4.2 and $\{m : m = 1, 2, \ldots, M\}$ is the symbol index. The vector $\tilde{\mathbf{x}}_m$ is formed at the receiver after removal of the cyclic prefix and FFT transform (Figure 3.1). At time $m$, $\mathbf{h}_m \equiv [h[0,m], h[1,m], \ldots, h[L-1,m], 0, \ldots 0] \in \mathbb{C}^{N\times 1}$ where $L \ll N$, is a sparse vector that is formed from padding a length $L$ vector with zeros. When the vector $\mathbf{h}_m$ is multiplied by the FFT matrix $\mathbf{F}$ the result, is the column vector $\tilde{\mathbf{h}}_m \equiv [H[0,m], H[1,m], \ldots, H[K-1,m]]^T$ of the channel matrix in (3.20) where $K = N$.

The structure of the OFDM signaling in equation (3.20) allows a channel estimator to use time and frequency correlations. Frequency correlations are observed in the columns $\tilde{\mathbf{h}}_m$ which are a sum of $L$ low frequency complex exponentials as a result of the Fourier transform of $\mathbf{h}_m$ with $L \ll K$. Time correlations for OFDM signalling can be understood by considering the Clarke's channel model introduced in Chapter 6. In general, time variance of the channel is caused by movement of the receiver at a given velocity or the various multipath mechanisms moving at random speeds [37]. When the channel is time variant, the relative path delays and attenuation of the individual multi-path components vary slowly but the phase shifts experience a Doppler effect and may vary rapidly.

In this thesis, it is assumed that *the QAM symbol transmission rate is high compared to the time variance of the channel and thus the channel impulse response is constant for the duration of an OFDM symbol.* If this is not the case, then each received QAM symbol will be the product of previously transmitted QAM symbols with different channel gain parameters. The simplifying assumption stated above is however supported by the strong time correlations observed when modeling channel gain parameters using Clarke's model. In the next section, the fundamental principles of one dimensional (time *or* frequency) and two dimensional (time *and* frequency) channel estimation in SU-SISO-OFDM systems are investigated.

### 3.2.1 One Dimensional Channel Estimation

Receiver complexity is reduced when one-dimensional channel parameter estimation is implemented in SISO-OFDM systems because time and frequency correlations may be exploited separately. The SNR performance of 1D channel estimators is however inferior to that of 2D channel estimators [37, 39] and the literature indicates that fewer pilots are required for 2D estimation leading to spectral efficiency [40]. In this section, the frequency correlation of the channel parameters are used to develop a low complexity 1D estimators for the SISO-OFDM wireless system. Temporal correlations may also be used based on the observation that the channel parameters in the time domain are a bandlimited stochastic process (Jakes Model [25]). The simplest channel estimator based on the frequency correlations [3] can be implemented by simply dividing the received QAM symbol by the transmitted QAM symbol. For a single OFDM symbol the flat fading channel for each sub-carrier can be estimated as follows (the index $m$ is omitted because the description here refers to the single training OFDM symbol)

$$\tilde{\mathbf{h}} = \tilde{\mathbf{r}}/\tilde{\mathbf{x}} \tag{3.21}$$

The division sign represents element wise division. The vectors in equation (3.21) apply to a single column in the system description given in equation (3.20). This estimator is referred to as the *Least Squares Estimator* in the

[3] these are the so called block-oriented estimators, and block refers to the QAM symbols that together form an OFDM symbol

literature [37] and [42] and has the major disadvantage of having an oversimplified channel model[4] i.e., the absence of AWGN and perfect equalization are assumed [37].

The frequency correlations of the channel gain for the OFDM symbol are linked to the finite maximum delay spread of the channel. For a well designed OFDM system, the duration of the OFDM symbol $NT_s$ is much longer the maximum channel delay $LT_s$, where $T_s$ is the QAM symbol period. Channel estimation can be performed in the time domain (solving for $\mathbf{h}_m$ rather that $\tilde{\mathbf{h}}_m$ in section 3.2) where there are fewer parameters. This leads to a low complexity solution with improved SNR performance. Considering without loss of generality that $\tilde{\mathbf{x}} = [1, 1, \ldots, 1]^T \in \mathbb{R}^{N\times 1}$, the received OFDM symbol can be written as

$$\tilde{\mathbf{r}} = \mathbf{F}\begin{bmatrix} \mathbf{h} \\ \mathbf{0} \end{bmatrix} + \tilde{\mathbf{n}} \tag{3.22}$$

$\mathbf{0}$ is an $(N - L) \times 1$ null vector, and $N = K$ is the length of the column vector $\tilde{\mathbf{r}}$. $\mathbf{F}$ is a $N \times N$ matrix that can be separated into the "signal subspace" and the "noise subspace", and the received OFDM symbol can be re-written with the partitioning of the $\mathbf{F}$ matrix.

$$\tilde{\mathbf{r}} = \begin{bmatrix} \mathbf{F_h} & \mathbf{F_n} \end{bmatrix}\begin{bmatrix} \mathbf{h} \\ \mathbf{0} \end{bmatrix} + \tilde{\mathbf{n}} = \mathbf{F_h}\mathbf{h} + \tilde{\mathbf{n}} \tag{3.23}$$

Relying on this model, the reduced space estimates of the channel can be calculated as follows

$$\hat{\mathbf{h}} = \mathbf{F}_\mathbf{h}^\dagger\tilde{\mathbf{r}} = \mathbf{h} + \mathbf{F}_\mathbf{h}^\dagger\tilde{\mathbf{n}} \tag{3.24}$$

$\mathbf{F}_\mathbf{h}^\dagger$ is the pseudoinverse of the signal subspace FFT matrix (Section 3.3.1). The so-called *Maximum Likelihood Estimator* [37] is then given by

[4]Practical systems may not be perfectly synchronized resulting in errors in burst detection and AWGN in the received symbol

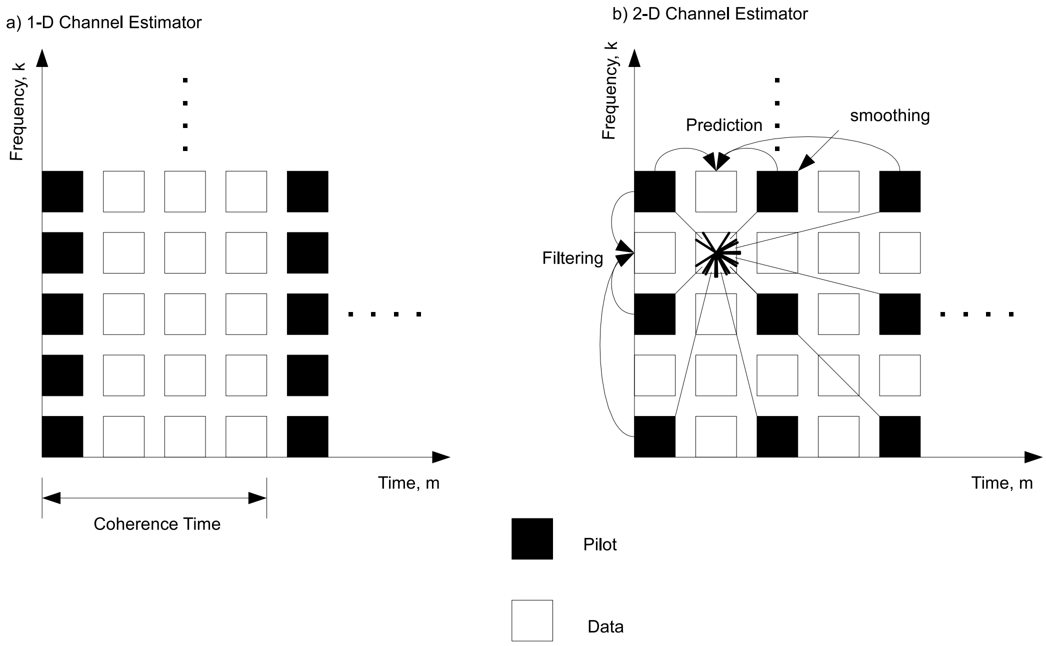


Figure 3.2: 1-D and 2-D SISO-OFDM channel estimation. The shaded sub-carriers contain training symbols. In 1-D channel estimation, the frequency correlation of the training sub-carriers is used to estimate the channel. In 2-D channel estimation, the time and frequency correlation of the training sub-carriers are used to estimate the channel.

$$\hat{\hat{\mathbf{h}}} = \mathbf{F}\hat{\mathbf{h}} \tag{3.25}$$

This estimator amounts to forcing the time channel estimator, which is constrained to a length $L$, back into the frequency domain. The placement of pilots for frequency domain channel estimation is depicted in Figure 3.2. Several data OFDM symbols are transmitted after the training OFDM symbol, and coherent detection is used to reduce the error in data detection. Note that due to the motion of the receiver or multipath mechanisms, training symbols are repeated within the coherence time, which is the time during which the channel parameters are valid.

### 3.2.2 Two Dimensional Channel estimation

For the SU-SISO-OFDM system, not all the sub-carriers are required for channel estimation because of the strong frequency correlations and the pilot QAM symbols can be spaced at interval in frequency to estimate the channels. The performance of the channel estimator can also benefit from the rather strong time correlations when pilot QAM symbols are spaced at interval in time (Figure 3.2). Exploiting both time and frequency correlations can significantly reduce the spectral inefficiency due pilot symbol placement whilst providing the functions of filtering, smoothing and prediction [37]–[43]. In order to explain the aforementioned functions, it is necessary to understand the process of 2D channel estimation. At the pilot sub-carrier time-frequency locations, an *a posteriori* least squares estimate of the channel parameters corrupted by additive white gaussian noise (AWGN) is given by

$$\hat{H}[\acute{k},\acute{m}] = \frac{\hat{R}[\acute{k},\acute{m}]}{X[\acute{k},\acute{m}]} = \frac{R[\acute{k},\acute{m}] + N[\acute{k},\acute{m}]}{X[\acute{k},\acute{m}]} \tag{3.26}$$

$$= H[\acute{k},\acute{m}] + \frac{N[\acute{k},\acute{m}]}{X[\acute{k},\acute{m}]} \tag{3.27}$$

Note that for the flat fading OFDM sub-carrier channel, the received QAM symbol is given by the product $R[k,m] = H[k,m]X[k,m]$, where $H[k,m]$ is the sub-carrier channel gain and $X[k,m]$ is a transmitted QAM symbol (data or pilot). An estimate of the sub-carrier channel gain at any given time-frequency location $\hat{H}[k,m]$ is given by a linear combination of the estimates $\hat{H}[\acute{k},\acute{m}]$ (3.27) at the pilot locations.

$$\hat{H}[k,m] = \sum_{[\acute{k},\acute{m}]} \omega[\acute{k},\acute{m}]\hat{H}[\acute{k},\acute{m}] = \boldsymbol{\omega}^H \hat{\hat{\mathbf{h}}} \tag{3.28}$$

The total number of pilots in the OFDM frame can be denoted by $N_{frame}$, where an OFDM frame refers to $M$ received OFDM symbols each containing

$K$ QAM symbols. The OFDM frame is used for both channel estimation and data detection in the 2-D estimator (Figure 3.2). $\hat{\hat{\mathbf{h}}} \in \mathbb{C}^{N_{frame} \times 1}$ is a vector formed from some arrangement of the least square channel parameter estimates $\{\hat{H}[\acute{k}, \acute{m}]\}$ (3.27) for the OFDM frame. This arrangement can be for example a collection of the estimates $\{\hat{H}[\acute{k}, \acute{m}]\}$ for increasing frequency index from the first to the last OFDM symbol in the OFDM frame. The optimal weights $\boldsymbol{\omega} \in \mathbb{C}^{N_{frame} \times 1}$, in the sense of minimizing the MSE ($E[|\hat{H}[k,m] - H[k,m]|^2]$) across all the time-frequency sub-carrier locations (the so-called 2-D Wiener filter coefficients), are given by

$$\boldsymbol{\omega}^H = \boldsymbol{\theta}^H \boldsymbol{\Phi}^{-1} \tag{3.29}$$

$\boldsymbol{\theta} \in \mathbb{C}^{N_{frame} \times 1}$ is a cross-correlation vector for the correlation between the estimated parameter and the least squares channel parameter estimates, $E\left[H[k,m]\hat{\hat{\mathbf{h}}}\right]$. $\boldsymbol{\Phi}^{N_{frame} \times N_{frame}}$ is a covariance matrix for the least squares channel parameter estimates $E[\hat{\hat{\mathbf{h}}}\hat{\hat{\mathbf{h}}}^H]$. However since these channel statistics are not known at the receiver, the elements of the cross-correlation vector $\boldsymbol{\theta}$ can be approximated as follows [43]

$$E\left[H[k]\hat{H}^*[\acute{k}]\right] = \frac{\sin\left(\pi\tau_{max}(k-\acute{k})F_s\right)}{\pi\tau_{max}(k-\acute{k})F_s} \tag{3.30}$$

$$E\left[H[m]\hat{H}^*[\acute{m}]\right] = \frac{\sin\left(2\pi f_D(m-\acute{m})(K+L)T_s\right)}{2\pi f_D(m-\acute{m})(K+L)T_s} \tag{3.31}$$

$$E\left[H[k,m]\hat{H}^*[\acute{k},\acute{m}]\right] = (H[k]\hat{H}^*[\acute{k}])(H[m]\hat{H}^*[\acute{m}]) \tag{3.32}$$

In the above formulation, $\tau_{max}$ is the maximum delay spread of the multipath channel, $F_s$ is the bandwidth of each sub-carrier, $f_D = \frac{vf_c}{c}$ is the Doppler frequency for a receiver traveling at a velocity $v$, for a carrier frequency $f_c$ and $c = 3 \times 10^8$ m/s is the velocity of Electromagnetic waves in free space. $K$ is the number of QAM symbols in the OFDM symbol, $L$ is the maximum number of non-zero elements in the CIR vector and $T_s$ is the QAM symbol period. The correlation of CSI in the frequency domain can be related to the power delay profile (PDP) as in Appendix C. Assuming that the correlations can be approximated by sinc functions is equivalent to assuming a rectangular power delay profile, and despite the fact the PDP has been modeled as exponentially decaying, the results obtained in this thesis and in the literature [43] are compelling. Similarly, the elements of the covariance matrix $\mathbf{\Phi}$ can be approximated by the formulation

$$E\left[\hat{H}[k]\hat{H}^*[\acute{k}]\right] = \frac{\sin\left(\pi\tau_{max}(k-\acute{k})F_s\right)}{\pi\tau_{max}(k-\acute{k})F_s} \tag{3.33}$$

$$E\left[\hat{H}[m]\hat{H}^*[\acute{m}]\right] = \frac{\sin\left(2\pi f_D(m-\acute{m})(K+L)T_s\right)}{2\pi f_D(m-\acute{m})(K+L)T_s} \tag{3.34}$$

$$E\left[\hat{H}[\acute{k},\acute{m}]\hat{H}^*[\acute{k},\acute{m}]\right] = (\hat{H}[k]\hat{H}^*[\acute{k}])(\hat{H}[m]\hat{H}^*[\acute{m}]) + \frac{\sigma_n^2}{E[X[\acute{k},\acute{m}]]}\delta_{\acute{k},\acute{m}} \tag{3.35}$$

$\delta_{\acute{k},\acute{m}}$ is the kronecker delta function and $\sigma_n^2$ is the noise variance at pilot sub-carrier locations. The assumption of sinc correlations for the OFDM CSI is equivalent to assuming a rectangular power spectral density. The power spectral density for the OFDM CSI at a single sub-carrier can be shown to be Jake's spectrum [25], but again, this simplifying assumption does not impair the wiener filter [43]. Channel estimation is performed for the data and pilot locations using the Wiener filter (3.28). In terms of 2-D channel estimation, filtering refers to the channel parameter estimates at the data carrying frequency indices which are in a sense an interpolated estimate due to Wiener filtering. Prediction refers to the channel parameters estimates at data carrying time indices which are procured through a process of time projection using the Wiener filter. Smoothing refers to a refinement of the initial 'noisy' least squares channel parameter estimates (3.27) at the pilot locations. 2-D Wiener Filter estimators, also called Minimum Mean Square Error (MMSE) estimators, have greatly increased computational complexity for the improved

| Parameter | Simulation Settings |
|---|---|
| Carrier Frequency | $f_c = 1.8 \times 10^9 Hz$ |
| OFDM Symbol length | $K = 16$ |
| OFDM Frame length | $M = 32$ |
| QAM Symbol Period | $T_s = 10 \times 10^{-6}(sec)$ |
| Maximum Delay spread | $\tau_{max} = 4 \times T_s(sec)$ |
| RMS Delay spread | $\tau_{rms} = 3.5 \times 10^{-6}(sec)$ |
| 2-D pilots frequency spacing | $N_f = 4$ |
| 2-D pilots time spacing | $N_t = 8$ |
| Number of 2-D pilots | $N_{frame} = 16$ |
| Number of 1-D pilots | $N_{frame} = 16$ |
| RF Channel Bandwidth | $F_s = 200 \times 10^3 Hz$ |

Table 3.1: Simulation Parameters for the comparison of 1-D and 2-D SISO-OFDM Channel Estimators.

SNR performance. For the implementation of the Wiener filter, see the Matlab code in appendix E. In order to model the time varying channel, Clarke's Model [13] was implemented. Simulation results indicate that the 2-D channel estimator has better SNR performance using the same number of pilots as the 1-D estimators (Least squares (LS) and Maximum Likelihood (MLE)). The results confirm that spacing the pilots at interval in frequency and time and implementing the Wiener filter achieves smoothing, filtering and prediction.

It is noted in the literature [39]–[43] that filtering in two dimensions will outperform filtering in just one dimension with respect to the number of pilots required and mean square error performance. However, two cascaded orthogonal 1-D filters are simpler to implement and are shown to be virtually as good as true 2-D filters. This observation motivates the separated 1-D approach pursued in this thesis, where optimization in the frequency and time domain are procured independently.

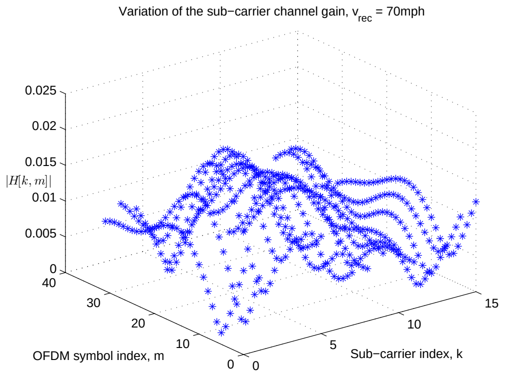


Figure 3.3: Random realization of the variation of OFDM channel parameters for $v = 70mph$.

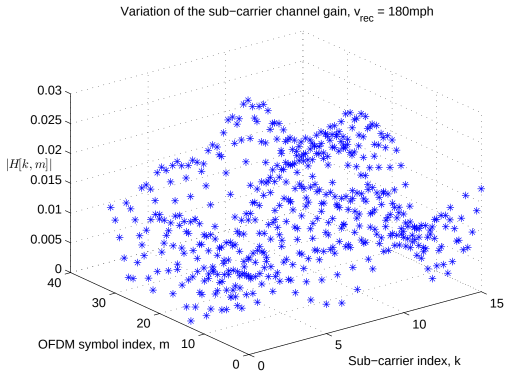


Figure 3.4: Random realization of the variation of OFDM channel parameters for $v = 180mph$.

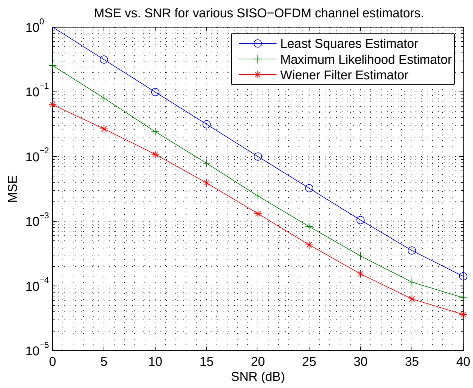


Figure 3.5: Simulation results for the Mean Square Error (MSE) in the channel parameter estimates vs. Signal to Noise Ratio (dB) for SISO-OFDM estimators for $v = 70mph$.

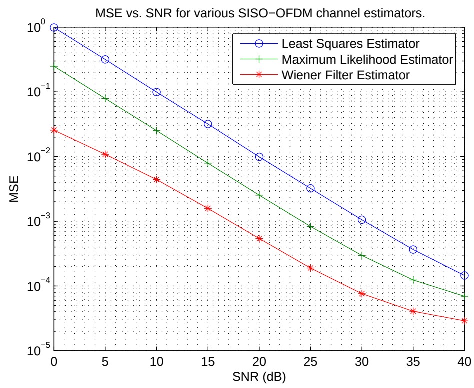


Figure 3.6: Simulation results for the Mean Square Error (MSE) in the channel parameter estimates vs. Signal to Noise Ratio (dB) for SISO-OFDM estimators for $v = 180mph$.

## 3.3 MIMO-OFDM Channel Estimation

Current research into SU-MIMO-OFDM channel estimation has mainly focused on least square (LS) channel estimation [45]. The main problem with this approach is the design of optimal training sequences, a problem that has been investigated in various literature [46, 47]. Recently, a common framework has been proposed for evaluating various (LS) channel estimation methods in [48]. The channel estimator described in this section uses the underlying convolution model of the communications channel in conjunction with available training data at the receiver to estimate the channel parameters in the time domain. This channel estimator is a modified version of the estimator in the literature [49] originally proposed for application to the Time Domain Multiple Access (TDMA) GSM frame. It can also be noted that the modified channel estimator is the generic MIMO-OFDM estimator presented in the literature [48].

### 3.3.1 Least Squares Solution

The forward problem $\mathbf{r} = \mathbf{Xh}$ can easily be formulated for the MISO-OFDM system using the convolution channel model. The forward solution predicts the outcome $\mathbf{r}$ as a function of known system inputs matrix $\mathbf{X}$ and channel vector $\mathbf{h}$. The channel vector $\mathbf{h}$ has a minimum length $L$ (Section 3.2) and the MISO system employs $(n_t, 1)$ antennas with $K$ sub-carriers for each transmit/receive antenna link. MISO-OFDM estimators can be generalized to MIMO-OFDM estimators by repeating the estimation process at each receive antenna at a time.

In the inverse problem, $N$ measured values of the system output $\mathbf{r}$ are used to estimate $n_t L$ unknown channel parameters [50]. Both the system output $\mathbf{r}$ and the system inputs matrix $\mathbf{X}$ are known at the receiver. In general $\mathbf{X}$ in non-invertible and a pseudoinverse must be used to solve the inverse problem.

$$\hat{\mathbf{h}} = \mathbf{X}^{\dagger}\mathbf{r} \tag{3.36}$$

The pseudoinverse $\mathbf{X}^{\dagger}$ is not the "normal" inverse of the matrix $\mathbf{X}$, and the products $\mathbf{D} = \mathbf{X}^{\dagger}\mathbf{X}$ is not necessarily equal to the identity matrix. The matrix $\mathbf{D} \in \mathbb{C}^{N\times N}$ is the *data resolution matrix* which is determined by the choice of the system input $\mathbf{X}$. The *residuals* are defined as $\mathbf{e} = \mathbf{r} - \mathbf{X}\hat{\mathbf{h}}$ and $L_2$ norm of the vector of residuals $\Gamma = \mathbf{e}^T \cdot \mathbf{e}$ is zero when $\mathbf{D} = \mathbf{I}$ and increases as $\mathbf{D}$ deviates from the identity matrix $\mathbf{I}$. The Least Squares (LS) solution corresponds to the minimum point of the error surface [50] and it is found by setting the derivative of the objective function $\Gamma$ with respect to $\mathbf{h}$ equal to zero $\frac{\partial \Gamma}{\partial \mathbf{h}} = 0$. The Moore-Penrose inverse $\mathbf{X}^{\dagger} = \left(\mathbf{X}^H\mathbf{X}\right)^{-1}\mathbf{X}^H$ yields the LS solution when $n_tL \leq N$. This LS solution is used for MIMO-OFDM estimators and has previously been used for SISO-OFDM Maximum Likelihood Estimators (Section 3.2.1). Note that the Least Square MIMO estimators are however different from SISO Least Squares estimators as presented in this thesis and in the literature [37] and [42].

### 3.3.2 Time Domain LS Channel Estimation

MIMO-OFDM channel gain estimation can be performed in the time domain by evaluating the CIR for the wireless links between the $n_t$ transmit antennas and a single receiver. The channel gain for the OFDM sub-carriers can be collected into a vector $\tilde{\mathbf{h}}_{i,j} \equiv [H_{i,j}[0], H_{i,j}[1], \ldots, H_{i,j}[K-1]]^T$ where $\tilde{\mathbf{h}}_{i,j} = \mathbf{F}\mathbf{h}_{i,j}$ and $(i, j)$ is the link between transmit antenna $i$ and receive antenna $j$. Note that the column vector of the CIR $\mathbf{h}$ in equation (2.50) for a MIMO link is a sparse vector. For a length $N$ CIR vector $\mathbf{h}$, only $L$ non-zero elements need to be estimated. This reduces the number of channel gain parameters to be estimated per MIMO-OFDM link from $N$ to $L$, and the number of channel gain parameters per receive antenna from $n_tN$ to $n_tL$ where $L \ll N$. Each received OFDM symbol of length $N$ (in the time domain) is used to estimate $n_tL$ channel gain parameters where[5] $n_tL \leq N$. After channel gain estimation

[5]Recall that $L$ is found by dividing the maximum delay spread $\tau_{rms}$ by the QAM symbol period $T_s$ so that the OFDM symbol length has to be long compared to the expected

in the time domain, the relationship $\tilde{\mathbf{h}} = \mathbf{F}\mathbf{h}$ is used to obtain frequency domain estimates.

The length $L$ CIR vectors of $n_t$ Multiple Input Single Output (MISO) links for the $j$th receiver can be written as a vector

$$\mathbf{h}_{MISO} \equiv \left[\mathbf{h}_{1,j}^T, \mathbf{h}_{2,j}^T, \ldots, \mathbf{h}_{n_t,j}^T\right]^T \tag{3.37}$$

$\mathbf{h}_{i,j}$ is the SISO CIR vector $\mathbf{h}$ in equation 2.50 for the $(i,j)$th MISO link that has been truncated to a length $L$. The transmitter sends unique training sequences from the $i$th antenna $\mathbf{x}_i = [x_i[0], x_i[1], \cdots, x_i[N+L-2]]^T \in \mathbb{C}^{(N+L-1)\times 1}$ which are length $N$ vectors with a cyclic prefix cf. section 3.2 of length $L-1$ QAM symbols. A circulant matrix of the training symbols may be observed at the receiver due to the convolution channel model based on the transmitted training sequence for antenna $i$.

$$\mathbf{X}_i = \begin{bmatrix} x_i[L-1] & \cdots & x_i[1] & x_i[0] \\ x_i[L] & \cdots & x_i[2] & x_i[1] \\ \vdots & \ddots & \vdots & \vdots \\ x_i[N+L-2] & \cdots & x_i[N] & x_i[N-1] \end{bmatrix} \in \mathbb{C}^{N\times L} \tag{3.38}$$

The first and last $L-1$ received QAM symbol of each burst are ignored in the formulation of the circulant matrix above. The circulant training sequence matrices in (3.38) are concatenated to form a larger matrix $\mathbf{X} = \begin{bmatrix} \mathbf{X}_1 & \mathbf{X}_2 & \ldots & \mathbf{X}_{n_t} \end{bmatrix} \in \mathbb{C}^{N\times n_t L}$ which can be used together with equation (3.37) to describe a received symbol vector

$$\mathbf{r} = \mathbf{X}\mathbf{h}_{MISO} + \mathbf{n} \tag{3.39}$$

$\mathbf{n}$ is Additive White Gaussian Noise (AWGN) vector. When referring to equation (3.39), the subscript $MISO$ will be omitted to simplify the notation.

maximum delay of the channel

| Parameter | Simulation Settings |
|---|---|
| Carrier Frequency | $f_c = 2.4 \times 10^9 Hz$ |
| OFDM Symbol length | $K = 128$ |
| QAM Symbol Period | $T_s = 11 \times 10^{-9}(sec)$ |
| Cluster arrival rate | $\Lambda = 1/200 \times 10^{-9}(sec^{-1})$ |
| Ray arrival rate | $\lambda = 1/5 \times 10^{-9}(sec^{-1})$ |
| Tx antenna gain | $G_t = 3(dB)$ |
| Rx antenna gain | $G_r = 3(dB)$ |
| Cluster power Delay Time Constant | $\gamma = 60 \times 10^{-9}$ |
| Ray power Delay Time Constant | $\Gamma = 20 \times 10^{-9}$ |

Table 3.2: Simulation Parameters for the analysis of the LS MISO-OFDM Channel Estimators. Refer to the Saleh-Valenzuela model Section 2.3

The vector $\mathbf{r} \in \mathbb{C}^{N\times 1}$ is the received symbol vector for the OFDM system, *before* the FFT operator, and is therefore considered a time domain vector. The Least Squares channel estimate can be found for equation (3.39) by pre-multiplying both sides of the equation by the Moore-Penrose inverse. Because the OFDM frame is designed such that $N \geq n_t L$, the LS solution is given by

$$\hat{\mathbf{h}} = \mathbf{X}^{\dagger}\mathbf{r} \approx \mathbf{h} \tag{3.40}$$

For a MU-MIMO-OFDM system with a large number of transmit antennas (Section 1.6), it becomes increasingly difficult to estimate the channel as the constraint $n_t L \leq N$ may not be met. An improvement to the estimator can be achieved by representing the channel gain for the SISO-OFDM sub-carriers in the form $\tilde{\mathbf{h}} = \mathbf{B}\mathbf{w}$ where $\mathbf{B}$ is an arbitrary basis and $\mathbf{w}$ has a length that is shorter than $\mathbf{h}$. This approach, which we shall refer to as Reduced Parameter Channel State Information (RP-CSI) Estimation, is investigated in chapter 4.

Note that channel fades independently for the channel between the receiver and transmit antennas 1 and 2 in figure 3.7–3.8. There is a small error in the estimated channel because the Saleh-Valenzuela model maximum delay of the Channel Impulse Response (CIR) is 200ns but the estimation considers a CIR

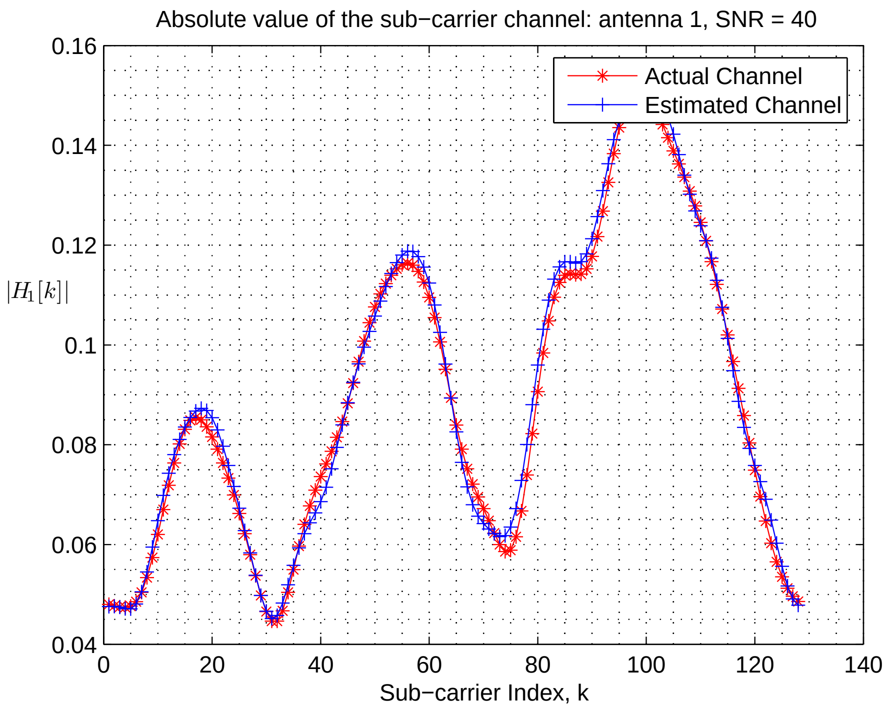


Figure 3.7: Absolute value of the sub-carrier channel gain for the actual and estimated channels using the LS MISO-OFDM estimator, channel 1.

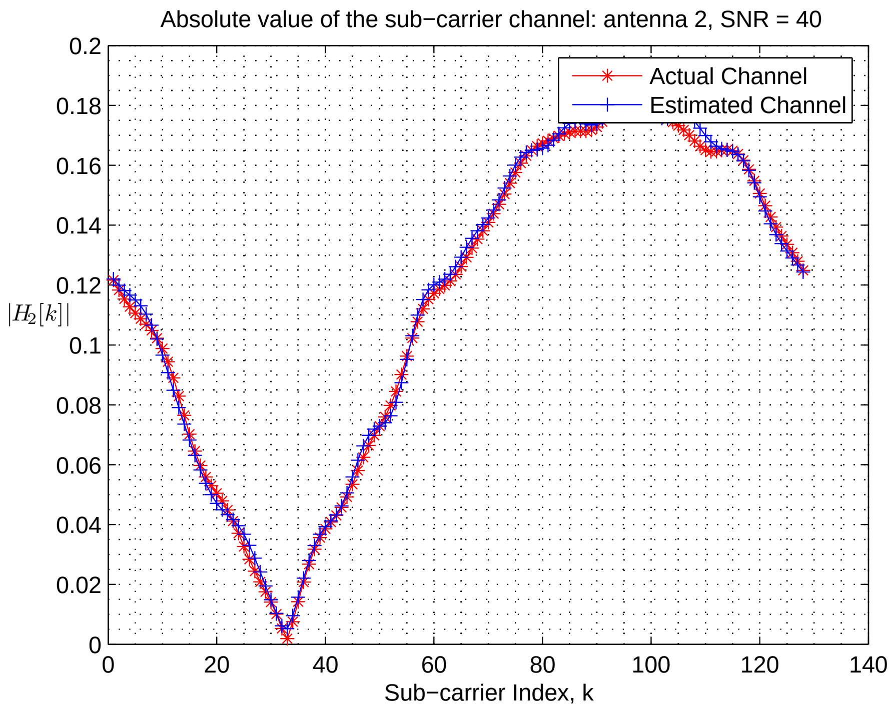


Figure 3.8: Absolute value of the sub-carrier channel gain for the actual and estimated channels using the LS MISO-OFDM estimator, channel 2.

with a maximum duration of $L \times T_s \approx 160$ns, where $L = 16$ and $T_s = 11$ns.

### 3.3.3 Performance of the Channel Estimator

The performance of the data aided channel estimator in equation 3.40 is degraded by the presence of Additive White Gaussian Noise (AWGN) in the received OFDM symbols. In this section, the effects of channel noise on the performance of the MIMO-OFDM estimator are quantified.

Using the noisy received symbols, the vector of the Least Squares channel gain parameters for the MISO-OFDM system are given by

$$\hat{\mathbf{h}} = \left(\mathbf{X}^H\mathbf{X}\right)^{-1}\mathbf{X}^H\left(\mathbf{X}\mathbf{h} + \mathbf{n}\right) \tag{3.41}$$

$$= \left(\mathbf{X}^H\mathbf{X}\right)^{-1}\left(\mathbf{X}^H\mathbf{X}\right)\mathbf{h} + \left(\mathbf{X}^H\mathbf{X}\right)^{-1}\mathbf{X}^H\mathbf{n} \tag{3.42}$$

$$= \mathbf{h} + \left(\mathbf{X}^H\mathbf{X}\right)^{-1}\mathbf{X}^H\mathbf{n} \tag{3.43}$$

The error in channel estimation is the difference between the actual channel gain vector and the estimated channel gain vector.

$$\hat{\mathbf{h}} - \mathbf{h} = \left(\mathbf{X}^H\mathbf{X}\right)^{-1}\mathbf{X}^H\mathbf{n} \tag{3.44}$$

The error covariance matrix [52] is defined as follows

$$P_D = E\left[\left(\hat{\mathbf{h}} - \mathbf{h}\right)\left(\hat{\mathbf{h}} - \mathbf{h}\right)^H\right] \tag{3.45}$$

$$= E\left[\left(\left(\mathbf{X}^H\mathbf{X}\right)^{-1}\mathbf{X}^H\mathbf{n}\right)\left(\left(\mathbf{X}^H\mathbf{X}\right)^{-1}\mathbf{X}^H\mathbf{n}\right)^H\right] \tag{3.46}$$

$$\tag{3.47}$$

The expression for the covariance matrix can be simplified further as follows

$$P_D = E\left[(\mathbf{X}^H\mathbf{X})^{-1}(\mathbf{X}^H\mathbf{n})(\mathbf{X}^H\mathbf{n})^H\left((\mathbf{X}^H\mathbf{X})^{-1}\right)^H\right] \tag{3.48}$$

$$= (\mathbf{X}^H\mathbf{X})^{-1}\mathbf{X}^H E\left[\mathbf{n}\mathbf{n}^H\right]\mathbf{X}\left((\mathbf{X}^H\mathbf{X})^{-1}\right)^H \tag{3.49}$$

$$= (\mathbf{X}^H\mathbf{X})^{-1}\mathbf{X}^H\sigma_n^2\mathbf{I}\mathbf{X}\left((\mathbf{X}^H\mathbf{X})^{-1}\right)^H \tag{3.50}$$

$$= \sigma_n^2(\mathbf{X}^H\mathbf{X})^{-1}(\mathbf{X}^H\mathbf{X})\left((\mathbf{X}^H\mathbf{X})^{-1}\right)^H \tag{3.51}$$

$$= \sigma_n^2\left((\mathbf{X}^H\mathbf{X})^{-1}\right)^H \tag{3.52}$$

The MSE of the channel estimator is related to the trace of the error covariance matrix $trace(P_D)$ as follows

$$MSE = \frac{trace(P_D)}{n_t L} \tag{3.53}$$

$n_t$ is the number of transmit antennas in the MISO-OFDM system and $L$ is the length of the CIR vector $\mathbf{h}$. Further analysis of the matrix $(\mathbf{X}^H\mathbf{X})$ shows that this matrix is a Toeplitz matrix which has dimensions $n_tL \times n_tL$ and contains delayed versions of the training sequence auto-correlations [44] for the $n_t$ transmitting antennas. The role of the training sequence on the performance of the MIMO-OFDM channel estimator is investigated for a RP-CSI MIMO-OFDM in Chapter 5. The RP-CSI estimator that is developed in Chapter 4 is more general that the estimator presented in this section and hence a similar MSE analysis to the one presented here is more informative. Simulation results comparing the analytical MSE to measured MSE for the LS MISO-OFDM estimator shows that the estimator is optimal for reducing MSE in channel estimates. The training sequence used for the simulation was the well known Hadamard codes also called the Walsh codes implemented in Chapter 11 of the literature [51].

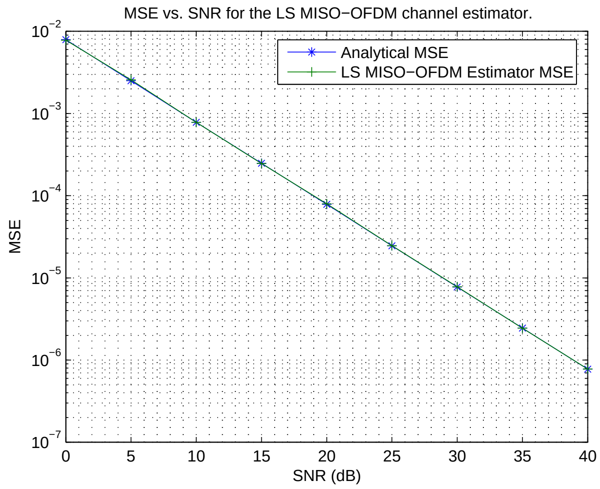


Figure 3.9: A comparison between the analytical and estimated MSE for the LS MISO-OFDM estimator.

## 3.4 Chapter Summary

In this chapter, several channel estimators for 1-D and 2-D SU-SISO-OFDM systems, as well as the generic SU-MIMO-OFDM estimator are discussed and their performance evaluated through extensive simulations. The OFDM channels are shown to vary in frequency as well as in time, as determined by well known channel models. Frequency domain channel parameter variation refers to the changes in the sub-carrier channel gain with increasing frequency index, $k$. A mathematically rigorous proof is presented to show that the sub-carrier channel gain is given by the product of the Fourier transformation matrix and the CIR vector, where the latter is a sparse matrix with a maximum of $L$ non-zero elements. The degree of variation of the channel parameters is related to the parameter $L$ such that the larger the value of $L$ the more rapid the variation of the channel parameters with $k$ and vice-versa. The parameter $L$ can be determined by dividing the maximum delay of the channel $\tau_{max}$ by the QAM symbol period, $T_s$. Time domain channel parameter variation refers to the changes in the sub-carrier channel gain at a particular frequency index $k$

with increasing time index, $m$. The variation of the CIR vector elements with time can be modeled using Clarke's model which predicts that the multipath amplitudes and relative delay are slowly varying, whilst the phase variations are rapid due to the effects of Doppler frequency related variation.

One dimensional channel estimators which exploit the frequency correlations of the OFDM channel improve the MSE performance of the SISO-OFDM system. Simulation results comparing the performance of Least Squares (LS) and the Maximum Likelihood Estimator (MLE) show that MLE estimators achieve a lower Mean Square Error at a particular SNR when compared to LS estimators. However, the 1-D MLE estimator is inferior to the 2-D channel estimator using the Wiener filter for $N_{frame}$ number of pilots that are spaced irregularly in time and frequency within the OFDM frame. In order to implement the Wiener filter, the CSI correlations in time and frequency are approximated using the sinc functions, with the first null being determined by the Doppler frequency and the maximum delay respectively. Simulation results show that the Wiener filter has improved SNR performance over the MLE 1-D estimator mainly due to the predictive function of the filter. However, 2-D estimators have a greatly increased computational complexity for the improved performance as numerous computations ($N_{frame}$ multiplications at each subcarrier) are required to evaluate each channel parameter in the OFDM frame. Because of this drawback, robust 1-D estimators are the focus of this thesis with optimized tracking of the time varying channel gain procured separately using the Kalman filter.

As a starting point to developing robust (optimal MSE performance for varying SNR) 1-D channel estimators for SU-MIMO-OFDM systems, the generic LS MIMO-OFDM channel estimator is derived and evaluated. This estimator represents a simple and accurate method of estimating the channel gain parameters based on pilot (training) sequences as well as the underlying convolution model of the frequency selective channel. The latter approach, also referred to as frequency-multiplex pilots (FMP) in the literature, may be argued to be bandwidth inefficient, since some sub-carriers must be assigned for pilots. However, alternative such as the Superimposed pilot (SIP) aided channel estimation (where data is linearly added to the pilots at a fraction of the total transmitted power) have performance limitation because the embedded data effectively acts as additive noise during channel estimation [54]–[59]. The spectral efficiency of the FMP approach adopted in this thesis can be improved by implementing channel tracking methods.

# Chapter 4

# Reduced Parameter Channel Estimation

*Get the facts right, you can distort them later - Mark Twain*

The frequency correlations of the channel parameters for the SISO-OFDM symbol can be used to develop low complexity receivers with robust Mean Square Error (MSE) performance. These frequency correlations are linked to the finite maximum delay of the channel between transmit and receive antenna in a multipath environment. The longer the maximum delay, the less the frequency correlations of the sub-carrier channel parameters and the more the number of parameters to be estimated. For multi-user MIMO-OFDM systems where the number of antennas to be trained is large, current methods of channel parameter estimation perform poorly.

This chapter introduces a generic MIMO-OFDM estimator that will be referred to as the Reduced Parameter Channel State Information (RP-CSI) estimator. The aim is to generate the MIMO-OFDM channel parameters (CSI) by using various methods that exploit the frequency correlations of the channel parameters. A basis that yields high SNR for low computation effort is one with few parameters that spans typical channel variation but is orthogonal to noise. Frequency correlations over OFDM sub-symbols are also examined.

## 4.1 CSI Frequency Correlations

It was noted in Section 3.1 that the channel parameters of a single MIMO-OFDM link (effectively SISO-OFDM) are the Fourier transform of the time domain CIR vector $\tilde{\mathbf{h}} = \mathbf{F}\mathbf{h}$. The Maximum Likelihood Estimator (Section 3.2.1) can be implemented for a single MIMO-OFDM link to exploit the frequency correlations of the channel. In this case, the FFT matrix $\mathbf{F}$ is separated into the "signal subspace" and the "noise subspace", and the vector of CSI for the single MIMO-OFDM link $\tilde{\mathbf{h}}$ can be re-written with the partitioning of the $\mathbf{F}$ matrix.

$$\tilde{\mathbf{h}} = \begin{bmatrix} \mathbf{F_h} & \mathbf{F_n} \end{bmatrix} \begin{bmatrix} \mathbf{h} \\ \mathbf{0} \end{bmatrix} \tag{4.1}$$

$\mathbf{0}$ is an $(N-L) \times 1$ null vector, and $N = K$ are the lengths of the column vector $\mathbf{h}$ and $\tilde{\mathbf{h}}$ respectively. $L$ is the maximum number of non-zero elements in the CIR vector which is found by dividing the maximum delay spread[1] $\tau_{max}$ by the symbol period $T_s$. The single MIMO-OFDM link (3.7–3.8) is therefore a *smooth* function of $L$ complex exponentials in the matrix $\mathbf{F_h} \in \mathbb{C}^{L \times N}$. This result can be evoked when solving for the CSI vector $\tilde{\mathbf{h}}$ using the basis $\mathbf{F}$ and reduced parameter set $\mathbf{h}$. The approach has been the focus of Least Squares MIMO-OFDM channel estimators and is presented in the literature [45],[46] and [69]. In this chapter, RP-CSI is generalized for the implementation of an arbitrary basis matrix $\mathbf{B}$ and reduced parameter set $\mathbf{w}$.

Before introducing the RP-CSI method, the measure of the "smoothness" of the single MIMO-OFDM wireless link in a multipath environment is discussed.

[1] the maximum delay spread is for the channel between MIMO antennas not the sub-carrier channels which are assumed to be flat fading

### 4.1.1 OFDM Frequency Correlations

Because the channel parameters of a single MIMO-OFDM link are the Fourier transform of the time domain CIR vector $\tilde{\mathbf{h}} = \mathbf{Fh}$, the vector of CSI $\tilde{\mathbf{h}}$ can be considered to be the channel frequency response. The strength of a relationship between channel parameter observations as a function of the frequency separation between them can be measured using the autocorrelation function. The autocorrelation function of the channel frequency response is given by

$$R(\Delta f) = \int_{-\infty}^{\infty} H(f)H^*(f + \Delta f)df \tag{4.2}$$

For channels with an exponential Power Delay Profile (PDP - Section 2.2.1) the autocorrelation can be computed as a statistical expectation. For a received signal with unity local mean power [37]

$$R(\Delta f) = E\left[H(f)H^*(f + \Delta f)\right] \tag{4.3}$$

The coherence bandwidth $B_{coh}$ gives a measure for the statistical average bandwidth over which the channel parameters are correlated. $B_{coh}$ is defined as the value of $\Delta f$ for which the autocorrelation function $R(\Delta f)$ of the channel frequency response has decreased by 3dB, which is half of peak power when the frequency deviation is zero.

$$\left.\frac{R(\Delta f)}{R(0)}\right|_{\Delta f = B_{coh}} = \frac{1}{2} \tag{4.4}$$

The coherence bandwidth $B_{coh}$ for the MIMO-OFDM antenna links can be related to the maximum delay spread of the channel. It was noted in Section 3.2.2 that the correlations of the OFDM channel gain parameters can be described approximately by a sinc function with a first null that is related to the maximum delay spread $\tau_{max}$ of the channel. In the next section, the maximum delay spread is shown to be inversely proportional to the coherence bandwidth. This implies that the greater the maximum delay spread $\tau_{max}$, the less the coherence bandwidth $B_{coh}$, and the more rapid are the channel parameter variations in frequency.

### 4.1.2 Effects of Multipath on Frequency correlations

This section is concerned with the relationship between the Power Delay Profile (PDP) cf. (4.5) and the correlation of the channel gain at particular sub-carrier frequencies cf. (4.3). The PDP was defined in Section 2.2.1 as the average received power as a function of delay $\tau$. This definition assumed that the channel has zero Doppler spread or equivalently that the transmitter and receivers are stationary [26]. In this thesis, it is assumed that the data rate is high and the channel remains constant during the transmission of an OFDM symbol. Zero Doppler spread of the channel can also be assumed in this instance.

$$p(\tau) = R_{\bar{\gamma}}(\tau, 0) = E\left[|\bar{\gamma}^*(\tau, t)|^2\right] \tag{4.5}$$

The WSSUS assumption means that the vector CIR $\mathbf{h}$ has uncorrelated elements so that $R_{\bar{\gamma}}(\tau_n, \tau_{n+k}, 0) = R_{\bar{\gamma}}(\tau_n, 0)\delta(\tau_n - \tau_{n+k})$. However, the CSI vector $\tilde{\mathbf{h}} = \mathbf{F}\mathbf{h}$ has elements $H[k]$ that are correlated within a bandwidth

$$B_{coh} \approx \frac{1}{\tau_{max}} \tag{4.6}$$

Such correlations can be modeled using the sinc function [67] which is a function of the maximum delay spread $\tau_{max}$ and the RF bandwidth of each sub-carrier $F_s$ cf. Section (3.2.2). From this definition we can re-classify the frequency selective and frequency flat channels described in Section 2.2.2 as follows

- Channels are said to exhibit frequency selective fading if the bandwidth per symbol $B = 1/2T_s$ is greater than the coherence bandwidth $B_{coh}$, $B > B_{coh}$.

- A channel is said to exhibit flat fading if the bandwidth per symbol $B$ is much smaller than the coherence bandwidth, $B \ll B_{coh}$.

The narrow band sub-carrier channels of a well designed MIMO-OFDM system are thus considered flat fading. The result (4.6) show how the Power Delay Profile, which indicates the extent of the multipath propagation for a wireless channel, can be related to the correlation of the channel gain at different sub-carrier frequencies. Section 4.3.2 shows how such correlations can be exploited to form channel estimates.

## 4.2 RP-CSI Basis Functions

The correlations of the CSI parameters in the vector $\tilde{\mathbf{h}}$ are determined by the maximum delay spread of the multipath channel $\tau_{max}$. When the elements of the CSI vector are highly correlated, an arbitrary Basis matrix $\mathbf{B}$ can be used to generate each MIMO-OFDM channel vector $\tilde{\mathbf{h}}$ through the transformation $\tilde{\mathbf{h}} = \mathbf{B}\mathbf{w}$. $\mathbf{w}$ is a column vector of the transform coefficients. Just as with the Fourier basis, the matrix $\mathbf{B}$ can be separated into the "signal subspace" and the "noise subspace". The CSI vector $\tilde{\mathbf{h}}$ can be re-written with the partitioning of the $\mathbf{B}$ matrix as follows

$$\tilde{\mathbf{h}} = \left[ \begin{array}{cc} \mathbf{B_w} & \mathbf{B_n} \end{array} \right] \left[ \begin{array}{c} \mathbf{w} \\ \mathbf{0} \end{array} \right] = \mathbf{B_w}\mathbf{w} \tag{4.7}$$

For a well designed basis, $\mathbf{0} \in \mathbb{C}^{(K-n_w)\times 1}$ is a null vector whose length $n_w$ is such that $n_w \ll K$ where $K$ is the length of the column vector $\tilde{\mathbf{h}}$ for a single MIMO-OFDM channel. Such a basis provides improved orthogonality to AWGN resulting in improved MSE for the channel estimator. In addition, the efficient representation of the MIMO-OFDM channel vector $\tilde{\mathbf{h}}$ has performance implications for MU-MIMO-OFDM systems when the number of antennas to be trained is large. The basis is orthogonal to noise when the CSI estimator rejects arbitrarily strong unwanted signals. It should be noted that orthogonality is never absolute as signal subspace is a within the noise subspace and the MSE of the estimator is a function of the noise variance [69], [70].

### 4.2.1 Wavelet Basis

This section describes how the wavelets transform can be used to reduce the number of channel estimation parameters, and hence lead to RP-CSI parameter estimation. As a starting point, the implementation of the discrete wavelet transform based on finite impulse response (FIR) filters is introduced, but the final RP-CSI implementation is achieved through vectorization of the wavelet synthesis and analysis equations.

The decomposition (analysis) coefficients in a wavelet orthogonal basis are computed with a fast algorithm that cascades discrete convolutions with the filters $\{h[n]\}$ and $\{g[n]\}$ and sub-samples the output[2] [60] (cf. Figure 4.1). The wavelet decomposition of a discrete CSI vector $\{H_i[k]\} \in \mathbb{C}^{K\times 1}$ at each cascade level $j \in \{0, 1, \dots, j_{max}\}$ can be written as the inner product.

$$a_j[l] = \sum_{n=0}^{2^{-j}K-1} H_i[2l+n]h[n] = (H_i * h)[2l] \tag{4.8}$$

$$= \langle H_i[2l+n], h[n]\rangle \tag{4.9}$$

$$d_j[l] = \sum_{n=0}^{2^{-j}K-1} H_i[2l+n]g[n] = (H_i * g)[2l] \tag{4.10}$$

$$= \langle H_i[2l+n], g[n]\rangle \tag{4.11}$$

There are $\frac{K}{2}$ decomposition coefficients $\{a_j[l] : l = 0, 1, \dots, \frac{K}{2} - 1\}$ and $\frac{K}{2}$ decomposition coefficients $\{d_j[l] : l = 0, 1, \dots, \frac{K}{2} - 1\}$ calculated at the first cascade level $j = 0$. Higher level wavelet decompositions are performed on the $\{a_j\}$ samples only (cf. Figure 4.1), hence the summation in equation 4.8 is

[2]these are the so called "wavelet filter" banks of the discrete wavelet transform.

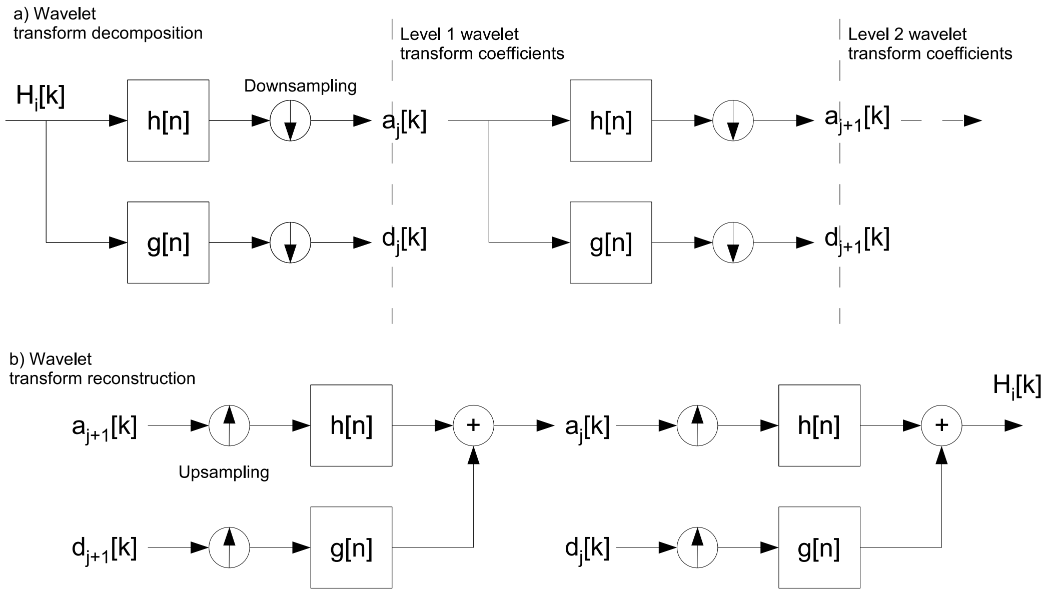


Figure 4.1: a) Wavelet filter banks for the decomposition and b) reconstruction of the CSI vector $\{H_i[k]\}$. The coefficients $d_j[n]$ are vanishingly small at the higher levels $j$ compared to $a_j[n]$.

performed over half as many samples ($a_j[n]$ replaces $H_i[n]$ in the equations 4.8 and 4.10) as at the previous level.

Note that $(x * y)[n] = \sum_{k=0}^{2^{-j}K-1} x[n+k]y[k]$ represents the $n$th element of the convolution of a signal vector $\{x[n]\}$ and general coefficient vector $\{y[n]\}$, where the elements of the later are in reverse order. In this thesis, $\{h[k]\}$ and $\{g[k]\}$ are the Daubechies filter coefficients [62] which are related via $g[k] = (-1)^{k-1}h[N-k+1]$. For example, the Daubechies filter coefficients $D4$ (The Daubechies filter coefficients $DN$ have $N$ non-zero elements) are $h[k] \equiv \left[\frac{1-\sqrt{3}}{4\sqrt{2}}, \frac{3-\sqrt{3}}{4\sqrt{2}}, \frac{3+\sqrt{3}}{4\sqrt{2}}, \frac{1+\sqrt{3}}{4\sqrt{2}}\right]$ and $g[k] \equiv \left[\frac{-1-\sqrt{3}}{4\sqrt{2}}, \frac{3+\sqrt{3}}{4\sqrt{2}}, \frac{-3+\sqrt{3}}{4\sqrt{2}}, \frac{1-\sqrt{3}}{4\sqrt{2}}\right]$ respectively. The maximum number of cascade levels that can be computed using the Daubechies filter coefficients $DN$ is given by $j_{max} = \log_2\left(\frac{N}{K}\right)$, where $N$ is the number of coefficients and $K$ is the number of OFDM subcarriers. The limit on the maximum number of cascade levels is incumbent on the matrix formulations presented in the following section.

The convolution operation in equations 4.8 and 4.10 can also be written as a dot product of the signal vector and coefficient vector (cf. 4.9 and 4.11). The dot product form of wavelet decomposition (which leads to matrix manipulations) will be used for CSI estimation in Section 4. Based on equations 4.8–4.11, consider the wavelet decomposition of a CSI vector resulting from the implementation of an 4 subcarrier OFDM modulation scheme in a single antenna system. The maximum number of cascade levels that can be computed using the Daubechies filter coefficients $D4$ is $j_{max} = \log_2(1) = 0$ i.e. a single level at $j = 0$. At each cascade level, the length of the vectors $\{h[k]\}$ and $\{g[k]\}$ are augmented by zero padding to obtain length $2^{-j}K$ vectors. However, according to equations 4.8 and 4.10, the calculation of the wavelet decomposition coefficients $a_0[1]$ and $d_0[1]$ presents a problem as it requires multiplication with CSI vector elements that do not exist (cf. 4.12).

$$\begin{bmatrix} a_0[0] \\ a_0[1] \\ d_0[0] \\ d_0[1] \end{bmatrix} = \begin{bmatrix} h[0] & h[1] & h[2] & h[3] & & \\ 0 & 0 & h[0] & h[1] & h[2] & h[3] \\ g[0] & g[1] & g[2] & g[3] & & \\ 0 & 0 & g[0] & g[1] & g[2] & g[3] \end{bmatrix} \begin{bmatrix} H[0] \\ H[1] \\ H[2] \\ H[3] \end{bmatrix} \tag{4.12}$$

In this thesis, this edge problem is overcome by assuming that the CSI vector is periodic, in other words the beginning of the CSI vector repeats after the last element. Several other alternative approaches are considered in the literature [63] but the one adopted here, despite being simple to implement, does not lead to any significant errors in CSI vector reconstruction (synthesis). This matrix formulation for the algorithm chosen to overcome the wrap around problem (cf. 4.122) indicates why a limit has been imposed on the maximum number of cascade level - no further wrapping around is possible.

$$\begin{bmatrix} a_0[0] \\ a_0[1] \\ d_0[0] \\ d_0[1] \end{bmatrix} = \begin{bmatrix} h[0] & h[1] & h[2] & h[3] \\ h[2] & h[3] & h[0] & h[1] \\ g[0] & g[1] & g[2] & g[3] \\ g[2] & g[3] & g[0] & g[1] \end{bmatrix} \begin{bmatrix} H[0] \\ H[1] \\ H[2] \\ H[3] \end{bmatrix} \tag{4.13}$$

$$\mathbf{w} = \mathbf{B}^T\mathbf{h} \tag{4.14}$$

The CSI vector $\{H_i[k]\}$ is reconstructed from the wavelet coefficients through up-sampling and convolution of the level $j = 0$ wavelet coefficients (c.f Figure 4.1). Upsampling [64] can be defined as follows: given a general vector of coefficients $y[p]$, where the index $p$ is such that $p \in \{0, 1, \ldots, K/2 - 1\}$, the up-sampled coefficients $\check{y}[n]$ with index $n$ such that $n \in \{0, 1, \ldots, K - 1\}$ can be written as follows

$$\check{y}[n] = \begin{cases} y[p] & \text{if } n = 2p \\ 0 & \text{if } n = 2p + 1 \end{cases} \tag{4.15}$$

In order to upsample the coefficients vector, each value of the index $p$ is applied to two different functions and the results compared to a single value of the index $n$ [64]. The value assigned to the upsampled vector $\check{y}[n]$ depends on conditions set on the equity of the two functions and the value of $n$. The process is repeated for the next value of $p$, until $2p = K-2$ and $2p+1 = K-1$. Note that the reconstructed CSI vector $\{H_i[k]\}$ is the sum of the output of the wavelet synthesis filters.

$$H_i[n] = \sum_{l=0}^{\frac{K}{2}-1} \check{a}_0[n-l]h[l] + \sum_{l=0}^{\frac{K}{2}-1} \check{d}_0[n-l]g[l] \tag{4.16}$$

$$= (\check{a}_0 * h)[l] + (\check{d}_0 * g)[l] = \langle \check{a}_0[n-l], h[l] \rangle + \langle \check{d}_0[n-l], g[l] \rangle \tag{4.17}$$

The convolution in the synthesis equation 4.16 differs from the convolution in the analysis equations 4.8–4.11, because the latter requires a lag (negative) delay rather than a lead (positive) delay. The reason why this formulation is adopted in this thesis is that it results in an inverse transformation matrix that is the transpose of the forward transformation matrix $\mathbf{B}^T$ (cf. 4.14). Assuming that the analysis coefficients are periodic *after* up-sampling, the system of synthesis equations is simply $\mathbf{h} = \mathbf{B}\mathbf{w}$. The reconstruction process in equation 4.16 recovers the $K$ elements of the vector $\{H_i[k]\}$ from $\frac{K}{2}$ coefficients $\{a_j[l]\}$ and $\{d_j[l]\}$.

For multilevel synthesis, the wavelet synthesis samples ($a_j$ and $d_j$) are determined from lower level synthesis samples samples ($a_{j+1}$ and $d_{j+1}$, where the level $j = 0$ is the highest level). The filters/coefficients $\{h[n]\}$ and $\{g[n]\}$ are chosen such that the energy of the signal from the decomposition using the coefficients $d_j[n]$ is vanishingly small compared to the energy of the signal from the decomposition using the coefficients $a_j[n]$ [61]. Note that because $\{d_j\}$ are small compared to $\{a_j\}$ the synthesis equations can be written as

$$\tilde{\mathbf{h}} \approx \begin{bmatrix} \mathbf{B_w} & \mathbf{B_n} \end{bmatrix} \begin{bmatrix} \mathbf{w} \\ \mathbf{0} \end{bmatrix} = \mathbf{B_w}\mathbf{w} \tag{4.18}$$

where $\mathbf{w} \equiv \{a_j\}$ and $\mathbf{0} \approxeq \{d_j\}$ is true for wavelet basis at a given level. Using the proposed scheme, the number of CSI parameters is halved at each level so that if $j = 3$, 16 coefficients can be used to generate the full set of 128 CSI unknowns for each channel cf. Figure 4.2. However, the error incurred in reconstructing the CSI vector $\{H_i[k]\}$ from the reduced parameter set depends ultimately on the design of the wavelet coefficients.

### 4.2.2 Principal Component Analysis Basis

The Principal Component Analysis (PCA) basis developed in this section exploits time and frequency correlations of a single MISO-OFDM channel vector. In the literature [65], the autocorrelation of the channel, i.e., its second-order statistic, is assumed to be known, and a Karhunen–Love transform (PCA) is

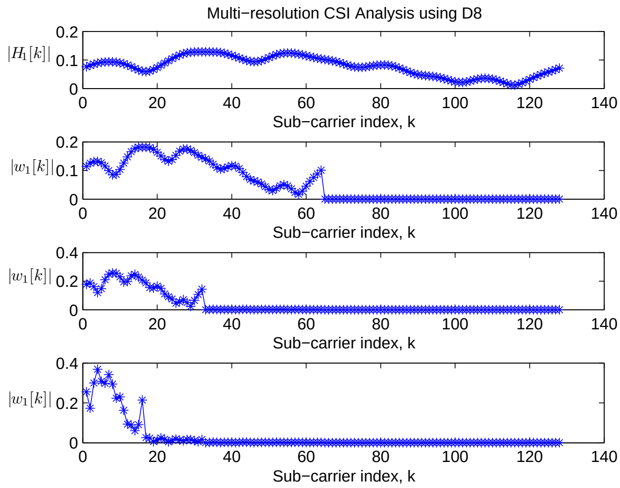


Figure 4.2: The multi-resolution analysis of a vector of CSI using the D8 wavelet.

applied. In this thesis, no assumption are made on the autocorrelation of the channel, and the PCA basis is derived from measurements. It can be shown that the eigen functions of the Saleh-Valenzuela channel covariance matrix are the Fourier transform exponentials cf. Appendix A.

The PCA basis can be generated from a matrix of MISO-OFDM vectors for a single transmit antenna where each column corresponds to the CSI for the $K$ sub-carriers of the MISO-OFDM channel and each row corresponds to the CSI for the $k$th sub-carrier for the $m$th channel parameter estimates.

$$\tilde{\mathbf{X}}_{\mathsf{T}} = \begin{bmatrix} H_i[0,0] & H_i[0,1] & \dots & H_i[0,M] \\ H_i[1,0] & H_i[1,1] & \dots & H_i[1,M] \\ \vdots & \vdots & \ddots & \vdots \\ H_i[K-1,0] & H_i[K-1,1] & \dots & H_i[K-1,M] \end{bmatrix} \tag{4.19}$$

The columns $\{H_i[k,m]\}$ are assumed to be in mean-deviation form (see Theorem 4.1) and are determined from $M$ channel measurements. The PCA basis is a matrix that transforms the CSI measurements in the matrix $\tilde{\mathbf{X}}_{\mathsf{T}}$ to another matrix $\mathbf{W}$ such that

$$\mathbf{W} = \mathbf{B}\tilde{\mathbf{X}}_{\mathsf{T}} \tag{4.20}$$

Note that matrices $\mathbf{W} \equiv [\mathbf{w}_1, \mathbf{w}_2, \cdots, \mathbf{w}_M]$ and $\tilde{\mathbf{X}}_{\mathsf{T}} \equiv \left[\tilde{\mathbf{h}}_1, \tilde{\mathbf{h}}_2, \cdots, \tilde{\mathbf{h}}_M\right]$ contain the transformation and CSI vectors respectively. The PCA basis $\mathbf{B}$ is chosen to diagonalize the covariance matrix $\mathbf{C}_{\mathbf{W}} = \frac{1}{(M-1)}\mathbf{W}\mathbf{W}^T$. It can be shown that the basis $\mathbf{B}$ can be generated from the measurement matrix $\tilde{\mathbf{X}}_{\mathsf{T}}$, such that $\mathbf{C}_{\mathbf{W}}$ is diagonal. We can begin by writing $\mathbf{C}_{\mathbf{W}}$ in terms of $\mathbf{B}$.

$$\begin{aligned}
\mathbf{C}_{\mathbf{W}} &= \frac{1}{(M-1)}\mathbf{W}\mathbf{W}^T && (4.21)\\
&= \frac{1}{(M-1)}(\mathbf{B}\tilde{\mathbf{X}}_{\mathsf{T}})(\mathbf{B}\tilde{\mathbf{X}}_{\mathsf{T}})^T && (4.22)\\
&= \frac{1}{(M-1)}\mathbf{B}(\tilde{\mathbf{X}}\tilde{\mathbf{X}}_{\mathsf{T}})^T\mathbf{B}^T && (4.23)\\
&= \frac{1}{(M-1)}\mathbf{B}\mathbf{C}_{\tilde{\mathbf{X}}_{\mathsf{T}}}\mathbf{B}^T && (4.24)\\
& && (4.25)
\end{aligned}$$

If we select $\mathbf{B}$ such that each row is an eigenvector of $(\tilde{\mathbf{X}}_{\mathsf{T}}\tilde{\mathbf{X}}_{\mathsf{T}}^T)$, which implies $\mathbf{B} = \mathbf{E}^T$ and $\mathbf{C}_{\tilde{\mathbf{X}}_{\mathsf{T}}} = \mathbf{B}^T\mathbf{D}\mathbf{B}$ such that $\mathbf{D} \equiv \mathsf{diag}(\lambda_0, \lambda_1, \ldots, \lambda_{K-1})$, then we can write

$$\begin{aligned}
\mathbf{C}_{\mathbf{W}} &= \frac{1}{(M-1)}\mathbf{B}(\mathbf{B}^T\mathbf{D}\mathbf{B})\mathbf{B}^T && (4.26)\\
&= \frac{1}{(M-1)}(\mathbf{B}\mathbf{B}^T)\mathbf{D}(\mathbf{B}\mathbf{B}^T) && (4.27)\\
&= \frac{1}{(M-1)}\mathbf{D} && (4.28)
\end{aligned}$$

**Theorem 4.1** For a given MISO-OFDM CSI vector $\tilde{\mathbf{h}}_i \equiv [H_i[0], H_i[1], \ldots, H_i[K-1]]^T$, with $\tilde{\mathbf{h}}_i \sim (\mu, \mathbf{E})$, the PCA vector $\mathbf{w}_i = \mathbf{E}^T(\tilde{\mathbf{h}}_i - \mu)$ has the properties (the vector $(\tilde{\mathbf{h}}_i - \mu)$ is in mean-deviation form [68])

$$var(\mathbf{w}_i[k]) = \lambda_k \tag{4.29}$$

$$cov(\mathbf{w}_i[k]) = 0 \tag{4.30}$$

$$var(\mathbf{w}_i[1]) \geq var(\mathbf{w}_i[2]) \geq \cdots \geq var(\mathbf{w}_i[K-1]) \geq 0 \tag{4.31}$$

**Proof**: The equations (4.29–4.31) are all proven in the result (4.28).

For $M$ MISO-OFDM CSI estimates for a given transmit antenna, the eigenvalues of the basis vector decay rapidly (Figure 4.3) due to the exponential power delay profile cf. Appendix A. The coefficients derived from the transformation $\mathbf{w}_i[m] = (\mathbf{B}\tilde{\mathbf{h}}_i)[k]$ therefore have a maximum variance of $\lambda_m$ and there are at most $M \leq K$ non-zero coefficients. The results are true for any vector $\tilde{\mathbf{h}}_i$ that results in the covariance matrix $\mathbf{C_W}$.

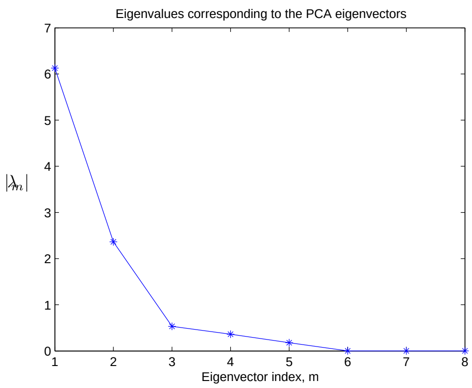


Figure 4.3: Eigenvalues for the PCA basis based on 32 sets of channel parameter estimates.

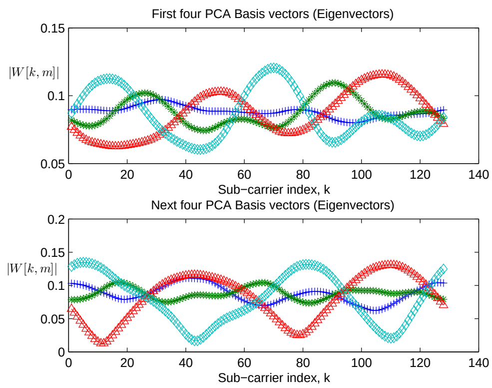


Figure 4.4: Eigenvectors for the PCA basis based on 32 sets of channel parameter estimates.

To obtain the results in Figures (4.3–4.4), it is assumed that the relative delays of the multipath components remain relatively constant over multiple OFDM symbols, whilst the amplitudes and phase of multipath components vary rapidly as indicated in the literature [87].

# 4.3 The Proposed Method

This section introduces two effective Reduced Parameter Channel State Information (RP-CSI) estimators. The OFDM symbol based estimators exploit the correlations of CSI elements across all the sub-carriers, and can achieve a significant reduction in the channel parameter estimates. However, there is a limit beyond which a reduction in the number of channel parameter estimates results in an irreducible error in the Mean Square Error (MSE). For example, the number of parameters below which an irreducible error in the MSE occurs for the Fourier basis is $L$, the maximum number of non-zero elements in the Channel Impulse Response (CIR) vector. Using the Saleh-Valenzuela model which predicts a maximum delay spread $\tau_{max} = 200$ns, and for a symbol period of $T_s = 10$ns, the expected maximum length of the CIR vector $L = \tau_{max}/T_s = 20$. An alternative to the OFDM symbol based estimators is the OFDM sub-symbol based estimators which exploit the strong correlations of CSI over a few sub-carriers to form channel estimates. It is shown that the performance of such estimators is limited by the knowledge of CSI correlations over the coherence bandwidth.

## 4.3.1 OFDM Symbol based correlations

In this section we develop a RP-CSI estimator that exploit the channel correlation in frequency so as to reduce the number of unknowns for each MISO-OFDM channel $\tilde{\mathbf{h}}_i$. We will refer to the vectors of CSI for channels from a given transmit antenna: $\tilde{\mathbf{h}}_i \equiv [H_i[0]\ H_i[1]\ \cdots\ H_i[K-1]]^T \in \mathbb{C}^{K\times 1}$ where the superscript $T$ denotes transposition, and the vectors of CSI for a given sub-carrier: $\tilde{\mathbf{h}}[k] \equiv [H_1[k]\ H_2[k]\ \cdots\ H_{n_t}[k]]^T \in \mathbb{C}^{n_t\times 1}$. These vectors are re-arrangements of the same parameters $\{H_i[k]\}$. Collecting the CSI for all transmit antennas and all sub-carrier yields two vectors:

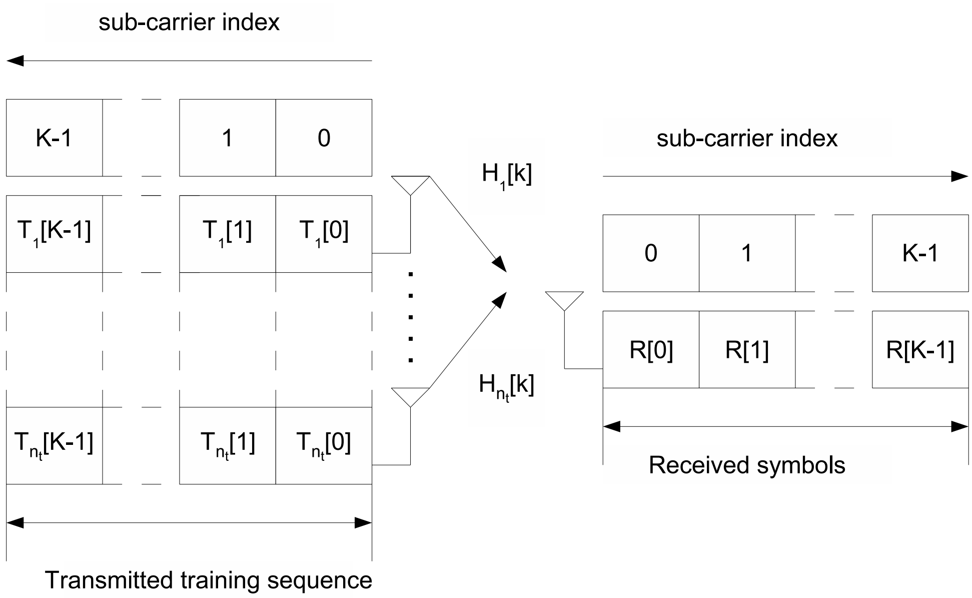


Figure 4.5: The MIMO-OFDM system.

$$\tilde{\mathbf{h}}_{\mathsf{S}} \equiv \left[\tilde{\mathbf{h}}^T[1], \tilde{\mathbf{h}}^T[2], \ldots, \tilde{\mathbf{h}}^T[K]\right]^T \in \mathbb{C}^{n_t K \times 1} \tag{4.32}$$

$$\tilde{\mathbf{h}}_{\mathsf{F}} \equiv \left[\tilde{\mathbf{h}}_1^T, \tilde{\mathbf{h}}_2^T, \ldots, \tilde{\mathbf{h}}_{n_t}^T\right]^T \in \mathbb{C}^{n_t K \times 1} \tag{4.33}$$

The subscript $\mathsf{F}$ indicates the parameters occur in sub-carrier order and $\mathsf{S}$ indicates the parameters occur in transmit antenna order. The vectors $\tilde{\mathbf{h}}_{\mathsf{F}}$ and $\tilde{\mathbf{h}}_{\mathsf{S}}$ contain the same information and are related by the orthonormal, square, permutation matrix $\mathbf{P} : \tilde{\mathbf{h}}_{\mathsf{S}} = \mathbf{P}\tilde{\mathbf{h}}_{\mathsf{F}}$.

Consider the CSI estimation problem for the MISO system as illustrated in Figure 4.5. During a single OFDM symbol period of duration $KT_s$ a training sequence is transmitted consisting of QAM symbol $T_i[k]$ from transmit antenna $i$ on sub-carrier $k$. Our objective is to estimate the vector of CSI $\mathbf{h}_{\mathsf{F}}$, cf. (4.33), based on the vector of received OFDM symbol $\tilde{\mathbf{r}} \equiv \{R[k]\}_{k=0,1,\ldots,K-1}$. When no noise is present, these vectors are related by the linear expression

$$\tilde{\mathbf{X}}\tilde{\mathbf{h}}_{\mathsf{S}} = \tilde{\mathbf{r}} \tag{4.34}$$

where

$$\tilde{\mathbf{X}}^T \equiv \begin{bmatrix} \tilde{\mathbf{t}}_{\mathsf{S},1} & \mathbf{0} & \cdots & \mathbf{0} \\ \mathbf{0} & \tilde{\mathbf{t}}_{\mathsf{S},2} & \cdots & \mathbf{0} \\ \vdots & \vdots & \ddots & \vdots \\ \mathbf{0} & \mathbf{0} & \cdots & \tilde{\mathbf{t}}_{\mathsf{S},K} \end{bmatrix} \in \mathbb{C}^{n_t K \times K} \tag{4.35}$$

and $\mathbf{0} \in \mathbb{R}^{n_t \times 1}$ and $\tilde{\mathbf{t}}_{\mathsf{S},k}$ are the vectors of training symbols transmitted from the antennas over sub-carrier $k$, i.e.,

$$\tilde{\mathbf{t}}_{\mathsf{S},k} \equiv [T_1[k] \; T_2[k] \; \cdots \; T_{n_t}[k]]^T \in \mathbb{C}^{n_t \times 1}. \tag{4.36}$$

For a system with $n_t = 1$, (4.35) is square and has full rank, and hence (4.34) has a unique solution. For $n_t > 1$, it is *underdetermined* and has an infinite number of solutions.

It is however possible to put constraints on the solution of the linear system (4.34) so that it can be solved in the LS sense using the Moore-Penrose inverse yielding a unique solution. Consider the introduction of the reduced basis approximation, i.e., $\tilde{\mathbf{h}}_{\mathsf{F},i} \cong \sum_{j=1}^{n_w} w_j \mathbf{b}_j$, which we can also write as

$$\tilde{\mathbf{h}}_{\mathsf{F},i} = \mathbf{B}_i \mathbf{w}_i \tag{4.37}$$

where $\mathbf{B}_i \equiv [\mathbf{b}_1 \; \mathbf{b}_2 \; \cdots \mathbf{b}_{n_w}] \in \mathbb{C}^{K \times n_w}$ and $\mathbf{w}_i \equiv \{w_i\} \in \mathbb{C}^{n_w \times 1}$ is a vector of basis weights describing CSI variation for the channels from transmit antenna $i$. Collecting the basis weight vectors for each antenna into a single vector yields

$$\tilde{\mathbf{h}}_{\mathsf{F}} = \mathbf{B}\mathbf{w} \tag{4.38}$$

where $\mathbf{B} \equiv \mathtt{diag}(\mathbf{B}_1, \mathbf{B}_2, \ldots, \mathbf{B}_{n_t}) \in \mathbb{C}^{n_t K \times n_t n_w}$ is a block-diagonal matrix and $\mathbf{w} \equiv \left[\mathbf{w}_1^T, \mathbf{w}_2^T, \ldots, \mathbf{w}_{n_t}^T\right]^T \in \mathbb{C}^{n_t n_w \times 1}$. Substituting this into (4.34) gives

$$\tilde{\mathbf{X}}\mathbf{P}\mathbf{B}\mathbf{w} = \tilde{\mathbf{r}}. \tag{4.39}$$

Equation 6.13 is an *overdetermined* system, with a reduced number of parameters $\mathbf{w}$ to be determined that generate the vector $\tilde{\mathbf{h}}_{\mathsf{F}}$ given a basis matrix $\mathbf{B}$. A minimum norm solution can be found using the Moore-Penrose inverse for an overdetermined system, i.e., if $\mathbf{A}\mathbf{x} = \mathbf{b}$, then the Moore-Penrose solution is $\left(\mathbf{A}^H\mathbf{A}\right)^{-1}\mathbf{A}^H\mathbf{b}$. Applying this method to (6.13), we have

$$\mathbf{w} = \left((\mathbf{XPB})^H \mathbf{XPB}\right)^{-1} (\mathbf{XPB})^H \tilde{\mathbf{r}}. \tag{4.40}$$

Due to the choice of the training sequence $\tilde{\mathbf{X}}$ and if $\mathbf{B}$ is the Fourier Basis, the matrix product to be inverted is the identity matrix (see section **??**). In other words if $\mathbf{Q} = (\tilde{\mathbf{X}}\mathbf{PB})^H$ then $\mathbf{Q}\mathbf{Q}^H = \mathbf{I}$, so that a solution for $\mathbf{w}$ may be calculated without matrix inversion, i.e.,

$$\mathbf{w} = \mathbf{Q}\tilde{\mathbf{r}}. \tag{4.41}$$

Moreover, the matrix $\mathbf{Q} = (\mathbf{XPB})^H$ may be calculated once and if $\mathbf{q}_i$ is the $i$th row of $\mathbf{Q}$, then (4.41) may be written as

$$\mathbf{w} = \sum_{i=1}^{K} R[i]\mathbf{q}_i. \tag{4.42}$$

The construction above is valid for any set of basis functions $\mathbf{B}$. For the PCA basis, there is an important alteration to be made to the RP-CSI framework above. The empirical mean is subtracted from the CSI for a antenna so that

$$\tilde{\mathbf{h}}_{\mathsf{F,i}} = \hat{\tilde{\mathbf{h}}}_{\mathsf{F,i}} + \mu_i \tag{4.43}$$

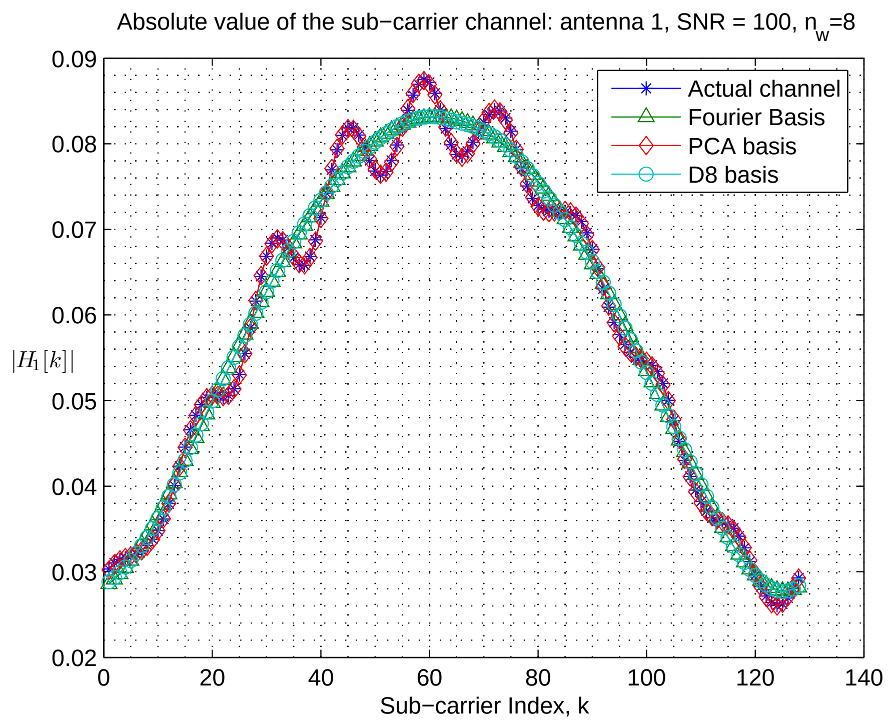


Figure 4.6: $|H_1[k]|$ for a (2,1) MISO-OFDM system based on the Fourier, PCA and Daubechies basis estimators. SNR=100dB, $n_w = 8$.

The vector $\mu_i \in \mathbb{C}^{K\times 1}$ is derived from a small set of measured CSI for each antenna. Also $\mathbf{QQ}^H \neq \mathbf{I}$ for the PCA basis and the wavelet basis. A basis that yields high SNR for low computation effort is one with few vectors that spans typical channel variation but is orthogonal to noise. In general noise and natural variation will not be totally separable and so a compromise is necessary.

Note that channel fades independently for the channel between the receiver and transmit antennas 1 and 2 in figure 3.7–3.8. The PCA basis outperforms the Fourier and the Daubechies because it provides the most compact representation of the CSI variations. Based on just $n_w = 8$ channel estimation parameters, the PCA basis is able to track the variation in CSI for each sub-carrier. The results above assume that the $p$th user is equipped with $n_t^p = 2$

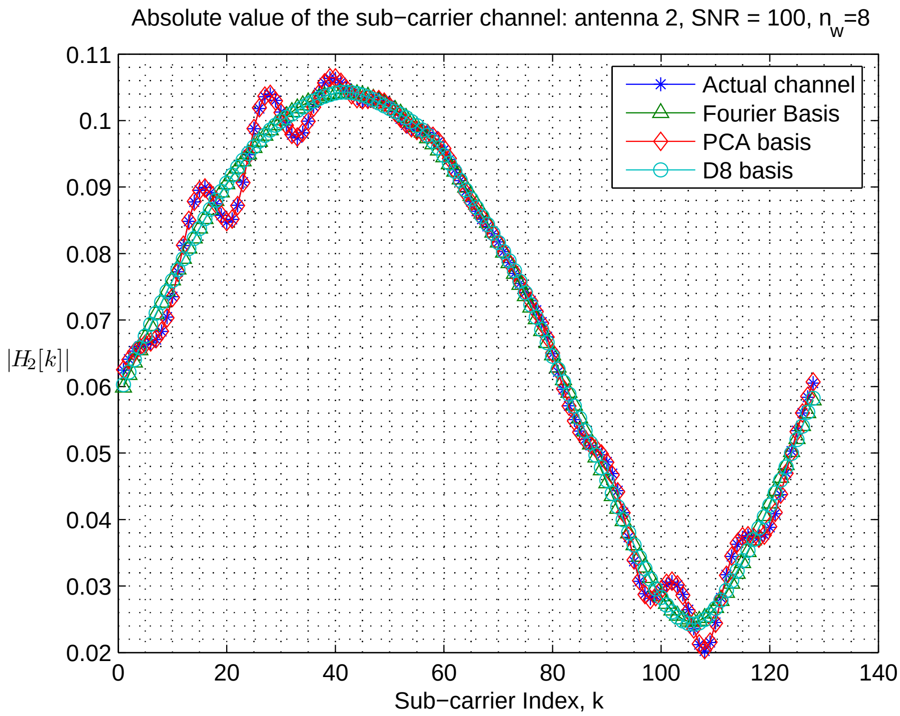


Figure 4.7: $|H_2[k]|$ for a (2,1) MISO-OFDM system based on the Fourier, PCA and Daubechies basis estimators SNR=100dB, $n_w = 8$.

number of transmit antennas and that $K = 128$.

### 4.3.2 OFDM sub-symbol based correlations

This section describes an effective MIMO-OFDM channel estimator that has been implemented in a Gigabit MIMO-OFDM prototype in the literature [51]. The estimator is based on the use of an orthogonal training sequence such as the Hadamard sequence and the correlations of MIMO-OFDM channels over OFDM sub-symbols ($K_{coh}$ sub-carriers) within a length $K$ OFDM symbol, where ($K_{coh} \ll K$). It was noted in Chapter 3 that the correlation of the OFDM CSI in frequency can be approximated by a sinc function, where the first null is related to the maximum delay spread ($\tau_{rms}$) of the channel. This result was used to develop the Wiener filter cf. (3.28) which was found to improve the MSE performance of a SISO-OFDM estimator at the cost of increased computational complexity at the receiver.

The concept of coherence bandwidth is particularly useful when describing the wireless channel for a multi-carrier system such as OFDM. To reiterate, the main advantage of OFDM is to eliminate Inter-Symbol Interference (ISI), which results when the duration of the transmitted symbol is shorter than the maximum delay of the wireless channel. ISI is eliminated by sending several symbols in parallel using evenly spaced carriers (referred to as sub-carriers), so that each symbol is transmitted for a longer duration. However, the channel is frequency selective, meaning that the Fourier transform of the Channel Impulse Response (CIR) is not flat. This in turn implies that the gain experienced by different sub-carriers varies as has been observed in the Chapter 3 for 1-D and 2-D channel estimation. The relationship between the maximum delay of the channel and correlation of the channel gain at different frequencies can be intuitively understood as follows: if the maximum delay is zero, the FFT of the CIR is unity for all frequencies from Fourier transform theory [11]. On the other hand, if the maximum delay is finite and non-zero, then the FFT of the CIR varies with frequency. The FFT of the CIR is the frequency response of the channel, that is, a description of how the channel gain varies with frequency, and the channel gain correlations can be derived from the resulting channel frequency response cf. Appendix C.

A rectangular CIR can be shown to result in a sinc correlation function as in Appendix C. If the power delay profile is the rectangular function

$$p(\tau) = \begin{cases} \frac{1}{\tau_{max}} & \text{if } |\tau| < \frac{1}{\tau_{max}} \\ 0 & \text{otherwise} \end{cases} \tag{4.44}$$

then the autocorrelation function is the sinc function.

$$R(\Delta f) = R\left((k - \acute{k})F_s\right) = \frac{\sin\left(\pi\tau_{max}(k - \acute{k})F_s\right)}{\pi\tau_{max}(k - \acute{k})F_s} \tag{4.45}$$

are well known Fourier transform duals [11],[67]. This observation motivates the *OFDM sub-symbol* based MIMO-OFDM channel estimators. The idea is that if the CSI is invariant for $K_{coh}$ sub-carriers, then a reduction in the number of CSI unknowns is possible leading to an accurate estimate of the CSI over $K_{coh}$ sub-carriers.

If the MIMO-OFDM system is equipped with $n_t$ transmit antennas and the channel estimation is performed at single receive antenna, the CSI $H_i[k]$ corresponding to the $i$th transmit antenna at the sub-carrier $k = k_0$ can be approximated by

$$\hat{H}_i[k_0] = \sum_{i=1}^{K_{coh}} R[k_0 + i - 1]T_i^*[k_0 + i - 1] \; \forall \, k_0 = 0, K_{coh}, \ldots, K - 1 \tag{4.46}$$

$z^*$ is the complex conjugate of a complex number $z$. For the MISO-OFDM system, the received QAM symbol is given by $R[k] = \sum_{i=1}^{n_t} H_i[k]T_i[k]$. The Hadarmard training sequence is an orthogonal training sequence such that

$$\sum_{k=k_0}^{k_0+K_{coh}-1} T_i[k]T_j^*[k] = \begin{cases} 1 & \text{if } i = j \\ 0 & \text{otherwise} \end{cases} \tag{4.47}$$

If the difference between the CSI for the $k$th sub-carrier and the $k_0$ sub-carrier is denoted by $\Delta\mathcal{H}_i^{k,k_0} = H_i[k] - H_i[k_0]$, the estimated CSI cf. (4.46) becomes

$$\hat{H}_i[k_0] = H_i[k_0] + \sum_{m=0}^{n_t-1}\sum_{n=0}^{K_{coh}-1} \Delta\mathcal{H}_{m+1}^{k_0+n,k_0} T_{i+m}[k_0+n]T_i^*[k_0+n] \tag{4.48}$$

The error in the estimated CSI $\delta\mathcal{H}_i[k_0]$ is the difference between the actual and estimated CSI. A simple rearrangement of equation 4.48 shows that the error in the estimated CSI is a function of the gradients $\Delta\mathcal{H}_i^{k,k_0} = H_i[k] - H_i[k_0]$.

$$\delta\mathcal{H}_i[k_0] = \hat{H}_i[k_0] - H_i[k_0] = \sum_{m=0}^{n_t-1}\sum_{n=0}^{K_{coh}-1} \Delta\mathcal{H}_{m+1}^{k_0+n,k_0} T_{i+m}[k_0+n]T_i^*[k_0+n] \tag{4.49}$$

Noise free transmission is assumed in equation (4.48). If coherence is assumed over the coherence bandwidth so that $\Delta\mathcal{H}_i^{k,k_0} \to 0$, then the error in the CSI estimate $\delta\mathcal{H}_i[k_0]$ tends towards zero. The advantage of the OFDM sub-symbol based channel estimator is that the strong correlations of the CSI over a few sub-carriers are used to form channel estimates. As such, the performance of the estimator for a large number of transmitting antennas is only limited by the knowledge of the change in CSI over $K_{coh} = n_t$ sub-carriers. The OFDM sub-symbol estimators can be used to train a large number of antennas by differentiating each antenna using a unique Hardarmard sequences cf. Section 5.3.2. However, the more the number of antennas in the MIMO-OFDM system, the fewer the number of estimated CSI as indicated in equation (4.46). The performance of the estimator is then limited by the interpolation requirements cf. Section 5.3.2.

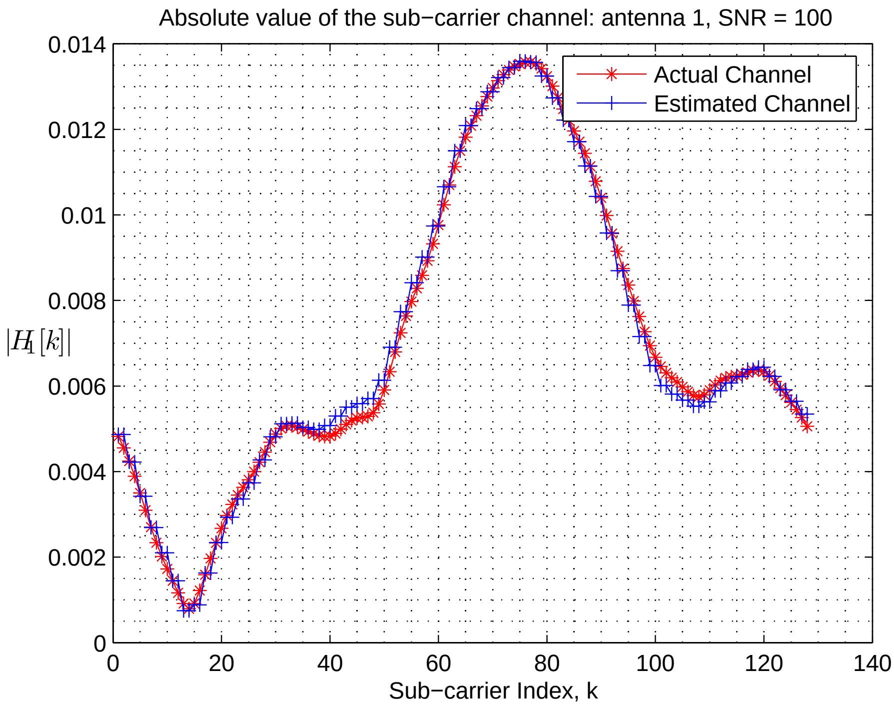


Figure 4.8: Absolute value of the sub-carrier channel gain for the actual and estimated channels using Orthogonal training sequence training for transmit antenna 1.

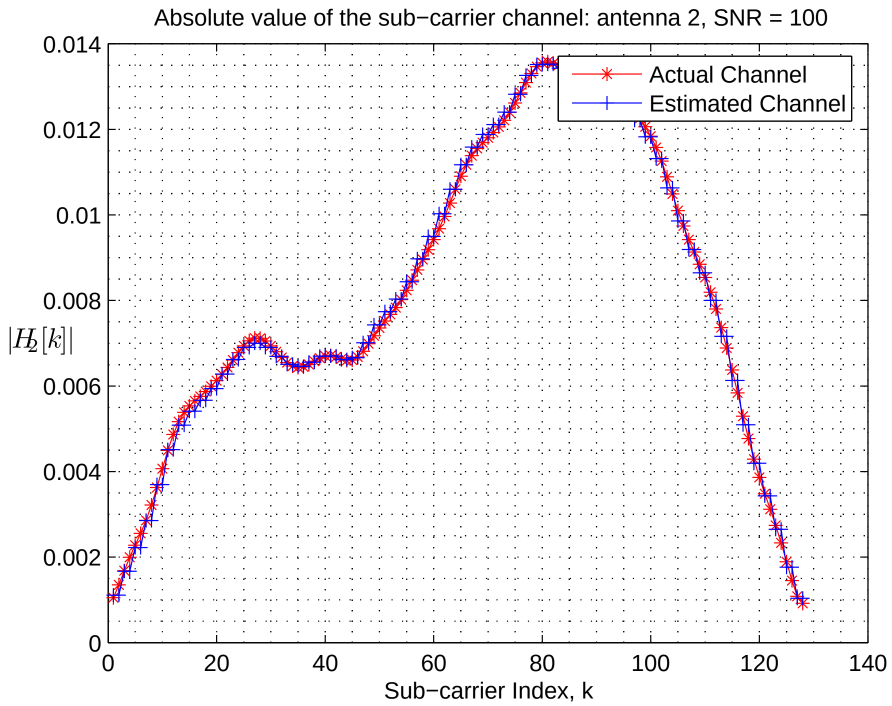


Figure 4.9: Absolute value of the sub-carrier channel gain for the actual and estimated channels using Orthogonal training sequence training for transmit antenna 2.

## 4.4 Chapter Summary

In this section, generic Reduce Parameter Channel State Information (RP-CSI) estimators for MIMO-OFDM systems are introduced. Unlike the traditional MIMO-OFDM channel estimators cf. Section 3.3.2, the generic RP-CSI estimators are not based on the convolution model of the RF channel and rely instead on the flat fading channel model due to Orthogonal Frequency Division Multiplexing (OFDM) modulation. The flat fading channel model, as well as the correlations of parameters within the CSI vector, can be used to develop MIMO-OFDM channel estimators with improved Mean Square Error (MSE) performance. The correlations of CSI elements can be modeled as a sinc function where the first null is related to the maximum delay spread $\tau_{rms}$ cf. Section 4.3.2. Due to this observation, various bases can be developed to represent the variations within the CSI vector with a few parameters. The matrices of the bases are a set of column vectors (basis vectors) whose linear combination can represent every vector in the CSI vector space. For an orthogonal basis, none of the basis vector can be represented as a linear combination of the other basis vectors.

In the first instance, the Fourier basis is a natural basis for CSI vector space. Using the Fourier transform matrix, $L$ Channel Impulse Response (CIR) components/parameters can be used to generate the CSI vector, a direct result of OFDM modulation cf. Section C. The accuracy of this approach is determined by the maximum delay of the channel $\tau_{max}$ and the number of antennas to be trained, $n_t$. The Least Squares (LS) solution implemented in RP-CSI estimators requires that the number of CSI unknowns $n_tL$ is less than or equal to the number of observation $K$, where $K$ is the number of QAM symbols in the OFDM symbol. As a consequence, when a large number of antennas is deployed, the number of CSI parameters that are calculated is reduced from

$L$ to $n_w$ such that $n_w < L$. However, solving for a number of parameter unknowns below $L$ using the Fourier basis leads to an irreducible error in the CSI estimates which negatively impacts the performance of a MIMO-OFDM system employing coherent detection.

This observation motivates the search for an arbitrary basis where $n_w$ parameters are sufficient to generate the CSI vector. Wavelets analysis of the CSI vector is investigated due to the properties of wavelets multi-resolution analysis. At each level of the multi-resolution analysis, the CSI vector is decomposed into two separate halves; one with large amplitude components which are the "coarse signal" representation, and another with negligibly small components representing the "details signal" required to reconstruct the original CSI vector, cf. Section 4.2.1. Further analysis of the "coarse signal" vector produces two quarter length signal which are again a "coarse signal" vector and "details signal" vector. In this way the length of the original signal vector can reduced in length by one half at every level of the multi-resolution analysis. Despite providing a reduced parameter representation of the CSI vector as required, the wavelet basis is inferior to the Fourier basis for the purposes of channel estimation.

Another alternative to reducing the number of CSI parameters is the use of the Principal Component Analysis (PCA) basis. PCA analysis is a well known mathematical technique used to reduce multidimensional data sets to lower dimensions for analysis. In terms of the CSI variations, the aim of Principal Component Analysis is to represent the variations within the CSI vectors using basis vectors that are orthogonal. Furthermore, it is desirable that the PCA parameters corresponding to the basis vectors should decay rapidly from the first to the last basis vector. The PCA basis can be determined using the covariance method where $M$ measurements of the CSI vector are stacked into a measurement matrix. The PCA basis is then found by determining the eigenvectors of the covariance matrix, calculated from the measurement matrix cf. Section 4.2.2. PCA analysis is found to provide a reduced parameter representation of the CSI vector which outperforms the Fourier Basis.

MIMO-OFDM estimators can also be developed based on the coherence of the CSI over a few sub-carriers. If the flat fading channel is assumed to be constant over a few sub-carriers, an orthogonal training sequence can be used to estimate the channel at a given sub-carrier. However, there are variations in the channel parameters within the coherence bandwidth which lead to errors in the estimated channel. The key to accurate CSI estimation for the OFDM sub-symbol based estimator is to have the knowledge of the variations in CSI. This knowledge of the variations in CSI can be deduced from the Fourier or PCA based estimation as described in the next chapter.

# Chapter 5

# Reduced Parameter Channel State Information Analysis

Traditionally, in the literature, the effect of the Signal to Noise Ratio (SNR) on the Mean Square Error (MSE) performance of MIMO-OFDM estimators is the primary consideration when designing an estimator. This chapter begins by showing that the OFDM symbol based estimators introduced in Section 4.3.1 achieve the Minimum MSE determined in the literature. The thesis then goes further by examining the effects of parameter reduction on the MSE performance of the MIMO-OFDM system when various bases are implemented in the RP-CSI estimator. Such considerations are warranted for high data rate systems deploying a large number of antennas in multipath channels. It becomes essential to have a basis that can accurately represent the CSI variations with fewer parameters in order to accurately train large number of antennas.

After investigating the potential for parameter reduction in RP-CSI estimators using the Fourier, Wavelet and PCA basis, suggestions are made on improving OFDM sub-symbol based estimators cf. Section 4.3.2. The advantage of such estimators is that their performance is linked to the variation of the CSI over a few sub-carriers, which is generally small enough to be ignored. However, knowledge gained about the CSI variation from bases interpolation may be used to enhance the performance of OFDM sub-symbol based estimators in a bid to procure Complete CSI (C-CSI) at the receiver.

## 5.1 The Lower Bound for MSE in Channel Estimate

In this section the lower bound for the MSE in channel estimate based on the RP-CSI framework and Fourier basis $\mathbf{B} = \mathbf{F}$ will be derived. Before investigating the effect of parameter reduction on the MSE performance of the MIMO-OFDM estimator, it is necessary to establish that the lower bound of the MSE achieved by the RP-CSI estimator based on Fourier basis is the Minimum MSE achievable. For the analysis, the length of the parameters vector is given by $n_w = L$, where $L$ is the maximum number of non-zero elements in the Channel Impulse Response (CIR) vector. It is well documented result in the literature, [44], [45] and [69], that evaluating $L$ CIR parameters followed by the FFT produces the Minimum achievable MSE for a given OFDM channel estimator.

The MSE for the proposed method is evaluated by considering the effects of Additive White Gaussian Noise (AWGN) on the received OFDM symbol in equation (6.13), so that

$$\tilde{\mathbf{r}} = \mathbf{Q}^H \mathbf{w} + \mathbf{n}. \tag{5.1}$$

where $\mathbf{n} \in \mathbb{C}^{K \times 1}$ is a vector of the i.i.d noise at the receiver. The Least Squares solution for the proposed the framework is then

$$\hat{\mathbf{w}} = \mathbf{w} + \mathbf{Q}\mathbf{n}. \tag{5.2}$$

Equation (4.41) for the coefficients of the MISO-OFDM CSI vector has been used. The error in channel estimate can be found by rearranging equation (5.2) and multiplying both sides by the basis matrix.

$$\mathbf{B}\left(\hat{\mathbf{w}} - \mathbf{w}\right) = \mathbf{BQn}. \tag{5.3}$$

so that

$$\left(\hat{\tilde{\mathbf{h}}}_{\mathsf{F}} - \tilde{\mathbf{h}}_{\mathsf{F}}\right) = \mathbf{BQn}. \tag{5.4}$$

The MSE in the channel estimate is then calculated using the error covariance matrix [52]which allows us to determine the relationship between the MSE and the maximum expected length of the CIR vector.

$$\begin{aligned} MSE &= \frac{1}{n_t K} E\left[\|\hat{\tilde{\mathbf{h}}}_{\mathsf{F}} - \tilde{\mathbf{h}}_{\mathsf{F}}\|^2\right] & (5.5)\\ &= \frac{1}{n_t K} E\Big[Tr\Big\{\left(\hat{\tilde{\mathbf{h}}}_{\mathsf{F}} - \tilde{\mathbf{h}}_{\mathsf{F}}\right)\left(\hat{\tilde{\mathbf{h}}}_{\mathsf{F}} - \tilde{\mathbf{h}}_{\mathsf{F}}\right)^H\Big\}\Big] & (5.6)\\ &= \frac{1}{n_t K} E\Big[Tr\Big\{\Big(\mathbf{BQn}\Big)\Big(\mathbf{BQn}\Big)^H\Big\}\Big] & (5.7)\\ &= \frac{1}{n_t K} Tr\Big\{\mathbf{BQ}E[\mathbf{nn}^H]\mathbf{Q}^H\mathbf{B}^H\Big\} & (5.8)\end{aligned}$$

Note that in equation (5.8), the $E[\mathbf{nn}^H] = \sigma_n^2\mathbf{I} \in \mathbb{R}^{K\times K}$, and we can write[1]

$$MSE = \frac{\sigma_n^2}{n_t K} Tr\Big\{\mathbf{BQQ}^H\mathbf{B}^H\Big\} \tag{5.9}$$

In the above equation, the MSE is depends on the training sequence and basis through the matrix $\mathbf{Q}$. We can define $\mathbf{Z} = \mathbf{BQ}$ so that $\mathbf{Y} = \mathbf{ZZ}^H$ in equation (5.9). We also define a diagonal matrix for the training symbols $\mathbf{T}_{\mathsf{S,i}} = \mathtt{diag}(T_i[k])$ and note the result $\mathbf{XP} = [\mathbf{T}_{S,1}\ \mathbf{T}_{S,2}\ \ldots\ \mathbf{T}_{S,n_t}]$. A diagonal matrix is a square matrix in which the entries outside the main diagonal are all zero. In this thesis, $\mathtt{diag}(a_1, \ldots, a_n)$ represents a diagonal matrix whose diagonal entries starting in the upper left corner are $a_1, \ldots, a_n$. We can then write for $\mathbf{Z} = \mathbf{BQ} = \mathbf{BB}^H(\mathbf{XP})^H$

[1]from the definition of noise spectral density

$$\mathbf{Z} = \left[\mathbf{B}_1\mathbf{B}_1^H\mathbf{T}_{\mathsf{S},1}^H \ \mathbf{B}_2\mathbf{B}_2^H\mathbf{T}_{\mathsf{S},2}^H \ \ldots \ \mathbf{B}_{n_t}\mathbf{B}_{n_t}^H\mathbf{T}_{\mathsf{S},\mathsf{n_t}}^H\right]^T \tag{5.10}$$

and using a similar argument for $\mathbf{Z}^H = (\mathbf{BQ})^H = (\mathbf{XP})\mathbf{BB}^H$, we deduce

$$\mathbf{Z}^H = \left[\mathbf{T}_{\mathsf{S},1}\mathbf{B}_1\mathbf{B}_1^H \ \mathbf{T}_{\mathsf{S},2}\mathbf{B}_2\mathbf{B}_2^H \ \ldots \ \mathbf{T}_{\mathsf{S},\mathsf{n_t}}\mathbf{B}_{n_t}\mathbf{B}_{n_t}\right]. \tag{5.11}$$

The matrix $\mathbf{Y} = \mathbf{ZZ}^H$ is then given by $\mathbf{Y} = (\mathbf{Y}_{m,n})_{n_t \times n_t}$ where $\mathbf{Y}_{m,n} = \mathbf{B}_i\mathbf{B}_i^H\mathbf{T}_{\mathsf{S},\mathsf{m}}^H\mathbf{T}_{\mathsf{S},\mathsf{n}}\mathbf{B}_i\mathbf{B}_i^H$. Analysis of the matrix the elements of the matrix $\mathbf{Y}$ shows that the diagonal elements are given by,

$$y_{l,l} = \frac{L}{K} \tag{5.12}$$

Therefore, when the training symbols are orthogonal, and a reduced Fourier basis is implemented, the MSE can be calculated as follows

$$MSE = \frac{\sigma_n^2}{n_tK}\sum_{l=1}^{n_tK} y_{l,l} \tag{5.13}$$

$$= \frac{\sigma_n^2}{n_tK}\sum_{l=1}^{n_tK} \frac{L}{K} \tag{5.14}$$

Using Cauchy's Mean theorem which states that the arithmetic mean is always greater than or equal to the geometric mean, we can expand the summation in the equation above so that

$$MSE \geq \frac{\sigma_n^2}{n_tK} n_tK \sqrt[n_tK]{\prod_{l=1}^{n_tK} \frac{L}{K}} \tag{5.15}$$

Equality is observed in equation (5.15) only when $y_{1,1} = y_{2,2} = \cdots = y_{n_tK,n_tK}$, which is a property that is determined by the basis for each transmit antennas CSI. However, the Fourier basis is used exclusively in the analysis of the MIMO-OFDM channel estimator, and it can be noted that $\prod_{l=1}^{n_tK} \frac{L}{K} = (\frac{L}{K})^{n_tK}$ so that

$$MSE \geq \frac{\sigma_n^2 L}{K} \tag{5.16}$$

This result agrees with the related analysis in [69] and the analysis in [70]. Equation (5.16) gives the minimum mean square error for the RP-CSI estimator, when the Fourier basis evaluates $L$ time domain channel parameters of the CIR vector (cf. Sections C–4.2). Because $L$ is the maximum number of non-zero elements in the CIR vector, the MSE increases if the number of parameters evaluated is less than $L$.

## 5.2 RP-CSI Simulation Results

In this section, the effect of reducing the number of channel estimation parameters for OFDM symbol based RP-CSI channel estimation is evaluated. The CSI estimation algorithm described in Section 4.3 will be used with the different basis functions described in Section 4.2. The channels linking each transmitter-receiver antenna pair are assumed to experience uncorrelated Rayleigh frequency selective fading as described by the model in Section 2.3. The systems and algorithms will be compared for a range of Signal-to-Noise Ratio (SNR) for various random realizations of the Saleh-Valenzuela channel model which has a root mean square (rms) delay spread of approximately $\tau_{rms} = 50ns$ and a maximum delay spread of $\tau_{max} = 200ns$.

Results were obtained for a symbol period of $T_s = 10ns$, for which an RF channel bandwidth of $B = 2/T_s = 200MHz$ is assumed. At this symbol rate and considering that multi-path components with delays in excess of $200ns$ were too small to be measured [32], a cyclic prefix of 16 symbols was chosen for 128 sub-carrier OFDM[2] . The RF channel bandwidth occupied by the OFDM transmission, the $200MHz$ (sub-carrier separation of $\frac{200(MHz)}{128} = 1.5625MHz$), is up-converted to 2.4GHz for transmission. [3]

### 5.2.1 Simulation Results for $L = 4$

The results for the computation of 4 coefficients for the RP-CSI estimator show that at high SNR, there are errors in the channel estimation because the basis is insufficient to span the variations in a given MIMO-OFDM CSI vector. At low SNR, the MSE is limited by the noise whilst at high SNRs the MSE plateaus for the reason above. These results can be used to indicate the MSE

[2]assuming L=16 considered multipath components within a maximum of 160ns. The estimator performs at the analytical limit despite an expected maximum delay of 200ns.

[3]This symbol rate for 4-QAM requires a bandwidth of 100MHz which compares with the gigabit MIMO-OFDM testbed http://iaf-bs.de/projects/gigabit-mimo-ofdm-testbed.en.html

| Parameter | Simulation Settings |
|---|---|
| Carrier Frequency | $f_c = 2.4 \times 10^9 Hz$ |
| OFDM Symbol length | $K = 128$ |
| OFDM Cyclic Prefix | $L = 16$ |
| QAM Symbol Period | $T_s = 10 \times 10^{-9}(sec)$ |
| Maximum Delay spread | $\tau_{max} = 200 \times 10^{-9}(sec)$ |
| RMS Delay spread | $\tau_{rms} = 50 \times 10^{-6}(sec)$ |
| RF Channel Bandwidth | $F_s = 200 \times 10^6 Hz$ |

Table 5.1: Simulation Parameters for the comparison of 1-D MISO-OFDM Channel Estimation based on 4-QAM. Different bases are implemented within the RP-CSI framework and the effect of reducing the number of channel estimation parameters on the MSE evaluated.

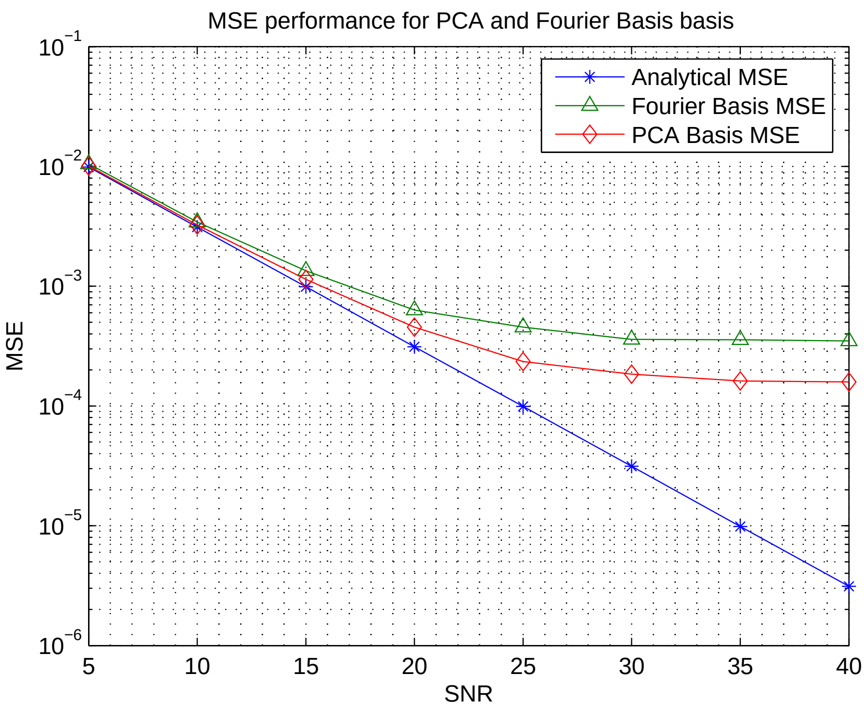


Figure 5.1: MSE vs. SNR for the Fourier Basis, L=4.

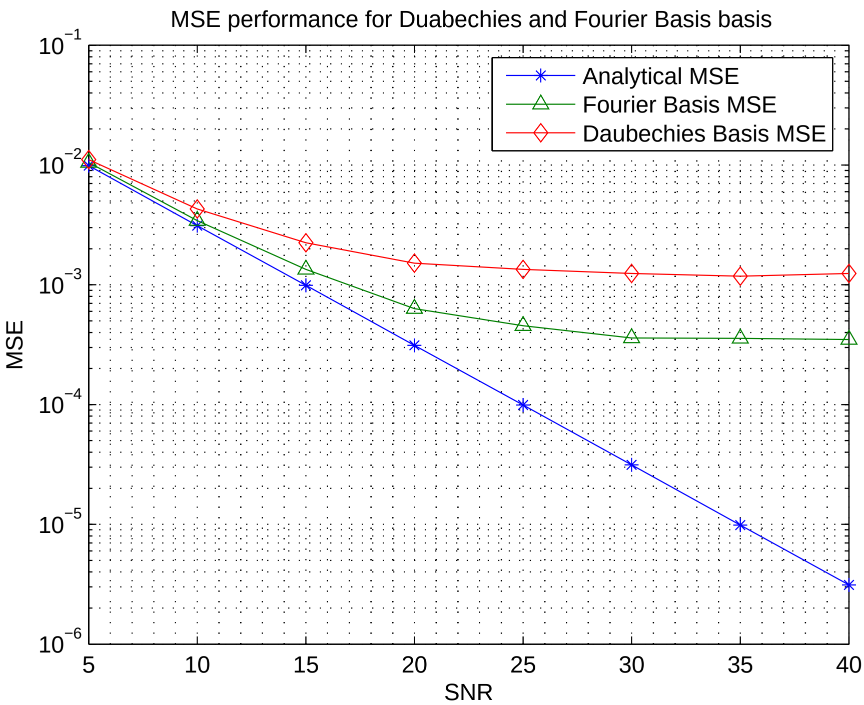


Figure 5.2: MSE vs. SNR for the Daubechies Basis, L=4.

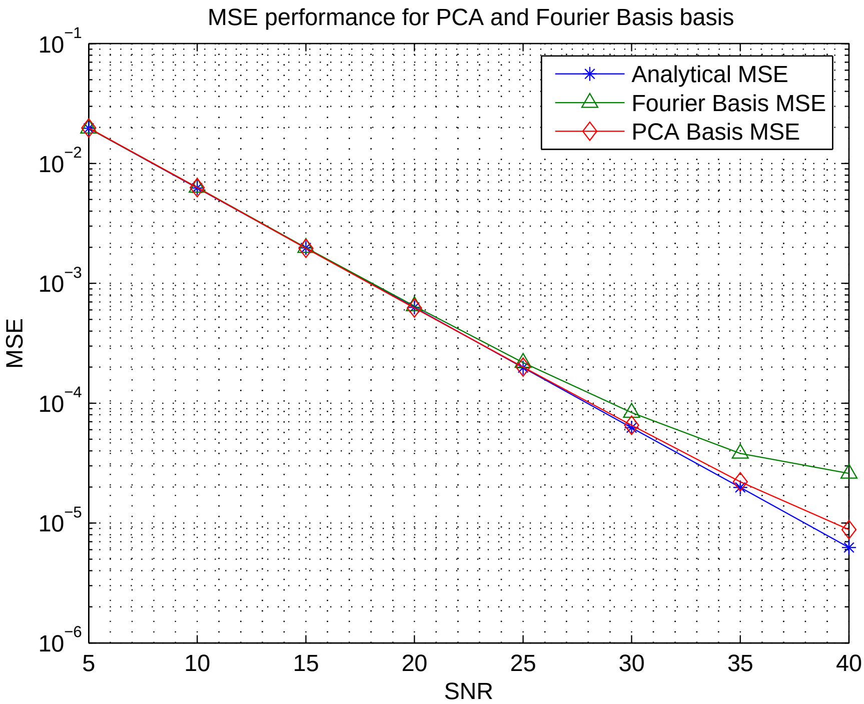


Figure 5.3: MSE vs. SNR for the Fourier Basis, L=8.

performance of a MU-MIMO-OFDM system where each user is equipped with $n_t = 2$ antennas, in which case the training of a total of 16 users can be performed simultaneously for a length $K = 128$ OFDM symbol. The Daubechies basis D4 is implemented and the number of measured CSI vectors for the PCA basis is $M = 64$.

### 5.2.2 Simulation Results for $L = 8$

When 8 coefficients are estimated for each user with RP-CSI, the MSE performance at high SNR is better than the performance using only 4 coefficients. However, for a MU-MIMO-OFDM system where each user is equipped with $n_t = 2$ antennas, the training of a total of 8 users can be performed simultaneously for a length $K = 128$ OFDM symbol. The Daubechies basis D8 is implemented and again the number of measured CSI vectors for the PCA basis

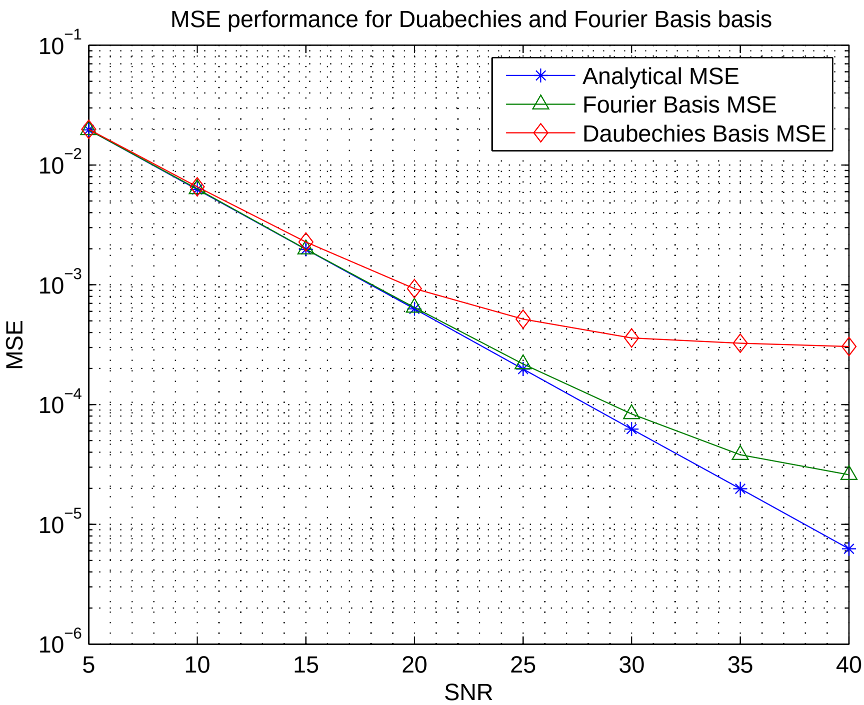


Figure 5.4: MSE vs. SNR for the Daubechies Basis, L=8.

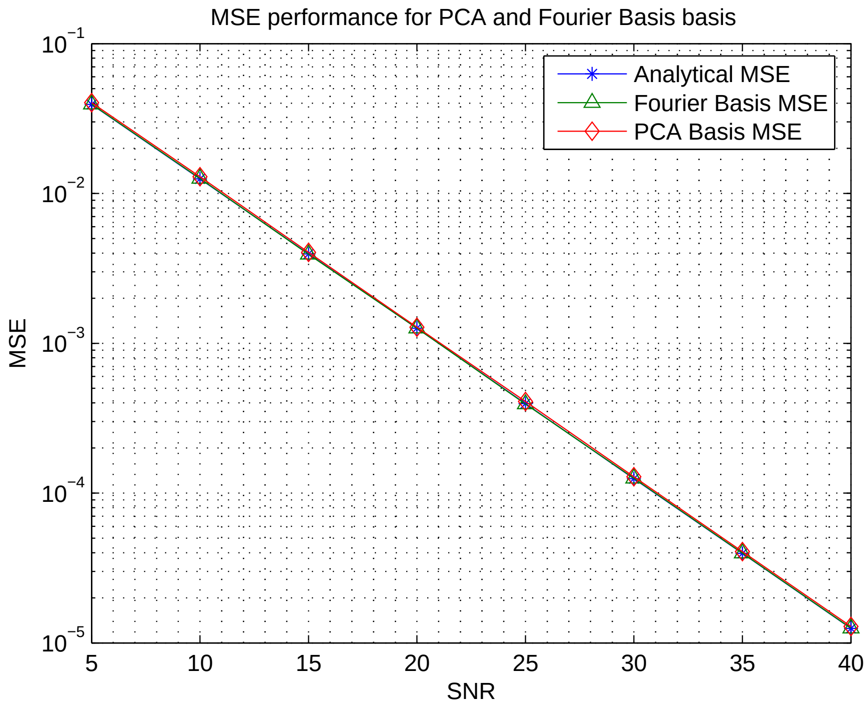


Figure 5.5: MSE vs. SNR for the Fourier Basis, L=16.

is $M = 64$.

### 5.2.3 Simulation Results for $L = 16$

The Daubechies basis D16 is implemented and the number of measured CSI vectors for the PCA basis is $M = 64$. It is clear that calculating more coefficients for RP-CSI produces the best results as expected. 16 coefficients are sufficient to produce the analytical MSE results for the Fourier and PCA basis, and near analytical MSE results for the Daubechies Basis. The comparatively poor performance of the Daubechies Basis indicates that the vanishingly small transformation coefficients play an important role in the accurate reconstruction of the CSI vector and are therefore not entirely negligible as postulated in cf. Section 4.2.1. It can be concluded that because the maximum delay spread of the channel is 200ns, computing 16 coefficients is sufficient to determine the

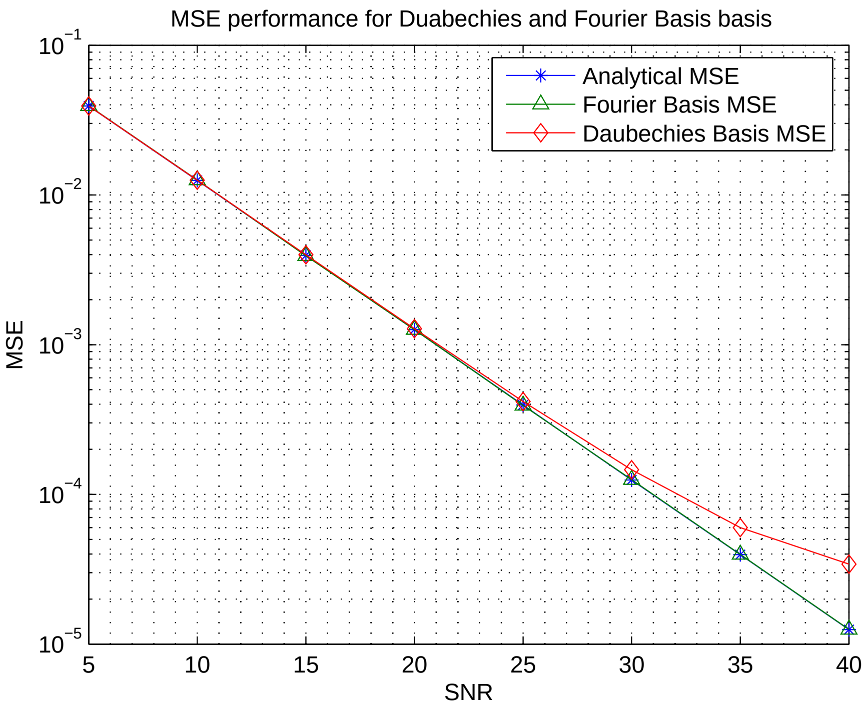


Figure 5.6: MSE vs. SNR for the Daubechies Basis, L=16.

significant multipath components in the time domain. The time domain vector can be processed using the Fourier transform in order to calculate the MIMO-OFDM CSI vector. However, only 4 users with $n_t = 2$ mobile devices can be trained simultaneously in the MU-MIMO-OFDM system. The PCA basis is superior to the Fourier basis as it achieves a lower MSE when the number of channel estimation parameters is less than $L$, where $L$ is the maximum number of non-zero elements in the CIR vector found by dividing the maximum delay spread of the multipath channel $\tau_{max}$ by the symbol period $T_s$.

## 5.3 OFDM Sub-symbol based MIMO-OFDM channel Estimation

In this section, an iterative algorithm to improve the accuracy of CSI estimation for OFDM sub-symbol based channel estimation is presented. As noted in Section 4.3.2, it can be assumed that the sub-carrier channel gain remains constant within the coherence bandwidth, which is typically a fraction of the total available RF channel bandwidth. It can therefore be inferred that the CSI remains constant over a few sub-carriers, leading to reduction in the parameters and accurate CSI estimates for high data rate MIMO-OFDM system [1], [51].

Another important aspect of OFDM sub-symbol based estimation is that the CSI for one in every $K_{coh}$ sub-carriers is estimated whilst the remaining CSI are interpolated. In the literature [51], a method of interpolation is described for an OFDM sub-symbol based estimator that improves the estimators MSE performance in the presence of AWGN. The method is based on the relationship

$$\tilde{\mathbf{h}} = \begin{bmatrix} \mathbf{B_w} & \mathbf{B_n} \end{bmatrix} \begin{bmatrix} \mathbf{w} \\ \mathbf{0} \end{bmatrix} = \mathbf{B_w w} \tag{5.17}$$

Because the length of the vector $\mathbf{w}$ is such that $n_w \ll K$ where $K$ is the length of the vector $\tilde{\mathbf{h}}$, the equation (5.17) is overdetermined. For $\frac{K}{K_{coh}}$ estimated CSI, the overdetermined equation cf. (5.17) can be used to solve for the CSI vector by replacing the rows corresponding to the missing CSI with rows of zeros. The advantage of such reduced rank interpolation is greatly improved MSE performance in the presence of AWGN. In this case, if the zero filled basis and CSI vectors are denoted as $\mathbf{B}_{\mathbf{w},z}$ and $\tilde{\mathbf{h}}_z$, then the CSI vector after interpolation is given by

$$\tilde{\mathbf{h}}_{intp} = \mathbf{B}_{\mathbf{w}} \left( \mathbf{B}^{\dagger}_{\mathbf{w},z} \tilde{\mathbf{h}}_z \right) \tag{5.18}$$

When a suitable basis is used in equation (5.18), interpolation can be performed for a smaller subset of estimated CSI vector $\tilde{\mathbf{h}}$. This motivates an investigation into the interpolation performance of the various basis introduced in this thesis. For a sufficient $n_w$ at high SNR, the accuracy of the interpolated CSI is limited by the accuracy of the estimated CSI, which in turn is related to the variation of the CSI within the coherence bandwidth. An iterative algorithm for improved channel estimation for overloaded MIMO-OFDM systems is presented that allows the receiver to procure Complete CSI (C-CSI) from the estimated Partial CSI (P-CSI). The approach is based on separating the *a posteriori* CSI estimates based on orthogonal training sequence estimation from the variation in CSI derived from interpolation based on a given CSI basis matrix.

### 5.3.1 Orthogonal Training Sequences for channel estimation

Using OFDM sub-symbol based estimators, the CSI over $K_{coh}$ sub-carriers is assumed to be invariant. This assumption is based on the sinc function model for the correlations between the CSI with increasing frequency index, where the first null is inversely proportional to the maximum delay spread $\tau_{rms}$ of the channel.

$$R(\Delta f) = R\left((k - \acute{k})F_s\right) = \frac{\sin\left(\pi\tau_{max}(k - \acute{k})F_s\right)}{\pi\tau_{max}(k - \acute{k})F_s} \tag{5.19}$$

As was noted in Section 4.3.2, the spaced-frequency correlation function can be determined by Fourier transform of the correlation function cf. Appendix B. The function $P(\Delta f)$ represents the correlation between the channels response to two narrowband sub-carriers with the frequencies $f_1$ and $f_2$ as a function of the difference $\Delta f$ [26]. Because the Fourier transform of the correlation function cf. (5.19) is the rectangular function [11] with a bandwidth $B_{coh} = 1/\tau_{max}$, the channel gain is assumed to be constant for the coherence bandwidth.

For a maximum delay spread of $\tau_{max} = 200ns$ and an RF channel bandwidth of $200MHz$, the coherence bandwidth is $B_{coh} = 1/\tau_{max} = 5MHz$ and approximately $128 \times 5MHz/200MHz \approx 3$ OFDM sub-carriers have the same gain for $K = 128$. In order to accurately train $n_t$ transmit antennas, the coherence assumption must hold for $K_{coh} \geq n_t$ sub-carriers and therefore a maximum of $n_t = 3$ antennas can be trained in the example given. In this thesis, it is argued that the CSI varies within the coherence bandwidth causing a significant error in CSI estimates. It is also shown that if such variation of CSI within the coherence bandwidth are taken into account, C-CSI can be achieved even when the coherence is assumed over $K_{coh} < n_t$ sub-carriers at high SNR.

The estimator in Section 4.3.2 is now reformulated to indicate how the number of transmit antennas $n_t$ affects the error in CSI estimation Figure 5.7. Given that the received QAM symbol at a given receiver of a MIMO-OFDM system is given by $R[k] = \sum_{i=1}^{n_t} H_i[k]T_i[k]$, the initial estimate of the CSI at a sub-carrier $k = k_0$ is given by

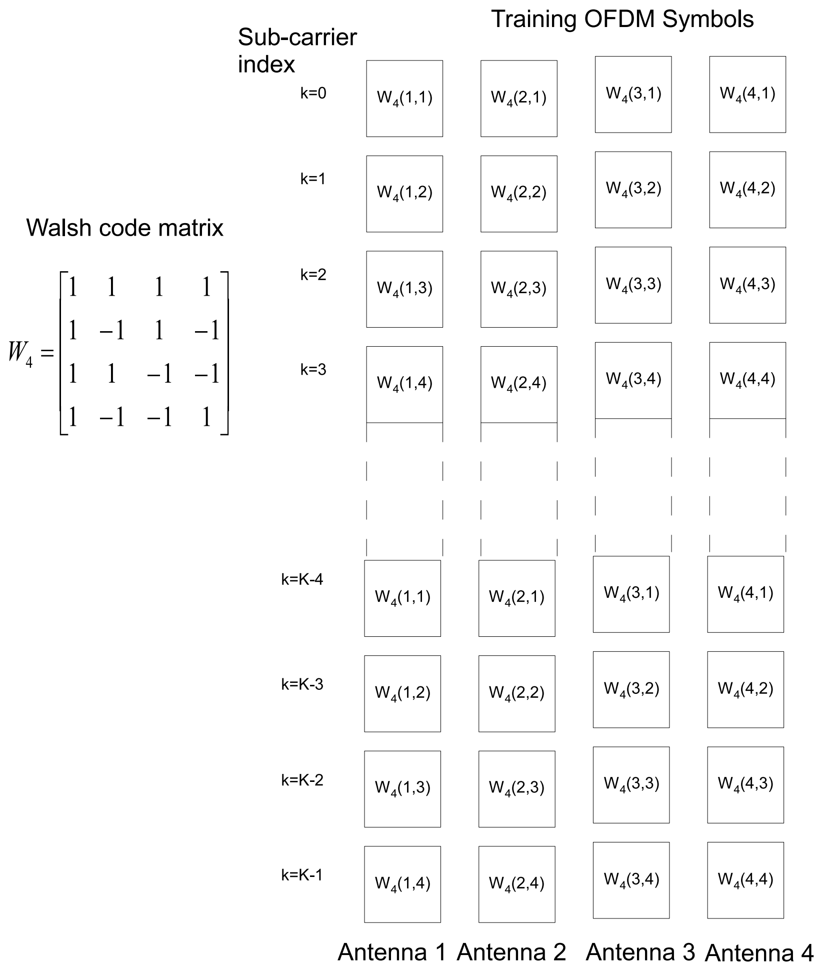


Figure 5.7: Training symbol placement for a QAM symbol based channel estimator for a (4,1) MISO-OFDM system. Each transmit antenna transmits a row of Walsh code (Hadamard) matrix which is used to uniquely identify the antenna at the receiver. $W_4(m, n)$ is the element in the $m$th row and $n$th column of the Walsh matrix.

$$\hat{H}_i[k_0] = \sum_{i=1}^{n_t} R[k_0 + i - 1]T_i^*[k_0 + i - 1] \,\forall\, k_0 = 0, n_t, \ldots, K - 1 \tag{5.20}$$

In the traditional sense, it is usual to assume that the coherence in CSI is observed over at least $K_{coh} = n_t$ number of sub-carriers. In this case, orthogonal Hadamard training sequences cf. (4.47) of length $n_t$ can be arranged within the OFDM symbol so as to determine the CSI after every $n_t$ sub-carriers cf. Figure 5.7. However it is known that the CSI will vary within the coherence bandwidth so that if the difference between the CSI for the $k$th sub-carrier and the $k_0$ sub-carrier is denoted by $\Delta\mathcal{H}_i^{k,k_0} = H_i[k] - H_i[k_0]$, then an error is incurred in estimating the CSI, which is given by

$$\hat{H}_i[k_0] = H_i[k_0] + \sum_{m=0}^{n_t-1}\sum_{n=0}^{n_t-1} \Delta\mathcal{H}_{m+1}^{k_0+n,k_0} T_{i+m}[k_0 + n]T_i^*[k_0 + n] \tag{5.21}$$

$$\delta\mathcal{H}_i[k_0] = \hat{H}_i[k_0] - H_i[k_0] = \sum_{m=0}^{n_t-1}\sum_{n=0}^{n_t-1} \Delta\mathcal{H}_{m+1}^{k_0+n,k_0} T_{i+m}[k_0 + n]T_i^*[k_0 + n] \tag{5.22}$$

In the next section, an iterative algorithm for reducing the error $\delta\mathcal{H}_i[k_0]$ is described. The algorithm is based on the notion that the gradients $\Delta\mathcal{H}_i^{k,k_0} = H_i[k] - H_i[k_0]$ can be accurately predicted through interpolation. The information on the gradients can be used to improve the *a posteriori* estimates $\hat{H}_i[k_0]$ and the gradients recalculated. The estimated and interpolated channels are depicted in Figure 5.8. If this process is repeated iteratively, it is expected that the estimated CSI will approach the actual CSI, providing C-CSI.

### 5.3.2 OFDM sub-symbol based MU-MIMO-OFDM channel estimation

In this section, an iterative algorithm is devised to improve CSI estimates when a large number of antennas is to be trained. It is assumed that the mobile station is equipped with $n_t = 2$ antennas and that RP-CSI is performed at a

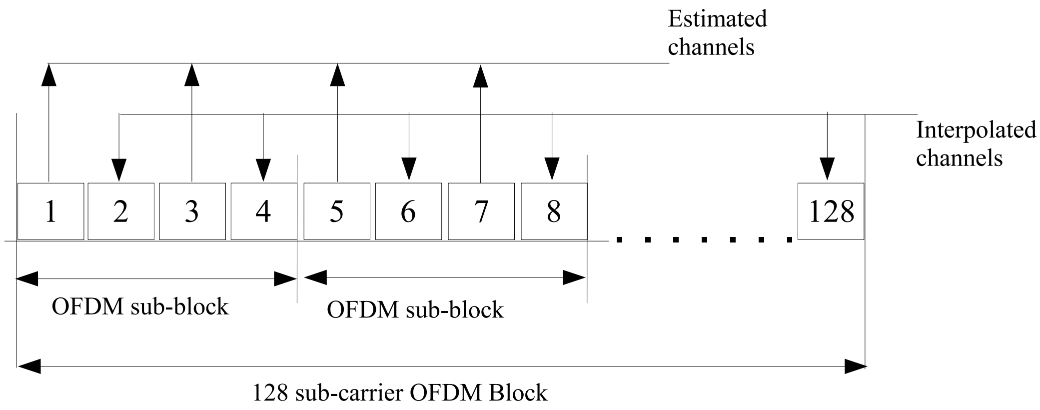


Figure 5.8: An example of the partitioning of 128 CSI estimates for the OFDM symbol into sub-symbols for a (2,1) MIMO-OFDM system.

single receive antenna at a time. The main idea is to exploit the channel correlation in frequency so that we could in a sense convert the underdetermined system into a determined system. To illustrate this, without loss of generality (WLOG), we consider only the first four sub-carriers, i.e., $k = 0, 1, 2, 3$, and assume there is no noise.

Firstly, given that $\{t_i[k]\}$'s are orthogonal pilot training sequences spanning two sub-carriers so that

$$\begin{aligned} |t_1[0]|^2 + |t_1[1]|^2 = |t_2[0]|^2 + |t_2[1]|^2 = 1, \\ t_1[0]t_2^*[0] + t_1[1]t_2^*[1] = 0, \end{aligned} \tag{5.23}$$

we can have a coarse estimate for $\tilde{H}_1[0], \tilde{H}_1[1], \tilde{H}_2[0], \tilde{H}_2[1]$ by linear combining the received signals

$$\begin{aligned} H_1^{\mathsf{est}}[0] &\triangleq t_1^*[0]r[0] + t_1^*[1]r[1] \\ &= H_1[0] + |t_1[1]|^2 \Delta\mathcal{H}_{1,0}^{(1)} + t_1^*[1]t_2[1]\Delta\mathcal{H}_{1,0}^{(2)} \\ &\approx H_1[0] \approx H_1[1] \end{aligned} \tag{5.24}$$

where

$$\begin{aligned}\Delta\mathcal{H}_1^{1,0} &\triangleq H_1[1] - H_1[0],\\ \Delta\mathcal{H}_2^{1,0} &\triangleq H_2[1] - H_2[0].\end{aligned} \tag{5.25}$$

Similarly, we also have

$$H_2^{\mathsf{est}}[0] = t_2^*[0]r[0] + t_2^*[1]r[1] \approx H_2[0] \approx H_2[1]. \tag{5.26}$$

Noting that perfect recovery of $\{H_i[k]\}$ is not possible even without noise because of the underdetermined structure, this conventional method incurs an irreducible error in the estimate for the channel pairs $(H_1[0], H_1[1])$ and $(H_2[0], H_2[1])$, which is inversely proportional to the degree of correlation for the channel pairs. That is to say, if the difference in the channel pairs, $\Delta\mathcal{H}_1^{1,0}$ and $\Delta\mathcal{H}_2^{1,0}$, is small, then the error in the estimate will be small. In an environment where there is a great degree of multi-path (i.e., large $\tau_{\mathsf{rms}}$), the channels are less correlated, and $\Delta\mathcal{H}_1^{1,0}$ and $\Delta\mathcal{H}_2^{1,0}$ are significant.

To describe our method, we find it useful to define

$$\begin{aligned}\delta\mathcal{H}_1[0] &\triangleq H_1^{\mathsf{est}}[0] - H_1[0]\\ &= |t_1[1]|^2\Delta\mathcal{H}_1^{1,0} + t_1^*[1]t_2[1]\Delta\mathcal{H}_2^{1,0},\end{aligned} \tag{5.27}$$

$$\begin{aligned}\delta\mathcal{H}_2[0] &\triangleq H_2^{\mathsf{est}}[0] - H_2[0]\\ &= t_1[1]t_2^*[1]\Delta\mathcal{H}_1^{1,0} + |t_2[1]|^2\Delta\mathcal{H}_2^{1,0},\end{aligned} \tag{5.28}$$

$$\begin{aligned}\delta\mathcal{H}_1[2] &\triangleq H_1^{\mathsf{est}}[2] - H_1[2]\\ &= |t_1[1]|^2\Delta\mathcal{H}_1^{3,2} + t_1^*[1]t_2[1]\Delta\mathcal{H}_2^{3,2},\end{aligned} \tag{5.29}$$

$$\begin{aligned}\delta\mathcal{H}_2[2] &\triangleq H_2^{\mathsf{est}}[2] - H_2[2]\\ &= t_1[1]t_2^*[1]\Delta\mathcal{H}_1^{3,2} + |t_2[1]|^2\Delta\mathcal{H}_2^{3,2}.\end{aligned} \tag{5.30}$$

$\{\delta\mathcal{H}_i[k]\}$'s can be viewed as the channel estimation errors between the estimated and actual channels. Therefore, (5.27)–(5.30) can be used to refine the channel estimates $\{H_i^{\mathsf{est}}[k]\}$ if $\{\Delta\mathcal{H}_{k,\ell}^{(i)}\}$ are known.

The proposed technique uses the estimates obtained from the conventional method (i.e., $\{H_i^{\mathsf{est}}[k]\}$) and exploits additional information (i.e., $\{\varrho_{k,\ell}^{(i)}\}$ introduced later) from estimation in subsequent frequency sub-carriers for channel pairs, $(H_1[2], H_1[3])$ and $(H_2[2], H_2[3])$, to further refine the estimates for the channel pairs, $(H_1[0], H_1[1])$ and $(H_2[0], H_2[1])$. An iterative algorithm will be developed to achieve a refined estimate.

In order to iterate for better estimates of the channel pairs, $(H_1[0], H_1[1])$ and $(H_2[0], H_2[1])$, the first step is to rewrite $H_1[0]$ and $H_2[0]$ as the subjects of (D.1) so that

$$\begin{aligned}\begin{pmatrix} H_1[0] \\ H_2[0] \end{pmatrix} &= \begin{pmatrix} t_1^*[0] & t_1^*[1] \\ t_2^*[0] & t_2^*[1] \end{pmatrix} \begin{pmatrix} r[0] \\ r[1] \end{pmatrix} \\ &- \begin{pmatrix} |t_1[1]|^2 & t_1^*[1]t_2[1] \\ t_1[1]t_2^*[1] & |t_2[1]|^2 \end{pmatrix} \begin{pmatrix} \Delta\mathcal{H}_1^{1,0} \\ \Delta\mathcal{H}_2^{1,0} \end{pmatrix}.\end{aligned} \tag{5.31}$$

(5.31) can be utilized to estimate the channels $H_1[0]$ and $H_2[0]$ if there is an estimate for the difference in the channel pairs, $\Delta\mathcal{H}_1^{1,0}$ and $\Delta\mathcal{H}_2^{1,0}$. Similarly for $(H_1[2], H_2[2])$ from $(\Delta\mathcal{H}_1^{3,2}, \Delta\mathcal{H}_1^{3,2})$.

Now, we intend to relate the channel estimates for adjacent sub-carriers by defining the following ratios

$$\varrho_{1,2}^{(1)} \triangleq \tfrac{H_1[1]-H_1[0]}{H_1[2]-H_1[0]} = \tfrac{\Delta\mathcal{H}_1^{1,0}}{H_1[2]-H_1[0]}, \tag{5.32}$$

$$\varrho_{1,2}^{(2)} \triangleq \tfrac{H_2[1]-H_2[0]}{H_2[2]-H_2[0]} = \tfrac{\Delta\mathcal{H}_2^{1,0}}{H_2[2]-H_2[0]}, \tag{5.33}$$

$$\varrho_{3,2}^{(1)} \triangleq \tfrac{H_1[3]-H_1[2]}{H_1[2]-H_1[0]} = \tfrac{\Delta\mathcal{H}_1^{3,2}}{H_1[2]-H_1[0]}, \tag{5.34}$$

$$\varrho_{3,2}^{(2)} \triangleq \tfrac{H_2[3]-H_2[2]}{H_2[2]-H_2[0]} = \tfrac{\Delta\mathcal{H}_2^{3,2}}{H_2[2]-H_2[0]}. \tag{5.35}$$

In practice, they can be approximated using the estimated even sub-carrier channels and the interpolated odd sub-carrier channels. For instance,

$$\varrho_{1,2}^{(1)} \approx \frac{H_1^{\mathsf{int}}[1] - H_1^{\mathsf{est}}[0]}{H_1^{\mathsf{est}}[2] - H_1^{\mathsf{est}}[0]} \tag{5.36}$$

where $H_1^{\mathsf{int}}[1]$ is the channel estimate obtained from interpolating the estimates $H_1^{\mathsf{est}}[0]$ and $H_1^{\mathsf{est}}[2]$. We observe that the approximated ratios are found to be about 95% accurate for $K_{coh} \leq 4$.

With these ratios, we have the following relations

$$\Delta\mathcal{H}_1^{1,0}\big|_{\mathsf{est}} = \varrho_{1,2}^{(1)}\left(H_1^{\mathsf{est}}[2] - H_1^{\mathsf{est}}[0]\right) \tag{5.37}$$

$$\Delta\mathcal{H}_2^{1,0}\big|_{\mathsf{est}} = \varrho_{1,2}^{(2)}\left(H_2^{\mathsf{est}}[2] - H_2^{\mathsf{est}}[0]\right) \tag{5.38}$$

$$\Delta\mathcal{H}_1^{3,2}\big|_{\mathsf{est}} = \varrho_{3,2}^{(1)}\left(H_1^{\mathsf{est}}[2] - H_1^{\mathsf{est}}[0]\right) \tag{5.39}$$

$$\Delta\mathcal{H}_2^{3,2}\big|_{\mathsf{est}} = \varrho_{3,2}^{(2)}\left(H_2^{\mathsf{est}}[2] - H_2^{\mathsf{est}}[0]\right) \tag{5.40}$$

which can be employed to estimate $\{\Delta\mathcal{H}_i^{k,\ell}\}$ that can then be used in (5.27)–(5.30) to get the estimation errors $\{\delta\mathcal{H}_i[k]\}$. From these, we can update the estimates for the even sub-carriers by

$$\begin{cases} H_1^{\mathsf{est}}[0] := H_1^{\mathsf{est}}[0] - \delta\mathcal{H}_1[0], \\ H_2^{\mathsf{est}}[0] := H_2^{\mathsf{est}}[0] - \delta\mathcal{H}_2[0], \\ H_1^{\mathsf{est}}[2] := H_1^{\mathsf{est}}[2] - \delta\mathcal{H}_1[2], \\ H_2^{\mathsf{est}}[2] := H_2^{\mathsf{est}}[2] - \delta\mathcal{H}_2[2]. \end{cases} \tag{5.41}$$

After $\{H_i^{\mathsf{est}}[k]\}$ are updated, they can be fed back into (5.37)–(5.40) to refine $\{\Delta\mathcal{H}_{k,\ell}^{(i)}\}$. As a consequence, we can iterate the estimation between $\{H_i^{\mathsf{est}}[k]\}$ and $\{\Delta\mathcal{H}_{k,\ell}^{(i)}\}$ to obtain a fine estimate for $\Delta\mathcal{H}_1^{1,0}, \Delta\mathcal{H}_2^{1,0}, \Delta\mathcal{H}_1^{3,2}, \Delta\mathcal{H}_2^{3,2}$. Finally, the channel estimates for the even sub-carriers can be readily obtained using (5.31). In addition, the odd sub-carrier channels can be easily found from

$$\begin{aligned} H_1^{\mathsf{est}}[1] &= H_1^{\mathsf{est}}[0] + \Delta\mathcal{H}_1^{1,0}\big|_{\mathsf{est}}, \\ H_1^{\mathsf{est}}[3] &= H_1^{\mathsf{est}}[2] + \Delta\mathcal{H}_1^{3,2}\big|_{\mathsf{est}}. \end{aligned} \tag{5.42}$$

The above iterative algorithm is summarized as follows:

**S1**) Estimate the even sub-carrier channels

$$H_1^{\mathsf{est}}[0], H_1^{\mathsf{est}}[2], \ldots, \text{ and } H_2^{\mathsf{est}}[0], H_2^{\mathsf{est}}[2], \ldots \tag{5.43}$$

based on the orthogonality of the training sequences [see (5.24) and (5.26)].

**S2**) Use the interpolation formulation to get the estimates for the odd sub-carrier channels from the estimated even sub-carrier channels:

$$H_1^{\mathsf{int}}[1], H_1^{\mathsf{int}}[3], \ldots, \text{ and } H_2^{\mathsf{int}}[1], H_2^{\mathsf{int}}[3], \ldots \tag{5.44}$$

**S3**) Obtain the estimates for $\{\varrho_{k,\ell}^{(i)}\}$ using (5.36).

**S4**) Update $\{\Delta\mathcal{H}_i^{k,\ell}\}$ using (5.37)–(5.40).

**S5**) Find $\{\delta\mathcal{H}_i[k]\}$ using (5.27)–(5.30), and then update the estimates for the even sub-carrier channels using (5.41). Go back to Step 4 until convergence.

**S6**) From the estimates $\{\Delta\mathcal{H}_i^{k,\ell}\}$, use (5.31) to get the estimates for the even sub-carrier channels, and then use (5.42) for the odd sub-carrier channels.

In the Appendix D, an algorithm that iteratively reduces the channel estimation error for an arbitrary number of antennas deployed in a high data rate systems is presented.

The proposed method attempts to procure C-CSI by devising ratios that relate the a posteriori CSI estimates to the interpolated CSI estimates. When orthogonal training sequences are used for CSI estimation, an error occurs due to the assumption of CSI equity within the OFDM sub-symbol. In actual fact, the CSI will vary within the OFDM sub-symbol, and this variation can be related to the resultant error in CSI estimation (5.27)–(5.30). If the variation in the CSI within the OFDM sub-symbol is known through interpolation, the estimated CSI can be improved. The information on the variations in CSI within the OFDM sub-symbol can then be updated based on the improvements in the estimated CSI only. Hence, the ratios relating the a posteriori CSI estimates to the interpolated CSI estimates can be used to iteratively improve

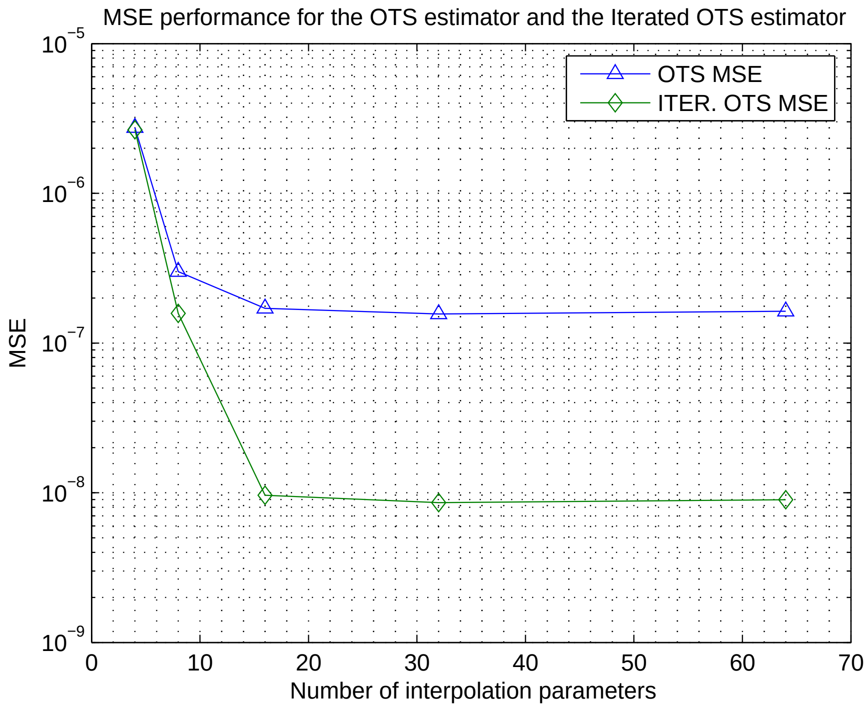


Figure 5.9: MSE vs. number of interpolation parameters for the Orthogonal Training Sequence (OTS), and the Iterated Orthogonal Training Sequence (ITER. OTS) estimators. The results show that the accuracy of interpolation affects the performance of the proposed ITER. OTS method - SNR = 100dB.

the a posteriori CSI estimates. The question, however, is the effect that errors in interpolation of CSI have on the iterative method. In order to train many MIMO transmitters (for example each user $p$ may be equipped with $n_t^p = 2$ antennas), equity has to be assumed for OFDM sub-symbols whose length is equal to the total number of antennas, $\sum_{p=1}^{P} n_t^p = n_t$. This reduces the number of interpolation parameters ($n_I$ a posteriori CSI estimates) in equation 5.18 and affects the accuracy of interpolation.

In figure 5.9, the MSE in channel estimates for increasing numbers of channel estimation parameters is evaluated for the orthogonal training sequence (OTS) method and the iterated (ITER) OTS method when $n_t^p = 2$ and $K = 128$. TDMA channel estimation is assumed, where non-overlapping rectangular functions are used to multiplex the users. In other words, each of the user's antennas transmits training sub-symbols of length $K_{coh} = 2$, then remains silent whilst another user is trained. This scheme is similar to the "time slots" used in GSM and the number of users being trained in the system is thus $P = K/(n_t^p \times n_I)$. Results in figure 5.9, relate to the Fourier transformation matrix basis where $L = 16$ and $L$ is the number of non-zero of parameters in the Channel Impulse Response (CIR) vector. As can be noted in figure 5.9, when $n_I < L$, the iterative method provides only marginal improvements.

In addition, the proposed algorithm is found to be unduly sensitive to AWGN in the received symbol, resulting in worse MSE performance at low SNR. This is thought to be because the least squares interpolation cf. (5.18) at low SNR provides unreliable information on CSI variation which further exacerbates the noisy posteriori CSI measurements when the iterative scheme is implemented.

## 5.4 Chapter Summary

A detailed analysis of the MSE performance of the RP-CSI estimator shows that for an orthogonal training sequence and Fourier basis, the lower bound of the MSE agrees with previously published results. Based on this analysis, the RP-CSI framework is used to evaluate the performance of various CSI bases that reduce the number of channel estimation parameters. These consideration are motivated by the training requirements for high data rate MIMO-OFDM systems deploying large number of transmit antennas, such as multi-user systems.

For uplink communications, the transmitting antennas from the $P$ users may be very large $\sum_{p=1}^{P} n_r^p = n_r$ when compared to the receiving antennas at the base station $n_t$. It becomes necessary for the base station to train the $n_r$ antennas simultaneously in order to enable coherent MIMO-OFDM communication based either on spatial multiplexing or space-frequency coding, cf. Section 1.5. Such overloaded communications systems can effectively be studied by considering a single user MISO-OFDM system for which the number of channel estimation parameters is reduced to reflect the number of users' communication simultaneously with the base station. This approach takes into account all the important variables, which are as follows:

- A maximum of $K$ OFDM sub-carriers are available for communications between the base station and the mobile station. RP-CSI estimators are based on correlations over this number of OFDM sub-carriers, therefore the OFDM symbol length is a limiting factor for any overloaded MIMO-OFDM system.

- Given a fixed resource $K$ for channel estimation, the LS solution implemented in OFDM symbol based RP-CSI estimators requires that the number of parameter unknowns is less than or equal to number of observations $K$. Each transmit antenna is associated with $n_w$ parameters which describe the multi-path channel so that the maximum number of antennas that can be simultaneously trained is given by $n_t = K/n_w$.

- Alternatively, the number of antennas that can be trained is determined by the availability of orthogonal training sequences. For a fixed resource $K$, a maximum of $n_t = K$ antennas can be trained simultaneously if a suitable training sequence is devised. However this provides a single CSI estimate over the whole OFDM symbol, which is undesirable as it is expected that the CSI will vary significantly with increasing sub-carrier index. A compromise is therefore necessary where the number of antennas that are trained is $n_t \ll K$ leading to $K/n_t$ CSI estimates per antenna. The remaining CSI are deduced through interpolation.

The above mentioned variables are carefully studied within this chapter in the context of the overloaded MIMO-OFDM system. This leads to an alternative performance criterion for MIMO-OFDM channel estimators, where performance is limited primarily by the maximum delay spread of the multipath channels. The Saleh-Valenzuela channel model which has a root mean square (rms) delay spread of approximately $\tau_{rms} = 50ns$ and a maximum delay of $\tau_{max} = 200ns$ is used in the evaluation of RP-CSI estimators. This sets the limit for the minimum number of channel estimation parameters using the Fourier basis as $L = \tau_{max}/T_s$, where $T_s$ is the QAM symbol period. This in turn means that the maximum number of antennas that can be trained is $n_t = K/L$ in order to implement the LS solution. Similar limitations are observed when OFDM sub-symbol estimators are implemented due to the interpolation LS solution cf. Section 5.3.

The performance of the Fourier Basis, the novel Wavelet Basis and the novel Principal Component Analysis (PCA) Basis are all investigated for reduced parameter channel estimation MSE performance. In the first instance, this performance is measured against the signal to noise ratio, which shows that the PCA basis has superior performance. The Fourier basis is then used for interpolation purposes in a new iterative scheme described in Section 5.3.2 and the MSE performance is again evaluated as a function of number of the number of channel estimation parameters. It is found that the posteriori CSI measurements based on orthogonal training sequence estimators can be improved by devising ratios which relate the measured CSI to interpolated CSI. These ratios are used to iteratively reduce the error in channel estimation due to CSI variations within the coherence bandwidth. Even so, AWGN adversely affects the performance of the proposed scheme and additional work on smoothing CSI measurements and obtaining reliable information on CSI variation at low SNR is necessary.

# Chapter 6

# Time Varying Channels

For Non-Line-of-Sight (NLOS) communications, the amplitude of the multipath gain is expected to vary according to Rayleigh distribution whilst the phase of the multipath gain is expected to be uniformly distributed due to the numerous propagation paths available. However, if the receiver were to move at a constant velocity, the carrier frequency for each multipath component will experience a different Doppler frequency shift because of the differing Angle of Arrival (AoA) relative to the moving vehicle for the various propagation paths. The phase of the multipath gain thus varies rapidly with receiver motion because it is a function of the Doppler frequency shift. The relative delay of the multipath components is however expected to vary slowly in such scenarios.

In this chapter, the Kalman filter approach for the tracking of time varying multipath channel gain is investigated. This discussion is motivated by the fact that training symbol based RP-CSI uses an entire OFDM symbol for 1-D, frequency domain channel estimation, and relies on the coherence of the channel in time for data detection in subsequent OFDM symbols. Clearly, when the receiver is mobile, a strategy is required to track the fast changes in the multipath gain during data transmission in order to ensure low error rates in data detection. Kalman tracking does not require the knowledge of the transmitted pilot sequence as Reduced Parameter CSI Estimation can utilize the detected data within the OFDM symbol. Data can be reliably detected in the OFDM symbols that are close to, or adjacent to the training symbol, and provided that the QAM symbol signaling is orthogonal, the detected data can be then be reprised as pilots for RP-CSI. In addition, Kalman filtering has the effect of reducing noise corrupted CSI through adherence to a model of the temporal variations of CSI. The main disadvantage of Kalman filtering is that orthogonal QAM symbol signaling is required, and as a consequence, the data rate of the MIMO-OFDM system decreases, particularly when the number of transmitting antennas is large. Clarke's Model is introduced to determine temporal channel variations and results from Kalman tracking are compared to time domain Discrete Prolate Spheroidal Sequence RP-CSI which are identified as optimal in the literature.

## 6.1 Clarke's Model

This section describes Clarke's model which is used to model the variations of the multipath channel gain with measurement time.

$$\bar{h}_{\bar{\gamma}}(t,\tau) = \sum_{n=0}^{N-1} \bar{\gamma}_n(\tau_n(t), t)\delta(t - \tau_n(t)) \tag{6.1}$$

The frequency selective channel model c.f (6.1) considered thus far for RP-CSI channel estimation is extended to include the effects of doppler frequency change and the performance of the estimator evaluated for the Discrete Prolate Spheroidal Sequence (DPSS) basis and the Kalman filter. The doubly selective channel model implemented, which is commonly referred to as Clarke's Model, is described in the literature [13] and [67]. In this model, the phase associated with the $n$th path is considered independent from the phase due to the Doppler frequency change. As it can be noted from the discussion below, the phase change due to path length is much greater than the phase change due to the Doppler frequency change which necessitates a distinction of the two quantities.

Clarke's Model can be derived from the equation for the received complex envelope for a signal transmitted at a carrier frequency $f_c$ cf. (2.6).

$$\bar{s}_m^{rx}(t) = \sum_{n=0}^{N-1} \gamma_n(t) e^{-j2\pi f_c \tau_n(t)} \bar{s}_m^{tx}(t - \tau_n(t)) \tag{6.2}$$

When the receiver is stationary, the complex channel gain $\bar{\gamma}_n(\tau_n(t), t) = \gamma_n(t)e^{-j2\pi f_c \tau_n(t)}$ can be modeled as an i.i.d complex process cf. Section 2.2.3. In order to separate the effect path length to those associated with the motion of the receiver, we shall start by expressing the phase of the multipath gain in the frequency selective model c.f. (6.1) as a function of path length. The phase of the multipath gain ($\phi_n = 2\pi f_c \tau_n(t)$ in 6.2) can be expressed as a function of path length $\ell_n$ by writing $\phi_n = \frac{2\pi}{\lambda_c}\ell_n$, where $\lambda_c$ is the wavelength of the RF carrier frequency. When the receiver is in motion at a constant velocity $v$, the phase of the multipath gain will change because of changes in the path lengths $\ell_n$. In addition, the frequency of the signal arriving via the $n$th path will experience a Doppler frequency shift which we denote as a variable $f_n$. The Doppler frequency shift $f_n$ for each multipath component is modified according to the azimuth Angle of Arrival (AoA) which we shall denote as $\theta_n$.

$$f_n = f_d \cos(\theta_n) = \frac{f_c v}{c} \cos(\theta_n) \tag{6.3}$$

$f_d = \frac{f_c v}{c}$ is the maximum Doppler frequency shift (Doppler bandwidth), which is attributed to the LOS multipath components. The phase of the multipath gain can be modeled as the summation of the path length induced and Doppler frequency induced phases when the receiver is moving.

$$\bar{s}_m^{rx}(t) = \sum_{n=0}^{N-1} \gamma_n(t) e^{j(2\pi f_n \tau_n(t) - 2\pi \frac{\ell_n}{\lambda_c})} \bar{s}_m^{tx}(t - \tau_n(t)) \tag{6.4}$$

We now introduce an alternative view to the signal received in a multipath environment in order to determine the measurement time variations in the complex channel gain $\bar{\gamma}_n(\tau_n(t), t)$. Consider that at some measurement time instant $t$, $N$ multipath components arrive with the same delay $\tau_n(t) = t$. The channel gain affecting the signal $\bar{s}_m^{rx}(t)$ in (6.4) at this measurement time is given by

$$\bar{\gamma}(t) = \sum_{n=0}^{N-1} \gamma_n(t) e^{j(2\pi f_n t - 2\pi \frac{\ell_n}{\lambda_c} + \alpha_n)} \tag{6.5}$$

$\alpha_n$ is a random phase associated with the $n$th path. The phase $\phi_n = (2\pi\ell_n/\lambda_c - \alpha_n)$ is independent of the measurement time and can be modeled using uniform distribution. This assumption generalizes the geometry of the communications system in terms of location of the transmitter, receiver and multipath mechanisms. The azimuth AoA ($\theta_n$) determines the Doppler frequency shift of the $n$th path as $\frac{f_c v}{c}\cos(\theta_n)$ and can also be modeled using uniform distribution. The amplitudes $\gamma_n(t)$ can be modeled using Gaussian distribution by virtue of the central limit theorem cf. Section 2.2.3. It is assumed that as the measurement time $t$ elapses, the amplitude of the multipath gain remains constant ($\gamma_n(t) = \gamma_n$). This model is Clarke's flat fading model [75]. Note that, in Clarke's model, path length induced phase for the different multipath components will be the same whilst the AoA-dependent Doppler induced phase will differ depending on the path. This is due to the fact that the $N$ multipath components arriving at the measurement time $t$ have the same delay $\tau_n(t) = t$ and hence the same path lengths $\ell_n$ but may have different AoAs. *Clark's model evaluates the gain of the channel $\bar{\gamma}_n(\tau_n(t), t)$ when $\tau_n(t) = t$ so that we are effectively considering a single multipath delay $\tau_n(t)$ as time elapses.*

The transformation of the complex channel gain $\bar{\gamma}_n(t)$ due to Doppler frequency induced phase changes results in the power spectral density

$$S(\nu) = \frac{1}{\pi f_d \left(1 - \frac{\nu}{f_d}\right)} \qquad |\nu| \leq f_d \tag{6.6}$$

$\nu$ is the frequency variable and $f_d$ is the maximum Doppler frequency. This

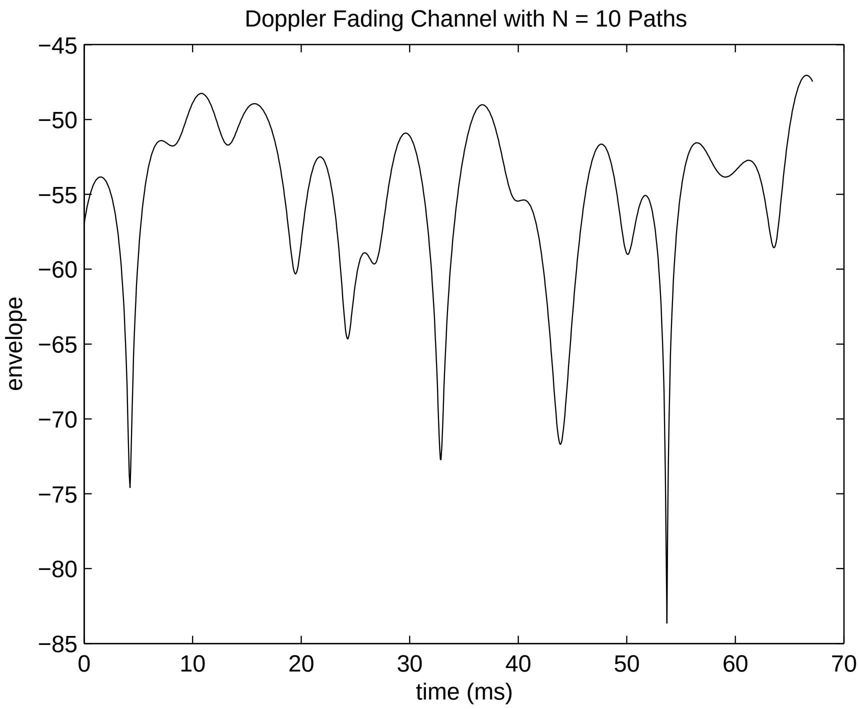


Figure 6.1: Channel $|\bar{\gamma}_n(t)|$ gain variations for a receiver travelling at a velocity of 50mph.

spectrum was derived by Jakes in the literature [25].

## 6.2 Slepian Basis Expansion

In Chapter 4, RP-CSI based on the 1-D correlations of the CSI in the frequency domain was introduced. Clarke's model can be used to show that the variations of CSI in the time domain show a high degree of correlation that can also be exploited for the purposes of channel estimation. This section introduces an optimal basis for time domain RP-CSI and it is assumed that training sequences are orthogonal in time rather than in frequency.

Slepian [88] showed that a time limited snapshot of a bandlimited sequence spans a low dimensional subspace, and this subspace is also spanned by Discrete Prolate Spheroidal Sequences (DPSS). The term sequence, as used here, refers to the vectors constructed for the gain of the multipath components as a function of measurement time. These vectors depict the variation of the gain of the multipath component as an ordered list (as a function of increasing measurement time). In the literature [89], one dimensional DPSS sequences are used for channel estimation in a multi-user Multi-Carrier Code Division Multiple Access (MC-CDMA) downlink in a time variant frequency selective channel. It is reported that the Slepian basis expansion per sub-carrier is three magnitudes smaller than the Fourier basis expansion and as such, represents an alternative basis within a RP-CSI framework. Here, the necessary background to facilitate similar comparisons is provided for the case where 1-D time domain basis are evaluated in RP-CSI estimators.

In order to derive the RP-CSI estimators for time domain based channel analysis, Clarke's model cf. Section 6.1 is used to describe multipath component gain variations as a function of measurement time. Clarke's model assumes that the multipath gain can be written as a sum of $N$ multipath components arriving simultaneously at a given measurement time $t$ cf. (6.5).

$$\bar{h}(t) = \sum_{n=0}^{N-1} \bar{\gamma}_n(t) e^{j2\pi f_n t} \tag{6.7}$$

In the equation (6.7) each multipath component is characterized by its complex weight $\bar{\gamma}_n(t) = \gamma_n(t)e^{-j\phi_n}$ cf. 6.5 which embodies the amplitude and phase shift, and additionally, the Doppler frequency shift induced phase $e^{j2\pi f_n t}$. Denoting the QAM symbol period of the communications system by $T_s$, the sampled multipath component gain can be written as

$$\bar{h}(mT_s) = \sum_{n=0}^{N-1} \bar{\gamma}_n(mT_s) e^{j(2\pi \nu_n m)} \tag{6.8}$$

where $\nu_n = f_n T_s$ is the normalized Doppler frequency shift for the $n$th multipath component. In order to establish the measurement intervals, we recall that in Section 2.2, the convolution model of the wireless channel was derived and it was determined that the received OFDM symbol of length $K$ is given by the convolution of the transmitted OFDM symbol and the CIR vector of length $L$. Note that the CIR vector for the convolution cf. (2.6) is a sequence of the multipath component gain as a function of the relative delays rather the measurement time required here. For the transmission of OFDM symbol in multipath channels, redundancy must be added to the transmitted OFDM symbol in order to maintain orthogonality of the sub-carriers [35] cf. Section 3.1. This is done by adding a repetition of some of the transmit QAM symbol to the beginning of each OFDM symbol burst resulting in a length $(K+L-1)$ transmit symbol. Taking these system considerations into account the 1-D representation of the multipath channel gain parameters cf. (6.8) as a function of measurement time can be arranges in a vector

$$\mathbf{h} = \begin{bmatrix} h(0) & h\left((K+L-1)T_s\right) & \ldots & h\left((M-1)(K+L-1)T_s\right) \end{bmatrix}^T \tag{6.9}$$

The time-variant fading process $\{h(mT_s)\}$ given by the model in (6.9) is band-limited to the region $W = [-\nu_d \; \nu_d]$, where $\nu_d$ is the maximum normalized

Doppler frequency shift. Note that the vector $\mathbf{h}$ is also time limited to the indices $I = [0, 1, \ldots, M]$ on which we calculate $\{h(mT_s)\}$.

**Definition 6.1** The one-dimensional Discrete Prolate Spheroid Sequences (DPSS) $v_k(m)$ with band-limit $W = [-\nu_d\ \nu_d]$ and concentration region $I = [0, 1, \ldots, M]$ are defined as the real solutions of

$$\sum_{n=0}^{M-1} \frac{\sin(2\pi\nu_d(m-n))}{\pi(m-n)} v_k(n) = \lambda_k v_k(m) \tag{6.10}$$

The LHS of the equation above is the dot product of two vectors of length $M$. The DPSS vectors $\mathbf{v}_k = [v_k(0), v_k(1), \ldots, v_k(M-1)]^T$ are the eigenvectors of the $M \times M$ matrix $\mathbf{S}$ with elements $S(m,n) = \sin(2\pi\nu_d(m-n))/\pi(m-n)$. The eigen decomposition of the square matrix $\mathbf{S}$ can thus be written as $\mathbf{SB} = \mathbf{B\Lambda}$, where $\mathbf{B} \equiv [\mathbf{v}_1, \mathbf{v}_2, \ldots, \mathbf{v}_k]$ and $\mathbf{\Lambda} \equiv \texttt{diag}(\lambda_1, \lambda_2, \ldots, \lambda_k)$. When considering RP-CSI, the concentration region $I = [0, 1, \ldots, M]$ is the time domain window c.f 6.9 that is used for channel estimation. The power density spectrum of these CSI samples is Jakes spectrum [25] which is non zero within the closed interval $W = [-\nu_d\ \nu_d]$.

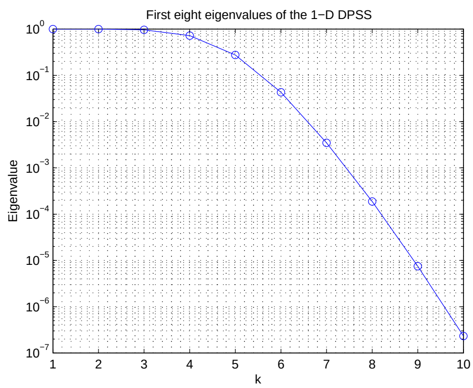


Figure 6.2: The first ten eigenvalues $\lambda_k, k = 1, 2, \ldots, 10$ for 1-D DPSS for $M = 256$ and $M\nu_d = 2$.

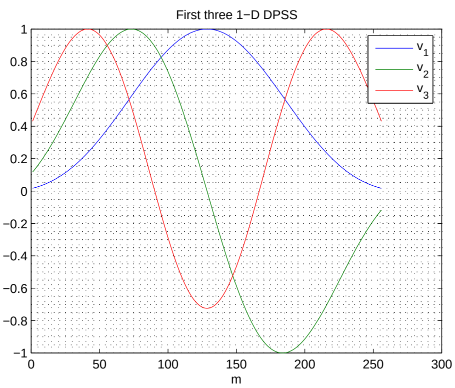


Figure 6.3: The first three eigenvectors $v_k, k = 1, 2, \ldots, 3$ for 1-D DPSS for $M = 256$ and $M\nu_d = 2$.

The eigenvalues of the matrix $\mathbf{S}$ decay exponentially and thus render numerical calculation difficult [90]. However, the inverse iteration method presented in the literature [91] enables fast and numerically stable calculation of DPSS. In this thesis, MATLAB functions are used to generate the DPSS.

**Theorem 6.2** The DPSS are orthogonal on the set $I$ and on $\mathbb{Z}$, the set of integers. In addition, every band-limited sequence $\mathbf{h}$ can be decomposed uniquely as $\mathbf{h} = \mathbf{B}\mathbf{w}$, where $\mathbf{B} \equiv [\mathbf{v}_1, \mathbf{v}_2, \ldots, \mathbf{v}_{k_{max}}]$ and $\mathbf{v}_k$ are DPSS.

For the proof of theorem 6.2 see the literature [88]. Parameter reduction is obtained through the DPSS property that the energy in the index-set $I$ is contained in the first $k_{max} = \lceil 2\nu_d M \rceil + 1$ DPSS vectors [90]. The CIR sequence cf. (6.9) is not readily available in the MIMO-OFDM system because the time domain received symbols are a convolution product cf. (3.1). In addition, because Clarke's model is used to depict the time varying changes in a flat fading channel, an alternative representation of the sub-carrier channel gain may be derived [89].

$$H[k,m] = \sum_{n=0}^{L-1} h[n,m] e^{-j\frac{2\pi kn}{L}} e^{j2\pi f_n mT} \tag{6.11}$$

$$H[k,m] = \sum_{n=0}^{L-1} \acute{h}[n,m] e^{j2\pi\nu_n m} \tag{6.12}$$

The equation (6.11) is evaluated at the measurement time intervals $T = (K + L - 1)T_s$ where $T_s$ is the QAM symbol period. In the CSI representation cf. (6.11), each multipath component at the delay $nT_s$ is associated with a doppler frequency shift and $L$ is the maximum number of non-zero elements in the CIR vector cf. Section 3.1. The representation cf. (6.12) compares to the representation cf. (6.8. The discrete time duration $m(K + L - 1)$ includes the duration of the OFDM symbol and the guard period due to the cyclic prefix. This representation makes it possible to use the DPSS basis for

| Parameter | Simulation Settings |
|---|---|
| Carrier Frequency | $f_c = 2.4 \times 10^9 Hz$ |
| OFDM Symbol length | $K = 128$ |
| OFDM Cyclic Prefix | $L = 16$ |
| QAM Symbol Period | $T_s = 10 \times 10^{-9}(sec)$ |
| Maximum Delay spread | $\tau_{max} = 200 \times 10^{-9}(sec)$ |
| RMS Delay spread | $\tau_{rms} = 50 \times 10^{-6}(sec)$ |
| Receiver velocity | $v = 27.8(meters/sec)$ |
| SNR | $\infty$ |
| Coherence Time | $20 \times (K + L)T_s(sec)$ |

Table 6.1: Simulation Parameters for the comparison of 1-D MISO-OFDM Channel Estimation based on 4-QAM.

reduced parameter channel estimation. When the CSI are stacked in a vector $\tilde{\mathbf{h}}_i \equiv [H_i[k, 0], H_i[k, 1], \ldots, H_i[k, M-1]]^T$, the RP-CSI framework cf. Section can be introduced to reduce the number of parameters in the time domain channel estimation problem as follows

$$\tilde{\mathbf{r}} = \tilde{\mathbf{X}}\mathbf{PBw} \tag{6.13}$$

Note that $\mathbf{B}$ is the matrix containing the DPSS. $\tilde{\mathbf{X}}$ is the training sequence matrix and $\mathbf{P}$ is permutation matrix cf. Section 4.3.1. The vector $\mathbf{w}$ has a length $n_t k_{max} \leq M$ where $M$ is the number of OFDM symbols that form a channel estimation frame.

Note that for the simulations, the SNR is infinity so as to reject the effects of the orthogonality of the basis to noise. Channel measurements are assumed to be performed after a coherence period has elapsed cf. Table 6.1. This was done because it was noted through several simulation trials that the channel parameters remained constant for a number of OFDM symbols at the given data rate. It was therefore decided to assume a coherence time in order to clearly demonstrate the variations of the CSI with time. An implementation of the RP-CSI framework for time domain CSI estimation shows that

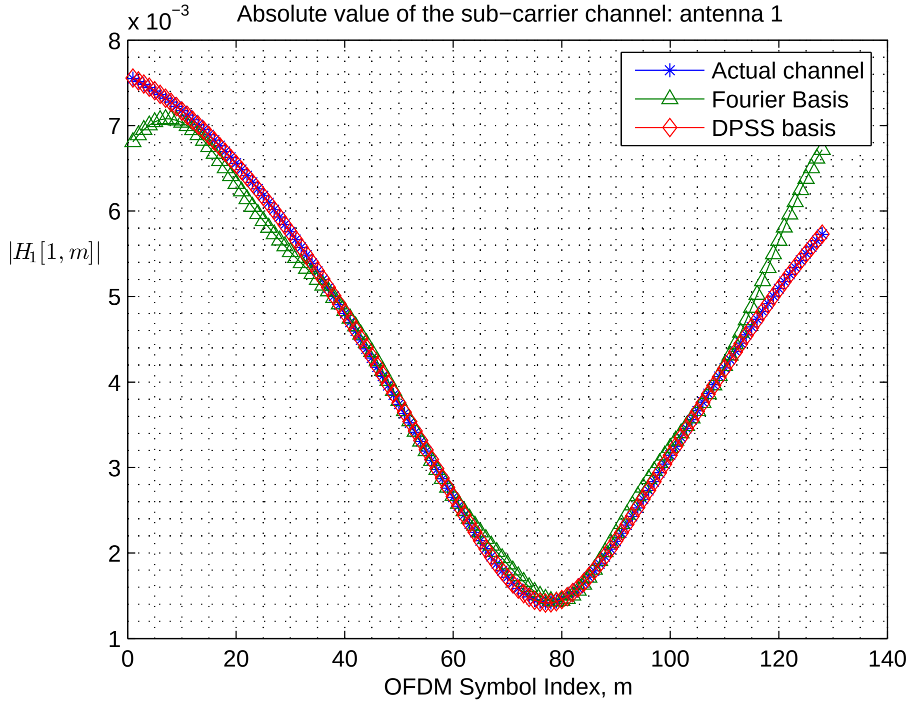


Figure 6.4: $|H_1[1, m]|$ for a (2,1) MISO-OFDM system based on the DPSS, and Fourier basis estimators. $n_w = 5$.

the DPSS basis outperforms the Fourier basis. Note that this result is true for 1-D CSI estimation in the time domain (increasing OFDM symbol index) but is generally not the case for 1-D CSI estimation in the frequency domain (increasing QAM symbol index).

In figure 6.6, the MSE in channel estimate is evaluated for an increasing number of channel estimation parameters $n_w$. The results in this figure are obtained for a user $p$ equipped with a MIMO transmitter with $n_t^p = 2$ antennas and $M = 128$. The total number of users that can be trained is given by $P = K/(n_t^p \times n_w)$. This number of users can be trained simultaneously using the RP-CSI estimator which does not require time slots as described for similar results in section 5.3.2. Note that for $n_w = k_{max} = 5$, where $k_{max} = \lceil 2\nu_d M \rceil + 1$ and $\nu_d M = 2$, the MSE is $10^{-10}$. Despite the fact that the SNR is assumed

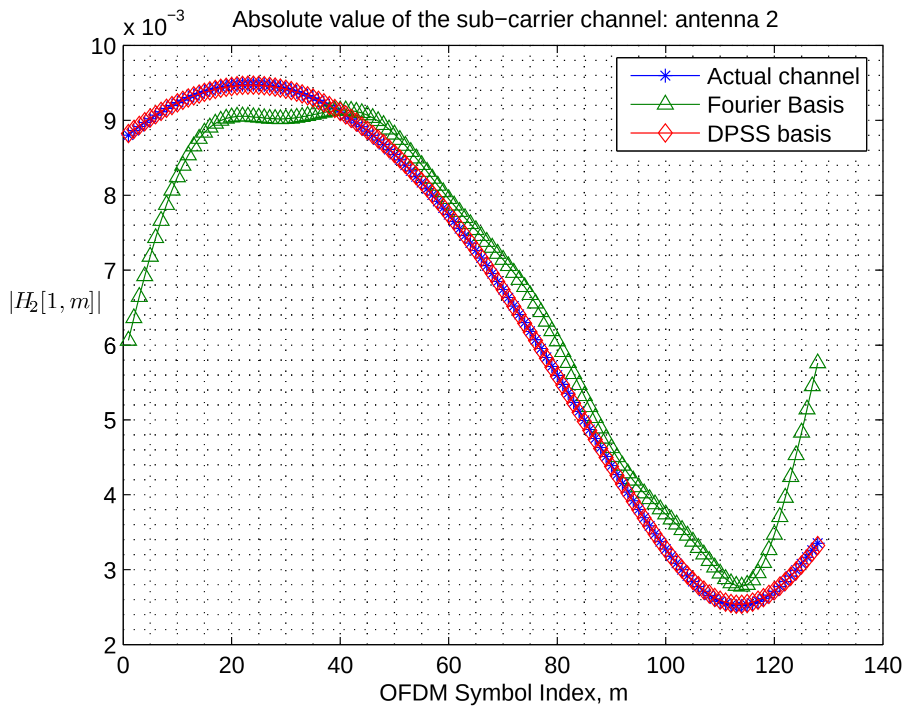


Figure 6.5: $|H_2[1, m]|$ for a (2,1) MISO-OFDM system based on the DPSS, and Fourier basis estimators. $n_w = 5$.

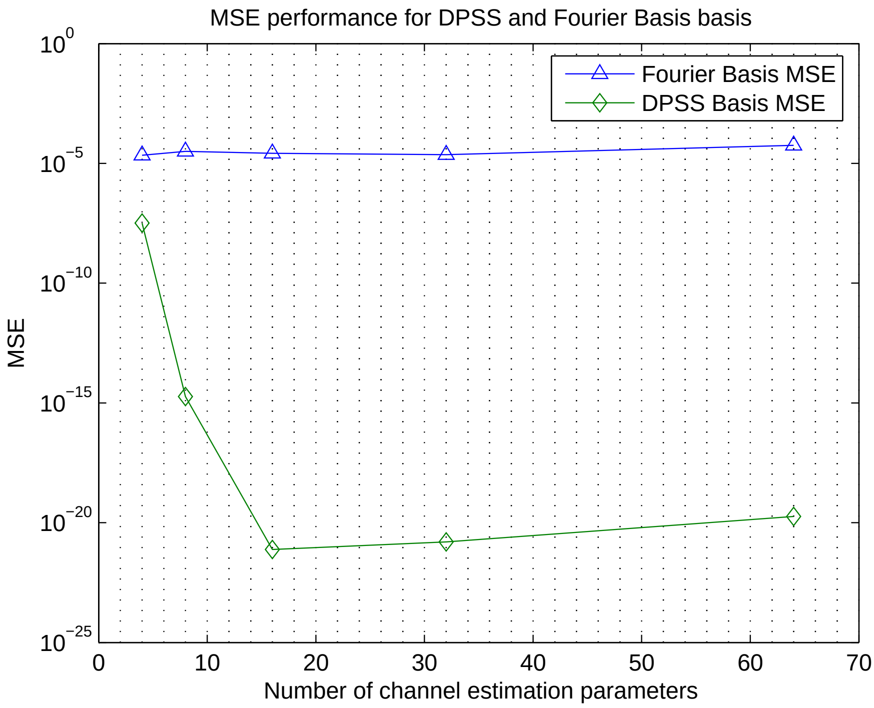


Figure 6.6: MSE vs. the number of estimated channel parameters for the Fourier and DPSS basis.

to be infinite, and unexpected result is that $n_w = 64$ results in a slight MSE degradation when compared to $n_w = 16$. At the time of writing this thesis, this result is still unexplained.

## 6.3 Kalman filter Tracking

The Kalman filter [76] is an efficient, recursive method of estimating the state of a discrete time varying process. The Kalman filter has previously been used to track the MIMO-OFDM channel gain as a time varying process in the literature [92]–[94]. The details of this application of the Kalman filter are provided here in order to highlight possible future developments for the RP-CSI time domain channel tracking.

Before describing the Kalman filter tracking algorithm, Clarke's channel model cf. (6.5) is related to the tapped-delay-line (TDL) model and to the channel model cf. (2.17) presented in Chapter 2. It has been shown that the received QAM symbol is a convolution of the transmitted QAM symbol with a $L$ length Channel Impulse Response of a communications channel which is characterized by multipath propagation cf. Section 2.2.2.

$$\bar{h}_{\bar{\gamma}}(t,\tau) = \sum_{n=0}^{L-1} \bar{\gamma}_n(\tau_n(t),t)\delta(t-\tau_n(t)) \tag{6.14}$$

The convolution of the QAM symbols with the CIR in (6.14) led to the tapped-delay-line (TDL) model of the system output (see Figure 2.3 in Section 2.2.2). This chapter considers the tracking of the TDL filter taps $\bar{\gamma}_n(\tau_n(t),t)$ by using Clarke's model to describe each TDL filter tap so that the notation $\bar{\gamma}(t)$ may be used for the multipath channel gain. The approach to deriving the discrete Kalman filter can be summarized as follows:

- Determine the mathematical description of the process whose state is to be estimated. In this case, the channel gain (TDL filter tap) which is based on Clarke's model is being tracked. This channel gain process is known to have a Doppler spectrum [25]. Hence, the Doppler spectrum for each TDL filter tap can be used to generate the time varying channel gain process from randomly generated i.i.d noise. This is approach forms the basis for the mathematical description of the process.

- Implement equations that describe how the process will vary with measurement time. As described above, a TDL filter tap can be generated by passing i.i.d noise though a bandpass filter whose frequency response is related to Jake's Spectrum. An autoregressive model is implemented in order to determine the relationship between previous states and current state of the TDL filter tap process.

- Determine the measurement equations. The TDL channel model relates the QAM symbol output of the channel to the QAM symbol input and the channel impulse response based on an underlying convolution model. This model was used to develop CSI estimators relating a known training sequence and received symbols to the unknown channel parameters. The RP-CSI estimators developed for MIMO-OFDM systems are used to develop measurement model relating measurements of the process to the current state of the process.

Using the first two steps described above, it can be determined that the time evolution of the channel gain process is governed by the *process model* and that the process model dictates the current state for the process based on a previous state. Let the $\mathbf{x}_k \in \mathbb{C}^{N\times 1}$ denote the channel gain process vector and suppose we formulate the following process model:

$$\mathbf{x}_k = \mathbf{F}_{k-1}\mathbf{x}_{k-1} + \mathbf{w}_{k-1} \tag{6.15}$$

$\mathbf{w}_{k-1} \in \mathbb{C}^{N\times 1}$ denotes the process noise vector which is assumed to be normally distributed with zero mean and covariance matrix $\mathbf{Q}$, so that we can write $p(w) \sim N(0, \mathbf{Q})$. $\mathbf{F}_{k-1} \in \mathbb{C}^{N \times N}$ is a matrix that relates the state of the channel gain process at a previous time step $k-1$ to the state at the current time step $k$. We will assume that $\mathbf{F}_{k-1}$ and the process noise covariance matrix $\mathbf{Q}$ are constant with each time step.

For the third step of deriving the Kalman filter, the flat fading model MIMO-OFDM model for the data based RP-CSI estimator is used to develop the *observation model*. The observation model relates measurements on the time varying process (in this case the noisy CIR estimates) to the actual state of the channel gain process. Suppose that the measurement model has been formulated as follows

$$\mathbf{z}_k = \mathbf{H}_k \mathbf{x}_k + \mathbf{v}_k \tag{6.16}$$

$\mathbf{H}_k \in \mathbb{C}^{M \times N}$ is a matrix that relates the state of the channel gain process $\mathbf{z}_k$ and the measured channel gain process $\mathbf{x}_k$ at the current time step $k$. $\mathbf{v}_{k-1} \in \mathbb{C}^{M \times 1}$ denotes the measurement noise vector which is assumed to be normally distributed with zero mean and covariance matrix $\mathbf{R}$, so that $p(v) \sim N(0, \mathbf{R})$. We will assume that $\mathbf{H}_k$ and the measurement noise covariance matrix $\mathbf{R}$ are constant with each time step.

If we define $\hat{\mathbf{x}}_k^-$ as our *a priori* estimate of the channel gain based on the process model (6.15) we can formulate an equation for the *a posteriori* state estimate $\hat{\mathbf{x}}_k$ based on the measurement model as follows

$$\hat{\mathbf{x}}_k = \hat{\mathbf{x}}_k^- + \mathbf{K}_k(\mathbf{z}_k - \mathbf{H}_k \hat{\mathbf{x}}_k^-) \tag{6.17}$$

$\mathbf{K} \in \mathbb{C}^{M \times N}$ is the Kalman gain/blending factor which is designed to minimize the a posteriori error covariance $\mathbf{P}_k = E[(\mathbf{x}_k - \hat{\mathbf{x}}_k)(\mathbf{x}_k - \hat{\mathbf{x}}_k)^T]$. One form of the Kalman gain that achieves this minimization [77] can be accomplished by

$$\mathbf{K}_k = \frac{\mathbf{P}_k^- \mathbf{H}_k}{\mathbf{H}_k \mathbf{P}_k^- \mathbf{H}_k^T + \mathbf{R}} \tag{6.18}$$

$\mathbf{P}_k^-$ is the a priori estimate covariance $\mathbf{P}_k^- = E[(\mathbf{x}_k - \hat{\mathbf{x}}_k^-)(\mathbf{x}_k - \hat{\mathbf{x}}_k^-)^T]$. The Kalman filter estimates the channel gain process by using a form of feedback control: the filter estimates the process state at some time using the process model and then obtains feedback in the form of the (noisy) measurement model.

| Discrete Kalman filter process update equations |
|---|
| $\hat{\mathbf{x}}_k^- = \mathbf{F}\hat{\mathbf{x}}_{k-1}$ <br> $\mathbf{P}_k^- = \mathbf{F}\mathbf{P}_{k-1}\mathbf{F}^T + \mathbf{Q}$ |

Table 6.2: Table of the process update equations.

The time update equations (6.2) project the state and covariance estimates forward from time step $k-1$ to step $k$. Initial conditions for the filter are given in the MATLAB code in Appendix E.

| Discrete Kalman filter measurement update equations |
|---|
| $\mathbf{K} = \frac{\mathbf{P}_k^- \mathbf{H}_k}{\mathbf{H}_k \mathbf{P}_k^- \mathbf{H}^T + \mathbf{R}}$ <br> $\hat{\mathbf{x}}_k = \hat{\mathbf{x}}_k^- + \mathbf{K}(\mathbf{z}_k - \mathbf{H}\hat{\mathbf{x}}_k^-)$ <br> $\mathbf{P}_k = (\mathbf{I} - \mathbf{K}\mathbf{H})\mathbf{P}_k^-$ |

Table 6.3: Table of the measurement update equations.

The process and measurement update equations for $\mathbf{P}_k^-$ and $\mathbf{P}_k$ are derived in the literature [78]. Note that the time step index $k$ is omitted form the matrices $\mathbf{K}$, $\mathbf{F}$ and $\mathbf{H}$ because we assume that they are time invariant.

### 6.3.1 Deriving the Kalman Filter Process Model

In order to simulate the wireless multipath channel when the receiver is mobile, we can generate the channel gain for a TDL filter tap by first of all generating a vector of a white, discrete time, Gaussian process to represent random changes of the TDL filter tap with time. After generating the noise vector, the power spectral density[1] of the noise process is "shaped" so that it assume the form of the Doppler spectrum (6.6) at each tap location. The shaping filter (impulse response) is real and has a pure amplitude transfer function $H(\nu) = \sqrt{S(\nu)}$ cf. (6.6).

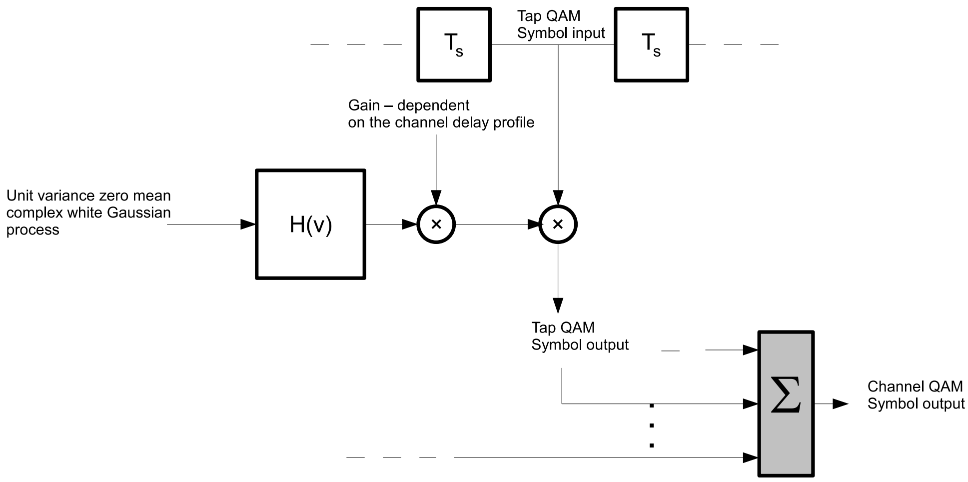


Figure 6.7: Tapped-delay-line model for diffuse multipath channels with tap generation.

Since $H(\nu)$ is a real and symmetric function, the impulse response of the spectrum shaping filter $h(t)$ can be derived from the cosine transform, which can be found in the literature [79].

$$h(t) = F^{-1}\left[H(\nu)\right] = A^{\frac{1}{2}} 2^{\frac{1}{4}} \pi^{\frac{1}{2}} f_d t^{-\frac{1}{4}} \Gamma\left(\frac{3}{4}\right) J_{\frac{1}{4}}(2\pi f_d |t|) \tag{6.19}$$

$J_{\frac{1}{4}}(\cdot)$ is the fractional Bessel function, $\Gamma(\cdot)$ is is the Gamma function, and $A^{\frac{1}{2}}$ is chosen such that $h(t)$ has the normalized power of 1 [26]. In order to derive the Kalman filter process model, the Finite Impulse Response (FIR) form of the channel gain process is converted into its equivalent Autoregressive model [80]. If the input of the FIR filter is Gaussian white noise then the output of the shaping filter is simply the convolution sum

[1]the power spectrum density of a Gaussian process is flat and wideband

$$x[n] = \sum_{m=0}^{M-1} w[n-m]h[m] \tag{6.20}$$

$h[n]$ is the sampled impulse response of the spectrum shaping filter $h(t)$ cf. (6.19), $w[n]$ is the vector of a white (discrete time) Gaussian process with zero mean and unit variance, and $x[n]$ is the channel gain with the Doppler power spectral density. Using the delay operator $z^{-1}$, the FIR model can be written as

$$x[n] = \left( \sum_{m=0}^{M-1} h[m](z^{-1})^m \right) w[n] \tag{6.21}$$

The summation in brackets can be regarded as a polynomial $P(z^{-1}) = \sum_{m=0}^{M-1} h[m](z^{-1})^m$ in the delay operator, so that we can write

$$x[n] = P(z^{-1})w[n] \tag{6.22}$$

$$\frac{1}{P(z^{-1})}x[n] = w[n] \tag{6.23}$$

This rational function $\frac{1}{P(z^{-1})}$ can be expanded using partial functions and using the geometric series expansion, $\frac{1}{1-pz^{-1}} = \sum_{i=0}^{\infty}(pz^{-1})^i$.

$$\begin{aligned}
\frac{1}{P(z^{-1})} &= \frac{1}{h_0 + h_1 z^{-1} + \ldots, +h_{M-1}(z^{-1})^{M-1}} && (6.24)\\
&= \frac{r_1}{1-pz^{-1}} + \frac{r_2}{1-pz^{-1}} + \cdots + \frac{r_{M-1}}{1-pz^{-1}} && (6.25)\\
&= r_1 \sum_{i=0}^{\infty}(pz^{-1})^i + r_2 \sum_{i=0}^{\infty}(pz^{-1})^i + \cdots + r_{M-1} \sum_{i=0}^{\infty}(pz^{-1})^i && (6.26)\\
&= \sum_{i=0}^{M-1} r_i + z^{-1} \sum_{i=0}^{M-1} p_i r_i + z^{-2} \sum_{i=0}^{M-1} p_i^2 r_i + \ldots && (6.27)
\end{aligned}$$

The infinite sum in (6.27) is formed by expanding the geometric series formulae in (6.26) and grouping together the like terms. In order to make the infinite sum tractable, it can be estimated as a summation of $N+1$ terms.

$$\frac{1}{P(z^{-1})} = \sum_{i=0}^{M-1} r_i + z^{-1}\sum_{i=0}^{M-1} p_i r_i + z^{-2}\sum_{i=0}^{M-1} p_i^2 r_i + \cdots + z^{-N}\sum_{i=0}^{M-1} p_i^N r_i \quad (6.28)$$

$$= \Pi_0 + z^{-1}\Pi_1 + z^{-2}\Pi_2 + \cdots + z^{-N}\Pi_N \quad (6.29)$$

In 6.29, the substitution $\Pi_n = \sum_{i=0}^{M-1} p_i^n r_i$ has been used for clarity. The result (6.29) can now be inserted into (6.23) in order to obtain an autoregressive model.

$$(\Pi_0 + z^{-1}\Pi_1 + z^{-2}\Pi_2 + \cdots + z^{-N}\Pi_N)x[n] = w[n] \quad (6.30)$$

$$\Pi_0 x[n] = -\Pi_1 x[n-1] - \Pi_2 x[n-2] - \cdots - \Pi_N x[n-N] + w[n] \quad (6.31)$$

$$x[n] = \frac{-\Pi_1}{\Pi_0}x[n-1] + \frac{-\Pi_2}{\Pi_0}x[n-2] + \cdots + \frac{-\Pi_2}{\Pi_0}x[n-N] + w[n] \quad (6.32)$$

$$x[n] = \sum_{i=1}^{N} \phi_i x[n-i] + w[n] \quad (6.33)$$

In (6.31) we use the result $z^{-v}x[n] = x[n-v]$ for multiplication with the delay operator $z^{-1}$. The autoregressive model cf. (6.23) can be used to develop a process model for a single TDL filter tap $x[n-1]$ by writing the matrix equation

$$\begin{bmatrix} x[n] \\ x[n-1] \\ x[n-2] \\ \vdots \\ x[n-N+1] \end{bmatrix} = \begin{bmatrix} \phi_1 & \phi_2 & \dots & \phi_{N-1} & \phi_N \\ 1 & 0 & \dots & 0 & 0 \\ 0 & 1 & \dots & 0 & 0 \\ \vdots & \vdots & \ddots & \vdots & \vdots \\ 0 & 0 & \dots & 1 & 0 \end{bmatrix} \begin{bmatrix} x[n-1] \\ x[n-2] \\ x[n-3] \\ \vdots \\ x[n-N] \end{bmatrix} + \begin{bmatrix} w[n] \\ 0 \\ 0 \\ \vdots \\ 0 \end{bmatrix} \quad (6.34)$$

$$\mathbf{x}_n = \mathbf{F}\mathbf{x}_{n-1} + \mathbf{w}_n \quad (6.35)$$

The equation (6.35) is in the form of the form (6.15). However, the equation (6.35) allows for the tracking of only a single TDL filter tap, and there are $L$

such taps that require tracking. We can expand the equation (6.35) to track several TDL filter tap by augmenting $L$ column vectors $\mathbf{x}_n^l$ and $\mathbf{x}_{n-1}^l$, where $l$ is the index of the filter tap. The same state transition matrix $\mathbf{F}$ is used for all the TDL filter taps [44].

### 6.3.2 Deriving the Kalman Filter Measurement Model

In Chapter 4, The RP-CSI estimator is introduced which can be used to reduce the number of parameters estimated for MIMO-OFDM channel estimation. It can be inferred that the RP-CSI estimator using the Fourier basis yields the truncated (to a length $L$ rather than $N$) time domain vector $\mathbf{h}$ in equation (2.50). In Section 6.3.1, a process model is developed for a single element of the truncated time domain vector $\mathbf{h}$ in equation (2.50). This section concludes the derivation of the Kalman filter by deriving the matrix $\mathbf{H}$ used in measurement equations.

Note that the RP-CSI estimator uses a received OFDM symbol $\tilde{\mathbf{r}}$ in order to calculate the CSI vector $\mathbf{h}$ using the Fourier basis. Because the received symbol is a function of $L$ TDL filter taps, some simplifiying assumptions are in order to track the $L$ channel parameters separately. It can be shown that the measurement matrix $\mathbf{H}$ is simply the identity matrix $\mathbf{I} \in \mathbb{R}^{L \times L}$.

Recall the equation for the channel estimates based on the basis $\mathbf{B}$ such that $\mathbf{Q} = (\tilde{\mathbf{X}}\mathbf{P}\mathbf{B})^H$, where $\mathbf{P}$ is an orthonormal, square, permutation matrix, $\tilde{\mathbf{X}}$ is a matrix of training symbols, and $\mathbf{B}$ is the Fourier basis matrix.

$$\hat{\mathbf{h}} = \mathbf{Q}\tilde{\mathbf{r}} = \mathbf{h} + \mathbf{Q}\mathbf{n} \tag{6.36}$$

$\mathbf{n}$ is an AWGN vector. Equation (6.36) can be used to derive the measurement model for the Kalman Filter. Each estimated TDL filter tap $\hat{\mathbf{h}}[l] = z^l[n]$ at the time index $n$ can be written as

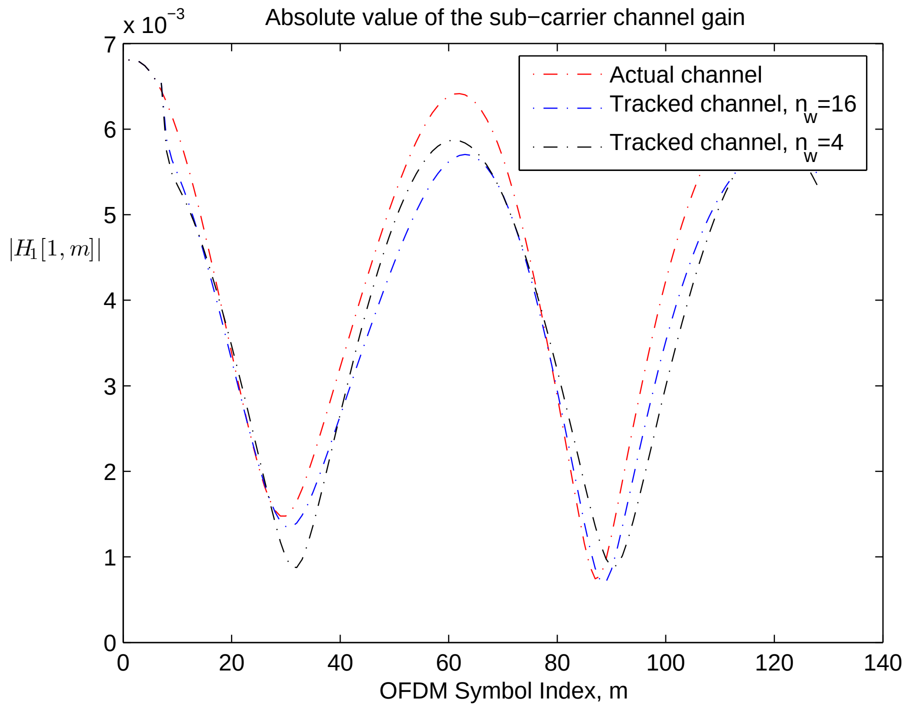


Figure 6.8: Simulation results showing the tracking of the channel gain at a single antenna for a single sub-carrier. Note that reducing the number of estimated parameters $n_w$ causes a marked change in the tracking output of the Kalman filter.

$$z[n] = x[n] + v[n] \tag{6.37}$$

$\{v[n]\}$ are the elements of the vector $\mathbf{Qn}[l] = v^l[n]$ and $\{x[n]\}$ are the TDL filter taps for a length $L$ CIR $\mathbf{h}[l] = x^l[n]$. In order to be consistent with the matrix form of the process model (6.35) we can write each element $\hat{\mathbf{h}}[l] = z^l[n]$ as a process in the time index $n$

$$\begin{bmatrix} z[n] \\ z[n-1] \\ z[n-2] \\ \vdots \\ z[n-N+1] \end{bmatrix} = \begin{bmatrix} 1 & 0 & \dots & 0 & 0 \\ 0 & 1 & \dots & 0 & 0 \\ 0 & 0 & \dots & 0 & 0 \\ \vdots & \vdots & \ddots & \vdots & \vdots \\ 0 & 0 & \dots & 0 & 1 \end{bmatrix} \begin{bmatrix} x[n] \\ x[n-1] \\ x[n-2] \\ \vdots \\ x[n-N+1] \end{bmatrix} + \begin{bmatrix} v[n] \\ v[n-1] \\ v[n-2] \\ \vdots \\ v[n-N+1] \end{bmatrix} \tag{6.38}$$

$$\mathbf{z}_n = \mathbf{H}\mathbf{x}_n + \mathbf{v}_n \tag{6.39}$$

In equation (6.39) it can be noted that the measurement matrix $\mathbf{H}$ is the identity matrix $\mathbf{I} \in \mathbb{R}^{L \times L}$. The Kalman filter can then be implemented as in described in section 6.3. As with the process model, the $L$ TDL filter taps can be tracked by augmenting the measurement vectors $\mathbf{z}_n$ and the process vectors $\mathbf{x}_n$ which are related by the same measurement matrix $\mathbf{H}$ [44].

A future challenge for the work presented in this section is to determine how measurements may be derived using the RP-CSI estimator based on some random data sequence in the matrix $\tilde{\mathbf{X}}$ cf. (6.36). In Figure 6.8, results are presented for Kalman tracking but importantly, it is assumed that the unknown data has the properties of an orthogonal Hadamard sequence cf. (4.47). Such requirements would reduce the throughput of the MIMO-OFDM system. If the unknown data does not have the orthogonal property, a solution may not be available based on the LS solution implemented in the RP-CSI estimator due to an insufficient number of independent observations in the received symbol vector. The results in Figure 6.8 show that there are differences in the tracking output when RP-CSI estimators for varying numbers of estimation parameters are implemented. Note also that for an adequate number of channel estimation parameters $n_w = 16$, the Kalman filter does not track the channel as well as the DPSS basis cf. Figure (6.4 and 6.5). A single iteration of the Kalman filter was considered in this comparison between the DPSS basis and the Kalman filter RP-CSI estimators.

Additional work may be done on the simulation and analysis of the tracking performance when estimated parameters and the CIR vector are related via $\mathbf{Bw} = \mathbf{Fh}$, so that $\mathbf{h} = \mathbf{F}^{-1}\mathbf{Bw}$.

## 6.4 Conclusions & Future Work

When QAM symbols are transmitted over a wireless channel, the detection error probability decays exponentially in SNR for the AWGN channel while it decays only inversely with the SNR for the fading channel [12]. The main reason why detection in the fading channel has poor performance is not because of the lack of knowledge of the channel at the receiver. It is due to the fact that the channel gain is random and there is a significant probability that the channel is in a "deep fade" [12]. Various authors have compared the performance of techniques such as adaptive coding which introducing tolerance to slow Rayleigh fading channels for radio access schemes [98]–[100]. In addition, the impact of channel uncertainty on the performance has been studied by various authors, including Medard and Gallager [95], Telatar and Tse [96] and Subramanian and Hajek [97]. The MIMO-OFDM technology exploits spatial and frequency diversity in order to increase the reliability of QAM symbol transmission through fading channels. Spatial diversity is achieved through the deployment of multiple antennas (MIMO) at both sides of the wireless link and it can be shown that the MSE is inversely proportional to the SNR raised to some power, and that the exponent of the SNR is the diversity gain [12]. Frequency diversity is achieved through a multi-carrier modulation scheme (OFDM) where transmit precoding is performed to convert the ISI channel into a set of non-interfering, orthogonal sub-carriers, each experiencing narrowband flat fading.

In the literature [1] the effects of imperfect CSI on a space time coding

MIMO system are evaluated through simulation. Space time coding systems are effectively the flat fading channel MIMO equivalent of the space frequency coding systems described in detail in Section 1.5.1. The difference is that Space frequency coding MIMO systems implement OFDM modulation that results in flat fading channels, but the coding is equivalent in frequency and time. In the literature [1], it is assumed that CSI is obtained through Orthogonal Training Sequence channel estimation and that errors in the CSI estimation are as a result of additive White Gaussian Noise (AWGN) in the received symbols. In the literature, [18], [101] and [102], the main result on the subject is that error below 15% are tolerable, such that the diversity advantage of the scheme is maintained. However, it was noted in Section 5.3.2 that errors in CSI estimates occur due to the assumptions on the correlation of CSI within the coherence bandwidth. A future aim of the work presented in this thesis is to extend the results cited here to include errors due to variations of CSI within the coherence bandwidth.

In the literature [103], a time-domain analysis of imperfect channel estimation in spatial multiplexing (cf. Section 1.5.2) OFDM-based multiple-antenna transmission systems is studied. It is noted, as in this thesis, that the channel estimator encountered with imperfect windowing results in an additional estimation error. This literature also considers the performance of orthogonal training sequences for channel estimation in spatial multiplexing systems. In all cases, Space time coding and spatial multiplexing, the diversity gain is of interest when evaluating the effects of imperfect CSI at the receiver. The analytical error probabilities for MIMO-OFDM systems in Rayleigh fading channel may be derived as in the literature [12] and the performance of the system with imperfect CSI at the receiver evaluated through simulation [1]. Future work to be undertaken includes establishing error performance bounds for spatial multiplexing and space frequency coding systems, where the diversity gain is degraded. This may be done by evaluating the analytical probability of error for various antenna configurations and evaluating the performance of a given MIMO-OFDM system with CSI errors. This analysis should be extended to the time domain tracking of channels with both directions of study (time and frequency domain channel estimation) taking into account various basis with reduced parameter properties.

In the literature [12], the sum capacity of the uplink and downlink flat fading channels for a multi-user system is related to the multi-user diversity gain. Compared to a system with a single transmitting user, the multi-user gain comes from two effects: optimal power allocation and the availability of numerous channels on which the power allocation is optimized. It is noted that the increase in the full CSI sum capacity comes from a multi-user diversity effect: when there are many users that fade independently, at any one time there is a high probability that one of the users will have a strong channel. The larger the number of users, the stronger tends to be the strongest channel, and the more the multi-user diversity gain [12]. An analysis of the effects of imperfect CSI on multi-user systems can be based on the results in the literature [74]. This literature provides a study on the lower and upper bounds of mutual information under channel estimation error, and it is shown that the two bounds are tight for Gaussian inputs. The effects of the number of users on the CSI estimation error in a multi-user system has been studied in this thesis. These results can be used to investigate the effects of CSI estimation error on multi-user diversity using the error bounds provided in the literature [74] and further efforts made on the design of an optimal CSI estimation basis.

# Bibliography

[1] S. Glisic, Advanced Wireless Communications 4G Technologies, John Wiley & Sons Ltd, 2004.

[2] A. Goldsmith, Wireless Communications, Cambridge University Press, 2005.

[3] Prof. W. Webb, Wireless Communications: The Future, John Wiley & Sons Ltd, 2007.

[4] W. Chu, Speech Coding Algorithms: Foundation and Evolution of Standardized Coders, John Wiley & Sons Ltd, 2004.

[5] H. Holma, and A. Toskala, WCDMA for UMTS : Radio Access for Third Generation Mobile Communications, John Wiley & Sons Ltd, 2004

[6] J. Heiskala, J. Terry, OFDM Wireless LANs: A Theoretical and Practical Guide, Sams Publishers, 2001.

[7] V. Kuhn, Wireless Communications over MIMO Channels: Applications to CDMA and Multiple Antennas Systems, John Wiley & Sons Ltd, 2006

[8] V. Tarokh, A. Naguib, N. Seshadri, and A. R. Calderbank, Combined array processing and space-time coding, *IEEE Transactions on Information Theory*, vol. 45, no. 4, pp. 1121–1128, May 1999.

[9] J. Yang and S. Roy, On joint transmitter and receiver optimization for multiple-input multiple-output (MIMO) transmission systems, *IEEE Transactions on Communications*, vol. 42, no. 12, pp. 3221–3231, Dec. 1994.

[10] S. Hirst and A. G. Burr, Investigating the Richness of the Finite Scatterers MIMO Wireless Channel, IEE Proc. Commun, Vol. 153 No. 4, Aug 2006, pp. 496-500.

[11] F. Stremler, Introduction to Communication Systems, Addison-Wesley, 1990

[12] D. Tse and P. Viswanath, Fundamentals of Wireless Communication, Cambridge University Press, 2005.

[13] F. Gross, Smart Antennas for Wireless Communications, The McGraw Hill Companies, 2005.

[14] R. W. Chang, Synthesis of band-limited orthogonal signals for multichannel data transmission, Bell System Technical Journal, 45, 17751796, 1966.

[15] B. R. Saltzberg, Performance of an efficient parallel data transmission system, IEEE Transactions on Communications, 15, 805811, 1967.

[16] H. Stern S. A. Mahmoud and L. E. Stern, Communications Systems Analysis and Design, Prentice Hall, 2004.

[17] Alamouti, S. M., "A simple transmit diversity technique for wireless communications, *IEEE Journ. Sel. Areas in Communs.*, pp. 1451–1458, Vol. 16, no. 8, Oct 1998

[18] V. Tarokh, H. Jafarkhani and A. R. Calderbank, Space-time block codes from orthogonal designs, IEEE Transactions on Information Theory, 48(5), 1999, 14561467.

[19] G. J. Foschini, Layered space-time architecture for wireless communication in a fading environment when using multi-element antennas, Bell Labs Technical Journal,vo. 1, no.2, pp. 41-59, 1996

[20] G. J. Foschini, and M. J. Gans, "On limits of wireless communication in a fading environment when using multiple antennas," *Wireless Personal Commun.*, Vol. 6, No. 3, pp. 311–355, Mar. 1998.

[21] J. H. Winters, J. Salz and R. D. Gitlin, The impact of antenna diversity on the capacity of wireless communication systems, IEEE Transactions on Communication, 42(24), Part 3, 17401751, 1994,

[22] A. M. Khachan, A. J. Tenenbaum, and R. S. Adve, Linear processing for the downlink in multiuser MIMO systems with mutiple data streams, in Proc. of IEEE ICC - To appear, June 2006.

[23] H. Karaa, R. Adve and A. Tenenbaum, "Linear precoding for Multiuser MIMO-OFDM Systems," *IEEE Int. Conf. On Communs.*, pp. 2797–2802, Jun. 2007.

[24] T. S. Rappaport, Wireless Communications: Principles and Practice, Prentice Hall, 2002.

[25] W. C. Jakes, Microwave Mobile Communications, New York: Wiley, 1974.

[26] M. Jeruchim, P. Balaban, K. Shanmugan, Simulation of Communications systems: Modelling, Methods and Techniques, Kluwer Academic Publishers, 2002.

[27] S. Kay, An Intuitive Probability and and Random Processes Using Matlab, Springer Science+Business Media, Inc., 2006.

[28] A. B. Carlson, P. B. Crilly, and J. C. Rutledge, Communications Systems. McGraw-Hill, 4th Edition, 2002.

[29] L. W. Couch, II, Digital and Analogue Communications Systems. Prentice Hall, 6th Edition, 2001.

[30] B. Sklar, Digital Communications: Fundamentals and Applications. Prentice Hall, 2th Edition, 2001.

[31] M. Cicerone, O. Simeone, U. Spagnolini, "Channel Estimation for MIMO-OFDM Systems by Modal Analysis/Filtering," *IEEE J. Trans. on Commun.*, vol. 54, Isuue. 11, pp. 2062–2074, Nov. 2006.

[32] Adel A. M. Saleh, and Reinaldo A. Valenzuela, "A statistical model for indoor multipath propagation," *IEEE J. Select. Areas Commun.*, vol. SAC-5, no. 2, pp. 128–137, Feb 1987.

[33] D. M. J. Devasirvantham, M. J. Krain, and D. A. Rappaport, "Radio propagation measurements at 850 GHz, 1.7 GHz, and 4.0 GHz inside two dissimiler office buildings," *IEE Elect. Letters*, vol. 26, no. 7, pp. 445–447, Jun. 1990.

[34] B. Vucetic and J. Yuan, Space-Time Coding, John-Wiley, 2003.

[35] A. Peled, and A. Ruiz, "Frequency domain data transmission using reduced computational complexity algorithms," *Proc. of IEEE Int. Conf. Acoustics Speech and Signal Processing*, vol. 5, pp. 964–967, Apr. 1980.

[36] E. Sjstrm , Singular Value Computations for Toeplitz Matrices, PhD Thesis, Department of Mathematics Linkping University, S-581 83 Linkping, Sweden, 1996.

[37] M. Engels, Wireless OFDM Systems: How to make them work, Kluwer Academic Publishers, 2002.

[38] S. Kaiser, Multi-Carrier CDMA Mobile Radio Systems - Analysis and Optimization of Detection, Decoding, and Channel Estimation, PhD Thesis published in *VDI-Verlag, Dusseldorf, Germany*, IBSN 3-18-353110-0, 1998.

[39] P. Hoeher, S. Kaiser, P. Robertson, Two-dimensional pilot-symbolaided channel estimation by Wiener filtering, in *Proc. ICASSP97, Munich, Germany*, pp. 1845-1848, April 1997.

[40] P. Hoeher, TCM on frequency-selective land-mobile fading channels, in *Proc. 5th Tirrenia Int. Workshop on Dig. Comm., Tirrenia, Italy, pp.* 317-328, Sept. 1991.

[41] P. Hoeher, S. Kaiser, P. Robertson, Pilot-symbol-aided channel estimation in time and frequency, in *Proc. IEEE Global Telecommunications Conference GLOBCOM97, Pheonix, USA*, pp. 90-96, Nov 1997.

[42] L. Hanzo, M. Munster, B. J. Choi, and T. Keller, OFDM and MC-CDMA for Broadband Multi-User Communications, WLANS and Broadcasting, IEEE press, John Wiley & Sons, 2003.

[43] K. Fazel, S. Kaiser, Multi-Carrier and Spread Spectrum Systems, Chap. 4, pp 139-158, John Wiley & Sons, 2003.

[44] R. Safaya, Mulipath Channel Estimation Algorithm using a Kalman Filter, Master's Thesis, pp 31-35, Illinois Institute Of Technology, Chicago, 1997.

[45] Y. Li, N. Nambirajan, and S. Ariyavisitakul, "Channel estimation for OFDM systems with transmitter diversity in mobile wireless channels," *IEEE J. Select. Areas Commun.*, vol. 17, pp. 1233–1243, Jul. 1999.

[46] I. Barhumi, G Leus and M. Moonen, "Optimal training design for MIMO in mobile wireless channels," *IEEE Trans. Sig. Proc.*, vol. 51, no.6, pp. 1615–1624, Jun. 2003.

[47] Y. Li, "Optimal training sequences for OFDM systems with multiple transmit antennas," *IEEE Trans. Commun.*, vol. 49, no. 12, pp. 2115–2123, Dec. 2001.

[48] A. Dietrich, and W. Utschick, "Pilot-assisted channel estimation based on second order statistics," *IEEE Trans. Sig. Proc.*, vol. 17, no. 3, pp. 461–471, Mar. 1999.

[49] P. Ranta, A. HOttinen, and Z. Honkalso, "Co-channel interference cancelling receiver for TDMA mobile sytem," *Proc. of IEEE Int. Conf. on Commun.*, vol. 1, issue. 18-22, pp. 17–21, Jun. 1995.

[50] S. J. Carlos and D. Fratta, Discrete signals and inverse problems; an introduction for engineers and scientists, John Wiley & Sons, 2005.

[51] G. Tsoulos, MIMO System Technoloy for Wireless Communications, taylor and Francis Group, 2006.

[52] J. Hamilton, Time Series Analysis, Princeton University Press, 1994.

[53] S. Colieri, M. Ergen, A. Puri, and A. Bahai, A study of channel estimation in OFDM systems, in Proc. of IEEE VTC, pp. 894-898, 2002.

[54] C. Kastenholtz and W. Birkemeir, A simultaneous information transfer and channel sounding modulation technique for wide-band channels, IEEE Transactions on Communication Technology pp.162175, June 1965.

[55] B. Farhang-Boroujeney, Pilot-based channel identification: proposal for semi-blind identification of communication channels, IEE Electronic Letters vol. 31, no. 13, pp.10441046, June 1995.

[56] G. Zhou, M. Viberg, and T. Mckelvey, Super-imposed periodic pilots for blind channel estimation, in Proceedings of 35th Asilomar Conference on Signals, Systems, and Computers Pacific Grove, CA, pp.653657, November 2001.

[57] N. Chen and G.Zhou, A superimposed periodic pilot scheme for semi-blind channel estimation of OFDM systems, in Proceedings of the 10th IEEE DSP Workshop Pine Mountain, GA, pp.362365, October 2002.

[58] J. Tugnait and W. Luo, On channel estimation using super-imposed training and first order statistics, in Proceedings of IEEE International Conference on Acoustic, Speech and Signal Processing Hong Kong, China, pp.624627, April 2003.

[59] A. G. Orozco-Lugo, M. M. Lara, and Des C. McLernon, Channel Estimation using Implicit Training, IEEE Transactions on Signal Processing, vol. 52, no. 1, pp. 240254, January 2004.

[60] S. Mallat, A Wavelet Tour of Signal Processing, Academic Press, 1998.

[61] W. Sweldens, "The lifting Scheme: a custon-design construction of second generation wavelets," *J. of Appl. and Comput. Harmonic Analysis*, vol. 3, no.2, pp. 186–200, Jun. 1996.

[62] I. Daubechies, "Orthonormal Bases of Compactly Supported Wavelets," *Comm. Pure Appl. Math.*, vol. 41, no. 7, pp. 909–996, Oct. 1988.

[63] Arne Jense and Anders la Cour-Harbo, Ripples in Mathematics: the Discrete Wavelet Transform, Springer Verlag 2001, ISBN 3-540-41662-5

[64] Stphane Mallat, A Wavelet Tour of Signal Processing, Academic Press 1999, ISBN : 0-12-466606-X

[65] M. Siala, Maximum a posteriori semi-blind channel estimation for OFDM systems operating on highly frequency selective channels, Ann. Telecommun., vol. 57, no. 9/10, pp. 873924, Sep./Oct. 2002.

[66] Golub, Gene H. & van Loan, Charles F. , Matrix Computations, 3rd edition, Johns Hopkins University Press, 1996

[67] S. Kaiser, Multi-Carrier CDMA Mobile Radio Systems - Analysis and Optimization of Detection, Decoding, and Channel Estimation, Dsseldorf: VDI-Verlag, Fortschritt-Berichte VDI, series 10, no. 531, 1998,

[68] D, Lay, Linear Algebra and its Applications, 3rd edition, Addison-Wesley Publishing Company, 2002

[69] T. Tung, and K. Yao, "Channel estimation and optimal power allocation for a multiple antenna OFDM system," *EURASIP Journ. on App. Signal Proc.*, vol. 2002, no. 3, pp. 330–339, Mar. 2002.

[70] Y. Li, "Simplified channel estimation for OFDM systems with multiple transmit antennas," *IEEE Trans. Wireless Commun.*, vol. 1, no. 1, pp. 67–75, Jan. 2002

[71] A. Viterbi, CDMA: Priciples of Spread Specctrum Communications, Addison-Wesley Publishing Company, 1995.

[72] T. M. Cover, J. A. Thomas, Elements of Information theory, John Wiley & Sons, Inc., 1991.

[73] M. Medard. The Effect upon Channel Capacity inWireless Communications of Perfect and Imperfect Knowledge of the Channel. IEEE Trans. Info. Theory, 46(3):933.946, May 2000.

[74] T. Yoo and A. Goldsmith. Capacity and Power Allocation for Fading MIMO Channels With Channel Estimation Error . IEEE Trans. Info. Theory, 52(5):2203.2214, May 2006.

[75] Haykin, S. and M. Moher, Modern Wireless Communications, Prentice Hall, New York, 2005.

[76] Kalman, R. E. 1960. A New Approach to Linear Filtering and Prediction Problems, Transaction of the ASMEJournal of Basic Engineering, pp. 35-45 (March 1960).

[77] Brown, R. G. and P. Y. C. Hwang, Introduction to Random Signals and Applied Kalman Filtering, Second Edition, John Wiley & Sons, Inc., 1992.

[78] Simon, D., (ed.), Optimal State Estimation; Kalman, H$\infty$ and Non-Linear Approaches, John Wiley & sons, inc., Publishers, 2006.

[79] H. Bateman, Table of Integral Transforms, Vol. I, McGraw-Hill, New York, 1954.

[80] George E.P. Box, Gwilym, M. Jenkins, Gregory C. Reinsel, Time series analysis: forecasting and control. Publisher: Prentice Hall, 1994.

[81] S. B. Weinstein and P. Embert, "Data transmission by frequency divison multiplexing using the discrete Fourier transform," *IEEE Trans. Commun. Tech.*, vol. 19, no. 5, pp. 628–634, Oct. 1971.

[82] I. Telatar, "Capacity of Multiantenna Gaussian Channels," *European Transactions on Telecommuncations*, vol. 10, no. 6, pp. 585–595, Noveember-December. 1999.

[83] R. Negi, and J. Cioffi, "Pilot tone selection for channel estimation in mobile OFDM systems," *IEEE Trans. Cons. Elec.*, vol. 44, no. 3, pp. 1122–1128, Aug. 1998.

[84] B. L. Hughes, "Differential space-time modulation," *IEEE Trans. Info. Theory*, vol. 46, no. 7, pp. 2567–2578, Nov. 2000.

[85] M. Dong, L. Tong, and B. M. Sadler, "Optimal insertion of pilot symbols for transmissions over time-varying flat fading channels," *IEEE Trans. Sig. Proc.*, vol. 52, no. 5, pp. 1403–1418, May 2004.

[86] H. Minn, D. I. Kim, and V. K. Bhargava, "A reduced-complexity channel estimation for OFDM systems with transmit diversity in mobile wireless channels," *IEEE Trans. Wireless Commun.*, vol. 50, no. 5, pp. 799–807, May 2002.

[87] M. Cicerone, Osvaldo Simeone, Umberto Spagnolini, "Channel Estimation for MIMO-OFDM Systems by Modal Analysis/Filtering," *IEEE Transactions on Communications*, vol. 54, no. 10, pp. 1896-1896, Nov 2006

[88] D. Slepian, Prolate spheroidal wave functions, Fourier analysis, and uncertaintyV: the discrete case, The Bell System Technical Journal, vol. 57, no. 5, pp. 13711430, 1978.

[89] T. Zemen and C. F. Mecklenbrauker, Time-variant channel estimation using discrete prolate spheroidal sequences, IEEE Transactions on Signal Processing, vol. 53, no. 9, pp. 35973607, 2005.

[90] Florian Kaltenberger, Thomas Zemen, and Christoph W. Ueberhuber, Low-Complexity Geometry-BasedMIMO Channel Simulation, EURASIP Journal on Advances in Signal Processing Volume 2007 (2007), Article ID 95281, 17 pages, May 2007

[91] Bell, B., Percival, D.B. and Walden, A.T. Calculating Thomson's Spectral Multitapers by Inverse Iteration, J. Comput. and Graph. Stat., 1993.

[92] D. Schafhuber, G. Matz, F. Hlawatsch, Kalman tracking of time-varying channels in wireless MIMO-OFDM systems, in Proc. of Asilomar-03, Pacific Grove (CA), Nov. 2003.

[93] M. Enescu, T. Roman, M. Herdin, Kalman-Based Estimation of Measured Channels in Mobile MIMO OFDM System, in XII. European Signal Processing Conference EUSIPCO-2004, September 6-10, Vienna Austria, pp. 1865-1868, 2004.

[94] T. Roman, M. Enescu, V. Koivunen, Joint Time-Roman Tracking of Channel and Frequency Offsets for MIMO OFDM Systems, in Wireless Personal Communications, Vol.31, pp.181-200, 2004.

[95] M. Mdard and R. G. Gallager, Bandwidth scaling for fading multipath channels, IEEE Transactions on Information Theory, 48(4), 840852, 2002.

[96] E. Telatar and D. Tse, Capacity and mutual information of wideband multipath fading channels, IEEE Transactions on Information Theory, 46(4), 13841400, 2000.

[97] V. G. Subramanian and B. E. Hajek, Broadband fading channels: signal burstiness and capacity, IEEE Transactions on Information Theory, 48(4), 809827, 2002.

[98] W. Webb and R. Steele, Variable rate QAM for mobile radio, IEEE Transactions on Communications, vol. 43, pp. 2223-2230, July 1995.

[99] R. Steele and L. Hanzo, eds., Mobile Radio Communications. New York, USA: IEEE Press - John Wiley & Sons, 2nd ed., 1999.

[100] D. Pearce, A. Burr, and T. Tozer, Comparison of counter-measures against slow Rayleigh fading for TDMA systems, in IEE Colloquium on Advanced TDMA Techniques and Applications, (London, UK), pp. 9/1-9/6, IEE, 28 October 1996. digest 1996/234.

[101] Gozali, R. and Woerner, B. D. (2002) The impact of channel estimation errors on spacetime trellis codes paired with iterative equalization/decoding, IEEE 55th Vehicular Technology Conference (VTC Spring 2002), 69 May 2002, 2, 826831.

[102] Garg, P., Mallik, R. K. and Gupta, H. M. (2002), Performance analysis of spacetime coding with imperfect channel estimation, IEEE International Conference on Personal Wireless Communications, December 1517 2002, pp. 7176.

[103] Y. You; H. Jung; W. Jeon; H. Cho, Impact of imperfect channel estimation in OFDM-based spatial multiplexing systems, IEEE Electronics Letters, Volume 38, Issue 24, 21 Nov 2002 pp 1589 - 1591.

# Appendix A

# Eigen Decomposition of the Channel Covariance Matrix

Consider a multipath channel where the reflected arrivals are a Poisson process with mean rate $\lambda$. For a specific realization, the delays relative to the Line-of-Sight (LoS) path are: $\{t_i : i = 1, 2, 3, \dots\}$. The complex amplitude of each tap $A(t)$, is a circular, zero mean, Normal random variable with an expected power that decays exponentially with delay:

$$E[A(t)A^*(t)] = ae^{-\mu t} \tag{A.1}$$

where $a$ and $\mu$ are constants. A specific realization of the channel impulse response $h(t)$ and its frequency response $H(\omega)$ may be written:

$$h(t) = \sum_{i=1}^{\infty} A(t_i)\delta(t - t_i) \tag{A.2}$$

$$H(\omega) = \sum_{i=1}^{\infty} A(t_i)e^{-j\omega t_i} \tag{A.3}$$

We wish to calculate the Eigen basis of the covariance of the transfer function $H(\omega)$. Note that $H(\omega)$ is zero-mean for all $\omega$ as $A(t)$ is zero-mean for all $t$. Therefore the covariance can be written as:

$$B(\omega_1,\omega_2) = E[H(\omega_1)H^*(\omega_2)] \tag{A.4}$$

$$= \sum_{i=1}^{\infty}\sum_{j=1}^{\infty} E[A(t_i)A^*(t_j)e^{-j\omega_1 t_i}e^{j\omega_2 t_j}] \tag{A.5}$$

Because the tap amplitudes are independent and zero mean, the cross terms in the expression cf. (A.5) do not contribute to the sum, i.e.,

$$B(\omega_1,\omega_2) = \sum_{i=1}^{\infty} E[A(t_i)A^*(t_i)e^{-j(\omega_1-\omega_2)t_i}] \tag{A.6}$$

For a Poisson process, the probability of a delay in the range $(t, t+dt)$ is $\lambda dt$ and the expression for the sum of expectations may be written:

$$B(\omega_1,\omega_2) = \int_0^{-\infty} ae^{-\mu t}e^{-j(\omega_1-\omega_2)t_i}\lambda dt \tag{A.7}$$

$$= \frac{\lambda a}{\mu + j(\omega_1-\omega_2)} \tag{A.8}$$

Note that the covariance is only a function of frequency difference i.e. $B(\omega_1,\omega_2) = B(\omega_1-\omega_2)$. This result may be used to show that Fourier basis functions are Eigen functions of the covariance of the transfer function $H(\omega)$. The Eigen functions $U(\omega)$ are the solutions of the integral equation:

$$\int_{-\infty}^{\infty} B(\omega_1,\omega_2)U(\omega_1) = \sigma^2 U(\omega_2) \tag{A.9}$$

The result in equation (A.8) may be used to simplify the expression for the Eigen functions cf. (A.9). Using the substitution $u = \omega_1 - \omega_2$ in equation (A.9) and assuming that $U(\omega_1) = e^{j\omega_1 t}$ in the expression cf. (A.9) yields

$$\int_{-\infty}^{\infty} B(\omega_1-\omega_2)e^{j\omega_1 t}d\omega_1 = \int_{-\infty}^{\infty} B(u)e^{j(u+\omega_2)t}du \tag{A.10}$$

$$= e^{j\omega_2 t}\int_{-\infty}^{\infty} B(u)e^{jut}du \tag{A.11}$$

The result cf. (A.11) shows that the function $U(\omega_1) = e^{j\omega_1 t}$ are the Eigen functions of the covariance of the transfer function $H(\omega)$. The Eigen values are $\sigma^2 = \int_{-\infty}^{\infty} B(u)e^{jut}du$.

# Appendix B

# Power Spectral Density

In this Appendix we provide proof for the relationship between the Power Spectral Density and the correlation functions in the time domain. This relationship has been used to determine the Power Delay Profile (PDP) from the Scattering function in Chapter 2 and also to determine the Coherence time when given the Doppler spectrum in Chapter (6). The proof is originally presented [11]

We shall start by defining the Power Spectral Density as a function of the signal $f(t)$. Let us define the Power Spectral Density function in the units (watts per Hz) whose integral yields the power in the time domain function $f(t)$. The time average power of a signal $f(t)$ that has been observed in the interval $(-T/2, T/2)$ is given by

$$P = \lim_{T\to\infty} \frac{1}{T} \int_{-T/2}^{T/2} |f(t)|^2 dt \tag{B.1}$$

$f(t)$ can be interpreted as the voltage $v(t)$ or current $i(t)$ applied to a 1ohm resistor. Parseval's theorem for the truncated function can be used to derive the Power Spectral Density function as follows

$$\int_{-T/2}^{T/2} |f(t)|^2 dt = \frac{1}{2\pi} \int_{-\infty}^{\infty} |F_T(\omega)|^2 d\omega \tag{B.2}$$

Hence the average power $P$ across a 1 $\Omega$ resistor is given by

$$P = \lim_{T\to\infty} \frac{1}{T}\int_{-T/2}^{T/2} |f(t)|^2 dt = \lim_{T\to\infty} \frac{1}{2\pi}\int_{-\infty}^{\infty} |F_T(\omega)|^2 d\omega \tag{B.3}$$

Combining the equation for Parseval's theorem (B.2–B.3), with our definition of the Power Spectral Density function $S_f(\omega)$ we have

$$\frac{1}{2\pi}\int_{-\infty}^{\infty} S_f(\omega) d\omega = \lim_{T\to\infty} \frac{1}{2\pi}\int_{-\infty}^{\infty} |F_T(\omega)|^2 d\omega \tag{B.4}$$

In addition, we insist that this relation should hold over each frequency increment so that equation (B.4) becomes

$$G_f(\omega) = \frac{1}{2\pi}\int_{-\infty}^{\omega} S_f(u) du = \lim_{T\to\infty} \frac{1}{2\pi}\int_{-\infty}^{\omega} |F_T(u)|^2 du \tag{B.5}$$

where $G_f(\omega)$ represents the cumulative amount of power for all frequency components below a given frequency $\omega$. For this reason $G_f(\omega)$ is called the cumulative power spectrum, or equivalently the integrated power spectrum of $f(t)$. If we interchange the order of the limiting operation and the integration is valid, equation (B.5) becomes

$$2\pi G_f(\omega) = \int_{-\infty}^{\omega} S_f(u) du = \int_{-\infty}^{\omega} \lim_{T\to\infty} \frac{1}{2\pi}\left|\frac{F_T(u)}{T}\right|^2 du \tag{B.6}$$

Note that the average or mean power contained in any frequency interval $(\omega_1, \omega_2)$ is $[G_f(\omega_2) - G_f(\omega_1)]$. In many cases, $G_f(\omega)$ is differntiable and we have

$$2\pi \frac{dG_f(\omega)}{d\omega} = S_f(u) \tag{B.7}$$

Under these conditions, equation B.6 gives

$$S_f(\omega) = \lim_{T\to\infty} \left|\frac{F_T(u)}{T}\right|^2 \tag{B.8}$$

Equation (B.8) is our desired result for the power spectral density of $f(t)$. We now show that the time domain autocorrelation is the operation which is equivalent to finding the power spectral density in frequency. If we assume that our relationship for the power spectral density is satisfied, the corresponding time domain operation is found by taking the inverse Fourier transform of (B.8)

$$F^{-1}\{S_f(\omega)\} = \frac{1}{2\pi}\int_{-\infty}^{\infty}\lim_{T\to\infty}\frac{1}{T}|F_T(\omega)|^2 e^{j\omega\tau}d\omega \tag{B.9}$$

We have purposefully chosen a new time variable, $\tau$, in equation (B.9) because the time variable $t$ is already in use in the definition of $F_T(\omega)$. Interchanging the order of operations yeilds

$$F^{-1}\{S_f(\omega)\} = \lim_{T\to\infty}\frac{1}{2\pi T}\int_{-\infty}^{\infty}F_T(\omega)^* F_T(\omega)e^{j\omega\tau}d\omega \tag{B.10}$$

$$= \lim_{T\to\infty}\frac{1}{2\pi T}\int_{-\infty}^{\infty}\int_{-T/2}^{T/2}f^*(t)e^{j\omega t}dt\int_{-T/2}^{T/2}f(t_1)e^{j\omega - t_1}dt_1 e^{j\omega\tau}d\omega \tag{B.11}$$

$$= \lim_{T\to\infty}\int_{-T/2}^{T/2}f^*(t)\int_{-T/2}^{T/2}f(t_1)\left[\frac{1}{2\pi}\int_{-\infty}^{\infty}e^{j\omega(t-t_1+\tau)}d\omega\right]dt_1 dt \tag{B.12}$$

The integral over $\omega$ within the brackets in (B.12) is now recognized as $\delta(t - t_1 + \tau)$, so that

$$F^{-1}\{S_f(\omega)\} = \lim_{T\to\infty}\int_{-T/2}^{T/2}f^*(t)\int_{-T/2}^{T/2}f(t_1)\delta(t - t_1 + \tau)dt_1 dt \tag{B.13}$$

$$= \lim_{T\to\infty}\int_{-T/2}^{T/2}f^*(t)f(t+\tau)dt \tag{B.14}$$

Equation (B.14) describes the operations in the time domain that correspond to the determination of $S_f(\omega)$ in frequency. The inverse Fourier transform of the power spectral density is the autocorrelation of $f(t)$ which we denote as $R_f(\tau)$.

$$F^{-1}\{S_f(\omega)\} = R_f(\tau) = \lim_{T\to\infty}\int_{-T/2}^{T/2}f^*(t)f(t+\tau)dt \tag{B.15}$$

# Appendix C

# Channel gain frequency correlations

In this Appendix, the mathematical expression for the correlations of the channel gain at different frequencies is formulated. As mentioned in the thesis, multi-carrier schemes such as OFDM can be used to overcome ISI due to multipath propagation. ISI is eliminated by simultaneously transmitting several symbols at a lower symbol rate using orthogonal (separable at the receiver) carriers. The channel gain will however vary from one sub-carrier to the next due to the frequency selectivity of the channel. Frequency selectivity results when the Channel Impulse Response (CIR) is an impulse train and the FFT of the CIR varies at different frequencies. In this case, because convolution in the time domain is equivalent to multiplication in the frequency domain, the symbol spectrum will experience different gain at different frequencies.

Consider the simple model of the discrete-time multipath channel. The CIR is an impulses train, where each impulse has a complex gain as described in Chapter 2.

$$\bar{h}_{\bar{\gamma}}(t,\tau) = \sum_{n=0}^{N-1} \bar{\gamma}_n(\tau_n(t),t)\delta(t-\tau_n(t)) \tag{C.1}$$

$\bar{\gamma}_n(\tau_n(t),t) = \gamma_n(t)e^{-j2\pi f_c \tau_n(t)}$ in (2.7) is the time varying channel gain of the $n$th path (the multipath gain). $\tau$ is the delay in arrival at the receiver of the $n$th multipath component relative to the first perceptible multipath component. $t$ is the measurement time instant which reflects changes in the CIR at separate time instances due to movement of the transmitter, receiver or the multipath mechanisms. Using the definition of the (continuous time) Fourier Transform, the frequency transfer function for this particular channel is

$$H(f) = \int_{-\infty}^{\infty} \sum_{n=0}^{N-1} \bar{\gamma}_n(\tau_n(t), t)\delta(t - \tau_n(t))e^{-j2\pi ft}dt = \sum_{n=0}^{N-1} \bar{\gamma}_n(\tau_n(t), t)e^{-j2\pi f\tau_n(t)} \tag{C.2}$$

The correlation between the transfer function at frequencies $f_1$ and $f_2$ is then

$$E\left[H(f_1)H^*(f_2)\right] = E\left[\sum_{n=0}^{N-1} \bar{\gamma}_n(\tau_n(t), t)e^{-j2\pi f_1\tau_n(t)} \sum_{m=0}^{M-1} \bar{\gamma}_m^*(\tau_m(t), t)e^{j2\pi f_2\tau_m(t)}\right] \tag{C.3}$$

To solve these sums analytically, we substitute $q = m - n$, and note that in the summing over $q$, only the term with $q = 0$ is non zero, so that

$$E\left[H(f_1)H^*(f_2)\right] = \sum_{n=0}^{N-1} \sum_{q=-n}^{M-1-n} E\left[\bar{\gamma}_n(\tau_n(t), t)\bar{\gamma}_{n+q}^*(\tau_{n+q}(t), t)\right] e^{-j2\pi f_1\tau_n(t)}e^{j2\pi f_2\tau_{n+q}(t)} \tag{C.4}$$

$$= \sum_{n=0}^{N-1} E\left[\bar{\gamma}_n(\tau_n(t), t)\bar{\gamma}_n^*(\tau_n(t), t)\right] e^{-j2\pi(f_1-f_2)\tau_n(t)} \tag{C.5}$$

It can be noted that equation C.5 is the discrete-time fast Fourier transform of the Power Delay Profile c.f (2.23). This result shows that if the PDP is assumed to be a square function, then the correlation is a sinc function, a result that is used extensively in Chapter 3.

# Appendix D

# WICOM-06 Conference Paper

Accurate channel state information (CSI) can be directly linked to the capacity and symbol-error-rate (SER) performance of a wireless system employing synchronized detection. Obtaining accurate CSI is particularly challenging when MIMO[1] antennas are implemented in conjunction with orthogonal frequency-division multiplexing (OFDM) modulation, for systems where the base station (BS) has more antenna than the mobile station (MS). The difficulty is that the received symbol vector at the mobile station is a sum of products of the transmitted symbols (data plus pilot) and several CSI unknowns, but that the later have to be resolved uniquely from the single, received symbol vector observation. Theoretically, perfect recovery of CSI is impossible even in the absence of noise as the number of unknowns is more than the number of observations, leading to an underdetermined system of linear equations. However, given that the CSI unknowns are correlated in frequency, this paper presents reduced rank algorithm to estimate the CSI at all sub-carriers from all of the antennas. Our proposed technique is inspired by the observation that a simple linear function can well approximate the channel variation in frequency and that permits us to have more CSI estimates than observations at the receiver. This paper can be thought of as a generalization of the approach previously proposed in [1] for any number of transmit antennas.

[1] The notation $(n_t, n_r)$ is used to denote a MIMO system with $n_t$ transmit antennas and $n_r$ receive antennas.

# I. Introduction

The principle of synchronous detection for which a channel estimate is formed and subsequently used for detection is applied in virtually all of today's digital wireless communications systems. The application of this principle to systems employing multiple-input multiple-output (MIMO) antennas and space time coding techniques is known to provide high quality, high data rate wireless communications. Systems that can achieve high channel capacity and low symbol error rates (SER) have been reported (e.g., [2]–[5]) and some are used in the third-generation wireless systems. Nonetheless, the capacity and SER performance of MIMO technologies, and synchronous detection systems in general, is directly linked to the availability of accurate channel state information (CSI) at the receiver. Without CSI, the channel capacity is simply not achievable although differential type of coding schemes can be used to obtain some advantages for improved performance [6]. Perfect CSI can be obtained for systems where symbols occupy a select few sub-carriers [7] but such systems are not spectrally efficient when compared to systems where the pilots are linearly added to the data and the resultant symbols occupy all available sub-carriers.

The channel estimation problem is challenging when MIMO antennas are used in conjunction with orthogonal frequency-division multiplexing (OFDM) modulation, and if the channels are to be estimated in one OFDM symbol [8]. OFDM modulation can be used to convert frequency selective channels to flat fading channels where the resultant received symbol is a product of a transmitted symbol and a single CSI variable. The problem is one where the observed received symbol is a sum of products of the transmitted symbols and the CSI unknowns, and practically there are more than one CSI variables to be estimated for each sub-carrier at each receive antenna. This gives rise to an underdetermined system for CSI estimation as obviously, multiple CSI estimates are required from one observation.

Conventional methods deal with this problem by presuming CSI congruence for at least $n_t$ sub-carriers, where $n_t$ is the number of transmit antennas. In effect, the number of CSI unknowns will be equal to the number of observations and the estimation problem reduces to the design of optimal training sequences. However, in practice, the CSIs in adjacent sub-carriers are not equal even though they might be highly correlated. This would impose an irreducible mean-square-error (MSE) floor in channel estimation even in the absence of noise. Though it is possible to estimate the time-sampled channels to generate different sub-carrier channel estimates, the underdetermined problem structure still exists and the optimal CSI estimates are not necessarily the true CSI even without noise [9, 10]. Most recently, Mung'au *et al.* proposed to apply the interpolation structure into refining the channel estimation for overloaded systems with only two transmit antennas [1]. Despite the promising result, it is not clear how the proposed scheme can be extended for more number of transmit antennas.

In this paper, we address the CSI estimation problem for a MIMO-OFDM system using orthogonal training sequences, where the data plus pilot symbol is assumed to be known through a maximum likelihood process. The main novelty is that we, in principle, regard the channels in frequency to be different, but correlated. Our method is thus able to produce multiple CSI estimates corresponding to different transmit antennas, at each sub-carrier. The work presented in this paper can be thought of as a generalization of the approach in [1] for any number of transmit antennas.

The paper is structured as follows. In Section II, we shall introduce the system model for an MIMO-OFDM system and formalize the channel estimation problem. Section III describes the proposed iterative channel estimation algorithm. Simulation results will be given in Section V. Finally, we have some concluding remarks in Section VI.

# II. MIMO-OFDM System Model and The Channel Estimation Problem

## D.0.1 OFDM Systems

For an OFDM system with multiple transmit antennas, at time $n$, information is transmitted in space and frequency by signals $\{t_i[n,k] : k = 0, 1, \ldots, K-1 \ \& \ i = 1, 2, \ldots, n_t\}$ in which $K$ is the number of sub-carriers and $n_T$ denotes the number of transmit antennas. Furthermore, $t_i[n,k]$ may be data, pilot or superimposed pilot with data or space-frequency encoded version of any of these [85].

At the $j$th receive antenna, the signal can be expressed as

$$r_j[n,k] = \sum_{i=1}^{n_t} H_{i,j}[n,k] t_i[n,k] + w_j[n,k] \tag{D.1}$$

where $H_{i,j}[n,k]$ denotes the channel response at the $k$th sub-carrier of the $n$th OFDM block, from the $i$th transmit antenna to the $j$th receive antenna, and $w_j[n,k]$ is the corresponding white noise perturbation with Gaussian distribution of zero-mean and $\sigma^2$-variance.

## D.0.2 The Fading Channel

The channel impulse response of the wireless channel can be described by a multi-ray model

$$h(t,\tau) = \sum_{\ell} \gamma_\ell(t) \delta(\tau - \tau_\ell) \tag{D.2}$$

where $\gamma_\ell(t)$ denotes the complex channel response of the $\ell$th path which we model it as a zero-mean complex Gaussian random variable following an exponential power profile, and $\tau_\ell$ is the delay of the $\ell$th path. The number of paths can be modelled by the Poisson distribution so that the inter-arrival time between paths is exponential distributed.

The frequency response of the channel (D.2) is hence given by

$$H(t,f) = \mathcal{F}\left\{h(t,\tau)\right\} = \sum_{\ell} \gamma_\ell(t) e^{-j2\pi f \tau_\ell}. \tag{D.3}$$

With proper cyclic extension and guard timing, the channel response, $H[n,k]$, can be written as [70]

$$H[n,k] \triangleq H(nT_f, k\triangle f) \tag{D.4}$$

where $T_f$ denotes the block length which includes the symbol duration and a guard interval, and $\triangle f$ represents the sub-carrier spacing. Usually, $T_f$ is long, at least when compared to the root-mean-square (rms) delay spread of the channel ($\tau_{\mathsf{rms}}$). Therefore, it is very likely that the channels will vary quite significantly from time $n$ to $n+1$. In this paper, we shall assume that $H[n,k]$ and $H[\tilde{n},k]$ are independent if $n \neq \tilde{n}$.

### D.0.3 The Overloaded Channel Estimation Problem

At sub-carrier $k$, the channel estimation aims to minimize the following MSE cost function:

$$\min_{\{\tilde{H}_i[k]\}:\forall i,k} \mathsf{MSE} \triangleq \sum_{i=1}^{n_t} \sum_{k=0}^{K-1} \left| \tilde{H}_i[k] - H_i[k] \right|^2 \tag{D.5}$$

where the indices for time and receive antenna are omitted for simplicity. However, as this MSE metric contains no known information, channel estimation is therefore usually done by minimizing [8]–[10]

$$\min_{\{H_i[k]\}:\forall i,k} \varepsilon \triangleq \sum_{k=0}^{K-1} \left| r[k] - \sum_{i=1}^{n_t} H_i[k] t_i[k] \right|^2. \tag{D.6}$$

Without multiple transmit antennas, the metric, $\varepsilon$, can achieve (D.5) perfectly in the absence of noise if $\{t_i[k]\}$'s are known pilot symbols. Unfortunately, problem arises when multiple transmit antennas are equipped because (D.6) becomes a well known underdetermined estimation problem. In this case, (D.6) is less meaningful as it has $K$ sum-of-squares with $n_t \times K$ variables. There are infinitely many solutions of $\{H_i[k]\}$ that could make $\varepsilon = 0$, and among them, there is only one set of solution which can minimize the MSE in (D.5). As a result, solving (D.6) does not help much in finding the best possible channel estimates for (D.5). In this paper, we look into finding a channel estimation method to achieve (D.5) instead of (D.6) due to the underdetermined system structure.

# III. The Proposed Method for $n_t > 1$

Our main idea is to exploit the channel correlation in frequency so that we could in a sense convert the underdetermined system into a determined system. As a starting point, the expression for the error in channel (CSI) estimate (assuming congruence over $n_t$ sub-carriers) will be derived for the case where there is no noise at the receiver.

Given that $\{t_i[k]\}$'s are orthogonal pilot training sequences spanning $n_t$ sub-carriers such that

$$\sum_{k=1}^{n_T} t_j^*[k] t_i[k] = \begin{cases} 1 & i = j, \\ 0 & i \neq j, \end{cases} \tag{D.7}$$

where $\{t_i^*[k]\}$ is the complex conjugate of $\{t_i[k]\}$, with the indices $i, j = 1, 2, ..., n_t$. We can have a coarse estimate for $\{H_i[k]\}$ by forming a linear combination of the received symbols, i.e.,

$$
\begin{aligned}
H_i^{\mathsf{est}}[k] &\triangleq t_i^*[k]r[k] + \cdots + t_i^*[k+n_t-1]r[k+n_t-1] \\
&= H_i[k] + t_i^*[k+1]t_1[k+1]\Delta\mathcal{H}_{k+1,k}^{(1)} + \cdots \\
&+ t_i^*[k+n_t-1]t_1[k+n_t-1]\Delta\mathcal{H}_{k+n_t-1,k}^{(1)} \\
&+ t_i^*[k+1]t_2[k+1]\Delta\mathcal{H}_{k+1,k}^{(2)} + \cdots \\
&+ t_i^*[k+n_t-1]t_2[k+n_t-1]\Delta\mathcal{H}_{k+n_t-1,k}^{(2)} + \cdots \\
&+ t_i^*[k+1]t_{n_t}[k+1]\Delta\mathcal{H}_{k+1,k}^{(n_t)} + \cdots \\
&+ t_i^*[k+n_t-1]t_{n_t}[k+n_t-1]\Delta\mathcal{H}_{k+n_t-1,k}^{(n_t)} \\
&= H_i[k] + \delta\mathcal{H}_i[k]
\end{aligned}
\tag{D.8}
$$

where $\{\delta\mathcal{H}_i[k]\}$'s can be viewed as the channel estimation errors between the estimated and actual channels with

$$\Delta\mathcal{H}_{\ell,k}^{(i)} \triangleq H_i[\ell] - H_i[k]. \tag{D.9}$$

For a given antenna $i$, in (D.8), there are $\frac{K}{n_t}$ channel estimates formed for the OFDM block and the variable $k$ assumes the values $k = 1, n_t+1, 2n_t+1, ..., K-n_t+1$ over the length $K$ of the OFDM block. Note that for the $i$th antenna, a single estimate is formed over $n_t$ sub-carriers for which congruence is assumed. The assumption of congruence imposes an error in the channel estimate $\delta\mathcal{H}_i[k]$ that increases as the number of transmit antennas increases. In addition, the error in the channel estimate is inversely proportional to the degree of correlation for the channel pairs [1]. That is to say, if the difference in the channel pairs, $\Delta\mathcal{H}_{\ell,k}^{(i)}$ for $\ell = (k+1), (k+2), ..., (k+n_t-1)$, is small, then the error in the estimate will be small. In an environment where there is a great degree of multi-path (i.e., large $\tau_{\mathsf{rms}}$), the channels are less correlated, and $\Delta\mathcal{H}_{\ell,k}^{(i)}$ is significant.

Standard interpolation of the estimated channel values over the length of the OFDM block can be used to determine the variations in the channels for which congruence is assumed. Our method proposes the use of the variations in the channels obtained from interpolation as well as two adjacent estimated channels to reduce the error in channel estimate defined in (D.8). For this purpose, the refinement in channel estimate will be carried out for sub-blocks of length $2n_t$ over the whole OFDM block in which there are two adjacent *estimated* channels and $2n_t - 2$ *interpolated* channels. [See figure D.2].

The error in the channel estimate of the two adjacent estimated channels can be evaluated using (D.8)

$$\begin{aligned}
\delta\mathcal{H}_i[k] \triangleq\ & H_i^{\mathsf{est}}[k] - H_i[k] \\
&= t_i^*[k+1]t_1[k+1]\Delta\mathcal{H}^{(1)}_{k+1,k} + \cdots \\
&+ t_i^*[k+n_t-1]t_1[k+n_t-1]\Delta\mathcal{H}^{(1)}_{k+n_t-1,k} \\
&+ t_i^*[k+1]t_2[k+1]\Delta\mathcal{H}^{(2)}_{k+1,k} + \cdots \\
&+ t_i^*[k+n_t-1]t_2[k+n_t-1]\Delta\mathcal{H}^{(2)}_{k+n_t-1,k} + \cdots \\
&+ t_i^*[k+1]t_{n_t}[k+1]\Delta\mathcal{H}^{(n_t)}_{k+1,k} + \cdots \\
&+ t_i^*[k+n_t-1]t_{n_t}[k+n_t-1]\Delta\mathcal{H}^{(n_t)}_{k+n_t-1,k},
\end{aligned} \tag{D.10}$$

$$\begin{aligned}
\delta\mathcal{H}_i[k+n_t] \triangleq\ & H_i^{\mathsf{est}}[k+n_t] - H_i[k+n_t] \\
&= t_i^*[k+n_t+1]t_1[k+n_t+1]\Delta\mathcal{H}^{(1)}_{k+n_t+1,k} + \cdots \\
&+ t_i^*[k+2n_t-1]t_1[k+2n_t-1]\Delta\mathcal{H}^{(1)}_{k+2n_t-1,k} \\
&+ t_i^*[k+n_t+1]t_2[k+n_t+1]\Delta\mathcal{H}^{(2)}_{k+n_t+1,k} + \cdots \\
&+ t_i^*[k+2n_t-1]t_2[k+2n_t-1]\Delta\mathcal{H}^{(2)}_{k+2n_t-1,k} + \cdots \\
&+ t_i^*[k+n_t+1]t_{n_t}[k+n_t+1]\Delta\mathcal{H}^{(n_t)}_{k+n_t+1,k} = \cdots \\
&+ t_i^*[k+2n_t-1]t_{n_t}[k+2n_t-1]\Delta\mathcal{H}^{(n_t)}_{k+2n_t-1,k}.
\end{aligned} \tag{D.11}$$

For the equation pairs, (D.10) and (D.11), the variable $k$ assumes the range $k = 1, 2n_t+1, 4n_t+1, \ldots, K-2n_t+1$. Standard interpolation can be used to estimate the variations in the channel $\{\Delta\mathcal{H}^{(i)}_{\ell,k}\}$. Therefore, (D.10)–(D.11) can be used to refine the channel estimates $\{H_i^{\mathsf{est}}[k]\}$ and having thus corrected for the errors in the channel estimate, re-interpolation provides more accurate estimates for the channels that are assumed to be congruent. In particular, the above observation is further qualified by rewriting the actual channels as a function of the received symbols $r[k]$ and the variation in the channels, so that

$$\begin{aligned}\begin{pmatrix} H_1[k] \\ \vdots \\ H_{n_t}[k] \end{pmatrix} &= \begin{pmatrix} t_1[k] & \cdots & t_{n_t}[k] \\ \vdots & \ddots & \vdots \\ t_1[k+n_t-1] & \cdots & t_{n_t}[k+n_t-1] \end{pmatrix}^{-1} \\ &\times \left[ \begin{pmatrix} r[k] \\ \vdots \\ r[k+n_t-1] \end{pmatrix} \right. \\ &- \begin{pmatrix} 0 & \cdots & 0 \\ \Delta\mathcal{H}^{(1)}_{k+1,k} & \cdots & \Delta\mathcal{H}^{(n_t)}_{k+1,k} \\ \vdots & \ddots & \vdots \\ \Delta\mathcal{H}^{(1)}_{k+n_t-1,k} & \cdots & \Delta\mathcal{H}^{(n_t)}_{k+n_t-1,k} \end{pmatrix} \\ &\times \left. \begin{pmatrix} t_1[k] & \cdots & t_1[k+n_t-1] \\ \vdots & \ddots & \vdots \\ t_{n_t}[k] & \cdots & t_{n_t}[k+n_t-1] \end{pmatrix} \right]. \end{aligned} \tag{D.12}$$

(D.12) can be utilized to estimate the channels $\{H_i[k]\}$ if there is an estimate for the variations in channel $\{\Delta\mathcal{H}^{(i)}_{\ell,k}\}$. A similar expression can be written for $\{H_i[k+n_t]\}$, the next *estimated* channels in the sub-block, by substituting the variable $k$ with $k+n_t$ in (D.12) above.

Note that if the initial estimate for the variations in the channel $\{\Delta\mathcal{H}^{(i)}_{\ell,k}\}$ in (D.10)–(D.11) are incorrect, it is not possible to correct for the error in the channel estimate as proposed here. Because of this assertion, we intend to relate the estimated channels and the interpolated channels by defining the following ratios, again considering the defined sub-block

$$\varrho^{(i)}_{\ell,k} \triangleq \frac{H_i[\ell] - H_i[k]}{H_i[k+n_t] - H_i[k]} = \frac{\Delta\mathcal{H}^{(i)}_{\ell,k}}{\Delta\mathcal{H}^{(i)}_{k+n_t,k}} \tag{D.13}$$

$$\varrho^{(i)}_{\ell,k+n_t} \triangleq \frac{H_i[\ell] - H_i[k+n_t]}{H_i[k+n_t] - H_i[k]} = \frac{\Delta\mathcal{H}^{(i)}_{\ell,k+n_t}}{\Delta\mathcal{H}^{(i)}_{k+n_t,k}} \tag{D.14}$$

In (D.13) $\ell = (k+1), (k+2), ..., (k+n_t-1)$ whereas in (D.14) $\ell = (k+n_t+1), (k+n_t+2), ..., (k+2n_t-1)$. In practice, these ratios can be approximated using the estimated channel and the interpolated channels. For instance, for a $(2,1)$ system,

$$\varrho^{(1)}_{2,1} \approx \frac{H_1^{\mathsf{int}}[2] - H_1^{\mathsf{est}}[1]}{H_1^{\mathsf{est}}[3] - H_1^{\mathsf{est}}[1]} \tag{D.15}$$

where $H_1^{\mathsf{int}}[2]$ is the channel estimate obtained from interpolating the estimates $H_1^{\mathsf{est}}[1]$ and $H_1^{\mathsf{est}}[3]$. We observe from numerical results that the approximated ratios are found to be about 95% accurate in most cases.

With these ratios, we have the following relations

$$\begin{aligned} \Delta\mathcal{H}^{(i)}_{\ell,k}\Big|_{\mathsf{est}} &= \varrho^{(i)}_{\ell,k}\left(H_i^{\mathsf{est}}[k+n_t] - H_1^{\mathsf{est}}[k]\right), \\ \Delta\mathcal{H}^{(i)}_{\ell,k+n_t}\Big|_{\mathsf{est}} &= \varrho^{(i)}_{\ell,k+n_t}\left(H_i^{\mathsf{est}}[k+n_t] - H_i^{\mathsf{est}}[k]\right). \end{aligned} \tag{D.16}$$

Observing that the estimated channel in (D.8) is related to the actual channel as $H_i^{\mathsf{est}}[k] = H_i[k] + \delta\mathcal{H}_i[k]$, (D.16) can be re-written as a function of the error in the channel estimate $\delta\mathcal{H}_i[k]$, allowing for an update of the variations in the channel $\Delta\mathcal{H}^{(i)}_{\ell,k}$.

$$\Delta\mathcal{H}^{(i)}_{\ell,k}\Big|_{\mathsf{est}} = \Delta\mathcal{H}^{(i)}_{\ell,k} + \varrho^{(i)}_{\ell,k}\left(\delta\mathcal{H}_i^{\mathsf{est}}[k+n_t] - \delta\mathcal{H}_1^{\mathsf{est}}[k]\right) \tag{D.17}$$

$$\begin{aligned} \Delta\mathcal{H}^{(i)}_{\ell,k+n_t}\Big|_{\mathsf{est}} &= \Delta\mathcal{H}^{(i)}_{\ell,k+n_t} \\ &\quad + \varrho^{(i)}_{\ell,k+n_t}\left(\delta\mathcal{H}_i^{\mathsf{est}}[k+n_t] - \delta\mathcal{H}_i^{\mathsf{est}}[k]\right) \end{aligned} \tag{D.18}$$

$\{\Delta\mathcal{H}^{(i)}_{\ell,k}\Big|_{\mathsf{est}}\}$ are updated, from the results in (D.10)–(D.11), using (D.17)–(D.18), and making the actual channel the subject of the formula. As a consequence, we can iterate the estimation between $\{\delta\mathcal{H}_i[k]\}$ and $\{\Delta\mathcal{H}^{(i)}_{\ell,k}\}$ to obtain a fine estimate for the later quantities. Finally, the estimated channels can be readily obtained using (D.12). In addition, the iterated channels can be easily found from

$$H_i^{\mathsf{est}}[\ell] = H_i^{\mathsf{est}}[k] + \Delta\mathcal{H}^{(i)}_{\ell,k}\Big|_{\mathsf{est}} \tag{D.19}$$

The above iterative algorithm is summarized as follows:

**S1**) Estimate the channels $H_i^{\mathsf{est}}[k]$ and $H_i^{\mathsf{est}}[k+n_t]$ for $k = 1, 2n_t+1, 4n_t+1, \ldots, K-2n_t+1$ based on the orthogonality of the training sequences [see (D.8)] for $i = 1, 2, \ldots, n_t$.

**S2**) Use standard interpolation function to get the estimates the channels: $H_i^{\mathsf{int}}[k+1], \ldots, H_i^{\mathsf{int}}[k+n_t-1]$ and $H_i^{\mathsf{int}}[k+n_t+1], \ldots, H_i^{\mathsf{int}}[k+2n_t-1]$.

**S3**) Obtain the estimates for $\{\varrho_{\ell,k}^{(i)}\}$ and $\{\varrho_{\ell,k+n_t}^{(i)}\}$ using (D.13) and (D.14), and the results of step 1 and 2 above.

**S4**) Find $\{\delta\mathcal{H}_i[k]\}$ and $\{\delta\mathcal{H}_i[k+n_t]\}$ using (D.10)–(D.11), and then update the estimates for the variations in the channels using (D.17) and (D.18). Repeat Step 4 until convergence.

**S5**) Use the updated $\{\Delta\mathcal{H}_{\ell,k}^{(i)}\}$ and $\{\Delta\mathcal{H}_{\ell,k+n_t}^{(i)}\}$ and (D.12) to recalculate the estimated channels.

**S6**) Use the updated $\{\Delta\mathcal{H}_{\ell,k}^{(i)}\}$ and $\{\Delta\mathcal{H}_{\ell,k+n_t}^{(i)}\}$ and the results from step 5 in (D.19) to recalculate the interpolated channels.

# IV. Simulation Results

Results were obtained for Rayleigh frequency selective fading channels under no noise conditions. In order to simulate the channel, Poisson distribution was used to simulate the number of significant multi-path elements with mean of 3 and also the exponential arrival times between the significant paths. A typical rms delay spread in an office building is $\tau_{\mathsf{rms}} = 270$ ns [12]. In figure D.3 where the rms delay spread is varied, results for the MSE in the channel estimate were provided for the range $0.5\tau_{\mathsf{rms}}$ to $1.5\tau_{\mathsf{rms}}$, for a $(2,1)$ system. Figure D.4 shows similar results for a $(3,1)$ system. Significant multi-path elements can be expected within $5\tau_{\mathsf{rms}}$, the so-called maximum delay. OFDM with 128 sub-carriers, symbol rate of 3.125 MHz was considered for the $(2,1)$ system. OFDM with 126 sub-carriers and the same symbol rate was considered for the $(3,1)$ system. The number of sub-carriers used has to be a multiple of $2n_t$ in order that refinement using the algorithm is possible for the whole OFDM block. Results for the conventional method that first estimates $\frac{K}{n_t}$ channels using orthogonal training sequences and then uses a standard interpolation function to obtain the remaining $K - \frac{K}{n_t}$ channels is provided for comparison. The results for the method that aims to minimize $\varepsilon$ in (D.6) is also provided [9].

As can be seen in figure D.3, the proposed algorithm can achieve nearly perfect channel estimates with MSE in the order of $10^{-7}$ as compared to the conventional method with MSE in the order of $10^{-3}$ for a $(2,1)$ system. Similar results are obtained for the $(3,1)$ system with MSE in the order of $10^{-5}$ as compared to the conventional method with MSE in the order of $10^{-2}$.

The performance of the proposed algorithm is superior to the conventional methods and the scheme in [9] for both systems considered. In particular, the proposed method can achieve several order of magnitude reduction in MSE for a wide range of rms delay spread.

## V. Conclusion

This paper has proposed an iterative algorithm for improved channel estimation for a MIMO-OFDM system. Our proposed method differs from the previous approaches in that we realize the underdetermined problem structure and introduce an approximate channel difference ratio to link the estimated and interpolated channels in frequency. The outcome is that we can significantly reduce the MSE in channel estimation by several orders of magnitude when compared to the known conventional methods. There is a limit to the improvement in the MSE and it can be noted that where there is significant multipath (i.e. for long $\tau_{\mathsf{rms}}$) and for the (3,1) system, the channel difference ratio is not accurate and the MSE is higher when compared to the MSE for shorter $\tau_{\mathsf{rms}}$ and fewer antennas. The improvement achieved however should translate to significantly increased capacity and SER performance for MIMO-OFDM systems.

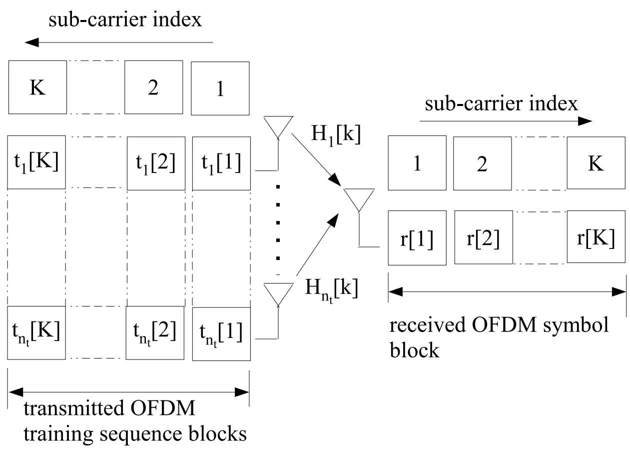


Figure D.1: The MIMO-OFDM system.

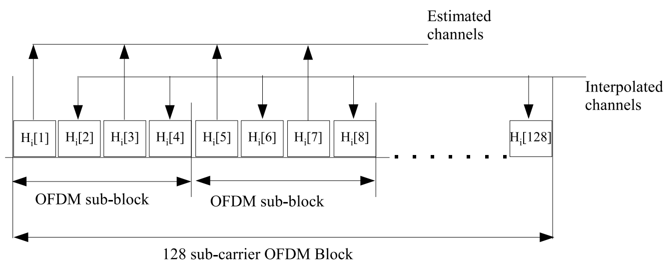


Figure D.2: Example of the partitioning of 128 channel estimates for the OFDM block into sub-blocks for a (2,1) MIMO-OFDM system.

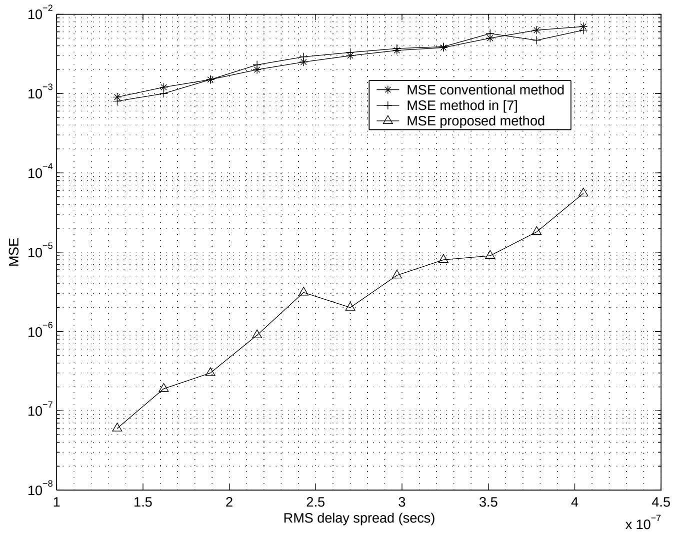


Figure D.3: Results comparing the MSE vs RMS delay spread for the estimated (conventional method), the method described in reference [7], and the iterated (proposed method) channels across 128 OFDM sub-carriers for a (2,1) system.

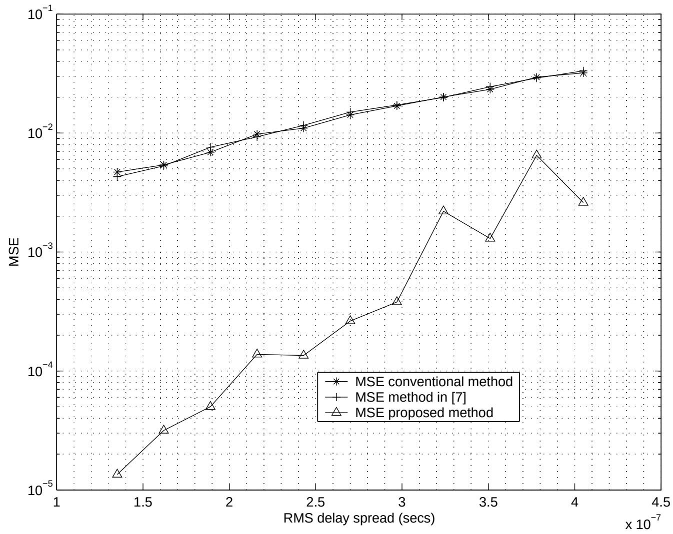


Figure D.4: Results comparing the MSE vs RMS delay spread for the estimated (conventional method), the method described in reference [7], and the iterated (proposed method) channels across 126 OFDM sub-carriers for a (3,1) system.

# Bibliography

[1] F. Mung'au, and K. K. Wong, "An improved channel estimation for MIMO-OFDM systems," to appear in *Int. Conf. Wireless Commun. Networking, and Mobile Computing*, 22-24 Sep. 2006, Wuhan, China.

[2] G. J. Foschini, and M. J. Gans, "On limits of wireless communication in a fading environment when using multiple antennas," *Wireless Personal Commun.*, Vol. 6, No. 3, pp. 311–355, Mar. 1998.

[3] V. Tarokh, N. Seshadri, and A. R. Calderbank, "Space-time codes for high data rate wireless communication: performance criterion and code construction," *IEEE Trans. Info. Theory*, vol. 6, pp. 744–765, Mar. 1998.

[4] S. M. Alamouti, "A simple transmit diversity scheme for wireless communications," *IEEE J. Select. Areas Commun.*, vol. 16, pp. 1451–1458, Oct. 1998.

[5] B. M. Hochwald, and S. ten Brink, "Achieving near-capacity on a multiple-antenna channel," *IEEE Trans. Commun.*, vol. 51, no. 3, pp. 389–399, Mar. 2003.

[6] B. L. Hughes, "Differential space-time modulation," *IEEE Trans. Info. Theory*, vol. 46, no. 7, pp. 2567–2578, Nov. 2000.

[7] R. Negi, and J. Cioffi, "Pilot tone selection for channel estimation in mobile OFDM systems," *IEEE Trans. Cons. Elec.*, vol. 44, no. 3, pp. 1122–1128, Aug. 1998.

[8] Y. Li, J. Chuang, and N. R. Sollenberger, "Transmit diversity for OFDM systems and its impact on high-rate data wireless networks," *IEEE J. Select. Areas Commun.*, vol. 17, pp. 1233–1243, Jul. 1999.

[9] Y. Li, "Simplified channel estimation for OFDM systems with multiple transmit antennas," *IEEE Trans. Wireless Commun.*, vol. 1, no. 1, pp. 67–75, Jan. 2002.

[10] H. Minn, D. I. Kim, and V. K. Bhargava, "A reduced-complexity channel estimation for OFDM systems with transmit diversity in mobile wireless channels," *IEEE Trans. Wireless Commun.*, vol. 50, no. 5, pp. 799–807, May 2002.

[11] M. Dong, L. Tong, and B. M. Sadler, "Optimal insertion of pilot symbols for transmissions over time-varying flat fading channels," *IEEE Trans. Sig. Proc.*, vol. 52, no. 5, pp. 1403–1418, May 2004.

[12] D. M. J. Devasirvantham, M. J. Krain, and D. A. Rappaport, "Radio propagation measurements at 850 GHz, 1.7 GHz, and 4.0 GHz inside two dissimiler office buildings," *IEE Elect. Letters*, vol. 26, no. 7, pp. 445–447, Jun. 1990.

# Appendix E

# MATLAB CODE

This section contains sample MATLAB code that was developed for simulations in the thesis. An attempt has been made to comment the cade as far as possible, but in order to understand the code, please refer to the relevant chapters.

## E.1 Saleh-Valenzuela Channel Model

```
function pdp=gen_SVstatpdp(show)
% a function to generate the saleh-velenzuela model
% channel
%************************************************%
% [1] - A statistical model for indoor multipath
% propagation.
% IEEE Jornal on selected areas of communications VOL.
% SAC 5. No 2. February 1997.

% here we try to simulate the 802.11n scenario

% For an OFDM system with a data rate of 540Mbps
% using 64-QAM (6 bits per symbol), the symbol_rate
% = bit_rate/bits_per_symbol = 90MSps. The symbol
% peiod = 1/symbol_rate.
```

```
if nargin==0
    show=0;
end

K=128; % number of subcarriers
T_sym=11e-9; % approximate symbol period

% at this symbol period, the maximum frequency of the
% subcarriers is bw=0.5*1/T_sym = 45Mhz. Sub-
% carrier frequency separation is bw/K = 0.3125MHz.
% similar to 802.11a.

% symbol period implies that a cyclic prefix of
% length 20 symbols is required so that 20*T_sym >
% tao_max of the multipath, with tau_max=200ns.

LAMBDA=1/(200e-9); % cluster rate
lambda=1/(5e-9); % ray rate

T_block=K*T_sym; % duration of the OFDM block

avg_clust=T_block*LAMBDA; % average number of clusters

% the clusters have poisson arrivals
nclust = poissrnd(avg_clust)+1; % avoid nclust=0;
clustdelays = exprnd((1/LAMBDA),[1 nclust]);

% monotonically intreasing delays...
monclustdelays=sort(clustdelays);

% the cluster delays should be less than the OFDM block length and non
% zero, if so they form TAO
TAO=[0,...
    monclustdelays(find(monclustdelays>0 & monclustdelays<T_block))];
```

```
% update the number of clusters...
nclust=length(TAO);

% because the delay of the first cluster is zero and the delay of the last
% cluster is less than T_block for the OFDM block
% length(TAO)=length(DELTA_TAO), but these will be used in context.
DELTA_TAO=zeros(1,length(TAO));
% calulate the number of rays in each cluster. First work out
% the delay between successive clusters. this is used to calculate t
% the expected number of rays in the cluster which is poisson with
% rate lambda=1/(5e-9)
for ii=1:nclust
    if ii < nclust
        DELTA_TAO(ii)=TAO(ii+1)-TAO(ii);
    else
        DELTA_TAO(ii)=T_block-TAO(ii);
    end
end

% for each cluster, make some rays...
% declare a variable to hold the number of rays in each cluster
nrays=zeros(1,length(DELTA_TAO));
for ii=1:length(DELTA_TAO)
    avgnum_rays=lambda*DELTA_TAO(ii);
    nrays(ii) = poissrnd(avgnum_rays)+1; % avoid nrays==0
end

% using the International Telecommunications Union's ITU1238
% model for the statistical description of a typical home's
% operating conditions, antenna gains G_t=G_r=3dB.

% the multipath power gain at one meter can be approx. by
% G = G_tG_r[lambda_0/4pi]^2
lambda0=3e8/2.4e9; % wavelength of the 2.4GHz
```

```
% multipath power gain
G=10^0.3*10^0.3*(lambda0^2/(4*pi));

% power delay time constant
gamma=20e-9;

% average power of the first ray of the first cluster
beta_rms00=G/(gamma*lambda);

% the power delay profile is sampled at the symbol period
pdp=zeros(1,K);
delay=0:T_sym:T_block; % declare the delays for the pdp

%generate the PDP
for ii=1:nclust
    %generate some ray delays
    raydelays = exprnd((1/lambda),[1 nrays(ii)]);
    %monotonically increasing delays
    monraydelays=sort(raydelays);
    %we do not want zero ray delays
    nzraydelays=[monraydelays(find(monraydelays~=0))];
    %add the cluster start time
    nzraydelays=TAO(ii)+nzraydelays;
    %ray delays should be less than the OFDM block
    tao=[TAO(ii), nzraydelays(find(nzraydelays<T_block))];
    %find the number of rays in the cluster
    nrayspclust=length(tao);
    %generate the PDP
    for jj=1:nrayspclust
        beta_rms=beta_rms00*exp(-TAO(ii)/60e-9)...
                                *exp(-tao(jj)/20e-9);
        for kk=1:K
            if (tao(jj)>=delay(kk))&(tao(jj)<=delay(kk+1))
                pdp(kk)=pdp(kk)+beta_rms;
```

```
            end
        end
    end
end

% generate delay in seconds for the power profile
taodelay=0:T_sym:(T_block-T_sym);

if show==1
    figure, stem(taodelay, abs(pdp))
    xlabel('Multi-path component delay: max = (N-1)T_s (sec) ')
    ylabel('$E[|\bar{\gamma}_n|^2]$','Interpreter','latex')
    title('PDP at QAM symbol period multiples: T_s=11e^-^9, N = 128')
    grid minor;
end


function chan=gen_SVstatchan(pdp,show)
% generate the channel impulse response

if nargin==1
    show=0;
end

K=128; % number of subcarriers
T_sym=11e-9; % approximate symbol period
T_block=K*T_sym; % duration of the OFDM block

% generate delay in seconds for the CIR
taodelay=0:T_sym:(T_block-T_sym);

for ii=1:length(pdp)
    % the standard deviation of the gaussian IQ channel gain
    % is calculated from the pdp
    std_dev=sqrt(pdp(ii)/2);
```

```
    % generate gaussian distributed x, mu = 0 and sigma = std_dev
    x = normrnd(0, std_dev);

    % generate gaussian distributed x, mu = 0 and sigma = std_dev
    y = normrnd(0, std_dev);

    % generate
    chan(ii) = x+j*y;
end

if show==1
    figure, stem(taodelay, abs(chan))
    xlabel('Multi-path component delay: max = (N-1)T_s (sec) ')
    ylabel('$|\bar{\gamma}_n|$','Interpreter','latex')
    title('Multi-path component gain amplitudes: T_s=11e^-^9, N = 128')
    figure, stem(taodelay, angle(chan))
    xlabel('Multi-path component delay: max = (N-1)T_s (sec) ')
    ylabel('$e^{-j2\pi f_c \tau_n}$','Interpreter','latex')
    title('Multi-path component gain phases: T_s=11e^-^9, N = 128')
end
```

## E.2 Wiener Filter Implementation

```
function errMat=WienerChanEst(tau_max, v_rec, SNR)
% tau_max = maximum delay of the channel
% v_rec = velocity of the receiver

K=16;  % OFDM symbol length
L=4;   % length of CP
M=32;  % OFDM frame length

T_s=10e-6; % symbol period
T_rms=3.5e-6; % rms delay spread
```

```
F_s=200e3/K; % subcarrier spacing

if nargin==0
    tau_max=4*T_s;
    v_rec=30;
    SNR=40; % SNR dB
    snr = 10^(SNR/10); % snr linear
end

f_c=1.8e9;
c=3e8;

f_Doppl=v_rec*f_c/3e8; % doppler frequency

N_f=4; % spacing of pilots in frequency
kp=0:N_f:K-1;
N_t=8; % spacing of pilots in time
mp=0:N_t:M-1;

F=gen_fftmatrix(K); % the FFT matrix

nfp=length(kp); % number of pilots in the frequency domain
ntp=length(mp); % number of pilots in the time domain

np=nfp*ntp; % number of pilots

% stack the pilot indices, down the frquency index first then accross tme
% index,...
pindx=zeros(np,2);
pcnt=1;
for ii=1:ntp
    for jj=1:nfp
        pindx(pcnt,1)=kp(jj);
        pindx(pcnt,2)=mp(ii);
        if pcnt<np
```

```
            pcnt=pcnt+1;
        end
    end
end

plt=rand(np,1)+i*rand(np,1); % some random data which will generate pilots
% generate some random QPSK pilots
for ii=1:np
    if real(plt(ii,1))>=0.5
        xx=1/sqrt(2);
    else
        xx=-1/sqrt(2);
    end

    if imag(plt(ii,1))>=0.5
        yy=1/sqrt(2);
    else
        yy=-1/sqrt(2);
    end

    plt(ii,1)=xx+i*yy;
end

% use clarke's model to generate a 2D channel
% generate the 2D OFDM channel, assume length 8 cyclic prefix
Nmp=10; % number of doppler multipath components
Nsigmp=3; % number of significant multipath
tau=[1,2,4]; % these are the OFDM indices with sig mp
cir=zeros(K,1); % the channel impulse response
hvec=zeros(K,1); % the OFDM channel vector
OFDMchan=zeros(K,M);
for ii=1:M
    if (ii==1)
        a=0.025*randn(Nmp,Nsigmp); % Gaussian amplitude coefficients/mp
                                   % component (/mpc)
```

```
        th=rand(Nmp,Nsigmp)*2*pi; % uniform azimuthal phase angles /mpc
        ph=rand(Nmp,Nsigmp)*2*pi; % uniform channel phase angles /mpc
    end

    for jj=1:Nsigmp
        mpgain=0;
        for kk=1:Nmp
            mpgain=mpgain+(a(kk,jj)*exp(j*ph(kk,jj))*...
                            exp(j*2*pi*f_Doppl*cos(th(kk,jj))*T_s*(K+L)*(ii-1)));
        end
        cir(tau(jj),1)=abs(mpgain)*exp(-tau(jj)*T_s/(2*T_rms))*exp(j*angle(mpgain))
    end
    %sum(abs(cir))
    %time=(0:K-1);
    %figure, plot(time,angle(cir),'*')
    %if ii==1
    %     cir(1:4,1)
    %end
    hvec=F*cir;
    OFDMchan(:,ii)=hvec(:,1);
    %freq=(0:K-1);
    %figure, plot(freq,abs(hvec),'*-')
end
% sum(abs(cir).^2) % gives an indication of the total multipath power,...
% according to the SV model this should be about max 0.01

%x=1:K;
%y=abs(OFDMchan(:,10));
%figure, plot(x,y)

%OFDMchan
% simulate data reception for the pilot symbols
rpSym=zeros(np,1);
for ii=1:np
    rpSym(ii,1)=OFDMchan(pindx(ii,1)+1,pindx(ii,2)+1)*plt(ii,1);
```

```
end

% add noise to the received symbols
rpSymn=awgn(rpSym,SNR);
nvect=rpSymn-rpSym; % noise vector
sigsqr=var(nvect);

% make the correlation matrix
psi = zeros(np,np);
for ii=1:np
    for jj=1:np
        theta_f=sinc(pi*tau_max*(pindx(ii,1)-pindx(jj,1))*F_s);
        theta_t=sinc(2*pi*f_Doppl*(pindx(ii,2)-pindx(jj,2))*(K+L)*T_s);
        if (pindx(ii,1)-pindx(jj,1)) == (pindx(ii,2)-pindx(jj,2))
            psi(ii,jj)=theta_f*theta_t+sigsqr;
        else
            psi(ii,jj)=theta_f*theta_t;
        end
    end
end

% make a matrix of data plus pilot
nfr=K*M; % total number of QAM symbols in the OFDM frame
findx=zeros(nfr,2);
fcnt=1;
for ii=0:M-1
    for jj=0:K-1
        findx(fcnt,1)=jj;
        findx(fcnt,2)=ii;
        if fcnt<nfr
            fcnt=fcnt+1;
        end
    end
end
```

```
%for ii=1:nfr
%    x(ii)=findx(ii,1);
%    y(ii)=findx(ii,2);
%    z(ii)=abs(OFDMchan(findx(ii,1)+1,findx(ii,2)+1));
%end

%figure, plot3(x,y,z,'*')
%xlabel('Sub-carrier index, k')
%ylabel('OFDM symbol index, m')
%zlabel('$|H[k,m]|$','Interpreter','latex')
%grid on;

% initial channel estimates at the pilot symbols
Hest=rpSymn./plt; % size(Hest)

for ii=1:nfr
    % make the autocorrelation matrix
    theta=zeros(np,1);
    for jj=1:np
        theta_f=sinc(pi*tau_max*(findx(ii,1)-pindx(jj,1))*F_s);
        theta_t=sinc(2*pi*f_Doppl*(findx(ii,2)-pindx(jj,2))*(K+L)*T_s);
        theta(jj,1)=theta_f*theta_t;
    end

    % calculate the wiener filter
    wfilt=psi.'\theta;

    % calculate the MMSE channel estimate at the data location
    OFDMchanestWF(findx(ii,1)+1,findx(ii,2)+1)=wfilt.'*Hest;
    %chanact=OFDMchan(findx(ii,1)+1,findx(ii,2)+1);
end

%chanact=OFDMchan(2,1)
%chanest=OFDMchanest(2,1)
%err=abs(OFDMchan(2,1)-OFDMchanest(2,1))
```

```
%OFDMchan

% calculate MSE
sqerrWF=0;
for ii=1:nfr
    err=OFDMchan(findx(ii,1)+1,findx(ii,2)+1)-...
        OFDMchanestWF(findx(ii,1)+1,findx(ii,2)+1);
    sqerrWF=sqerrWF+abs(err)^2;
end

rmserrWF=sqerrWF/nfr;

%Nfideal=1/(2*tau_max*F_s)
%Ntideal=1/(4*f_Doppl*(K+L)*T_s)

% spacing of data in frequency
dind=1;
for ii=1:nfp
    for jj=1:N_f-1
        kd(1,dind)=kp(ii)+jj;
        dind=dind+1;
    end
end

%kd
%length(kd)

% identify the data indices
nfd=length(kd);
nd=nfr-np;
pind=1;
dind=1;
dindx=zeros(nd,2);
for ii=0:M-1
    % use special data spacing at the pilot OFDM symbols
```

```
    if ii==(mp(1,pind))
        for jj=0:nfd-1
            dindx(dind,1)=kd(jj+1);
            dindx(dind,2)=ii;
            if dind<nd
                dind=dind+1;
            end
        end
        if pind<ntp
            pind=pind+1;
        end
    else
        for jj=0:K-1
            dindx(dind,1)=jj;
            dindx(dind,2)=ii;
            if dind<nd
                dind=dind+1;
            end
        end
    end
end

%dindx(1:15,1)

dat=rand(nd,1)+i*rand(nd,1); % some random data which to be transmitted
for ii=1:nd
    if real(dat(ii,1))>=0.5
        xx=1/sqrt(2);
    else
        xx=-1/sqrt(2);
    end

    if imag(dat(ii,1))>=0.5
        yy=1/sqrt(2);
    else
```

```
        yy=-1/sqrt(2);
    end

    dat(ii,1)=xx+i*yy;
end

% simulate symbol reception for the data symbols
rdSym=zeros(nd,1);
for ii=1:nd
    rdSym(ii,1)=OFDMchan(dindx(ii,1)+1,dindx(ii,2)+1)*dat(ii,1);
end

% add noise to the received symbols
rdSymn=awgn(rdSym,SNR);

OFDMchanestMLE=zeros(K,M);
OFDMchanestLS=zeros(K,M);

% make the 1D OFDM symbol
OFDMsym=zeros(K,1);
OFDMsym(kp+1,1)=rpSymn(1:K/N_f,1);
OFDMsym(kd+1,1)=rdSymn(1:(K-K/N_f),1);
%OFDMsym

% make the 1D data vector
X=zeros(K,1);
X(kp+1,1)=plt(1:K/N_f,1);
X(kd+1,1)=dat(1:(K-K/N_f),1);
%size(XX)
% make a data matrix for the hadamard product
XX = zeros(K,L);
for ii=1:L
    XX(:,ii)=X(:,1);
end
```

```
% signal subspace Fourier matrix
Fsig=F(:,1:L);
% make the matrix of data times Fourier
QQ =XX.*Fsig;
% estimate the channel in the time domain
hestvect=pinv(QQ)*OFDMsym;
hestlvect=[hestvect; zeros(K-L,1)]; % estimated zero padded channel
% estimate the channel in the fourier domain
hest1DMLE=F*hestlvect;

% the 1-D LS estimator
hest1DLS=OFDMsym./X;

% estimated the first 32 OFDM symbol channels
for ii=1:M
    OFDMchanestMLE(:,ii)=hest1DMLE(:,1);
    OFDMchanestLS(:,ii)=hest1DLS(:,1);
end

% calculate MSE
sqerrMLE=0;
for ii=1:nfr
    err=OFDMchan(findx(ii,1)+1,findx(ii,2)+1)-...
            OFDMchanestMLE(findx(ii,1)+1,findx(ii,2)+1);
    sqerrMLE=sqerrMLE+abs(err)^2;
end

rmserrMLE=sqerrMLE/nfr;

% calculate MSE
sqerrLS=0;
for ii=1:nfr
    err=OFDMchan(findx(ii,1)+1,findx(ii,2)+1)-...
            OFDMchanestLS(findx(ii,1)+1,findx(ii,2)+1);
    sqerrLS=sqerrLS+abs(err)^2;
```

```
end

rmserrLS=sqerrLS/nfr;

% lets do some data error rates
serrWF=0;
serrMLE=0;
serrLS=0;

SERWF=serrWF/nd;
SERMLE=serrMLE/nd;
SERLS=serrLS/nd;

errMat=zeros(3,2);
errMat(1,1)=rmserrWF;     errMat(1,2)=SERWF;
errMat(2,1)=rmserrMLE;    errMat(2,2)=SERMLE;
errMat(3,1)=rmserrLS;     errMat(3,2)=SERLS;
```

## E.3 RP-CSI Estimator

```
function errMat=MISOOFDMchanEst3(SNR, n_w, show)
% a function to simulate the performance of a multi-transmitter
% system.
% SNR - signal to noise ratio
% n_w - number of coefficients in RP-CSI
% show - do you want to see result displays

% for simulation we shall call L_0=n_w to calculate the
% analytical MSE
L_0=n_w;
if nargin == 1
    L_0=16;
    show = 0;
end
```

```
n_t=2; % number of transmit antennas

% define the number of subcarriers.
Ndata = 128;
hNdata = Ndata/2;
% declare the length of the cir
vv = 16;
% define a useful parameter due to convolution
convlen = Ndata + vv - 1;
% sub-carrier steps for training sequence placement
deltaf = 2;
% find linear snr
snr = 10^(SNR/10);

%****************************************%
% transmission and reception OFDM matrices %
%****************************************%
F=gen_fftmatrix(Ndata);
Finv=F';

% generate a power delay profile
pdlyp=gen_SVstatpdp;
% generate the channel impulse response
cir1=gen_SVstatchan(pdlyp);
cir2=gen_SVstatchan(pdlyp);
% generate rayleigh channel matrix
hmatrix1=gen_SVstatchanmat(cir1,Ndata,vv);
hmatrix2=gen_SVstatchanmat(cir2,Ndata,vv);
% make circula hmatrix
chmatrix1=gen_SVstatcircchanmat(cir1,Ndata);
chmatrix2=gen_SVstatcircchanmat(cir2,Ndata);
% calculate the diagonal hmatrix
diag_hmatrix1 = F*chmatrix1*Finv;
diag_hmatrix2 = F*chmatrix2*Finv;
```

```
%[BPCA,muv]=MIMOOFDMoptbasis(L_0,0);

%****************************************%
% generate training OFDM symbols-Walsh code %
%****************************************%

a=0.7071;

% orthogonal training sequence
X_1 = (a+i*a);      X_2 = (a+i*a);
Y_1 = (a+i*a);      Y_2 =-(a+i*a);

% generate the OrthoNormal training sequences
for ii = 1:deltaf:Ndata
    TX1Block(ii,1)   = X_1;  TX2Block(ii,1)   =  Y_1;
    TX1Block(ii+1,1) = X_2;  TX2Block(ii+1,1) =  Y_2;
end

% find the ifft of the OrthoNormal complex signal
OFDMTBlock1 = Finv*TX1Block;
OFDMTBlock2 = Finv*TX2Block;

% add cyclic prefix to the OrthoNormal training block
cycOFDMTBlock1 = addCyclicPrefix(OFDMTBlock1, Ndata, vv);
cycOFDMTBlock2 = addCyclicPrefix(OFDMTBlock2, Ndata, vv);

%****************************************%
% simulate MISO-OFDM tx and rx           %
%****************************************%

% model the received training signal, r = hs + n
recCycOFDMTBlock  = (hmatrix1*cycOFDMTBlock1) + ...
                    (hmatrix2*cycOFDMTBlock2);
```

```
% add complex noise at the receiver
recCycOFDMTBlockwn=awgn(recCycOFDMTBlock,SNR);

nvar=var(recCycOFDMTBlockwn-recCycOFDMTBlock);

% remove training cyclic prefix
recOFDMTBlockwn = recCycOFDMTBlockwn(vv:convlen,1);

% calculate received symbol via FFT
symBlockwn = F*recOFDMTBlockwn;

%*****************************************%
% calculate analytical MSE and capacity    %
%*****************************************%

L_max=16; % this is the expected maximum delay of the channel

for ii=1:Ndata
    H_1(ii,1)=diag_hmatrix1(ii,ii);
    H_2(ii,1)=diag_hmatrix2(ii,ii);
end

subRT=symBlockwn([1:2:Ndata])/(a+i*a);

aMSE=nvar*L_0/Ndata;

%****************************%
% use the Fourier basis RP-CSI %
%****************************%
fhMatrixEst1=zeros(Ndata,Ndata);
fhMatrixEst2=zeros(Ndata,Ndata);

% make an R matrix
for ii=1:Ndata
    R(ii,1)=symBlockwn(ii);
```

```
end

T=(a+j*a); % training symbol
TBlock=[T   T;...
            T -T];
X=gen_tSeqMatrix(Ndata,n_t,TBlock);
P=gen_Permatrix(Ndata,n_t)';
B=gen_invFB(Ndata,n_t,L_0);

Q=(X*P*B)';
w=Q*R;
h_F=B*w;

for ii=1:Ndata
     fhMatrixEst1(ii,ii)=h_F(ii+0*Ndata);
     fhMatrixEst2(ii,ii)=h_F(ii+1*Ndata);
end

%*******************************%
% use the wavelet basis RP-CSI   %
%*******************************%
dhMatrixEst1=zeros(Ndata,Ndata);
dhMatrixEst2=zeros(Ndata,Ndata);

NL=log2(Ndata/L_0);
Nwavlet=8;

B=analyseDaubechies(Ndata,NL,n_t,Nwavlet);
Q=(X*P*B);

% this matrix is not the identity
invQ=pinv(Q);
w=invQ*R;
h_F=B*w;
```

```
for ii=1:Ndata
    dhMatrixEst1(ii,ii)=h_F(ii+0*Ndata);
    dhMatrixEst2(ii,ii)=h_F(ii+1*Ndata);
end

%****************************%
% use the PCA basis RP-CSI    %
%****************************%
phMatrixEst1=zeros(Ndata,Ndata);
phMatrixEst2=zeros(Ndata,Ndata);

L_M=64;

for nn=1:L_M
    % generate the channel impulse response
    cir=gen_SVstatchan(pdlyp);
    % make circula hmatrix
    chmat=gen_SVstatcircchanmat(cir,Ndata);
    % calculate the diagonal hmatrix
    Tdiag_hmat = F*chmat*Finv;

    XX(:,nn)=diag(Tdiag_hmat);
end

uu=mean(XX,2);

hh=ones(1,L_M);

BB=XX-uu*hh;

CC=(1/L_M)*BB*BB';

[VV,DD] = eig(CC);

B=[VV(:,1:L_0) zeros(size(VV(:,1:L_0)));...
```

```
    zeros(size(VV(:,1:L_0))) VV(:,1:L_0)];

mu=[uu;uu];

R_pca=R-(X*P*mu);

Q=(X*P*B)';
w=inv(Q*Q')*Q*R_pca;
h_F=B*w+mu;

for ii=1:Ndata
    phMatrixEst1(ii,ii)=h_F(ii+0*Ndata);
    phMatrixEst2(ii,ii)=h_F(ii+1*Ndata);
end

%*****************************%
% calculate C, C_LB and MSE   %
%*****************************%

fMSE=0; % calculate Fourier MSE
pMSE=0;
dMSE=0;
for ii = 1:Ndata
    fMSE=fMSE+...
            (abs(fhMatrixEst1(ii,ii)-diag_hmatrix1(ii,ii))^2)+...
            (abs(fhMatrixEst2(ii,ii)-diag_hmatrix2(ii,ii))^2);

    pMSE=pMSE+...
            (abs(phMatrixEst1(ii,ii)-diag_hmatrix1(ii,ii))^2)+...
            (abs(phMatrixEst2(ii,ii)-diag_hmatrix2(ii,ii))^2);

    dMSE=dMSE+...
            (abs(dhMatrixEst1(ii,ii)-diag_hmatrix1(ii,ii))^2)+...
            (abs(dhMatrixEst2(ii,ii)-diag_hmatrix2(ii,ii))^2);
end
```

```
fMSE=fMSE/(n_t*Ndata);
pMSE=pMSE/(n_t*Ndata);
dMSE=dMSE/(n_t*Ndata);

errMat=[aMSE; fMSE; pMSE; dMSE];

%****************************%
% display results            %
%****************************%

if show == 1
    for ii = 1:Ndata
        yy1(1,ii)=abs(diag_hmatrix1(ii,ii));
        zz1(1,ii)=abs(diag_hmatrix2(ii,ii));

        yy2(1,ii)=abs(fhMatrixEst1(ii,ii));
        zz2(1,ii)=abs(fhMatrixEst2(ii,ii));

        yy3(1,ii)=abs(phMatrixEst1(ii,ii));
        zz3(1,ii)=abs(phMatrixEst2(ii,ii));
    end

    xx=1:Ndata;

    NN=L_0;

    figure, plot(xx,yy1,'*-',xx,yy2,'^-',xx,yy3,'d-')
    grid minor;
    legend('true channel','Fourier Basis','PCA basis',1)

    figure, plot(xx,zz1,'*-',xx,zz2,'^-',xx,zz3,'d-')
    grid minor;
    legend('true channel','Fourier Basis','PCA basis',1)
```

```
    vect1=abs(diag(DD)).';
    nnv=1:NN;
    figure, plot(nnv,vect1(1:NN),'*-')
    title('Eigen values for channel 1')
    xlabel('Eigenvector index, m')
    ylabel('$|\lambda_m|$','Interpreter','latex')

    pb11=VV(:,1);         pb15=VV(:,5);
    pb12=VV(:,2);         pb16=VV(:,6);
    pb13=VV(:,3);         pb17=VV(:,7);
    pb14=VV(:,4);         pb18=VV(:,8);

    figure, subplot(2,1,1), plot(xx,abs(pb11),'+-',xx,abs(pb12),'*-',...
                                 xx,abs(pb13),'^-',xx,abs(pb14),'d-')
    title('First four PCA Basis vectors (Eigenvectors) for channel 1')
    xlabel('Sub-carrier index, k')
    ylabel('$|W[k,m]|$','Interpreter','latex')
            subplot(2,1,2), plot(xx,abs(pb15),'+-',xx,abs(pb16),'*-',...
                                 xx,abs(pb17),'^-',xx,abs(pb18),'d-');
    title('Next four PCA Basis vectors (Eigenvectors) for channel 1')
    xlabel('Sub-carrier index, k')
    ylabel('$|W[k,m]|$','Interpreter','latex')

    fMSE

    pMSE

end
```

## E.4 Wavelet Basis

```
function ID=analyseDaubechies(nData,res,nAnt,DN)
% a function to analyse the daubechies wavelet
```

```
% transform of a sine wave

if nargin==1
    res=1;
    nAnt=1;
    DN=8;
elseif nargin==3
    DN=8;
end

N=DN;
%N=4;

maxresdim=nData/(2^(res));

if maxresdim<N
    disp('ERROR: The resolution depth is not achievable with DN!');
    ID=0;
    return;
end

DB=eye(nData,nData);

for ii=1:res
    TM=eye(nData,nData);
    resdim=nData/(2^(ii-1));
    D=gen_DaubMatrix(resdim, N);

    TM(1:resdim,1:resdim)=D(:,:);

    DB=TM*DB;
end

IDB=DB';
```

```
trunc_IDB=IDB(:,1:maxresdim);


%**************************************%
% test routines                        %
%**************************************%
%K=128;
%v=8;

%trunc_IDB'*trunc_IDB

%kk=1:K;

%f_kk=sin((2*pi*(kk-1)*v)/K)';

%wt=DB*f_kk;

%figure, plot(kk,wt,'*-')

%trunc_wt=wt(1:maxresdim,1);

%rf_kk=trunc_IDB*trunc_wt;

%figure, plot(kk,f_kk,'*-',kk,rf_kk,'+-')
%***************************************%
% end test routine                      %
%***************************************%

nCoeffs=maxresdim;

for antNum=0:nAnt-1
    for kk=1:nData
        for vv=1:nCoeffs
            kkmod=(nData*antNum)+kk;
            vvmod=(nCoeffs*antNum)+vv;
```

```
            ID(kkmod,vvmod)=trunc_IDB(kk,vv);
        end
    end
end
```

## E.5 Slepian/ Discrete Prolate Spheroidal Sequences

```
function w = dpssw(M,Wc,kchan);
%function [w,A,V] = dpssw(M,Wc);

% DPSSW - Compute Digital Prolate Spheroidal Sequence window of
%           length M, having cut-off frequency Wc in (0,pi).

k = (1:M-1);
s = sin(Wc*k)./ k;
c0 = [Wc,s];
A = toeplitz(c0);
[V,evals] = eig(A); % Only need the principal eigenvector
[emax,imax] = max(abs(diag(evals)));

w=zeros(M,kchan);
for ii=1:kchan
    w(:,ii) = V(:,M-ii+1);
    if ii==1
        w(:,ii) = w(:,ii) / max(abs(w(:,ii)));
    else
        w(:,ii) = -w(:,ii) / max(abs(w(:,ii)));
    end
end

lamda_n=zeros(1,kchan);
```

```
for ii=1:kchan
    lamda_n(1,ii)=evals(M-ii+1,M-ii+1)/evals(M,M);
end

%size(w)

%t = 1:M;
%figure, plot(t,w(:,1),t,w(:,2),t,w(:,3))
%legend('v_1','v_2','v_3',1)
%xlabel('m')
%title('First three 1-D DPSS')
%grid minor;
%n=1:kchan;
%figure, semilogy(n,lamda_n,'o-')
%xlabel('n')
%ylabel('Eigenvalue')
%title('First eight eigenvalues of the 1-D DPSS')
%grid minor;
```

## E.6 Orthogonal Training Sequence Training

```
function MISOOFDMchanEst6(SNR,show)
% a function to simulate the performance of a multi-transmitter
% system.
% SNR - signal to noise ratio
% show - do you want to see result displays

if nargin == 0
    SNR=100;
    show = 1;
end

n_t=2; % number of transmit antennas
```

```
% define the number of subcarriers.
Ndata = 128;
hNdata = Ndata/2;
% declare the length of the cir
vv = 16;
% define a useful parameter due to convolution
convlen = Ndata + vv - 1;
% sub-carrier steps for training sequence placement
deltaf = 2;
% find linear snr
snr = 10^(SNR/10);

%*****************************************%
% transmission and reception OFDM matrices %
%*****************************************%
F=gen_fftmatrix(Ndata);
Finv=F';

% generate a power delay profile
pdlyp=gen_SVstatpdp;
% generate the channel impulse response
cir1=gen_SVstatchan(pdlyp).';
cir2=gen_SVstatchan(pdlyp).';

% flat fading OFDM channels
chan1=F*cir1;
chan2=F*cir2;

%******************************************%
% generate training OFDM symbols-Walsh code %
%******************************************%

a=0.5;
% orthogonal training sequence
X_1 = (a+i*a);      X_2 = (a+i*a);
```

```
Y_1 = (a+i*a);        Y_2 =-(a+i*a);

abs(X_1)^2;

% generate the OrthoNormal training sequences
for ii = 1:2:Ndata
    TX1Block(ii,1)   = X_1;  TX2Block(ii,1)   =  Y_1;
    TX1Block(ii+1,1) = X_2;  TX2Block(ii+1,1) =  Y_2;
end

%****************************************%
% simulate MISO-OFDM tx and rx           %
%****************************************%
recSym=(TX1Block.*chan1)+(TX2Block.*chan2);

% add complex noise at the receiver
recSymn=awgn(recSym,SNR);

%************************************%
% use the orthogonal training seuqences %
%************************************%
estchan1=zeros(Ndata,1);
estchan2=zeros(Ndata,1);
for ii=1:deltaf:Ndata
     estchan1(ii,1)=recSymn(ii,1)*conj(TX1Block(ii,1))+...
                    recSymn(ii+1,1)*conj(TX1Block(ii+1,1));
    %estchan1(ii+1,1)=estchan1(ii,1);
     estchan2(ii,1)=recSymn(ii,1)*conj(TX2Block(ii,1))+...
                    recSymn(ii+1,1)*conj(TX2Block(ii+1,1));
    %estchan2(ii+1,1)=estchan2(ii,1);
end


%************************************%
%Do some interpolations              %
```

```
%**************************************%
L=32; % number of foureir coeffs for intrepolation
Fint=F(:,1:L);
Fsub=F(:,1:L);
for ii=1:deltaf:Ndata
    Fint(ii+1,:)=zeros(1,L);
end

estchan1=Fsub*(pinv(Fint)*estchan1);
estchan2=Fsub*(pinv(Fint)*estchan2);



if show==1
    mm=(1:Ndata).';
    figure, plot(mm,abs(chan1),'-.r',mm,abs(estchan1),'-.b')
    xlabel('Sub-carrier Index, k')%,mm,abs(iestchan1),'-.k')
    ylabel('$|H_1[k]|$','Interpreter','latex')
    title('Absolute value of the sub-carrier channel: antenna 1, SNR = 100')
    legend('Actual Channel','Estimated Channel',1)

    mm=(1:Ndata).';
    figure, plot(mm,abs(chan2),'-.r',mm,abs(estchan2),'-.b')
    xlabel('Sub-carrier Index, k')%,mm,abs(iestchan2),'-.k')
    ylabel('$|H_2[k]|$','Interpreter','latex')
    title('Absolute value of the sub-carrier channel: antenna 2, SNR = 100')
    legend('Actual Channel','Estimated Channel',1)
end
```

## E.7 Kalman Filter

```
function errMat=MISOOFDMchanEst5(SNR,L_0,show)
% a function to simulate the performance of a multi-transmitter
% system.
```

```
% SNR - signal to noise ratio
% show - do you want to see result displays

if nargin==0
    SNR=100;
    snr = 10^(SNR/10);
    L_0=16;
    show=1;
end

if nargin == 0
    SNR=100;
    show = 1;
end

n_t=2; % number of transmit antennas

% define the number of subcarriers.
Ndata = 128;
K=Ndata;
M=128;
hNdata = Ndata/2;
% declare the length of the cir
vv = 16;
L=vv;
% define a useful parameter due to convolution
convlen = Ndata + vv - 1;
% sub-carrier steps for training sequence placement
deltaf = 2;
% find linear snr
snr = 10^(SNR/10);

v_rec=70;
f_c=2.4e9;
c=3e8;
```

```
f_Doppl=v_rec*f_c/3e8; % doppler frequency

T_s=10e-9; % QAM symbol period

%***************************************%
% Kalman filter design                  %
%***************************************%

F_Sampl=16*560; % sample frequency
T_Sampl=1/F_Sampl;

lenfilt=8; % this is the length of the CIR
tt = (1:lenfilt); % time during which we canclulate CIR for jakes process

A=1/pi;

hjakes=zeros(1,lenfilt);
for ii=1:lenfilt
    xx=2*pi*f_Doppl*tt(ii)*T_Sampl;
    %hjakes(ii)=2^(1/4)*f_Doppl*xx^(-1/4)*gamma(3/4)*besselj(1/4,xx);
    hjakes(ii)=A^(1/2)*2^(1/4)*pi^(1/2)*f_Doppl*xx^(-1/4)*gamma(3/4)*...
        besselj(1/4,xx);
end

% nemerator
b=1;

% denominator
a=hjakes;

% find the partial fraction representation
[r,p,k] = residuez(b,a);

% read the thesis chapter 6 for the rest of the code
```

```
Nclac=length(r);

PIvect=zeros(1,Nclac);
for ii=1:Nclac
    sum=0;
    for jj=1:Nclac
        sum=sum+r(jj)*p(jj)^(ii-1);
    end
    PIvect(ii)=sum;
end

psi=zeros(1,Nclac-1);

for ii=1:Nclac-1
    psivect(ii)=-PIvect(ii+1)/PIvect(1);
end

arlen=length(psivect); % length of the autoregressive model

sigsqrn=9.7809e-014; % constant representing noise variance, we have no,...
% noise

deltMat=zeros(arlen,arlen);
deltMat(1,1)=1;

%deltaMat

P = eye(arlen,arlen); % posteriori error covariance

H = eye(arlen,arlen); % measurement model matrix

% make the process model matrix
A = zeros(arlen,arlen);
A(1,:) = psivect(1,1:arlen);
delta_kron=zeros(1,arlen);
```

```
delta_kron(1,1)=1;
for ii=2:arlen
    A(ii,:)=circshift(delta_kron,[0 (ii-2)]);
end

Q = 2*sigsqrn*deltMat; % process noise covariance matrix

R = sigsqrn*eye(arlen,arlen);

%****************************************%
% transmission and reception OFDM matrices %
%****************************************%
F=gen_fftmatrix(Ndata);
Finv=F';

% generate a power delay profile
pdlyp=gen_SVstatpdp;
% generate the channel impulse response
cir1=gen_SVstatchan(pdlyp).';
cir2=gen_SVstatchan(pdlyp).';

% gerenare the time variant channel
th=rand(K,1)*2*pi; % uniform azimuthal phase angles /mpc
fn=f_Doppl.*cos(th); % doppler freq shifts

% calculate channel with phase, we do T_s*20 to exaggerate the changes in
% channel parameters for this data rate
cir1doppl=zeros(K,M);
cir1doppl=zeros(K,M);
for ii=1:M
    cir1doppl(:,ii)=cir1.*exp(j*2*pi*fn*(ii-1)*(K+L-1)*20*T_s);
    cir2doppl(:,ii)=cir2.*exp(j*2*pi*fn*(ii-1)*(K+L-1)*20*T_s);
end

% generate the OFDM flat fading channel
```

```
fltchan1=zeros(K,M);
fltchan1=zeros(K,M);
for ii=1:M
    fltchan1(:,ii)=F*cir1doppl(:,ii);
    fltchan2(:,ii)=F*cir2doppl(:,ii);
end

%*****************************************%
% Initial conditions for the process vectors %
%*****************************************%

s1=zeros(arlen,1); % initial prediction is zero
s2=zeros(arlen,1); % initial prediction is zero
% initial data estimates
x1=zeros(arlen,1);
x2=zeros(arlen,1);
for ii=1:arlen
    x1(ii,1)=fltchan1(1,(arlen-ii+1));
    x2(ii,1)=fltchan1(1,(arlen-ii+1));
end

% initialixe a tracking channel vector
hchantrack1=zeros(M,1);
hchantrack1(1:arlen,1)=fltchan1(1,1:arlen,1);

hchantrack1=zeros(M,1);
hchantrack1(1:arlen,1)=fltchan1(1,1:arlen,1);
hchantrack2=zeros(M,1);
hchantrack2(1:arlen,1)=fltchan1(1,1:arlen,1);

%****************************************%
% generate training OFDM symbols-Walsh code %
%****************************************%

a=0.7071;
```

```
% orthogonal training sequence
X_1 = (a+i*a);       X_2 = (a+i*a);
Y_1 = (a+i*a);       Y_2 =-(a+i*a);

% generate the OrthoNormal training sequences
for ii = 1:2:M
    TX1Block(ii,1)   = X_1;  TX2Block(ii,1)   =  Y_1;
    TX1Block(ii+1,1) = X_2;  TX2Block(ii+1,1) =  Y_2;
end

% make some RP-CSI vectors,...
Tvec=(a+j*a); % training symbol
TBlock=[Tvec  Tvec;...
    Tvec -Tvec];
Xmat=gen_tSeqMatrix(M,n_t,TBlock);
Pmat=gen_Permatrix(M,n_t).';
Bmat1=gen_invFB(M,n_t,L_0);
Bmat2=gen_invFB(M,n_t,(L_0/4));

Qmat1=(Xmat*Pmat*Bmat1);
Qmat2=(Xmat*Pmat*Bmat2);
mpinvQ1=pinv(Qmat1);
mpinvQ2=pinv(Qmat2);

for ii=arlen+1:M
    %*****************************************%
    % simulate MISO-OFDM tx and rx            %
    %*****************************************%

    % Prediction for state vector and covariance:
    s1 = A*s1;
    s2 = A*s2;
    P = A*P*A' + Q;

    % Compute Kalman gain factor:
```

```
KK = P*H'*inv(H*P*H'+R);

% Correction based on observation:
s1 = s1 + KK*(x1-H*s1);
s2 = s2 + KK*(x2-H*s2);
P = P - KK*H*P;
%end

% store away the tracked channel
hchantrack1(ii,1)=s1(1,1);
hchantrack2(ii,1)=s2(1,1);

% update the measurements, use RP-CSI,...
x1 = circshift(x1,[1 0]);
x2 = circshift(x2,[1 0]);

% here we implement RP-CSI for the this OFDM symbol because we know
% the data,... chan predict in s -> data est now become pilots ->,
% ... chan est thr RP-CSI
chan1=fltchan1(:,ii);
chan2=fltchan2(:,ii);

% make the rx symbol,..
Rvec=(TX1Block.*chan1)+(TX2Block.*chan2);
% if we have the rx, and our detected data are now our pilots, we can
% use RP-CSI to get the latest 'measured channel',...
wvec1=mpinvQ1*Rvec;
wvec2=mpinvQ2*Rvec;
h_F1=Bmat1*wvec1;
h_F2=Bmat2*wvec2;

% now we update the measured channel matrix
x1(1,1) = h_F1(1,1);
x2(1,1) = h_F2(1,1);
%pdatest=x(1,1)
```

```
end % end the time tracking ,...
%

%hchantrack(arlen+1,1)
%fltchan1(arlen+1,1)


if show==1
    mm=1:M;
    figure, plot(mm, abs(fltchan1(1,:)),'-.r',mm, abs(hchantrack1),'-.b',...
        mm,abs(hchantrack2),'-.k')
    legend('Actual channel','Tracked channel, n_w=16','Tracked channel, n_w=8',1)
    xlabel('OFDM Symbol Index, m')
    ylabel('$|H_1[1,m]|$','Interpreter','latex')
    title('Absolute value of the sub-carrier channel: antenna 1')
end
```